UNIVERSITÉ DE SHERBROOKE
Faculté de génie
Département de génie mécanique

Développement d'une méthode hybride éléments finis-matrice de transfert pour la prédiction de la réponse vibroacoustique de structures avec traitements acoustiques

Development of a hybrid finite element-transfer matrix methodology for the modeling of vibroacoustic systems with attached noise control treatments

Thèse de doctorat
Specialité : génie mécanique

Luca Alimonti

Jury: Noureddine Atalla (Directeur)
Alain Berry (Codirecteur)
Raymond Panneton (Rapporteur)
Franck Sgard (Examinateur)
Christian Soize (Examinateur)

Sherbrooke (Québec) Canada December 2014

RÉSUMÉ

Les véhicules aériens et terrestres sont constitués de systèmes bâtis complexes. La structure principale est généralement composée de panneaux légers renforcés par des éléments rigides. Cette solution de conception est répandue parce qu'elle allie la force et un faible poids. Cependant, on sait qu'elle offre des résultats vibroacoustiques médiocres, c'est à dire que l'effet des perturbations externes qui touchent le système peut générer un niveau de bruit excessif à l'intérieur de la cabine des passagers. C'est une préoccupation majeure chez les fabricants, parce que ce niveau de bruit nuit sensiblement au confort ressenti par les clients et peut causer de la fatigue chez les conducteurs et les pilotes. Pour cette raison, les composants passifs constitués de matériaux dissipatifs assemblés en mode multicouche sont généralement intégrés à la structure. Ces assemblées bordées intègrent surtout des matériaux poroélastiques, qui sont plutôt répandus, grâce à l'agencement intéressant de bonnes propriétés d'isolation sonore et de faible poids.

L'intégration en amont des traitements de contrôle du bruit au processus de conception est la clé de succès d'un produit. Pour ce faire, des outils pratiques numériques en mesure de capter le comportement dynamique des systèmes vibroacoustiques impliquant les structures, les cavités et les matériaux d'insonorisation sont requis. D'une part, la modélisation de ces systèmes couplés en utilisant des procédés à base d'éléments finis peut être, bien que précis, irréalisable pour des applications pratiques. D'autre part, les approches analytiques telles que la méthode de matrice de transfert sont souvent préférées grâce à leur facilité d'utilisation, même si elles manquent de précision en raison des hypothèses rigoureuses inhérentes au cadre analytique. Dans ce contexte, les procédures de structuration hybrides sont récemment devenues très populaires. En effet, les différentes techniques de modélisation sont généralement recherchées pour décrire les systèmes vibroacoustiques complexes arbitraires sur la plus large gamme de fréquences possible.

L'objectif du projet proposé est de mettre au point un cadre hybride offrant une méthodologie simple pour tenir compte des traitements de contrôle du bruit dans l'analyse vibroacoustique par éléments finis. A savoir, le modèle de calcul qui en découle conserve la souplesse et la précision de la méthode des éléments finis en bénéficiant de la simplicité et de l'efficacité de la méthode de matrice de transfert pour obtenir une réduction de la charge de calcul pour la modélisation de composants acoustiques passifs. La performance de la méthode pour prédire la réponse vibroacoustique de structures planes homogènes avec des traitements acoustiques attachées est évaluée. Les résultats démontrent que la méthode hybride proposée est très prometteuse, parce qu'elle permet une réduction de l'effort de calcul tout en conservant suffisamment de précision par rapport à l'analyse complète par éléments finis. En outre, la méthode de matrice de transfert proposée de modélisation des traitements de contrôle des bruits est générale, comme on peut l'appliquer dans d'autres cadres outre l'application de l'élément fini considéré dans ce travail.

Mots-clés : vibroacoustique, méthode des éléments finis, méthode matrice de transfert, modélisation hybride, perte par transmission, absorption, traitement acoustique

ABSTRACT

Aerial and terrestrial vehicles consist of complex built-up systems. The main structure is typically made of light panels strengthened by stiffer components. Such design solution is widely used as it combines strength and low weight. However, it is known to give poor vibroacoustic performances, i.e. the effect of external disturbances acting on the system may generate an excessive noise level inside the passengers cabin. This is a main concern for the manufacturers, as it significantly affects the comfort experienced by the costumers and may fatigue drivers and pilots. For this reason, passive components consisting of dissipative materials assembled in a multilayer fashion are typically integrated within the structure. These lined assemblies mainly involve poroelastic materials, which are commonly used thanks to the appealing combination of good noise insulation properties and low weight.

The early integration of noise control treatments in the design process is the key to a successful product. For this purpose, practical numerical tools able to capture the dynamic behavior of vibroacoustic systems involving structures, cavities and noise proofing materials are demanded. On the one hand, modeling such coupled systems using finite element based methods can be, albeit accurate, time consuming for practical applications. On the other hand, analytical approaches such as the transfer matrix method are often preferred thanks to their ease of use, although they suffer from a lack of accuracy due to the stringent assumptions inherent within the analytical framework. In this context, hybrid substructuring procedures have recently become quite popular. Indeed, different modeling techniques are typically sought to describe arbitrarily complex vibroacoustic systems over the widest possible frequency range.

The aim of this thesis is to devise a hybrid framework providing a simple methodology to account for noise control treatments in vibroacoustic finite element analysis. Namely, the resulting computational model retains the flexibility and accuracy of the finite element method while taking advantage from the simplicity and efficiency of the transfer matrix method to obtain a reduction of the computational burden in the modeling of passive acoustic components. The performance of the method in predicting the vibroacoustic response of flat structures with attached homogeneous acoustic treatments is assessed. The results prove that the proposed hybrid methodology is very promising, as it allows for a reduction of the computational effort while preserving enough accuracy with respect to full finite element analysis. Furthermore, the proposed transfer matrix based methodology for noise control treatments modeling is general, as it can be used in alternative frameworks besides the finite element application considered in this work.

Keywords: vibroacoustics, finite element method, transfer matrix method, hybrid modeling, transmission loss, absorption, sound package

TABLE OF CONTENTS

LIST OF FIGURES

LIST OF TABLES

CHAPTER 1

INTRODUCTION

This chapter aims at introducing the reader to the topic of this research, namely the numerical modeling of vibroacoustic systems involving noise control treatments. First, the industrial context is briefly described and the scientific problem is presented. Next, a literature review is performed in order to define the state of the art concerning the modeling techniques. The objectives of this work are then presented. The chapter ends with the outline of the thesis.

1.1 Industrial context

Nowadays, the design of automotive and aerospace vehicles is driven by the twofold need to reduce costs and respect eco-friendly requirements. Thus, to achieve both an abatement of manufacturing costs and an increase of fuel efficiency while protecting the environment, modern cars and aircrafts take advantage from lightweight structural designs involving light panels strengthened by stiffer components such as beams. However, such design solutions typically lead to poor vibroacoustic performances, as the effect of an external disturbance acting on the system may generate an excessive noise level inside the aircraft or car cabin. This is a main concern for the manufacturers. Indeed, the noise inside vehicles significantly affects the comfort experienced by the occupants and may fatigue drivers and pilots. As a result, the requirement of a safety and healthy environment is always an essential part of the design specifications. In this context, a successful product depends (i) on an accurate detection of the potential disturbances as well as (ii) on the design of passive and/or active components which can guarantee the required noise insulation.

The experimental and mathematical characterization of the noise sources involved in practical applications is a very important topic. For instance, in the context of modern turbojet aircraft, the overall noise is mainly due to (i) aerodynamic noise associated to the Turbulent Boundary Layer (TBL) developing over the fuselage and lifting surfaces, and (ii) engine noise associated to the exhausted flow. For typical automotive applications, the aerodynamic noise is important at high speeds while the noise generated by power unit and wheels may be an important source also at lower speeds because of the vibrations mechanically induced to the car structural frame.

The noise insulation properties of lightweight structures involved in aerial and terrestrial vehicles can be enhanced by integrating passive or active solutions within the structure. However, the complexity of the required components (i.e. sensors, actuators and source of energy) together with the necessity of a robust design make active solutions, although attractive, yet difficult to be integrated in practical systems. Thus, passive solutions are rather preferred, thanks to their ease of use, range of possible designs and combinations. In this context, highly dissipative materials such as viscoelastic and poroelastic materials are typically employed to reduce the noise level. Such passive components are assembled in a multilayer fashion and attached onto the structure. These assemblies of dissipative materials are equivalently referred to as *noise control treatments*, *acoustic trims* or *sound packages*.

Nevertheless, the enhanced acoustic performance of the passively treated vibroacoustic system must be obtained by minimizing the overall weight. For this reason and because of the strong coupling between the noise control treatment and the vibroacoustic system (i.e. main structure and cabin), the early integration of such passive components in the design process is the key to a successful product. To this end, numerical tools able to capture the dynamic behavior of these multiphysics systems are needed. This latter aspect is the main concern of this work.

1.2 Problem description

Without loss of generality, practical vibroacoustic systems described above mainly involves three coupled domains, i.e. (i) an external acoustic domain (i.e. emission side), (ii) the main structure and (iii) the interior environment (i.e. receiver side). The latter is the cabin where specific noise level requirements must be satisfied. The disturbances are applied on the emission side (e.g. TBL, engine noise) or directly on the main structure (e.g. vibrations transmitted by wheels and engine). The dynamic response of such systems in the frequency domain is of interest. Under these circumstances, the effectiveness of the noise insulation design is evaluated in terms of vibroacoustic indicators based on global (i.e. averaged) or local (e.g. pressure at a given location) quantities. Among all, the following indicators will be considered in this work.

– Structural and acoustic vibrational energies in terms of space averaged quadratic velocity and pressure, respectively.

– Power radiated into the receiver domain, often presented in terms of Transmission Loss (TL), defined on as the ratio between the incident (i.e. external source) and the radiated powers.
– Noise transfer functions from the external source to the driver or passengers ear.

As already briefly discussed, the external sources are ideal models of the actual disturbances and may be of different kinds. For instance, *acoustic-borne* noise is modeled by acoustic sources placed on the emission side. They represent the effects of external sources (e.g. engine and wheels) as fluctuating pressure excitations, acoustic monopoles, dipoles and quadrupoles. Air-borne noise paths mainly depend on the mass properties of the structure-sound package system. Such non-resonant path typically depicts very good insulation properties at high frequencies. In this context, double wall (DWL) configurations are widely used to enhance the TL at low frequencies. Namely, the sound package is made of an assembly of one or more dissipative layers with a heavy screen on top. Such configuration results in a *spring-mass* behavior able to induce a decoupling frequency (i.e. the DWL resonance) above which a satisfactory noise attenuation is obtained. Hence, the noise control treatment can be designed by optimizing the position of the DWL resonance depending on the specific needs.

On the other hand, *structure-borne* noise due to vibrating parts (e.g. engine mounts) is usually modeled by displacement constraints or mechanical forces applied directly onto the structural frame. Differently from the case of acoustic sources, the energy path involoved in the structure-borne noise is due to the resonant coupling between the mechanical excitation, the structure and the cabin. As a result, although DWL system are still effective, the noise control treatment must also inhibit strong modal transmission paths, for instance optimizing the damping performance of the structural and acoustic domains using, respectively, viscoelastic layers and absorptive elements. In particular, the desired cabin absorption is typically obtained by means of *light* acoustic treatments, involving one or few layers of poroelastic materials which can give optimal damping performance over the mid and high frequency range.

Therefore, the need for an effective design under various excitations and conditions implies the use of fairly complicated sound packages. For instance, a DWL design strategy would result in a satisfactory TL above the decoupling frequency, while no broadband absorption would be provided to the cabin. Hence, the DWL configuration must be combined with other solutions to retrieve the missing performance, for instance adding on the top of the heavy screen other layers of poroelastic materials. However, while providing the desired

acoustic performance, the volume of the sound package must be minimized to obtain the highest possible noise-reduction-efficiency-to-weight ratio.

1.2.1 Poroelastic materials

As already mentioned above, poroelastic materials are widely used in noise control treatments thanks to the combined acoustic efficiency and low weight. Such materials consist of an elastic solid frame saturated by a fluid. In the context of this work, the solid phase defines the structure of the material while air occupies the pores. The effectiveness of poroelastic materials in noise control applications is related to the dissipation mechanisms involved in the coupling between the two phases. Namely, the energy flowing through a poroelastic media is dissipated by (i) structural damping provided by the solid frame itself, (ii) viscous losses due to fluid-structure interaction phenomena at the pores level and (iii) thermal coupling effects between the two phases.

The multiphysics nature of poroelastic materials along with the complexity of the small scales involved in the aforementioned physical mechanisms suggest that a feasible mathematical description of these media may be obtained through the definition of an appropriate equivalent homogeneous material. In this context, the Biot theory [13–15] accounts for the dissipative mechanisms listed above in a simplified manner, namely introducing a macroscopic description of the two-phases medium. Since its first appearance, the Biot theory has been improved and, nowadays, is widely used as a reliable mathematical model of poroelastic materials. Moreover, it is possible to simplify further the Biot model when the solid phase can be considered motionless or limp, in which cases the poroelastic domain can be treated as an equivalent dissipative fluid. For a comprehensive documentation of the modern theory of poroelasticity and its application to passive noise control the reader can refer to the book by Allard and Atalla [3].

1.3 Literature review

The aim of this section is to present the state of the art in the numerical modeling of vibroacoustic systems. First, the most widely used techniques are introduced and classified according to their range of applicability. Then, the literature review is specified to the case of vibroacoustic systems with attached noise control treatments involving poroelastic materials, which is the subject of this work. The main concern of this section is to convey that, broadly speaking, a unique methodology which can provide a feasible and reliable full spectrum analysis (i.e. from low to high frequencies) of complex coupled systems

involving domains with very different physical properties (e.g. stiff and soft structures, acoustic fluids, noise control treatments etc...) can hardly be devised. Consequently, the coexistence of various methodologies in a *hybrid* framework is presented as a possible solution to such modeling issue.

1.3.1 Modeling strategies for vibroacoustic applications

Numerical methods in vibroacoustics have come a long way during the past decades (see the overview in Ref. [100] for instance). They are usually classified as low and high frequency approaches. Namely, deterministic methods are used in the low frequency range, i.e. when the wavelength is long compared to the size of the system, while statistical approaches are preferred at higher frequencies, i.e. when the wavelength is short compared to the system dimensions. Alternatively, simple analytical methods are often employed to obtain quick estimations and tendencies in the preliminary design stage. Besides, hybrid methodologies involving different modeling techniques within the same built-up system are becoming quite common to obtain fast and reliable results over the widest possible frequency range.

Deterministic methods

The Finite Element Method [10] (FEM), is the most common technique to model wave propagation phenomena in complex multiphysics systems. Indeed, thanks to the element based polynomial interpolation, the detail and flexibility provided by the FEM can be hardly found in any other numerical or analytical method. This aspect makes the FEM an almost universal methodology, in theory applicable to arbitrary complex systems. However, its strengths soon become weaknesses. Indeed, the fact that the mesh size must be small enough compared to the wavelength of the physical phenomenon leads to practical limitations when the vibroacoustic response of large structures like cars, aircrafts and trains is considered over a wide range of audible frequencies. Namely, as the frequency increases, the wavelengths propagating in the physical domains become shorter and shorter, leading to huge discrete models and thus rendering the FEM unfeasible in terms of required computational time and resources.

Although several attempts have been made to enhance the efficiency of finite element based techniques (e.g. hierarchical shape functions [117, 118] and *hp*-adaptivity [129]) and to develop alternative approaches (e.g. Trefftz methods [36, 41, 42, 87, 113–116, 124–126] and semi-analytical methods [39, 71, 82, 89]), the FEM is still the most common numerical method used for industrial applications. The reason of this is twofold. First of all, due to the complexity of practical systems, the use of more efficient methodologies is

often prevented by poor geometrical flexibility and numerical issues (e.g. ill-conditioning and cumbersome numerical integration of high order polynomials or oscillatory functions). Second, well-established Model Order Reduction (MOR) techniques have been developed and implemented in modern commercial softwares thus enhancing the computational efficiency of standard finite element models (see Ref. [31] for a review of the most common approaches). In this context, the most widely used MOR technique is *modal synthesis*. Basically, the orthogonal modes of a conservative system are calculated solving the associated eigenvalue problem and then the size of the discrete model is reduced by projection onto the reduced order space spanned by the mode shapes. To successfully extend modal techniques to complex coupled systems, the Component Mode Synthesis (CMS) has been introduced (see for instance Refs. [27, 38, 121]). Essentially, the system is divided into components, or subdomains, on which a modal synthesis is independently performed.

On the other hand, *non modal* techniques have been also attempted. In these approaches, the reduced basis is found matching some meaningful properties of the original dynamic model. In this context, Padé approximants by explicit and implicit moment matching have been object of intensive research [8, 22, 55, 56, 70, 70, 88].

Among the others, another noteworthy MOR technique is the Patch Transfer Function (PTF) method [7, 77, 83]. This substructuring technique allows for speeding up vibroacoustic finite element analysis by means of a substructuring approach based on a coarse discretization of the subdomains interfaces into elementary areas called patches. The methodology consists in studying each subsystem independently, in order to build a set of transfer functions among the patches. Then, the final system is assembled by using the superposition principle and continuity relations at the patches, leading to a downsized problem and thus allowing for faster computations.

Statistical methods

Standard finite element methodologies based on substructuring and modal synthesis are intrinsically limited to low frequency analysis because of the following reasons. First, as already mentioned, the FEM is obviously not practical in the high frequency regime as it leads to huge computational models. The second reason is instead phenomenological. Namely, the dynamic response of a system in the high frequency range does not clearly exhibit separated resonance peaks because of the overlapping of successive modes. Basically, a huge number of modes is computed but their contribution is not distinguishable as the response of the system appears smooth. Consequently, the effectiveness of a modal synthesis becomes questionable. Furthermore, it may be argued that the exact sequence of

natural frequencies and associated mode shapes is very sensitive to small modifications of the built-up system - which is inherently uncertain - raising doubts about the usefulness of deterministic models when a large number of modes participate to the dynamic response.

For the reasons above, alternative approaches have been developed. Among all, Statistical Energy Analysis [73] (SEA) is the most widely used tool for high frequency analysis in industrial applications. It relies on a substructuring methodology which assumes the vibrational energy of each subsystem to be uniform in the space. Each subsystem is thus assumed to be in a state of vibrational equilibrium, being its energy equally distributed among its modes (analogously to the definition of thermal equilibrium in thermodynamics). From a wave standpoint, such hypothesis is often referred to as the *diffuse field* assumption [40]. Under these circumstances, the energies of each subsystem are considered the main variables of the methodology. Such energies are strictly averages over an ensamble of subsystems, although the interpretation in terms of frequency and space average is often employed. Assuming light lossless coupling between adjacent subsystems (i.e. the amount of energy dissipated within the subsystems is larger than that exchanged at the interface) a simple law arises as the energy exchanged between two connected subsystems is proportional to the difference between their internal modal energies. As a result, the coupled response of the assembled system can be found by simply imposing the energy balance (i.e. input power equals dissipated power) over each subsystem.

The most obvious advantage of the SEA is computational. Indeed, differently from the FEM, the statistical model involves only few unknowns (i.e. the energies of each subsystem), thus drastically reducing the cost of the calculations. Besides, the details of the actual system (i.e. geometrical complexity) are neglected, resulting in a simplification of the modeling problem. The model input are instead reduced to simple physical parameters, such as the subsystem Damping Loss Factor (DLF), Coupling Loss Factor (CLF) and modal density. These parameters can be obtained by experimental procedures [21], analytical solutions [73], or by means of a detailed numerical model of the subsystem. In the latter case, the periodic structure theory has been successfully employed to find the SEA parameters of complex two-dimensional subsystem (see Ref. [76] for an overview and Ref. [24] for an application to typical aircraft panels). Alternatively, also the waveguide-FEM [47] can be an efficient tool for the identification of SEA parameters in specific cases. This methodology couples a standard finite element discretization of the waveguide cross-section with the analytical wave solution in the propagation direction. A similar approach has been developed in Ref. [39]. Some interesting applications can be found in Refs. [9, 71, 72, 103].

While imposing itself as a valuable prediction tool thanks to its ease of use, the applicability and accuracy of the SEA is still subject of ongoing research. Conventional SEA is indeed limited to (i) wide-band and uncorrelated excitations, (ii) large modal overlap, (iii) equipartition of energy (i.e. diffuse wave fields) and (iv) light coupling. Strictly speaking, these conditions are only met in the high frequency limit, for low damping and for weakly coupled subsystems [74, 75]. Moreover, the validity of these assumptions may be hard to verify for complex assemblies like cars and aircrafts, considering, in addition, that the accuracy of an SEA model typically depends on how the subsystems are chosen. Consequently, the reliability of full SEA models is often questionable.

For these reasons, alternative methodologies often interpreted as generalizations of the energetic and statistical framework involved in the SEA have been developed. Among all, much effort has been devoted to relax the diffuse field (or, from a modal viewpoint, equipartition of modal energy) hypothesis in order to retrieve the spatial energy distribution in the subsystems. For instance, the approach proposed in Ref. [120] consideres modal energies rather than global energies of subsystems. Conversely, other methodologies favor a wave based approach leading to integral representations of the vibrational field (see for instance Refs. [18, 119], [48, 128] and [67, 68]). Such attempts to retrieve the spatial distribution of the vibrational energy are however not costless, as the computational burden generally increases with respect to standard SEA.

Analytical methods

An alternative to sophisticated deterministic and statistical approaches relies in fast analytical methodologies. Indeed, multilayered structures (e.g. main structure and attached sound package) are often modeled by analytical approaches to perform almost costless predictions and fast parametric studies. However, to solve analytically the coupled partial differential equations governing the system, several assumptions must be introduced. Namely, the multilayer system is assumed (i) homogeneous, (ii) flat and (iii) laterally unbounded. The system remains, instead, bounded in the thickness direction. Under these conditions, the Fourier Transform can be employed to move from the physical space (x, y) to the wavenumber domain (k_x, k_y). As a result, the boundary value problem can be reformulated as a set of ordinary differential equations in terms of the thickness coordinate z. Given the set of interface conditions between different layers, the analytical solution for each traveling wave (k_x, k_y) can be found. In this context, the Transfer Matrix Method [3] (TMM) allows for a compact and general formulation leading to the solution of a small linear system. This methodology is widely used to calculate transmission and absorption coefficients of multilayered structures and, under the aforementioned hypotheses, provides

quick and accurate estimations for the case of acoustic-borne noise [90, 93], i.e. when modal transmission paths are not relevant. Besides, since the assumption of unbounded layers is not justified at low frequency, a finite size correction has been developed [91] to extend the prediction capability of the classical TMM.

The knowledge of the analytical solution in the wavenumber domain can also be used to retrieve the acoustic impedance [3, 86] (or, from a mathematical standpoint, the Green function) of an infinitely extended multilayer structure. Indeed, once the (k_x, k_y)-space has been properly sampled, the inverse Fourier transform can be employed to find the solution in the physical domain. This analytical procedure was used in Ref. [44] to calculate the acoustic impedance of a sandwich panel. A similar methodology is proposed in Ref. [54] to obtain the self and mutual piston impedances of a dissipative elastic layer radiating in a semi-infinite fluid medium. As it will be argued later on, these simple and efficient analytical approaches may find a potential application in the approximation of the acoustic impedance of noise control treatments.

Hybrid methods

The transition between low and high frequency regime of a complex built-up system may be hard to identify. Indeed, the physical properties (i.e. wavelength) of different components of the vibroacoustic system may be such that in the considered frequency spectrum neither deterministic nor statistical methods can be efficiently and effectively applied. Namely, whilst a FE modeling of the entire system typically leads to complicated and huge numerical models, a simple SEA model is not accurate enough to capture the physics of the coupled system. As a result, hybrid techniques are typically required for the practical modeling of real life systems.

A first attempt in modeling heterogeneous systems involving long and short wavelength components in a hybrid framework can be found in the theory of structural fuzzy [107, 108]. Essentially, the system is described as a primary structure with secondary "attachments". The former is deterministically known and constitutes the long wavelength part of the assembled structure. The secondary components are instead considered uncertain and/or not accessible to conventional modeling strategies (e.g. FEM). Such subsystems are referred to as structural fuzzy and they are assumed to be attached to the primary structure by point connections. The fuzzy structural theory aims at defining the energy transfer at the attachment points between the primary deterministic structure (e.g. modeled by standard FEM) and the secondary imprecisely known subsystems by random impedance operators. As in an SEA model, some physical parameters must be experimentally or

numerically identified to fully define the impedance of the attached fuzzy part. The extension to continuous fuzzy attachments can be found in Ref. [112] to answer to the practical need of modeling efficiently complex heterogeneous structures whose dynamic behavior is characterized by global (i.e. deterministic part) and local elastic modes (i.e. imprecisely known details). An alternative methodology was proposed in Ref. [65], where the local modes are instead modeled as SEA subsystems rather than fuzzy components.

The latter approach has been further developed in Ref. [104] to extend the range of applicability of SEA towards lower frequencies. Essentially, this hybrid methodology is presented as a possible solution to the following modeling problem. Let us consider two subsystems, connected by a one- or two-dimensional junction. In this context, even though the two subsystems alone meet the SEA requirements (i.e. diffuse wave field), the energy flow through the junction (i.e. CLF) may depend on an amount of details that can be accurately captured only by a deterministic model of the connection. In addition, the impedance of the junction can also be a function of the subsystems geometry (i.e. boundary conditions) in case their dimensions are comparable with the wavelength. Hence, it could happen that one subsystem meets the SEA requirements, whereas a deterministic model of the other subsystem and the junction must be accounted for to get reliable results. The solution of this modeling problem relies on the reciprocity condition between the way the power is injected from the deterministic connection into the statistical subsystem and the blocked force acting on the deterministic degrees of freedom as a consequence of the resulting reverberant diffuse field in the statistical subsystem. Such theoretical result is often referred to as diffuse field reciprocity relationship [64, 106] and provides the framework within which deterministic (i.e. FEM) and statistical (i.e. SEA) modeling strategies can be employed in the same computational model. Applications of such hybrid methodology can be also found in Refs. [25, 66].

It may be argued that the fuzzy theory and the diffuse field reciprocity are two possible answers to the following practical issues.

- A tradeoff between accuracy and computational efficiency in the numerical modeling of typical vibroacoustic systems is sought to perform feasible and reliable analysis over a wide range of audible frequencies.
- Some parts of the assembled system may be inherently unknown because, for instance, associated to industrial process which cannot guarantee their deterministic knowledge (e.g. mounting conditions, material uncertainties, etc. . .).

The arguments above may be generalized as follows. A practical predictive tool should model each subsystem of a complex multiphysics system by means of the more appropriate methodology. the latter is the one that allows to describe the subsystem with the minimum amount of information while preserving "sufficient" accuracy. The resulting hybrid strategy would avoid expensive (short wavelengths) or meaningless (unknown details) finite element models of those components which do not actually need to be accurately modeled to capture their "average" effect on the assembled system response.

In this context, several hybrid methodology have been proposed to combine the strengths of different approaches within the same framework. For instance, in Ref. [59] the accurate deterministic model of a long-wavelength main structure is coupled with simple analytical tools to capture the effect of the uncertain and/or short-wavelength components. An application of this hybrid modeling strategy to beam-stiffened plate systems can be found in Ref. [60]. Another example of hybrid modeling is the methodology presented in Refs. [49, 61], which allows to retain a detailed finite element model of the main structure while taking advantage from an efficient Trefftz approach to model large acoustic cavities.

It is herein stressed that the generalized concept of hybrid modeling discussed above perfectly embraces the motivations of the present work, as it will be clarified later on in this chapter.

1.3.2 Noise control treatments modeling

In this section the modeling of vibroacoustic systems with attached noise control treatments is specifically discussed through a review of the most common approaches. The main issue in the approximation of the dynamic behavior of such acoustic components is associated to the presence of highly dissipative and soft materials which require the use of complex material models. As a result, the numerical approximation of the vibroacoustic system may become cumbersome. For this reason, analytical approaches are typically preferred thanks to their ease of use and computational efficiency, although accurate finite element models of the full system (master structure, acoustic cavity and sound package) are often needed to obtain reliable results for arbitrary configurations (e.g. cars and aircrafts) in the low frequency range.

Analytical methods

A preliminary assessment of the noise control treatment insulation properties (i.e. TL and absorption) is typically performed by means of the TMM. As already mentioned, due to the stringent hypotheses inherent within its analytical framework, the TMM is limited

to high frequencies and acoustic-borne noise. Moreover, the TMM is also widely used to account for noise control treatments in SEA models. Indeed, sound packages cannot be considered subsystems in the SEA sense because of the strong dissipation which prevent the establishment of a diffuse field. Thus, the effect of acoustically treated parts on the response of SEA models must be differently accounted for, for instance by modifying the subsystems SEA parameters (i.e. DLF and CLF). This can be quickly done by solving simple transfer matrix problems, as discussed for instance in Refs. [23, 90].

However, the assumptions of laterally unbounded systems is not justified at low frequency, especially when structure-borne paths dominates the energy flow through the built-up system (e.g. point forces). For this reason, attempts have been recently made to extend the TMM framework in order to account for the modal behavior of the main structure. In this context, it is noteworthy the methodology proposed in Refs. [90, 92, 93] to model flat rectangular plates with attached multilayer treatments. The approach relies on a description of the structural displacement by superposition of orthogonal trigonometric functions (i.e. Ritz method), while the effect of the noise control treatment on each mode is approximated by solving small TMM problems. However, more accurate deterministic models are typically needed in the low frequency range to capture the modal transmission energy paths between an arbitrary complex main structure and the receiver acoustic domain (e.g. passengers' cabin).

Deterministic methods

Consequently, the presence of acoustic treatments has to be often included in a finite element framework. In this context, the most practical way to account for the dynamic effects of a sound package on the structural and acoustic domains (i.e. main structure and cavity) consists in a costless impedance boundary conditions to be applied over the acoustically treated surface (see for instance Ref. [37]). Typically, the impedance condition is measured by testing a sample of the sound package in an impedance tube facility. On the one hand, this approach has the undeniable advantage of simplifying the modeling and avoiding the identification of the sound package mechanical and acoustic parameters. However, on the other hand, it implicitly assumes that the behavior of the noise treatment is local, meaning that the impedance at a given point of the multilayer treatment depends only on the local values of displacement and pressure.

For this reason, accurate finite element models of acoustic materials in the low frequency range are often required to obtain more accurate predictions. However, when poroelastic materials are involved in noise control treatments, using finite element based method-

ologies can be, even if accurate, computationally expensive. Indeed, the Biot model is typically taken into account to obtain a good accuracy [84] for general configurations and a broad range of excitation frequencies. However, the (u, p) formulation [5] of the Biot theory, albeit more efficient compared to other formulations (e.g. displacement based formulation [85]), still needs four unknowns per node. Therefore, a large number of degrees of freedom is necessary to describe short wavelengths and dissipation involved in poroelastic materials. Furthermore, classical mesh criteria, i.e. six linear or four quadratic elements per wavelength, do not provide a sufficient condition to get reliable results, due to the coupling between the two phases and because of the dissipation mechanisms [30]. Consequently, a large number of elements are always needed in order to capture the dynamics of sound packages, especially as the frequency range of interest increases.

Several attempts have been made to alleviate this drawback. On the one hand, much work has been devoted to improve the efficiency of the FEM for poroelastic materials modeling. For instance, hierarchical formulations of the elements [57, 94], simplified 2D models [19, 58] and enrichment methods [20] have been investigated. In addition, the complex frequency dependency of the finite element matrices describing the coupling between fluid and solid phases in poroelastic materials make standard eigenvalue solvers difficult to apply. Despite several attempts to develop modal based MOR techniques for porous materials [32, 33, 96], their effectiveness remains questionable as a huge number of modes, whose participation to the global response of the system is not clear apriori [97], has to be taken into account. The use of Padé-like approximants have also been attempted for acousto-poroelastic problems [95], showing interesting performance.

Due to mathematical difficulties and questionable effectiveness of modal based MOR techniques, a condensation of the acoustic treatment degrees of freedom is typically preferred [53]. In this case, the final discrete model of the coupled system involves only the amplitudes of the master subsystems generalized coordinates (e.g. structural and acoustic modal amplitudes). The effect of the acoustic treatment is, instead, held in an added (boundary) operator which contains the effect of the condensed degrees of freedom on the generalized coordinates. Such operator can be seen as an equivalent interface impedance which, differently from the extremely simplified local impedance models discussed above, accounts for the exact non local behavior of the sound package.

Alternatively, new approaches have been developed to avoid the difficulties arising from a finite element discretization of the acoustic treatment. More specifically, wave based techniques have been proposed. The rationale behind these methods consists in enriching or replacing the piece-wise polynomials used in classical finite element analysis by piece-wise

plane waves, as these are exact solution of the homogeneous problem. In this framework, the Wave Based Method [36] (WBM) has been developed and applied to porous media [35]. Also, the Discontinuous Galerkin Method (DGM) has been used for poroelastic applications [34]. Differently, the rationale of the enrichment methods is to combine the strengths of finite element and wave based methodologies. In this context, an application of the Partition of Unity FE Method [79] (PUFEM) to dissipative acoustic materials can be found in Ref. [20].

Although the aforementioned wave based methodologies can achieve a drastic reduction of the degrees of freedom compared to conventional finite element models, their application to complex three-dimensional systems is still subject of ongoing research. Hence, the FEM is still the most widely used prediction tool in an industrial context, thanks to its accuracy and versatility. Such approach, although well-established for real life structures (e.g. stiffened plates, junctions etc...) and complex shaped acoustic domains, typically leads to expensive and complicated models when noise control treatments are considered, as discussed above. The main issues can be summarized as follows.

– First, several degrees of freedom are typically needed to capture the short and damped waves travelling within the poroelastic layers, especially as the frequency range of interest increases. Moreover, classical MOR techniques (i.e. modal synthesis) are not as effective as for lightly damped structures and acoustic enclosures.
– Second, a preprocessing phase is always required to mesh all the layers involved in the treatment. Thus, for each design of the acoustic trim, a new mesh must be created, making the FEM not suitable for the early stage of the design process, when the optimal configuration of the acoustic trim has to be identified.
– Third, noise control treatments can be quite complex systems, so that mounting conditions might not be exactly known, hard to model in a finite element framework or, from an industrial standpoint, vary for each realization of the system (e.g. assembled car).

Experimental methods

From an industrial standpoint, the characterization of the materials involved in typical sound packages can be an important issue, also because mechanical and acoustic properties may be modified when the noise control treatment is assembled. For this reason, it would be preferable to directly characterize the acoustic impedance of the assembled noise control treatment. In this context, an experimental PTF methodology has been proposed in Ref. [127]. In this approach, the two sides of the sound package are divided in patches whose self and transfer impedances are experimentally measured and coupled with the PTF models

of the structural and acoustic domains. However, the experimental characterization is not free of drawbacks. For instance, the patch size is limited by practical aspects, potentially preventing the convergence of the PTF (as a matter of fact, the effect of the sound package on the system might be filtered by a coarse discretization of the acoustically treated area). In addition, non local effects (i.e. transfer impedances) may be hard to measure due to dissipative effects, thus limiting the accuracy of the experimental methodology.

Hybrid methods

Ultimately, it may be argued that the most common methodology to account for noise control treatments in finite element analysis is by means of a boundary operator accounting for generalized stiffness, mass and damping added to the vibroacoustic system. On the one hand, the calculation of such operator by a full finite element model of the noise control treatment is, albeit accurate, computationally expensive, as already pointed out. On the other hand, extremely simplified impedance models (e.g. plane wave impedance) may be, although costless from a computational standpoint, inaccurate to describe the actual behavior of typical sound packages.

Consequently, a question arises on how noise control treatments can be accurately modeled while avoiding expensive finite element approaches as well as poor impedance models. Namely, while standard finite element models of main structure and acoustic enclosure are nowadays an industrial standard, different approaches must be devised for passive acoustic treatments. Thus, the following scientific question may be raised: what is the minimum amount of information (i.e. model complexity) that is needed to correctly capture the dynamic effects of an acoustic treatment while saving computational time and virtual prototyping efforts? An understanding of the physical behavior of such dissipative components is necessary to answer to this question.

A possible interpretation is proposed in Refs. [45, 46] and can be summarized as follows. In addition to short wavelengths and dissipation, noise control treatments are also characterized by variability of geometry, materials properties and mounting conditions (among layers and at the interface with the main structure) induced by industrial process. This argument suggests that the sound package may be effectively modeled as a structural fuzzy component. Thus, the treatment is simply characterized by a random impedance operator, whose parameters must be identified by experimental measurements and finite element analysis. However, although the "fuzzy acoustic trim" perfectly fits a statistical description and allows for system uncertainties to be accounted for in the context of a

robust design, it still oversimplifies the mathematical model of the impedance operator, which is essentially considered a stochastic one-dimensional spring-mass-damper system.

On the other hand, since the TMM has become an industrial standard in the design of sound insulating materials, there is a growing interest in embedding a simple analytical model of the sound package in vibroacoustic finite element analysis. Indeed, although the hypotheses of laterally unbounded and flat system cannot be met at low frequency for structural components or acoustic cavities, the short wavelengths and high damping involved in the acoustic trim suggest that the TMM could be successfully employed for such subsystems. The advantages of a hybrid Finite Element-Transfer Matrix Method (FE-TMM) are twofold. The most obvious one is again computational. Namely, the sound package is considered as an equivalent two-dimensional reacting surface, thus reducing the number of degrees of freedom with respect to a standard finite element modeling. Second, it provides a simple and automated (i.e. neither mesh nor measurements required) procedure to characterize the sound package impedance, thanks to the use of the well-established TMM. As a matter of fact, the latter advantage can be very important during the design process, when an optimal configuration of the acoustic treatmet is sought.

Only a few finite element-transfer matrix models have been proposed in the past. They may be classified as locally or non locally reacting models, depending on the assumed impedance model. When the sound package is assumed to behave as a locally reacting system, the transfer matrix between the two ends of the multilayer is used to calculate the acoustic impedances (i.e. pressure over normal velocity) seen by the main structure and the acoustic cavity. On the other hand, more sophisticated approaches are needed to account for non local behavior. Essentially, the impedances are considered a function of the space (or, equivalently, of the wavenumber) rather then a constant (like in locally reacting materials). Under these circumstances, the mathematical problem can be formulated in an integral form involving spatial convolutions of sources and Green functions. The latter are calculated in the wavenumber domain by means of the TMM. Due to the assumption inherent within the transfer matrix framework, the finite lateral extent of the sound package, which is assumed to be homogeneous and flat, is neglected. As a consequence, the non local surface impedance is approximated considering only the direct field contribution to the sound package response, thus neglecting the reflected field emanating from the lateral boundaries. Such apparently stringent assumption is justified, besides the softness of acoustic materials, by the fact that waves impinging onto the boundaries of the sound package quickly dies out after being reflected, because of dissipative phenom-

ena. Hence, one can argue that the effect of the reflected field is likely negligible and the dynamic response could be approximated only by the direct field contribution only.

In what follows the hybrid FE-TMM formulations available in the literature are briefly described.

- Tournour *et al.* [122] proposed a simple hybrid model wherein the acoustic treatment is accounted for in a locally reacting sense by the frequency dependent coefficients of the multilayer transfer matrix evaluated at a given couple (k_x, k_y). Typically, the analytical problem is solved for a normal plane wave excitation, i.e. $k_x = k_y = 0$, although an average over different angle of incidence (e.g. diffuse fields) can also be considered. An application of this methodology to an optimization problem can be found in Ref. [130]. Even though this hybrid model can achieve a drastic reduction of the computational burden, its main drawback resides in the choice of the locally reacting impedance value which is, generally speaking, hard to justify since typical sound packages do not exhibit a local behavior (the most obvious example is perhaps the case of spring-mass layups, usually employed in automotive applications). Nonetheless, it could be argued that the choice would be partially justified only under particular cases of external disturbances, such as plane waves.
- Shorter and Mueller [105] proposed a formulation in terms of self and mutual piston impedances to couple the finite element model of a structure with a transfer matrix model of the sound package radiating in a semi-infinite fluid medium. Consequently, this methodology can account for the non local behavior of acoustic treatments. The mathematical framework relies on a weak form of the integral equation (i.e. spatial convolution between external excitation and Green function) in the wavenumber domain. As a result the discrete piston impedances are directly calculated in the (k_x, k_y)-space by numerical integration of the analytical kernel (i.e. Green function). The approach follows the methodology proposed by Langley [63] to calculate the radiation impedance of a bare structure (i.e. without noise control treatment). The main advantage of introducing a set of shape functions (e.g. pistons) to approximate the displacement at the main structure-acoustic trim interface is computational, as it avoids the exact calculation of the inverse Fourier transform by filtering the integrand high wavenumber content and thus preventing from the numerical integration of highly oscillating functions.
- Courtois and Bertolini [26] developed a similar integral approach which relies instead on a standard finite element approximation of the integral equations. As a result, the Green functions in the physical domain must be retrieved from the transfer matrix calculations by means of the inverse Fourier transform. However, this methodology has

some drawbacks. In fact, for generic sound packages involving poroelastic materials (i) a slow convergence of the inverse Fourier transform is typically observed, leading to the integration of a highly oscillating function at high wavenumbers, and (ii) singularities may occur for some particular cases, leading to improper integrals to be evaluated. In addition, once the analytical kernels in the physical domain are known, further numerical integrations are required to calculate the finite element matrices, making this approach less appealing from a computational standpoint compared to a full wavenumber domain methodology.

It can be pointed out that, potentially, these hybrid FE-TMM formulations may be very efficient. Indeed, the sound package is entirely characterized by analytical kernels which can be quickly evaluated at each frequency employing the TMM. Moreover, a three-dimensional model of the sound package is no longer needed, saving time and resources during the preprocessing phase. On the other hand, the methodology assumes the noise control treatment to be homogeneous, flat and of infinite lateral extent.

However, the open literature on the accuracy and limitations of these hybrid methodologies is lacking. Indeed, in the few works briefly described above, a comprehensive theoretical background for the sound package model is not provided. Moreover, the generic properties of such hybrid FE-TMMs (i.e. domain of validity of the approximation, accuracy and computational efficiency with respect to well-established finite element based substructuring procedures) can hardly be inferred. In particular, the effect of the infinite lateral extent assumption, inherent in the TMM, is completely ignored.

1.4 Motivations and objectives

Numerical tools are necessary to optimize and validate the design of industrial products (e.g. cars, aircraft, trains etc...). However, as discussed in section 1.3, the modeling of vibroacoustic systems is definitely not trivial. Namely, multiphysics (i.e. structural, acoustic and poroelastic domains interact with each other) and broadband frequency analysis (the frequency of interest can run from few Hz to several KHz) make the development of practical numerical tools quite challenging. As the literature review conveys, tradeoffs (i) between accuracy and computational efficiency, and (ii) between flexibility and ease of use, are the major key to a successfull modeling tool.

This work is mainly concerned with the low frequency modeling. In such frequency range (e.g. up to 1 KHz for typical automotive applications) conventional finite element models of the primary subsystems (i.e. main structure and acoustic cavities) constitute a well-

established industrial standard. However, such methodology is not totally justified to model passive noise control treatments, mainly due to practical reasons (among all, complexity of typical sound packages and poor computational efficiency of the resulting model). On the other hand, arbitrary complex sound packages can be easily and efficiently modeled (under some specific assumptions) by analytical methods (e.g. TMM). This context seems then to suggest the development of a hybrid framework combining (i) the accuracy and flexibility of the FEM and (ii) the efficiency and ease of use of the TMM. These two modeling tools are widely used and typically accessible in commercial and open source softwares.

This work aims at developing a hybrid finite element-transfer matrix framework to tackle the modeling of noise control treatments attached onto a main structure and radiating in a bounded or unbounded acoustic domain. Because of the simplifications inherent within the analytical model of the sound package, the behavior of the hybrid model must be carefully studied. As a matter of fact, the feasibility and potentiality of this hybrid methodology must be still fully assessed, as confirmed by the only few works available in the literature. This is therefore the ultimate objective of this work. The latter can be summarized in the following three tasks.

- Define the best strategy in terms of accuracy/efficiency tradeoff to integrate a transfer matrix model of the noise control treatment in a finite element model of the vibroacoustic system.
- Provide a comprehensive assessment (i.e. domain of validity) of the hybrid methodology by considering different configurations and materials typically employed in practical applications.
- Compare the accuracy and computational efficiency of the developed model with established industrial standards, namely the FEM (accuracy standard) and locally reacting impedance models.

The present work is concerned with the assessment of the main assumption behind the hybrid finite element-transfer matrix methodology, that is the infinite lateral extent of the noise control treatment. The effects of the other assumptions inherent within the use of the TMM (i.e. homogeneous and flat configurations) are instead not studied in this thesis, because considered as a further step in the assessment of the hybrid model. Under this circumstances, the main outcome of this research is expected to be a critic overview of the proposed hybrid FE-TMM and guidelines for its proper use.

1.5 Outline

The thesis is organized in seven chapters. The main contributions of this work are contained in four scientific papers. Chapters 2-3 gather early work, whose main contributions are (i) the comprehensive presentation of the theoretical background behind the hybrid FE-TMM and (ii) the preliminary assessment of its performance. In chapter 2, the main theoretical part of this work is developed. This chapter consists of a scientific paper published in the *Journal of Acoustical Society of America*, where a first application of the hybrid methodology to the noise radiation of structures with attached acoustic treatments is considered. Chapter 3 extends the formulation to plate-cavity systems. This analysis is presented in the form of a scientific paper submitted to the *Journal of Acoustical Society of America*.

Chapters 4-5 gather recent work, whose main contribution is the development of an enhanced formulation of the hybrid FE-TMM. In particular, chapter 4 introduces the new framework, studying the effect of different mathematical formulations. A better understanding of the hybrid FE-TMM strengths and limitations is achieved within this chapter. Its importance within the thesis is thus primary, as it collects the conclusions of chapters 2-3 (perhaps reinterpreted more consciously) while proposing further insight into the behavior of the proposed hybrid model. The content of chapter 4 is presented in the form of a scientific paper, which is yet to be submitted. The latter is conceived as the Part I of a two-parts paper, whose Part II is instead the content of chapter 5. Therein, a simple correction is proposed to retrieve some of the accuracy that is inherently lost when the finite lateral extension of the acoustic treatment is neglected.

Next, chapter 6 presents results concerning the application of the hybrid modeling strategy to the radiation of structures into unbounded fluid domains. Indeed, this class of problems requires a careful analysis since the numerical approximation become even more burdensome due to the presence of the unbounded fluid. To this purpose, different hybrid strategies based on the models presented throughout chapters 2-5 are discussed. Furthermore, their performance are compared for the case of a simplified automotive configuration. Finally, chapter 7 summarizes the main conclusions of this work and its and perspectives.

CHAPTER 2

THEORETICAL FRAMEWORK OF THE HYBRID FE-TMM AND APPLICATION TO TRANSMISSION PROBLEMS

In this chapter the theoretical framework of the hybrid FE-TMM proposed in this thesis is presented. Namely, the integral formulation employed to model the acoustic treatment is introduced as well as its numerical approximation. The hypotheses inherent within the mathematical framework are presented and discussed. The methodology is then employed to predict the noise radiation of a vibrating structure with an attached noise control treatment. This chapter mainly refers to the paper published on the *Journal of Acoustical Society of America* (Ref. [1]). However, the contents of the original paper have been slightly altered in order to include the analysis published on a later erratum (Ref. [2]). Moreover, a final section (i.e. section 2.8) has been added to integrate the paper in the context of the thesis.

Auteurs et affliation:

L. Alimonti: Étudiant au doctorat, Université de Sherbrooke, Faculté de Génie, Department de génie mécanique

N. Atalla: Professeur, Université de Sherbrooke, Faculté de Génie, Department de génie mécanique

A. Berry: Professeur, Université de Sherbrooke, Faculté de Génie, Department de génie mécanique

F. Sgard: Chercheur chez Institut de recherche Robert-Sauvé en santé et en sécurité du travail (IRSST)

Date d'acception: 2 avril 2014

État de l'acceptation: publiée

Revue: Journal of Acoustical Society of America (JASA)

Référence: [1]

Titre français: Évaluation d'un modéle hybride éléments finis - matrice de transfert pour les structures planes avec traitements acoustiques homogénes

Contribution au document: Dans ce article, le cadre théorique de le modéle hybride éléments finis - matrice de transfert est présentée. La méthodologie est ensuite util-

isée pour prédire la radiation de bruit de une structure vibrante avec un traitement acoustique.

Résumé français: La modélisation de systèmes vibroacoustiques complexes, y compris les matériaux poroélastiques, par des méthodes fondées sur des éléments finis peut être impraticable pour des applications pratiques. Pour cette raison, les méthodes analytiques telles que la méthode de matrice de transfert sont souvent préférées afin d'obtenir une estimation sommaire des paramètres vibroacoustiques. Cependant, les hypothèses fortes et inhérentes à la méthode de matrice de transfert conduisent à un manque de précision dans la description de la géométrie du système. En conséquence, la méthode de matrice de transfert est intrinsèquement limitée à la plage de haute fréquence. Aujourd'hui, les procédures de structuration hybrides sont devenues très populaires. En effet, les différentes techniques de modélisation sont généralement recherchées à décrire les systèmes vibroacoustiques complexes sur la plus large gamme de fréquences possible. Par conséquent, la souplesse et la précision de la méthode des éléments finis et l'efficacité de la méthode de matrice de transfert peuvent être couplés au sein d'une technique hybride pour obtenir une réduction de la charge de calcul. Dans ce travail, une méthode hybride est proposée. Les performances de la méthode pour prédire les indicateurs vibroacoustiques des structures planes avec des traitements acoustiques homogènes attachés sont évaluées. Les résultats démontrent que, sous certaines conditions, le modèle hybride permet une réduction de l'effort de calcul tout en conservant une précision suffisante par rapport à la solution complète des éléments finis.

Note: -

2.1 Abstract

Modeling complex vibroacoustic systems including poroelastic materials using finite element based methods can be unfeasible for practical applications. For this reason, analytical approaches such as the transfer matrix method are often preferred to obtain a quick estimation of the vibroacoustic parameters. However, the strong assumptions inherent within the transfer matrix method lead to a lack of accuracy in the description of the geometry of the system. As a result, the transfer matrix method is inherently limited to the high frequency range. Nowadays, hybrid substructuring procedures have become quite popular. Indeed, different modeling techniques are typically sought to describe complex vibroacoustic systems over the widest possible frequency range. As a result, the flexibility and accuracy of the finite element method and the efficiency of the transfer matrix method could be coupled in a hybrid technique to obtain a reduction of the computational

burden. In this work a hybrid methodology is proposed. The performances of the method in predicting the vibroacoustic indicators of flat structures with attached homogeneous acoustic treatments are assessed. The results prove that, under certain conditions, the hybrid model allows for a reduction of the computational effort while preserving enough accuracy with respect to the full finite element solution.

2.2 Introduction

Passive acoustic treatments used to control the noise level generated by vibrating systems typically involve dissipative materials assembled in a multilayer fashion. The acoustic treatment, also called sound package or acoustic trim, can be attached to a structure and be in contact with a fluid medium. One or more layers of these passive components usually contain poroelastic materials. Such materials consist of a solid and fluid phase. The coupling between these two phases causes dissipation by viscous and thermal effects while structural damping is provided by the frame. The Biot theory [13–15] accounts for these mechanisms and can be used as a reliable mathematical model [3]. Although it is possible to simplify the Biot model when the solid phase can be considered motionless or limp, for general multilayer systems and for a broad range of excitation frequencies both phases must be taken into account to obtain a good accuracy [84].

Even though the numerical approximation of vibroacoustic problems is still an open issue [100] and an optimal approach has not been devised yet, the Finite Element Method [10] (FEM) is typically used to model arbitrarily complex systems in the low and mid frequency range. However, when poroelastic materials are involved in passive treatments, using finite element based methodologies can be, even if accurate, computationally expensive. Indeed, a large number of degrees of freedom is necessary to describe the two phases of the porous material; for instance, the (u, p) formulation [5] of the Biot theory, albeit more efficient compared to other formulations (e.g. displacement based formulation [85]), still needs four unknowns per node. Furthermore, classical mesh criteria, i.e. six linear or four quadratic elements per wavelength, do not provide a sufficient condition to get reliable results, due to the coupling between the two phases and because of the dissipation mechanisms [30]. Therefore, a large number of elements are always needed in order to capture the solution. Several attempts have been made to alleviate this drawback. On the one hand, much work has been devoted to improve the efficiency of the FEM. Hierarchical formulations of the elements [57, 94], simplified 2D models [19, 58], enrichment methods like the Partition of Unity FEM [20] (PUFEM) and model reduction techniques [32, 53, 95, 96] have been investigated. Still, these methods remain computationally expensive

and may introduce further mathematical issues. On the other hand, new approaches have been developed to avoid the difficulties arising from a full finite element discretization of the system. For instance, the Wave Based Method [36] (WBM) has been applied to poroelastic domains [35]. However, convergence issues due to bad conditioning of the final system may appear for domains of arbitrary shape, limiting the application of the WBM to simple configurations. Recently, a Discontinuous Galerkin Method (DGM) with plane wave interpolants has been proposed by Dazel and Gabard [34] and applied to 2D poroelastic domains. The approach has shown interesting properties, as an improved conditioning of the final system is achieved compared to other wave-based methodologies (e.g. WBM and PUFEM).

An alternative to these sophisticated numerical approaches relies in fast analytical methodologies. However, to solve analytically the coupled Partial Differential Equations (PDEs) which govern the vibroacoustic system, several assumptions must be introduced. Namely, the multilayer system is assumed homogeneous, flat and laterally unbounded. The system remains, instead, bounded in the thickness direction. Under these conditions, the Fourier Transform (FT) can be employed to move from the physical space (x, y) to the wavenumber domain (k_x, k_y). As a result, the boundary value problem can be reformulated as a set of Ordinary Differential Equations (ODEs) in terms of the thickness coordinate z. Given the set of interface conditions between different layers, the analytical solution for each traveling wave (k_x, k_y) can be found. In this context, the Transfer Matrix Method [3] (TMM) allows for a compact and general formulation leading to the solution of a small linear system. Once the solution in the wavenumber domain has been properly sampled, the Inverse Fourier Transform (IFT) can be employed to find the solution in the physical domain. This methodology can be used to construct the acoustic impedance of a multilayer system, as well as, from a more mathematical point of view, its Green function. Faverjon and Soize [44] considered this approach to find the acoustic impedance of a three-layer system consisting in a poroelastic layer sandwiched between two plates. The experimental set up considered to validate the analytical methodology exhibited a few discrepancies at low frequencies, because of finite size effects. Later on, Hassan [54] used the analytical approach to obtain the self and mutual piston impedances of a viscoelastic layer radiating in a semi-infinite fluid medium.

Overall, although it can be argued that such analytical approaches capture the physics of the system in the thickness direction, the assumption of unbounded layers is not justified at low frequency. However, it can be stated that finite size effects are mainly confined in the master systems, i.e. structures and cavities, whereas the acoustic treatment is less

affected by the presence of physical boundaries. Indeed, (i) the dissipation provided by poroelastic and viscous layers and (ii) the short waves propagating through these media suggest that the information regarding the geometry could be neglected. In this context, several approaches have been developed to couple a detailed description of the elastic and acoustic domains with a simple analytical model of the acoustic treatment. For instance, Rhazi and Atalla [92, 93] proposed a hybrid methodology to model flat rectangular plates with attached multilayer treatments. The displacement of the simply supported plate was described in terms of superposition of orthogonal trigonometric functions (i.e. Ritz method) while the effect of the multilayer treatment on each mode was approximated using the TMM. To model complex structures or cavities, attempts have been made to include a simplified model of the acoustic treatment in a finite element framework. As a first approximation, the acoustic treatment can be taken into account by its wall impedance [3, 86], which can be determined experimentally or calculated by means of analytical models such as the TMM. Since experimental approaches are not contemplated in the present work, only the latter methodology is herein considered. In this context, Tournour *et al.* [122] proposed a simple hybrid model wherein the acoustic treatment is accounted for in a locally reacting sense by the frequency dependent coefficients of the transfer matrix evaluated at a given couple (k_x, k_y). An application of this methodology to an optimization problem can be found in the work of Yamamoto *et al.* [130]. However, to account for complex sound packages, more accurate approaches based on integral formulations (i.e. Green function) are typically sought. For instance, the approach proposed by Shorter and Mueller [105] employs a formulation in terms of self and mutual piston impedances to couple the finite element model of a structure with a transfer matrix model of the sound package radiating in a semi-infinite fluid medium. On the other hand, the approach of Courtois and Bertolini [26] uses the IFT methodology to explicitly find the exact Green functions of the laterally unbounded acoustic treatment placed between a structure and a cavity. Finally, note that simplified models to account for sound packages in finite element analysis has also been proposed in a stochastic framework [45, 46].

Thus, it can be pointed out that, potentially, these hybrid Finite Element-Transfer Matrix Methods (FE-TMMs) may be very efficient from the computational point of view. Indeed, the sound package is entirely characterized by analytical kernels which can be evaluated quickly at each frequency employing the TMM. Moreover, a 3D model of the sound package is no longer needed, saving time and resources during the preprocessing phase. However, the open literature on the accuracy and limitations of these hybrid methodologies is lacking. Indeed, in the few works briefly described above [26, 105, 122], a complete theoretical background for the analytical model of the sound package is not provided. Moreover,

the assessment of the performances of the hybrid method is typically restricted to global vibroacoustic indicators (i.e. TL, quadratic velocity or pressure). This work wants to partially fill this gap by (i) providing a critical overview of the analytical modeling of flat and homogeneous multilayer systems by means of the Green function formalism, (ii) proposing an efficient methodology to use the analytical model of the multilayer acoustic trim in a finite element framework and (iii) assessing the validity of the hybrid model by a comprehensive analysis. In section 2.3 and 2.4 a hybrid methodology based on the Green function formalism is proposed. The approach differs from the one proposed by Courtois and Bertolini [26] by the fact that the sound package problem is entirely formulated in the wavenumber domain, avoiding the issues related to the direct computation of the Green function by IFT. On the other hand, the approach can be seen as a generalization of what was proposed by Shorter and Mueller [105]. The Green function formalism is introduced and discussed in section 2.3, giving an overview of the approaches proposed in other works and showing the advantages of the methodology suggested by the authors. Although the approach can be extended to couple the analytical model of the sound package with finite element domains of different nature (e.g. fluid and solid media), this work is restricted to the analysis of flat structural systems with an attached homogeneous acoustic treatment radiating in an unbounded fluid domain. Thus, in section 2.4, the substructuring approach to take into account the analytical model of the sound package into the finite element model of a generic structure is presented. In section 2.5, two analysis are performed to assess the accuracy of the hybrid methodology. First, the attention is focused on the dynamic response of the acoustic treatment alone. Then, a second analysis aims at assessing the accuracy of the assembled hybrid model for a treated structure excited by acoustic and mechanical disturbances. The results in terms of typical vibroacoustic indicators obtained by means of the FE-TMM are discussed and compared with the full finite element solution. However, as already mentioned above, such analysis is typically not sufficient (i) to provide a comprehensive understanding of the behavior of the hybrid model and (ii) to identify its strengths and limitations. Therefore, to provide such answers, further analysis are proposed.

2.3 Analytical formulation

In this section the Green function based formulation to model the response of generic multilayer systems is presented. The system is assumed flat and of infinite lateral extent (see Fig. 2.1). The two faces which define the finite thickness of the treatment are referred to as side A and B. The planar coordinates $\mathbf{x} = (x, y)$ define the position of each point

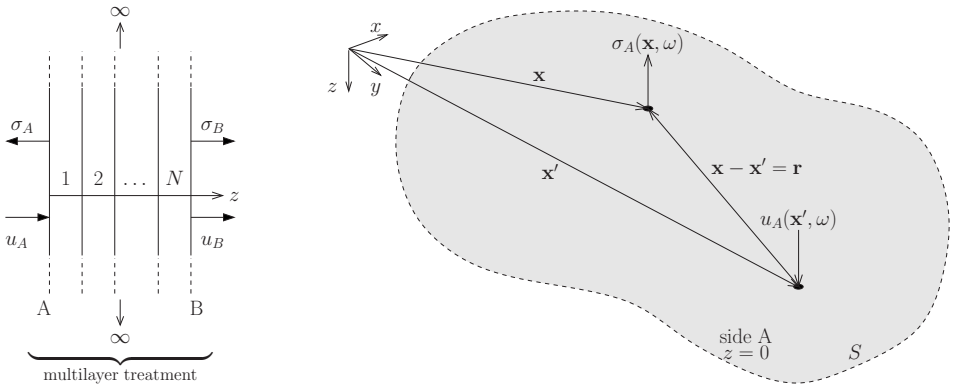

Figure 2.1 Geometry of the multilayer system. Through-the-thickness view of the treatment (left) and top view of the excited surface S on side A (right).

over these faces. The normal displacements at side A and B are denoted by u_A and u_B, respectively. Similarly, the normal stresses exerted on the two sides of the treatment are σ_A and σ_B, respectively. All the displacements and stresses are functions of the space variable $\mathbf{x}$ and of the circular frequency ω (i.e. the time dependency $e^{\imath\omega t}$ is implicitly assumed). Without loss of generality, let the normal stress σ_A be the output of the system when a displacement u_A is applied over a finite area S (see Fig. 2.1) and a set of boundary conditions are applied to side B (e.g. hard wall condition $u_B = 0$, pressure release condition $\sigma_B = 0$ or mixed condition $Z_B u_B + \sigma_B = 0$). In this context, assuming a homogeneous system with respect to the planar coordinates $\mathbf{x}$, the Green function formalism can be employed to write the solution as

$$\sigma_A(\mathbf{x}, \omega) = \int_S d(\mathbf{x} - \mathbf{x}', \omega) u_A(\mathbf{x}', \omega) \, \mathrm{d}\mathbf{x}' \,, \tag{2.1}$$

where $d(\mathbf{x} - \mathbf{x}', \omega)$ is the Green function of the problem. The domain S represents the support of the normal displacement u_A (i.e. side A of the multilayer is embedded into a rigid planar baffle). The distance vector pointing from $\mathbf{x}'$ to $\mathbf{x}$ is denoted by $\mathbf{r}$. It should be observed that, for a generic non-homogeneous system, the Green function depends on both the planar coordinates $\mathbf{x}$ and $\mathbf{x}'$, i.e. $d(\mathbf{x}, \mathbf{x}', \omega)$. Then, assuming a homogeneous system and boundary conditions over side B, the dependency from the absolute position over the planar surface can be removed, leading the Green function to be a function of the relative distance $\mathbf{r}$ only. Introducing some appropriate shape functions $\psi_j(\mathbf{x})$, the displacement can be expanded as

$$u_A(\mathbf{x}, \omega) = \psi_j(\mathbf{x}) \, a_j(\omega) \,, \tag{2.2}$$

where the sum over repeated index is implicitly assumed. The coefficient $a_j(\omega)$ is the participation factor of the j^{th} shape function $\psi_j(\mathbf{x})$. If the basis is such that $u_A(\mathbf{x}_j, \omega) = a_j(\omega)$, then $a_j(\omega)$ is the nodal displacement $U_{A_j}(\omega)$ (i.e. the basis has the Kronecker delta property, as the finite element shape functions). Otherwise, an interpolation scheme is sought to relate the coefficients $a_j(\omega)$ to the nodal values $U_{A_j}(\omega)$, like in intrinsic meshless methods [81]. Using Eq. 2.2 in Eq. 2.1, premultiplying by $\psi_i(\mathbf{x})$ and integrating over the surface S gives

$$\int_S \psi_i(\mathbf{x})\sigma_A(\mathbf{x},\omega)\,\mathrm{d}\mathbf{x} = \int_S \psi_i(\mathbf{x}) \int_S d(\mathbf{x}-\mathbf{x}',\omega)\psi_j(\mathbf{x}')\,\mathrm{d}\mathbf{x}'\,\mathrm{d}\mathbf{x}\,a_j(\omega)\,, \tag{2.3}$$

which is the projection of Eq. 2.1 onto the finite dimensional space spanned by the selected shape functions.

2.3.1 Formulation in the wavenumber domain

Let $f(\mathbf{x})$ be a function of the 2D space. Its FT and IFT are defined as

$$\hat{f}(\mathbf{k}) = \int_{\mathbf{x}} f(\mathbf{x}) e^{-\imath\,\mathbf{k}\cdot\mathbf{x}}\,\mathrm{d}\mathbf{x} \tag{2.4}$$

$$f(\mathbf{x}) = \frac{1}{(2\pi)^2}\int_{\mathbf{k}} \hat{f}(\mathbf{k}) e^{\imath\,\mathbf{k}\cdot\mathbf{x}}\,\mathrm{d}\mathbf{k}\,, \tag{2.5}$$

where $\mathbf{k} = (k_x, k_y)$ denotes the wavenumber domain coordinates and $\imath$ is the complex unit. The direct application of the IFT formula to the Green function leads to

$$d(\mathbf{r},\omega) = \frac{1}{(2\pi)^2}\int_{\mathbf{k}} \hat{d}(\mathbf{k},\omega) e^{\imath\,\mathbf{k}\cdot\mathbf{r}}\,\mathrm{d}\mathbf{k}\,. \tag{2.6}$$

Assuming an isotropic system with respect to the planar coordinates $\mathbf{x}$, the Green function becomes a function of the distance only, i.e. $d(|\mathbf{r}|,\omega) = d(r,\omega)$. In this case, the IFT in Eq. 2.6 can be expressed in polar coordinates (k,ϕ) yielding to the following one-dimensional integral

$$d(r,\omega) = \frac{1}{2\pi}\int_0^\infty \hat{d}(k,\omega) J_0(kr) k\,\mathrm{d}k\,, \tag{2.7}$$

where $k = |\mathbf{k}|$ is the modulus of the wavenumber and $J_0(kr)$ is the Bessel function of zero order of argument kr. Eq. 2.7 gives the Green function relating displacement and stress for a given distance r over side A in terms of an infinite sum of wavenumber contributions. The fundamental kernel $\hat{d}(k,\omega)$ can be computed by simple analytical approaches, such as the TMM. Therefore, one can be tempted to find back the Green function $d(r,\omega)$ of a given multilayer by applying Eq. 2.7. This methodology was considered by Faverjon and Soize [44] to find the Green function of a multilayer consisting of a poroelastic layer sandwiched between two thin plates. However, it has some drawbacks. In fact, for generic sound packages involving poroelastic materials (i) a slow convergence of the integral in Eq. 2.7 is typically observed, leading to the integration of a highly oscillating function at high wavenumbers, and (ii) singularities may occur for some particular cases at $r = 0$, leading to improper integrals to be evaluated (i.e. $\hat{d}(k,\omega)$ might be unbounded as $k \to \infty$).

As a consequence, a more efficient procedure should be used in order to overcome the aforementioned issues. Thus, employing the convolution theorem, with further manipulations, Eq. 2.3 can be rewritten as

$$\int_S \psi_i(\mathbf{x})\sigma_A(\mathbf{x},\omega)\,\mathrm{d}\mathbf{x} = \frac{1}{(2\pi)^2}\int_{\mathbf{k}} \hat{\psi}_i^*(\mathbf{k})\hat{d}(\mathbf{k},\omega)\hat{\psi}_j(\mathbf{k})\,\mathrm{d}\mathbf{k}\,a_j(\omega)\,, \tag{2.8}$$

where it has been assumed that the displacement $u_A(\mathbf{x},\omega)$ is zero outside the surface S. This assumption allows to interpret the region S as the infinite plane at $z = 0$, so that the FT formulas can be employed. The superscript * indicates the conjugate of a complex number. Let the basis of the approximation space be spanned by generic radially symmetric functions obtained by translation and associated to a set of collocation points $\mathbf{x}_i$, i.e.

$$\psi_i(\mathbf{x}) = \psi(|\mathbf{x} - \mathbf{x}_i|) = \psi_i(r)\,. \tag{2.9}$$

Its FT reads

$$\hat{\psi}_i(\mathbf{k}) = \hat{\psi}(k)\,e^{-\imath\,\mathbf{k}\cdot\mathbf{x}_i}\,, \tag{2.10}$$

where

$$\hat{\psi}(k) = 2\pi\int_0^R \psi(r)J_0(kr)r\,\mathrm{d}r\,. \tag{2.11}$$

In Eq. 2.11 it has been implicitly assumed that the function $\psi(r)$ has a compact support of radius R. Using Eq. 2.10 in Eq. 2.8 gives:

$$\begin{aligned} R_{A_i}(\omega) &= \int_S \psi_i(r)\sigma_A(\mathbf{x},\omega)\,\mathrm{d}\mathbf{x} = \\ &= \left[\frac{1}{2\pi}\int_0^\infty \hat{d}(k,\omega)J_0(kr)k|\hat{\psi}(k)|^2\,\mathrm{d}k\right] a_j(\omega) = D_{AA}(r,\omega)\,a_j(\omega)\,, \end{aligned} \tag{2.12}$$

where R_{A_i} is the normal stress projected onto the i^{th} degree of freedom and $D_{AA}(r,\omega)$ is the discrete Green function based dynamic stiffness seen from side A of the flat and laterally infinite multilayer system. Finally, $r = |\mathbf{r}|$ is the distance between the j^{th} and i^{th} nodes. The definition of the discrete Green function $D_{AA}(r,\omega)$ in Eq. 2.12 differs from the analytical function $d(r,\omega)$ in Eq. 2.7 by the presence of the term $|\psi(k)|^2$, which acts as a filter on the system, cutting off the waves propagating above a certain wavenumber. As a consequence, this choice would circumvent the issues related to the integration of Eq. 2.7. On the other hand, Eq. 2.12 allows for the direct calculation of the projected (i.e. filtered) Green function $D_{AA}(r,\omega)$ (dimensionally a force, in the considered case), which differs from the analytical function $d(r,\omega)$ (dimensionally a stress). It is finally noted that the procedure showed above is general, as different projected Green functions can be defined employing the desired input and output in Eq. 2.1.

2.3.2 Type of radially symmetric functions

Different types of shape functions $\psi(r)$ have been used in the literature. The use of cylindrical pistons has been investigated by Hassan [54] and by Shorter and Mueller [105]. However, the resulting filter may not be effective because of the high frequency content related to the presence of a sharp edge at $r = R$. To avoid this issue a linear transition region can be added, avoiding the discontinuity [54]. It is worth noting that, although the finite aperture of the shape functions is able to filter the high wavenumber content of the integral in Eq. 2.12, the convergence may still be problematic, since the cut-off wavenumber generally depends on the considered system. To overcome this issue, Langley [63] proposed the use of the jinc function ($\text{jinc}(x) = \frac{J_1(x)}{x}$, where $J_1(x)$ is the Bessel function of first order of argument x). Such wavelet functions have the advantage to avoid sharp edges and having a band-limited FT, removing the convergence issue. However, the definition of the mapping between the amplitude of the wavelet (i.e. a_j) and the related physical variable (i.e. U_{A_j}) is not straightforward for arbitrary geometries.

In the present work, the authors investigate the performance of linear functions, i.e.

$$\psi(r) = \begin{cases} 1 - \dfrac{r}{R} & \text{if } r \leq R \\ 0 & \text{if } r > R \end{cases}, \tag{2.13}$$

with FT

$$\hat{\psi}(k) = 2\pi R^2 \text{jinc}(kR) - \frac{2\pi}{R} \int_0^R r^2 J_0(kr)\, \mathrm{d}r\,, \tag{2.14}$$

Eq. 2.13 provides a more effective filter compared to the cylindrical pistons. Moreover, it allows to mimic the effect of classical finite element linear functions. Thus, in the present work, the collocation points $\mathbf{x}_i$ on the treated surface are associated to a structured FE mesh which involves elements of the same size. Each nodal displacement defined on the FE mesh is then approximated by Eq. 2.13. In this context, the compact support R of the radial linear basis functions (Eq. 2.13) is chosen such that

$$\int_S N_i(\mathbf{x})\, \mathrm{d}\mathbf{x} = \int_S \psi(\mathbf{x} - \mathbf{x}_i)\, \mathrm{d}\mathbf{x}\,, \tag{2.15}$$

where $N_i(\mathbf{x})$ and $\psi(\mathbf{x} - \mathbf{x}_i)$ are the finite element and radially symmetric shape functions associated to the same i^{th} node. Consequently, in analogy with the finite element shape functions, the coefficients a_j are assumed to be the normal displacements U_{A_j} associated to each collocation point (i.e. node) of the meshed surface S, so that Eq. 2.12 can be rewritten as

$$R_{A_i}(\omega) = D_{AA}(r, \omega)\, U_{A_j}(\omega)\,, \tag{2.16}$$

where $D_{AA}(r, \omega)$ is then the approximated boundary dynamic stiffness of the acoustic treatment seen from side A for a given distance r between two nodes belonging to the finite element mesh of the treated surface S.

2.4 Hybrid finite element-transfer matrix model

Let the acoustic treatment be attached onto a structure over side A. The following approximations are introduced to employ the analytical tool: the acoustic treatment is assumed (i) isotropic and (ii) homogeneous in the plane (i.e. thickness, lay-up and material properties do not change over the surface S), (iii) flat (unwrapped if any curvature is present) and (iv) of infinite extent (lateral mounting conditions are neglected). Under these assumptions, the surface S defines the treated interface between the structural domain and the sound package. By a classical finite element approximation, the linear system describing the dynamic of the master subsystem (i.e. elastic solid) is

$$\mathbf{K}(\omega)\mathbf{U}^s(\omega) = \begin{bmatrix} \mathbf{K}_{AA}(\omega) & \mathbf{K}_{Ai}(\omega) \\ \mathbf{K}_{Ai}^{\mathrm{T}}(\omega) & \mathbf{K}_{ii}(\omega) \end{bmatrix} \begin{Bmatrix} \mathbf{U}_A^s(\omega) \\ \mathbf{U}_i^s(\omega) \end{Bmatrix} = \begin{Bmatrix} \mathbf{R}_s(\omega) \\ \mathbf{0} \end{Bmatrix} + \mathbf{F}(\omega)\,, \tag{2.17}$$

where the following partition of the master degrees of freedom has been assumed

$$\mathbf{U}^s(\omega) = \begin{Bmatrix} \mathbf{U}_A^s(\omega) \\ \mathbf{U}_i^s(\omega) \end{Bmatrix}. \tag{2.18}$$

The vector $\mathbf{U}^s$ contains the structural degrees of freedom, also called master degrees of freedom. The vector $\mathbf{U}_A^s$ contains the nodal normal displacements over the treated surface S, while $\mathbf{U}_i^s$ refers to the internal degrees of freedom. Matrix $\mathbf{K}$ is the dynamic stiffness of the structure. $\mathbf{F}$ is the external load vector (i.e. the disturbance). $\mathbf{R}_s$ gather the interface normal forces due to the presence of the acoustic treatment. A relation between the latter forces and the master degrees of freedom $\mathbf{U}_A^s$ is sought to account for the effect of the sound package into the finite element model (Eq. 2.17). In what follows it will be shown how to retrieve this relation using an analytical model of the sound package alone. Namely, the Green function approach as presented in section 2.3 and the simplified locally reacting approach [122] will be used to build the hybrid finite element-transfer matrix model.

2.4.1 Green function based FE-TMM

Given a set of nodes over the treated surface S, Eq. 2.16 can be rearranged in matrix form, yielding

$$\mathbf{R}_A(\omega) = \mathbf{D}_{AA}(\omega)\mathbf{U}_A(\omega)\,, \tag{2.19}$$

which gives, for a given boundary condition over side B, the interface forces $\mathbf{R}_A$ due to the displacements $\mathbf{U}_A$ imposed over side A of the treatment attached onto the structure. Assuming that the collocation points of the Green function formulation (Eq. 2.19) coincide with the finite element nodes of the structural domain, continuity conditions on the displacements and interface forces can be easily imposed. Thus, Eq. 2.19 can be assembled into the finite element system in Eq. 2.17, leading to the following hybrid model

$$\left[\begin{array}{cc} \mathbf{K}_{AA}(\omega) - \mathbf{D}_{AA}(\omega) & \mathbf{K}_{Ai} \\ \mathbf{K}_{Ai}^{\mathrm{T}}(\omega) & \mathbf{K}_{ii}(\omega) \end{array} \right] \left\{ \begin{array}{c} \mathbf{U}_A^s(\omega) \\ \mathbf{U}_i^s(\omega) \end{array} \right\} = \mathbf{F}(\omega)\,, \tag{2.20}$$

where $\mathbf{D}_{AA}(\omega)$ can be interpreted as an added dynamic stiffness accounting for the presence of the acoustic treatment. The efficiency of the assembled hybrid model in Eq. 2.20 can be improved by projection onto the structural modal basis. It is worth noting that the effect of an external fluid in contact with the sound package over side B is taken into account in matrix $\mathbf{D}_{AA}(\omega)$, avoiding expensive boundary element formulations. However, this methodology replaces the exact finite size radiation impedance seen by side B of the laterally bounded sound package by a simple plane wave impedance, i.e. imposing $p_B(k,\omega) = \imath\omega \frac{\rho_0 c_0 k_0}{\sqrt{k_0^2 - k^2}} u_B(k,\omega)$ in the TMM when solving for $\hat{d}(k,\omega)$ with ρ_0 and c_0 the density and speed of sound in the unbounded fluid and $k_0 = \frac{\omega}{c_0}$ the acoustic wavenumber in the medium (see appendix A). On the other hand, when the fluid loading is neglected, the pressure release condition $p_B(k,\omega) = 0$ is imposed in the TMM to calculate $\hat{d}(k,\omega)$. In any case, once the system in Eq. 2.20 has been solved, the power radiated Π_{rad} can be evaluated as

$$\begin{aligned} \Pi_{\mathrm{rad}} &= \frac{\omega^2}{2\,(2\pi)^2} \int_{\mathbf{k}} \hat{u}_A^*(\mathbf{k},\omega)\, \mathrm{Re}\big\{ \hat{Z}_\infty(k,\omega) \big\} |\hat{d}_{A\to B}(k,\omega)|^2\, \hat{u}_A(\mathbf{k},\omega)\, \mathrm{d}\mathbf{k} = \\ &= \frac{\omega^2}{2} U_{A_i}^{s^*}(\omega)\, Z_{ij}^{\mathrm{rad}}(\omega) U_{A_j}^s(\omega)\,, \end{aligned} \tag{2.21}$$

where $\hat{Z}_\infty(k,\omega) = \frac{\rho_0 c_0 k_0}{\sqrt{k_0^2 - k^2}}$ is the plane wave radiation impedance and $\hat{d}_{A\to B}(k,\omega)$ is the coupling Green function, i.e. the displacement at side B due to an imposed displacement at side A. Again, $\hat{d}_{A\to B}(k,\omega)$ is evaluated by means of the TMM and can account for the effect of an external fluid at side B (see appendix A), as explained above. Eq. 2.21 can be reduced to a one-dimensional integral as it has been shown in section 2.3 for Eq. 2.12. The matrix Z_{ij}^{rad} is the effective radiation impedance seen by the structure.

2.4.2 Locally reacting FE-TMM

If the sound package is assumed to have a locally reacting behavior, the Green function is approximated by a function independent of the wavenumber k, i.e. $\hat{d}(k,\omega) = \hat{d}_0(\omega)$. As a result, all the waves are guided through the thickness of the treatment according to $\hat{d}_0(\omega)$, irrespective of the particular wavelength. Thus, Eqs. 2.12 can be rewritten in the physical domain, as the wave domain representation of the Right Hand Side (RHS) integral is no more justified. A classical finite element approximation can be used instead, yielding to the following hybrid model

$$\begin{bmatrix} \mathbf{K}_{AA}(\omega) - \hat{d}_0(\omega)\mathbf{C}_{AA} & \mathbf{K}_{Ai}(\omega) \\ \mathbf{K}_{Ai}^{\mathrm{T}}(\omega) & \mathbf{K}_{ii}(\omega) \end{bmatrix} \begin{Bmatrix} \mathbf{U}_A^s(\omega) \\ \mathbf{U}_i^s(\omega) \end{Bmatrix} = \mathbf{F}(\omega)\,, \tag{2.22}$$

where $\mathbf{C}_{AA}$ is the structural normal displacements self-coupling term. The computational efficiency of such approximation is evident: the effect of the acoustic treatment is described by a simple and frequency independent geometrical coupling term (i.e. $\mathbf{C}_{AA}$) involving products of the finite element shape functions over the surface S. However, the choice of the local kernel $\hat{d}_0(\omega)$ is, generally speaking, hard to justify. It could be argued that the choice would be partially justified only for the case of external disturbances which force a given wavenumber on the system (e.g. plane wave). In what follows, the local kernel is chosen as $\hat{d}(k_t,\omega)$ in the case of a plane wave excitation (k_t is the forced trace wavenumber on the structural excited plane) and $\hat{d}(0,\omega)$ in case of a mechanical excitation (e.g. point force).

As explained in section 2.4.1, the effect of the fluid loading can be either considered or neglected in the computation of the locally reacting Green function $\hat{d}_0(\omega)$. Then, in the postprocessing phase, the power Π_{rad} radiated by the sound package can be evaluated using the locally reacting kernel $\hat{d}_{A\to B_0}(\omega)$ in Eq. 2.21, yielding

$$\begin{aligned} \Pi_{\mathrm{rad}} &= |\hat{d}_{A\to B_0}(\omega)|^2 \frac{\omega^2}{2\,(2\pi)^2} \int_{\mathbf{k}} \hat{u}_A^*(\mathbf{k},\omega)\,\mathrm{Re}\big\{\hat{Z}_\infty(k,\omega)\big\}\,\hat{u}_A(\mathbf{k},\omega)\,\mathrm{d}\mathbf{k} = \\ &= |\hat{d}_{A\to B_0}(\omega)|^2 \frac{\omega^2}{2} U_{A_i}^{s^*}(\omega)\, Z^{\mathrm{rad}}_{\mathrm{bare}_{ij}}(\omega) U^s_{A_j}(\omega)\,, \end{aligned} \tag{2.23}$$

where $Z^{\mathrm{rad}}_{\mathrm{bare}_{ij}}$ is the radiation impedance of the bare structure. Therefore, the locally reacting approximation is employed (i) to find $U^s_{A_j}$ by solving Eq. 2.22 and (ii) to evaluate the displacement at side B of the acoustic treatment using $\hat{d}_{A\to B_0}(\omega)$. Then, the power

radiated by the resulting velocity profile is exactly evaluated (Eq. 2.23), as far as the case of a flat surface S is concerned.

2.5 Results

In this section the performance of the Green function based FE-TMM presented in section 2.3 and 2.4 is assessed. For this purpose, two different analysis are proposed. First, the added dynamic stiffness $\mathbf{D}_{AA}(\omega)$ approximated by the analytical method (Eq. 2.19) is compared with the exact calculation obtained by a finite element model of the sound package alone. This analysis is restricted to the acoustic treatment only, as the master structure is not involved in the calculations. Next, an academic benchmark consisting in a rectangular plate treated by two different sound packages and excited by an acoustical or a mechanical source is considered to assess the accuracy of the hybrid methodology. Notably, the Green function based FE-TMM is compared with the locally reacting FE-TMM and with the FEM. The latter is considered as the reference model. Only flat systems will be treated in the present analysis, as the effect of the curvature of the trimmed area is beyond the scope of this paper.

It is noted in passing that in all the following cases, a thin air gap was placed at the first layer of the treatment (e.g. between the master structure and a poroelastic layer) in order to only take into account continuity of normal components over the treated surface S, so that a meaningful comparison with the full finite element model can be established. However, the hybrid methodology is not limited to such configurations, as the model described in section 2.4 allows to handle generic layups as long as only the continuity of normal displacement and stress is assumed at the interface with the solid. For instance, if a solid phase domain (e.g. poroelastic or solid layer) is placed at the first layer of the treatment (i.e. side A), the stress component lying on the surface S (i.e. shear component) must be forced to zero in order to be able to solve the transfer matrix problem to obtain the desired Green function. In other words, the state vector of the transfer matrix model of the treatment at side A has to be reduced to normal components only (see appendix A).

2.5.1 Assessment of the analytical model

This case involves a three-layers acoustic treatment of planar dimensions $0.8 \times 1.7\,\mathrm{m}^2$ consisting, from side A, of a 1 mm air gap, a 2 cm poroelastic foam and a $1.2\,\mathrm{kg/m}^2$ heavy layer (see Tab. 2.1 for the material properties). The latter was modeled as a 1 mm thick

limp solid layer with Young's modulus 1 MPa, Poisson's ratio 0.3 and zero loss factor. A pressure release condition is applied over side B of the sound package. The finite element model of the acoustic treatment involves a mesh of 30×60 elements in the (x, y) plane while one, three and one Hexa-8 fluid, poroelastic and solid elements are used along the thickness direction. The finite element model is assumed to slide along its lateral boundaries.

The generic component (i, j) of matrix $\mathbf{D}_{AA}(\omega)$ comes from the integration in the wavenumber domain of the kernel $\hat{d}(k, \omega)$ for a given distance r between the i^{th} and j^{th} nodes (see Eq. 2.16). The same component can be obtained by means of the finite element model of the acoustic treatment described above. Figs. 2.2 and 2.3 show one element of matrix $\mathbf{D}_{AA}(\omega)$ related to a nodes pair located approximately at the middle of the treated area S, far from the boundaries. The figures show an extra-diagonal term (i.e. $r = 0.1983\,\text{m}$) for the case of a poroelastic (i.e. Biot) and limp model of the foam, respectively. Concerning the Biot model (see Fig. 2.2), some discrepancies between the analytical model and the FEM are observed around 800 Hz, where a peak controlled by the shear waves in the poroelastic layer appears. Indeed, generally speaking, it has been found that the effect of structural borne thickness resonances, such as the shear waves controlled peak in Fig. 2.2, is typically underestimated by the analytical model. Therefore, larger dimensions are required for the finite size system to converge to the analytical solution of the laterally unbounded treatment. The same analysis was also performed employing a limp model of the foam (see Fig. 2.3). In this case the shear waves are neglected (i.e. the elasticity of the solid phase is not accounted for) and an almost perfect correlation between the analytical and finite element models is observed. Moreover, Figs. 2.2 and 2.3 show that no important size effects are shown around the thickness resonance of the acoustic treatment at 300 Hz.

Overall, it can be pointed out that, for the considered system, the analytical solution for the infinite system appears to approximate adequately the behavior of the actual bounded system even at low frequency. However, it should appear clear that, as the nodes pair (i, j) gets closer to the boundaries, more discrepancies between the analytical model and the FEM are expected due to the effect of the reflected field. As a result, although the present analysis can provide qualitative observations, it does not allow to fully assess the global accuracy of the analytical model of the sound package. Thus, in order to do so, a different analysis will be presented in the next section.

2.5.2 Assessment of the FE-TMM

The second analysis involves a 2 mm thick steel plate with an attached acoustic treatment. Two different layups are considered for the sound package. Namely, a two-layers treatment

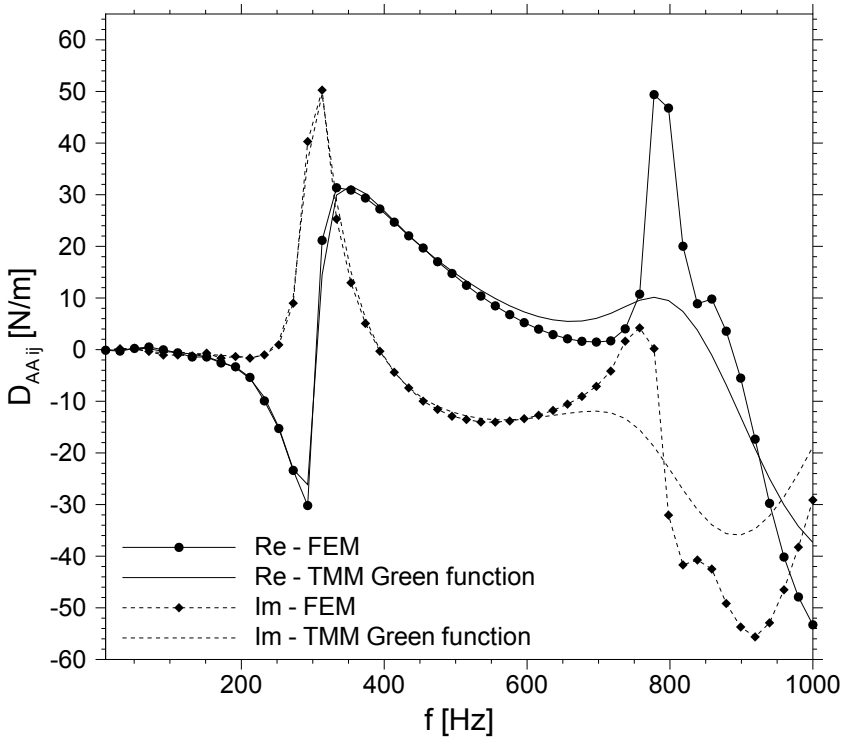

Figure 2.2 Extra-diagonal term of the discrete Green function $D_{AA_{ij}}$ (dynamic stiffness). Real (Re) and imaginary (Im) parts. The distance between the two nodes is $r = 0.1983\,\mathrm{m}$. The FEM solution refers to a nodes pair (i, j) placed approximately at the middle of the treated surface S. Solution according to the Biot model of the foam.

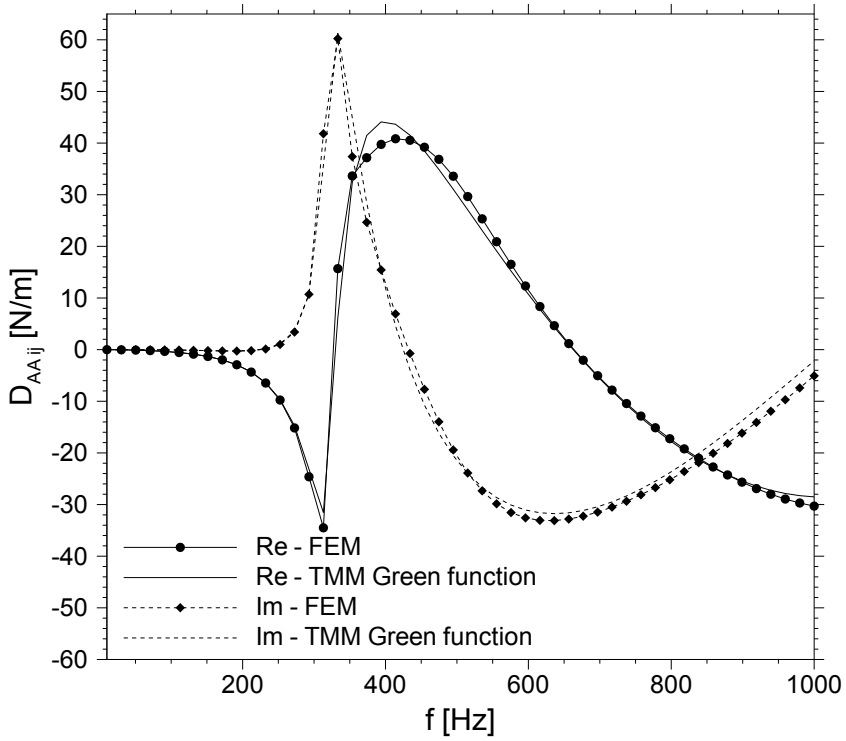

Figure 2.3 Extra-diagonal term of the discrete Green function $D_{AA_{ij}}$ (dynamic stiffness). Real (Re) and imaginary (Im) parts. The distance between the two nodes is $r = 0.1983\,\mathrm{m}$. The FEM solution refers to a nodes pair (i, j) placed approximately at the middle of the treated surface S. Solution according to the limp model of the foam.

Table 2.1 Materials used in the numerical simulations.

Material	**Properties**	
	Acoustic	**Mechanical**
Steel plate		density = $8000\,\mathrm{kg/m^3}$ Young's modulus = 200 GPa Poisson's ratio = 0.33 loss factor = 0
Air	density = $1.21\,\mathrm{kg/m^3}$ speed of sound = $342.2\,\mathrm{m/s}$	
Melamine	porosity = 0.99 resistivity = $10900\,\mathrm{kg/m^3 s}$ tortuosity = 1.02 viscous length = $100\,\mu$m thermal length = $130\,\mu$m	density = $8.8\,\mathrm{kg/m^3}$ Young's modulus = 80 kPa Poisson's ratio = 0.4 loss factor = 0.17
Mass		density = $1200\,\mathrm{kg/m^3}$ Young's modulus = 10^3 kPa Poisson's ratio = 0.3 loss factor = 0

consisting, from the plate side (i.e. side A), of a 1 mm air gap and a 2 cm foam and (ii) a three-layers treatment consisting, in the same order, of a 1 mm air gap, a 2 cm foam and a $1.2\,\mathrm{kg/m^2}$ heavy layer (see Tab. 2.1 for the material properties). Two different boundary conditions are considered over side B of the sound package, namely, a radiation condition into an unbounded fluid and a pressure release condition. In the finite element model, the radiating side of the acoustic treatment is assumed to be embedded in a rigid baffle. In this context, the impedance condition for the case of the radiating foam (i.e. the two-layers lay-up) is modeled by the boundary formulation proposed by Atalla *et al.* [6]. Concerning the hybrid model, the methodology explained in section 2.4.1 is employed to account for the fluid loading. The radiated power is thus retrieved by means of Eqs. 2.21 and 2.23. The untreated (i.e. excitation) side of the plate is assumed to vibrate in-vacuo. In what follows, unless differently specified, the Biot model is employed for the poroelastic layer involved in the two considered sound packages.

The first case refers to a simply supported plate of dimensions $0.4 \times 0.85\,\mathrm{m^2}$ excited by a plane wave impinging onto the structure with a $45°/45°$ angle of incidence. The two-layers treatment is attached onto the plate and radiates in the receiver domain, where the presence of an unbounded fluid is modeled as explained above. The structure was modeled with 55×110 linear quadrilateral plate elements. For the acoustic treatment the same number of elements was used in the (x, y) plane while one and seven Hexa-8 fluid and poroelastic elements were used in the thickness direction to model the two layers

of the acoustic treatment. The latter is assumed to slide along its lateral boundaries. Figs. 2.4 and 2.5 show the space averaged quadratic velocity of the plate and the TL of the system, respectively, predicted by the FE-TMM (Green function and locally reacting based) and the FEM. The quadratic velocity (Fig. 2.4) is well captured by the Green function based FE-TMM. On the other hand, the locally reacting approximation leads to an overestimation of the dissipation at the peaks of the response. This is due the fact that the plane wave radiation condition used in a locally reacting sense is not a reliable approximation at low frequencies, as also observed by Atalla *et al.* [6]. Fig. 2.5 shows, instead, the TL of the system. The hybrid models seem to overestimate the TL below 2 KHz (besides, it has been observed that the error increases as the treatment becomes thicker while preserving the planar dimensions of the system), as a convergent behavior towards the reference finite element solution can only be inferred at higher frequencies. Therefore, the Green function based FE-TMM seems to be able to capture the kinetic energy of the plate but it underestimates the power radiated by the back of the foam (i.e. side B), leading to a higher TL prediction.

To understand this misbehavior, the resistive and reactive contributions seen by the plate due to the added dynamic stiffness $\mathbf{D}_{AA}(\omega)$ are assessed in terms of energetic indicators. Indeed, the resistive part of $\mathbf{D}_{AA}(\omega)$ is related to the power dissipated by the sound package, i.e.

$$\Pi_{\text{res}} = -\frac{1}{2}\,\text{Re}\left[\mathbf{V}_A^{s^*}(\omega)\mathbf{T}_A^s(\omega)\right] = \frac{1}{2}\,\text{Re}\left[\mathbf{U}_A^{s^*}(\omega)\,\imath\omega\mathbf{D}_{AA}(\omega)\,\mathbf{U}_A^s(\omega)\right]\,, \tag{2.24}$$

where $\mathbf{V}_A^s = \imath\omega\mathbf{U}_A^s$. The minus sign has been used for coherence with Eq. 2.20. On the other hand, the reactive part of $\mathbf{D}_{AA}(\omega)$ is related to the imaginary part of the same physical quantity, or, equivalently, to the real part of the potential energy associated to the sound package itself, i.e.

$$\Pi_{\text{rea}} = \frac{1}{2}\,\text{Im}\left[\frac{1}{\omega}\,\mathbf{V}_A^{s^*}(\omega)\mathbf{T}_A^s(\omega)\right] = -\frac{1}{2}\,\text{Re}\left[\mathbf{U}_A^{s^*}(\omega)\mathbf{T}_A^s(\omega)\right] = -\frac{1}{2}\,\text{Re}\left[\mathbf{U}_A^{s^*}(\omega)\,\mathbf{D}_{AA}(\omega)\,\mathbf{U}_A^s(\omega)\right]\,. \tag{2.25}$$

Fig. 2.6 (resp. 2.7) shows the difference between the resistive (resp. reactive) indicator calculated by the FEM and the Green function based FE-TMM. It can be seen that, on average, both the indicators lie within 0.5 dB over the observed frequency range. However, since the mass and stiffness added to the plate by the sound package are negligible

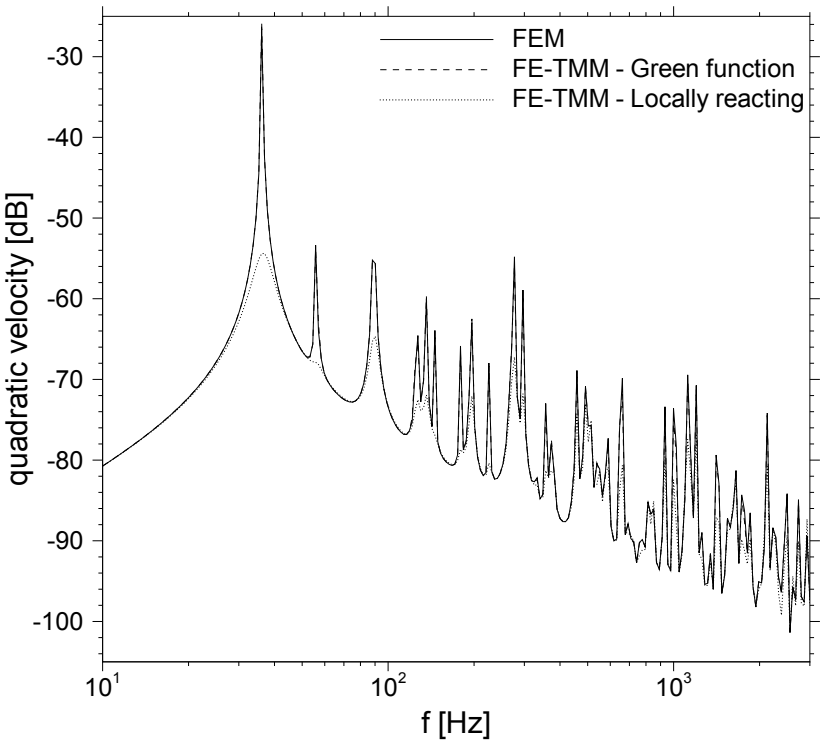

Figure 2.4 Quadratic velocity of the simply supported steel plate excited by a 45°/45° plane wave and attached to the two-layers lay-up. Comparison between the FEM, the Green function based FE-TMM and the locally reacting FE-TMM.

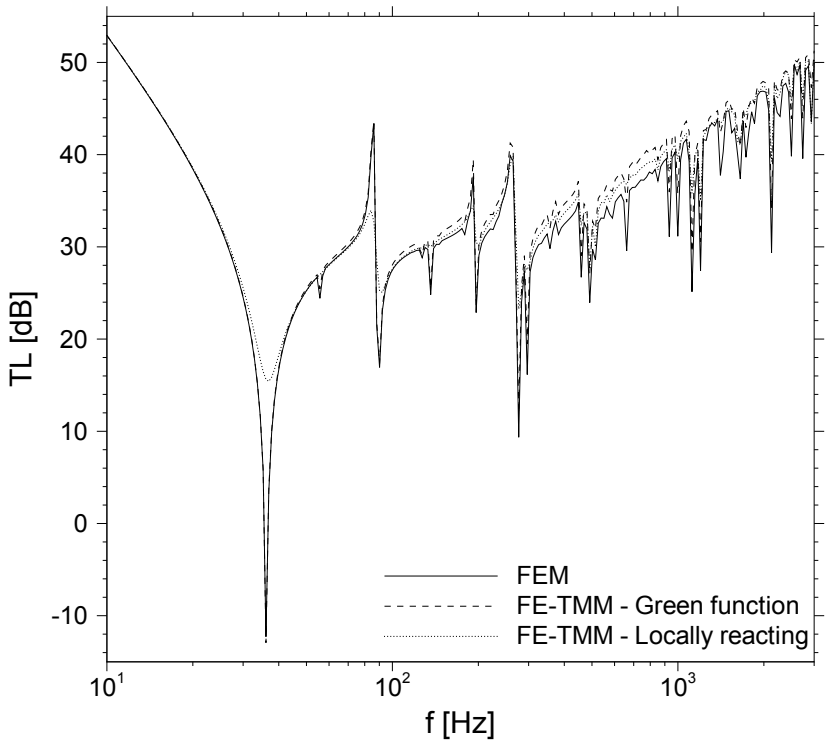

Figure 2.5 TL of the simply supported steel plate excited by a 45°/45° plane wave and attached to the two-layers lay-up. Comparison between the FEM, the Green function based FE-TMM and the locally reacting FE-TMM.

compared with the reactive terms of the structure itself, the quadratic velocity is well predicted (see Fig. 2.4). On the contrary, the TL (see Fig. 2.5) converges to the reference solution only as the approximation of the reactive part becomes accurate enough.

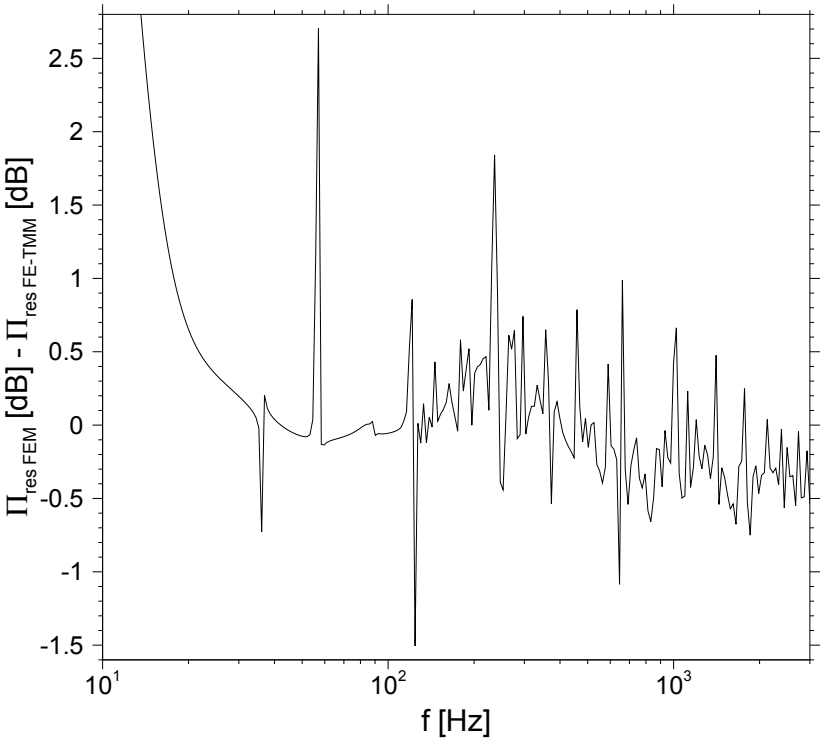

Figure 2.6 Difference between the resistive indicator Π_{res} (Eq. 2.24) calculated by the FEM and the Green function based FE-TMM. Simply supported steel plate excited by a 45°/45° plane wave and attached to the two-layers lay-up. The effect of the fluid loading at side B is accounted for in both models.

Although the system described above cannot be accurately approximated neglecting the pressure loading exerted by the fluid over the back of the foam, for the sake of argument, the same analysis was run with a pressure release condition at side B of the foam. Only the difference between the reactive indicator calculated by the reference and the hybrid FE-TMM is reported in Fig. 2.8, as the resistive indicator exhibits the same accuracy. The figure shows that, when a pressure release condition is applied on side B of the treatment, the reactive effects are accurately solved (i.e. the difference is almost zero on average). Therefore, the lack of accuracy experienced by the Green function based FE-TMM in Fig. 2.5 indicates that the effect of an unbounded fluid is not accurately approximated by the analytical model. This is basically due to the fact that the finite size system is

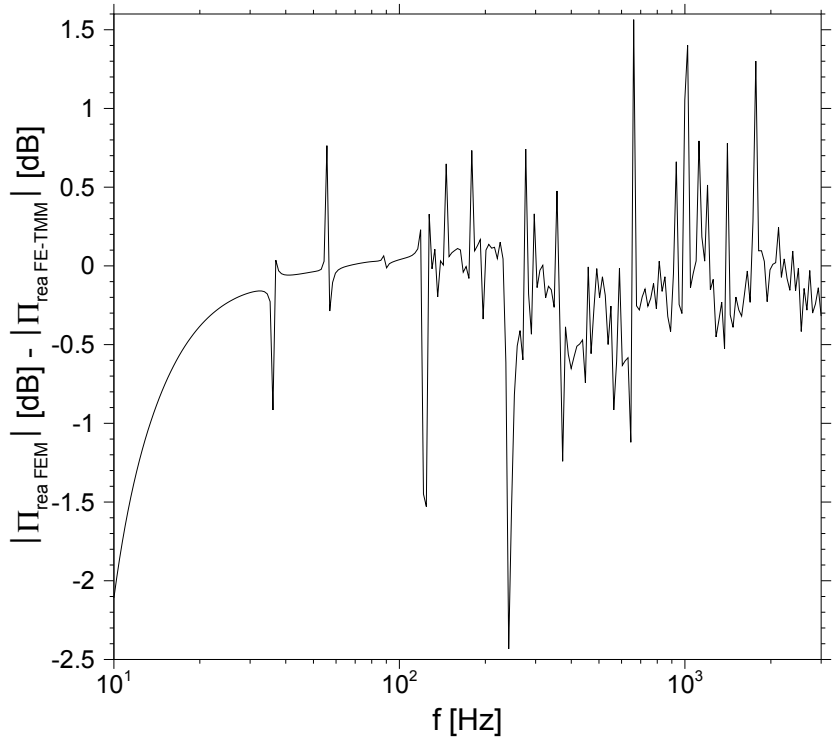

Figure 2.7 Difference between the absolute value of the reactive indicator Π_{rea} (Eq. 2.25) calculated by the FEM and the Green function based FE-TMM. Simply supported steel plate excited by a 45°/45° plane wave and attached to the two-layers lay-up. The effect of the fluid loading at side B is accounted for in both models.

actually baffled at the radiating side (i.e. side B), while the analytical model of the sound package (Eqs. 2.19 and 2.21) requires only side A (i.e. the structural side) to be inserted into a rigid baffle. Thus, a surface bigger than the treated surface S is in contact with the unbounded fluid over side B of the sound package and, consequently, the effective fluid loading is overestimated. Generally speaking, this effect is dominant below the coincidence frequency, when the acoustic wavelength is longer than the structural wavelength. This argument is confirmed by the results in Fig. 2.9, where the radiation impedance of two representative plate modes (with clamped boundary conditions) calculated by means of the Green function based FE-TMM (Eq. 2.21) is compared with the FEM prediction. It is clear that the hybrid model is not accurate enough below the coincidence frequency of each mode (i.e. when the acoustic wavelength equals the wavelength of the considered plate mode). However, when the plate is excited by a plane wave with angle of incidence θ, the acoustic trace wavenumber $k_t = (\omega/c_0)sin(\theta)$ is enforced on the structure, so that, after a low frequency region where the structural response is mostly modal, the structure vibrates with a wavelength longer than the acoustic wavelength (being $k_t < k_0$). As a result, the hybrid method converges to the reference solution before the critical frequency. On the contrary, it was found that, when the structure is mechanically excited (i.e. point force), discrepancies between the hybrid and the reference FEM solution must be expected up to the coincidence frequency (with a maximum error comparable with that one in Fig. 2.5), due to the fact that the plate vibrates at each frequency according to its bending wavenumber.

Consequently, the Green function based FE-TMM is expected to perform better when the pressure loading at side B is neglected. To confirm this argument, the case of a sound package involving an impervious mass attached at the back of the foam is now considered. In fact, for this kind of layups, it is known that the fluid loading affects the plate-sound package system at low frequency mainly adding damping around the double wall resonance. Thus, if one accepts to neglect this effect, the dynamic response of the system system can be solved in-vacuo and the radiated power can be retrieved in the postprocessing phase. For this analysis, the same steel plate with doubled dimensions (i.e. $0.8 \times 1.7\,\mathrm{m}^2$) attached to the three-layers treatment (i.e. air gap-foam-mass lay-up) is considered. The plate is clamped and excited along the z-axis by a 1 N point force applied at $(0.0582\,\mathrm{m}, 1.6382\,\mathrm{m})$. Similar results were obtained for a plane wave excitation. However, a different excitation and size are here used to illustrate the accuracy of the method for various excitations and dimensions. As mentioned above, the effect of the fluid loading at the receiver side is neglected in the FE-TMM and in the FEM. The structure was modeled with 55×110 linear quadrilateral plate elements while one, three and one Hexa-8 fluid, poroelastic and

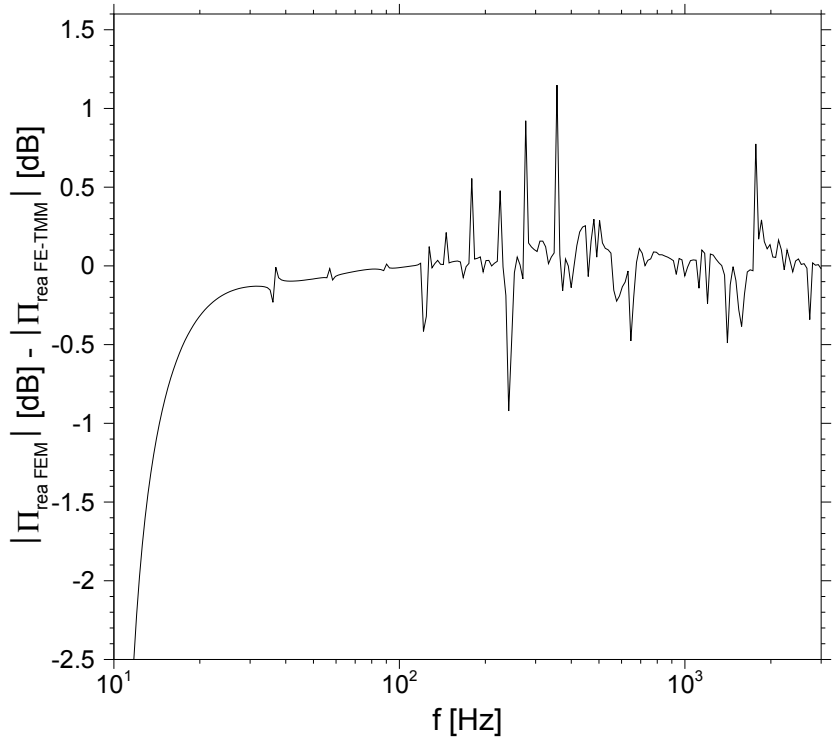

Figure 2.8 Difference between the absolute value of the reactive indicator Π_{rea} (Eq. 2.25) calculated by the FEM and the Green function based FE-TMM. Simply supported steel plate excited by a 45°/45° plane wave and attached to the two-layers lay-up. The effect of the fluid loading at side B is neglected in both models.

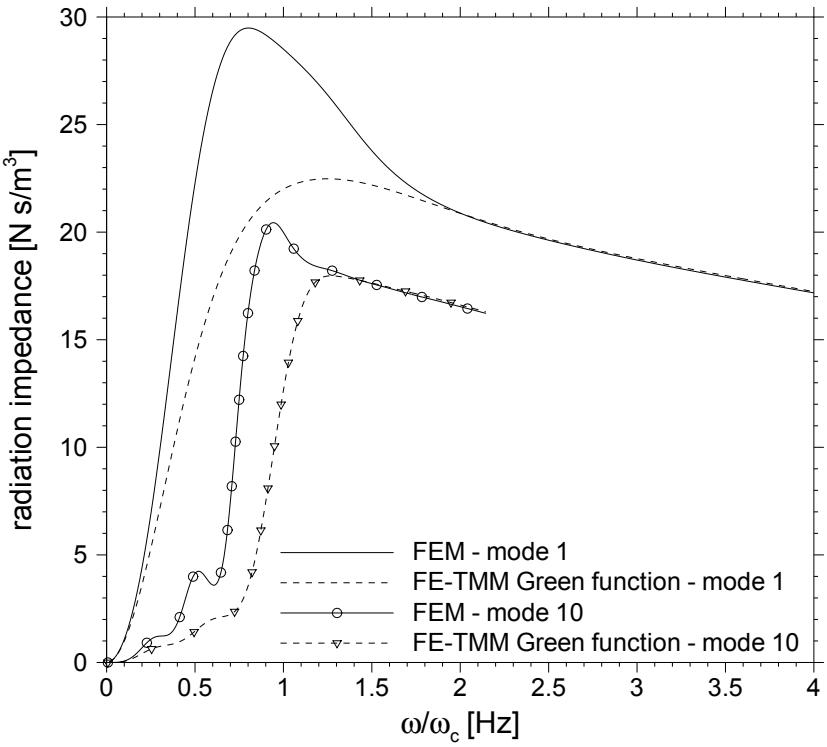

Figure 2.9 Radiation impedance Z_{ij}^{rad} (Eq. 2.21) seen by a clamped steel plate with an attached 2 cm thick melamine foam (limp model). Comparison between the FEM and the Green function based FE-TMM. The circular frequency at which the coincidence between the modal wavelength and the acoustic wavelength occurs is denoted by ω_c (different for the mode 1 and 10)

solid elements were used in the thickness direction to model the three layers of the acoustic treatment. Figs. 2.10 and 2.11 show the space averaged quadratic velocity of the plate and the radiated power, respectively, obtained by the hybrid FE-TMM and the FEM. A very good agreement between the Green function based FE-TMM prediction and the reference is now observed not only for the quadratic velocity but also for the radiated power. Few discrepancies appear around the double wall resonance at 300 Hz and at the end of the spectrum, where the shear waves resonance previously discussed occurs. Figs. 2.12 and 2.13 show the resistive and reactive indicators of the added dynamic stiffness $\mathbf{D}_{AA}(\omega)$ and confirm that the hybrid model perform well when a pressure release condition is applied. However, it is worth noting that the reactive indicator (see Fig. 2.13) is in better agreement with the reference before the double wall resonance, suggesting that the mass effects (below 300 Hz) are better captured than the stiffness effects (above 300 Hz) for the considered system. In fact, the effect of the three-layers treatment on the plate is approximately equivalent to that of a spring-mass system, mass-controlled at low frequencies, damping-controlled around the spring-mass resonance (i.e. 300 Hz) and stiffness-controlled at higher frequencies. However, the stiffness added by the acoustic treatment is negligible compared with the stiffness of the structure itself, so that the quadratic velocity in Fig. 2.10 is still well captured despite the error observed in Fig. 2.13. Finally, it should be noted that the locally reacting assumption (see Figs. 2.10 and 2.11) fails over the considered frequency range for the three-layers sound package. Indeed, the mass at the top of the foam and the strong modal response due to the mechanical disturbance excite particularly the non local response of the treatment. As a result, this class of complex acoustic treatments cannot be modeled as locally reacting subsystems, limiting the use of this simplification to simple layups.

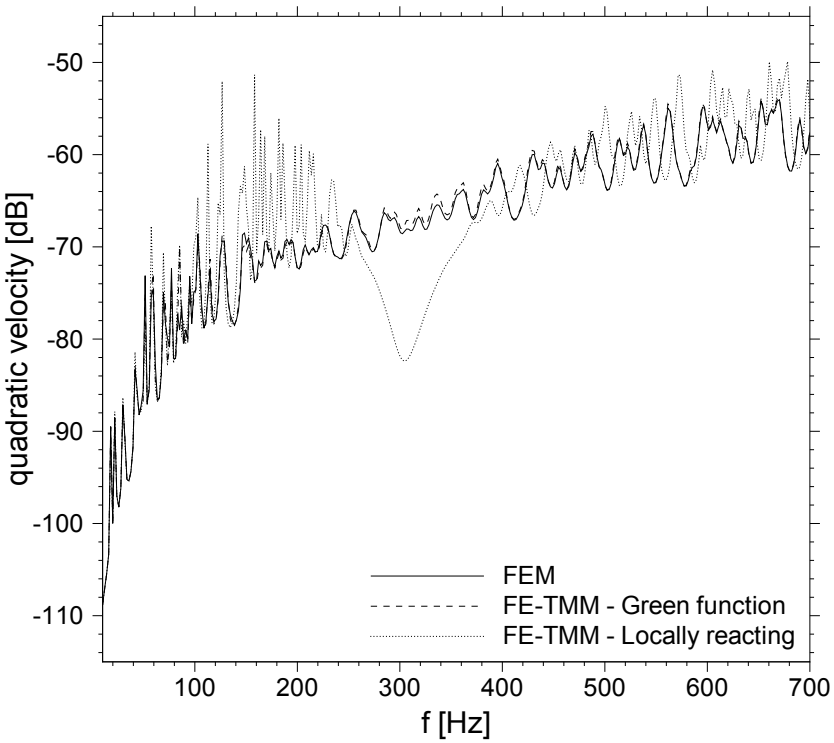

Figure 2.10 Quadratic velocity of the clamped steel plate excited by a point force and attached to the three-layers lay-up. Comparison between the FEM, the Green function based FE-TMM and the locally reacting FE-TMM.

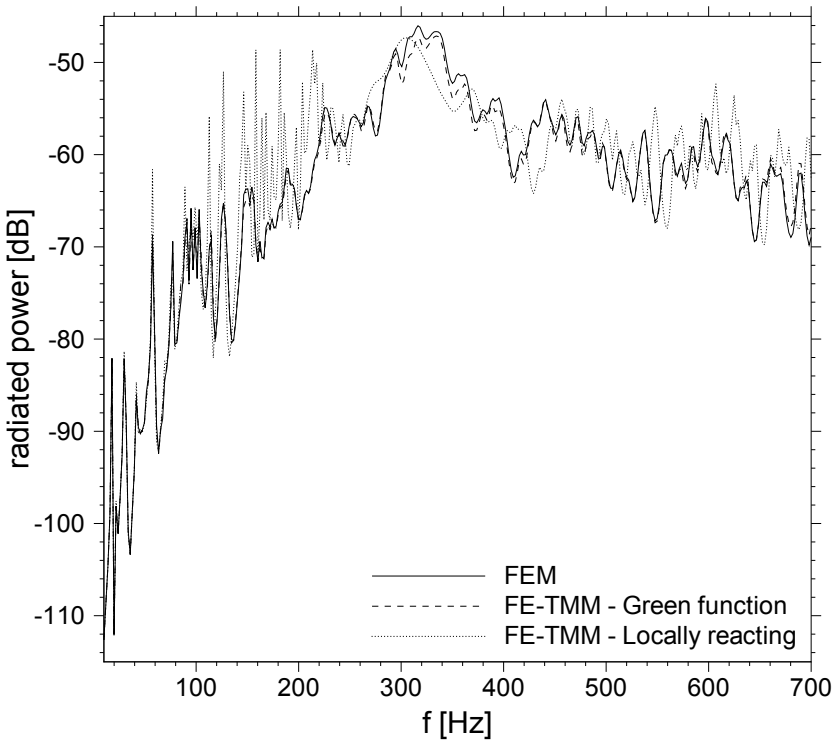

Figure 2.11 Radiated power Π_{rad} of the clamped steel plate excited by a point force and attached to the three-layers lay-up. Comparison between the FEM, the Green function based FE-TMM and the locally reacting FE-TMM.

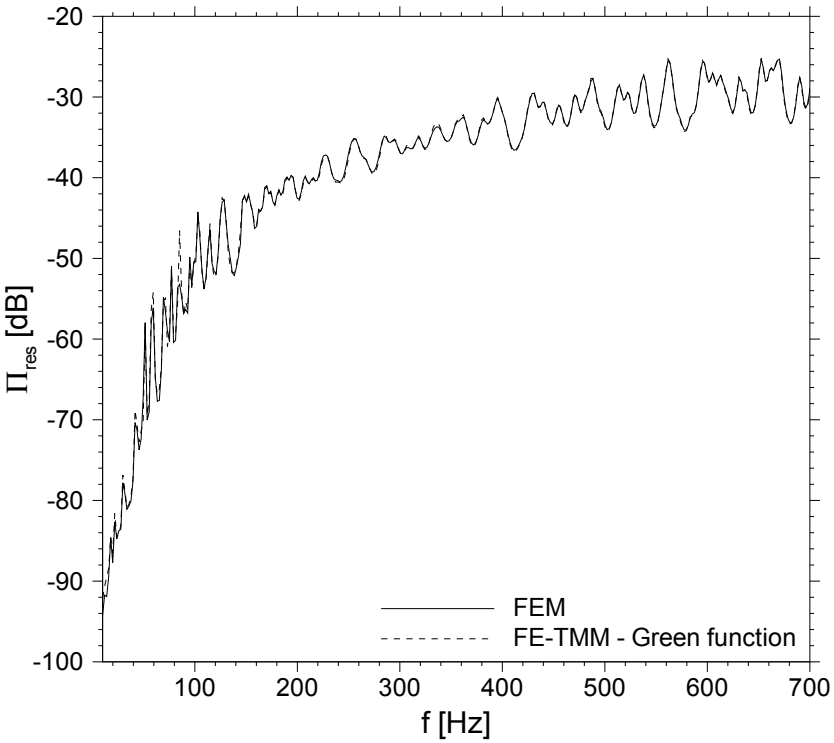

Figure 2.12 Resistive indicator Π_{res} (Eq. 2.24) for the clamped steel plate excited by a point force and attached to the three-layers lay-up. Comparison between the FEM and the Green function based FE-TMM.

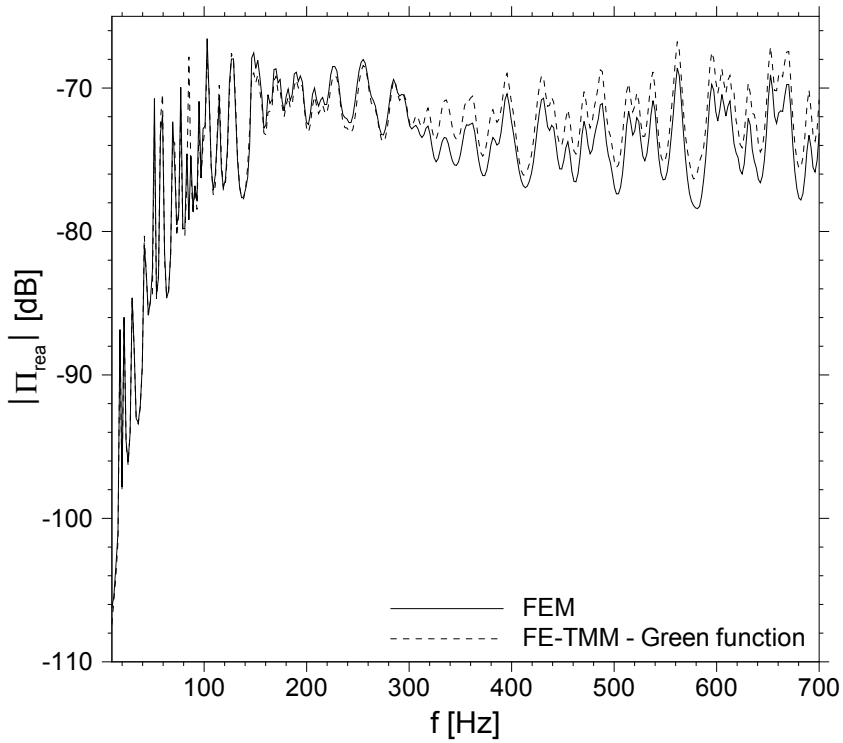

Figure 2.13 Absolute value of the reactive indicator Π_{rea} (Eq. 2.25) for the clamped steel plate excited by a point force and attached to the three-layers lay-up. Comparison between the FEM and the Green function based FE-TMM.

2.6 Implementation aspects

The efficiency of the Green function based FE-TMM resides mainly in the numerical quadrature involved in Eqs. 2.12 and 2.21, as the calculation of the analytical kernels $\hat{d}(k,\omega)$ and $\hat{d}_{A\to B}(k,\omega)$ can be performed quickly using the TMM. In the present work, the following procedure is used for the evaluation of matrices $\mathbf{D}_{AA}$ and $\mathbf{Z}^{\text{rad}}$. First, (i) a preprocessing module is run to calculate the analytical kernels by means of the classical TMM. Then, for each frequency step where the system in Eq. 2.20 has to be be solved, (ii) the converged value of the integral is obtained by an adaptive numerical quadrature algorithm (i.e. the open source QUADPACK library was used). The numerical integration is performed at discrete values of the distance r, typically between $r_{min} = 0$ and $r_{max} = \max(r)$, i.e. the maximum distance between two points lying over the treated surface S. It should be noted that the convergence of the integral in in Eqs. 2.12 depends, for a given sound package, on the decay rate of $|\hat{\psi}(k)|^2$ (see Eq. 2.12). However, depending on the structural boundary conditions along the perimeter of the surface S, the global displacement of the structure may provide a far more effective filter than the one provided by the shape functions (i.e. $|\hat{\psi(k)}|^2$). As a result, the integral could be truncated before its actual convergence, leading to a faster numerical quadrature. However, in this case, a general truncation rule would be hard to define, as the displacement of the structure is an unknown of the problem. For the two-layers (resp. three-layers) lay-up considered above, the integration step was performed in about 1 s (resp. 2 s) at 100 (resp. 200) grid points between r_{min} and r_{max} (data relatives to a serial implementation on a 2.2 GHz AMD processor). Once the integral has been approximated between r_{min} and r_{max}, (iii) an interpolation is performed to obtain all the independent (i,j) components of matrices $\mathbf{D}_{AA}$ and $\mathbf{Z}^{\text{rad}}$. This step strongly depends on the particular implementation (i.e. serial/parallel and adopted interpolation routine). Thus, since the latter aspect was not optimized in the current implementation, the computational time required to perform step (iii) is not reported.

Finally, it should be noted that the computational time is only weakly dependent on the frequency. Indeed, the acoustic treatment is solved analytically in the thickness direction, so that steps (ii) and (iii) only depends on the number of nodes over the treated surface S. On the contrary, a finite element model of the sound package requires a finer mesh in the thickness as the frequency increases, leading to a larger system to be solved. However, a direct comparison with the computational time required by the FEM is not provided. Indeed, the efficiency of the in-house finite element code used in this work is not repre-

sentative of the typical computational cost of modern finite element procedures based on substructuring [53].

2.7 Conclusions

A hybrid FE-TMM has been proposed to couple the finite element with an analytical model of the acoustic treatment. The analytical formulation is based on the Green function formalism and assumes flat, laterally unbounded, homogeneous and isotropic treatments. A first analysis has been performed to show that the analytical model can capture the behavior of the actual bounded sound package even at low frequencies. It has been found that poroelastic layers modeled by means of the Biot model exhibit size effects mostly at the solid phase controlled resonances, which are typically underestimated by the analytical model. Then, the accuracy of the FE-TMM has been assessed for a typical vibroacoustic problem consisting of a plate treated by a sound package radiating in an unbounded fluid medium. Two representative treatment layups were considered in the numerical examples, namely a two-layers lay-up (i.e. air gap-foam configuration) and a three-layers lay-up (i.e. air gap-foam-mass configuration). It has been found that, when the effect of fluid loading on the sound package is taken into account, the power radiated in the unbounded fluid estimated by the FE-TMM converges to the FEM calculation only at higher frequencies. In the case of a plane wave excitation, the convergence is obtained as soon as the structural response stops to be strongly modal. On the contrary, in case of mechanical excitations (e.g. point force), no convergence can be expected before the coincidence frequency. Nonetheless, the quadratic velocity of the plate is qualitatively and quantitatively well captured for the considered sound packages. Conversely, when the effect of the fluid on the back of the treatment is neglected, a very good agreement was observed for both the considered indicators (i.e. space averaged quadratic velocity and radiated power) in case of mechanical and acoustic excitations.

Other parameters have been found to affect the accuracy of the FE-TMM. For instance, the ratio between the lateral dimensions and the thickness of the sound package as well as the boundary conditions applied on the structural displacement (i.e. structural boundary conditions) along the perimeter of the treated surface S may affect the accuracy of the hybrid methodology. Nevertheless, for typical sizes, layups and boundary conditions, the effect of the fluid loading over the back of the treatment was found to be the most critical parameter for the considered systems. Overall, the FE-TMM has shown interesting performances, revealing itself as an improvement over the locally reacting approach, which confirmed, instead, its limitation to simple configurations. Finally, it should be stressed

that, due to the strong assumptions considered in the hybrid formulation (i.e. the actual finite size acoustic treatment is replaced by a baffled and laterally unbounded one), a perfect correlation with the FEM cannot be expected at low frequencies. Despite that, under the conditions mentioned above, the FE-TMM provides a fast and reliable estimation of the acoustic performance of a trimmed structure.

2.8 Further comments

The main conclusions of this chapter can be summarized as follows.

– The dissipation added to the structural domain due to the presence of the sound package is typically well captured by the proposed hybrid methodology.
– The power transmitted to the fluid (i.e. receiver side) may be instead poorly captured.

The reason of the latter was found to be related to the modeling of the unbounded fluid. Indeed, both the sound package and the fluid domain have been modeled by means of the TMM. On the one hand, this strategy allows for an efficient approximation of the unbounded fluid domain. However, on the other hand, it neglects the fact that only a finite area S of the sound package is actually in contact with the fluid over side B. It was found that this approximation introduces the following errors.

– The added mass due to the presence of a foam seen from the structure is overestimated (Figs. 2.7 and 2.8).
– The radiation efficiency seen by the structure is poorly captured below the coincidence frequency (Fig. 2.9). This is not surprising since the baffling condition is known to have a non negligible effect over this frequency range.

As a result, in order to improve the accuracy, the presence of the fluid at side B must be confined within the actual wetted surface S. To this purpose, the performance of the hybrid methodology in modeling noise treatments placed between a finite element structural and acoustic domain must be assessed. This analysis will be comprehensively developed throughout chapters 3-5. The acoustic radiation into unbounded acoustic domains will be again considered in chapter 6 to formally conclude the analysis started in this chapter.

CHAPTER 3

EXTENSION OF THE FE-TMM TO ACOUSTICALLY TREATED PLATE-CAVITY SYSTEMS

In this chapter, the hybrid FE-TMM is assessed for the case of treated plate-cavity systems. The noise control treatment is thus placed between a finite element structure and acoustic cavity. Hence, differently from the model considered in the previous chapter, a finite size area is coupled with a finite element domain on both sides of the sound package. The hybrid model is obtained as an extension of the framework developed in Chapter 2. The paper submitted to the *Journal of Acoustical Society of America* follows. Furthermore, a final section (i.e. Section 3.6) has been added to integrate the paper in the context of the thesis.

Auteurs et affliation:

L. Alimonti: Étudiant au doctorat, Université de Sherbrooke, Faculté de Génie, Department de génie mécanique

N. Atalla: Professeur, Université de Sherbrooke, Faculté de Génie, Département de génie mécanique

A. Berry: Professeur, Université de Sherbrooke, Faculté de Génie, Département de génie mécanique

F. Sgard: Professeur, Chercheur chez Institut de recherche Robert-Sauvé en santé et en sécurité du travail (IRSST)

Date d'acception: -

État de l'acceptation: soumis le 20 Mai 2014

Revue: Journal of Acoustical Society of America (JASA)

Référence: -

Titre français: Un modéle hybride éléments finis - matrice de transfert pour les systémes vibroacoustiques avec traitements acoustiques planes et homogénes

Contribution au document: Dans ce article, le modéle hybride éléments finis - matrice de transfert est évaluée dans le cas des systémes traités plaque-cavité.

Résumé français: Les systèmes vibroacoustiques pratiques comprennent des traitements acoustiques passifs constitués de milieux très dissipatifs, comme les matériaux poroélas-

tiques. La modélisation numérique de ces systèmes à des fréquences basses et moyennes repose généralement sur des méthodologies de sous-structuration fondées sur des modèles d'éléments finis. À savoir, les sous-systèmes de base (c.-à-d. les domaines structuraux et acoustiques) sont décrits par un ensemble fini de modes découplés, tandis que les procédures de condensation sont généralement préférées pour les traitements acoustiques.Cependant, bien que précise, cette méthode est coûteuse en ressources informatiques lorsque les applications concrètes sont envisagées. Une éventuelle réduction de la charge de calcul peut être obtenue par une approximation de l'effet du traitement acoustique de sous-systèmes de base sans introduire de degrés physiques de liberté. Pour ce faire, le traitement doit être présumé homogène, plat et d'une étendue latérale infinie. Sous ces hypothèses, des outils d'analyse simples comme la méthode de matrice de transfert peuvent être utilisés. Dans cet article, on propose une méthode de matrice de transfert de l'élément fini hybride. L'impact des hypothèses restrictives inhérentes au cadre analytique est évalué pour le cas des systèmes de plaques cavité impliquant des traitements acoustiques planes et homogènes. Les résultats démontrent que le modèle hybride peut capter le comportement qualitatif du système vibroacoustique, tout en réduisant l'effort de calcul.

Note: -

3.1 Abstract

Practical vibroacoustic systems involve passive acoustic treatments consisting of highly dissipative media such as poroelastic materials. The numerical modeling of such systems at low to mid frequencies typically relies on substructuring methodologies based on finite element models. Namely, the master subsystems (i.e. structural and acoustic domains) are described by a finite set of uncoupled modes, whereas condensation procedures are typically preferred for the acoustic treatments. However, although accurate, such methodology is computationally expensive when real life applications are considered. A potential reduction of the computational burden could be obtained by approximating the effect of the acoustic treatment on the master subsystems without introducing physical degrees of freedom. In order to do that, the treatment has to be assumed homogeneous, flat and of infinite lateral extent. Under these hypotheses, simple analytical tools like the transfer matrix method can be employed. In this paper a hybrid finite element-transfer matrix methodology is proposed. The impact of the limiting assumptions inherent within the analytical framework are assessed for the case of plate-cavity systems involving flat and homogeneous acoustic treatments. The results prove that the hybrid model can capture

the qualitative behavior of the vibroacoustic system while reducing the computational effort.

3.2 Introduction

Typical vibroacoustic systems involve an acoustic cavity surrounded by structural components, such as plates. In automotive and aeronautical applications, the use of lightweight structures typically leads to poor vibroacoustic performances, as the structural frame vibrational energy produced by an external source is transferred significantly to the acoustic fluid enclosed by the structure. As a result, the noise level inside the cavity may become an issue, especially when the final product has to guarantee a healthy and comfortable interior environment. Thus, passive acoustic treatments, also called sound packages, are used to introduce dissipation in the system. They typically consist of highly dissipative materials assembled in a multilayer fashion and attached onto the structure. One or more layers of these passive components usually contain poroelastic materials. Such materials are made up of a solid and fluid phase and can provide damping by the vibration of the solid phase itself and by the coupling between the two phases. The Biot theory [13–15] describes these complex phenomena for a homogeneous porous medium and can be used as a reliable mathematical model [3]. Although it is possible to simplify the Biot model when the solid phase can be considered motionless or limp (i.e. negligible structural rigidity), for general multilayer systems and for a broad range of excitation frequencies both phases must be taken into account to obtain a good accuracy [84].

Good modeling tools are essential to save resources during the design process. The Finite Element Method [10] (FEM) is typically employed in the low frequency range. Namely, substructuring solution strategies are used to improve the computational efficiency of finite element analysis. On the one hand, the structural (e.g. plates) and acoustic (e.g. cavity) domains that exhibit a modal behavior over the considered frequency range are described by a finite set of uncoupled modes, computed from the respective finite element models. Such subdomains will be herein referred to as *master* subsystems. On the other hand, an optimal modeling strategy for the acoustic treatment has not been devised yet. Indeed, the complex frequency dependency of the finite element matrices describing the coupling between fluid and solid phases in poroelastic materials make standard eigenvalue solvers difficult to apply. Despite several attempts to develop modal techniques for porous materials [32, 33, 96], their effectiveness remains questionable as a huge number of modes, whose participation to the global response of the system is not clear a priori [97], has to be taken into account. As a consequence, a condensation of the acoustic treatment

degrees of freedom is typically preferred [53]. Thus, the final discrete model of the coupled system involves only the amplitudes of the master subsystems generalized coordinates (e.g. structural and acoustic modal amplitudes). The effect of the acoustic treatment is, instead, held in an added (boundary) operator which contains the effect of the condensed degrees of freedom on the generalized coordinates. Such operator can be seen as an equivalent interface impedance.

However, when poroelastic materials are involved in passive treatments, relying on a finite element model of the sound package can be, even if accurate, computationally expensive. Indeed, the (u, p) formulation [5] of the Biot theory, albeit more efficient compared to other formulations (e.g. displacement based formulation [85]), still needs four unknowns per node. Moreover, even at low frequencies, a very fine mesh is typically required to describe the shortest wavelength propagating inside the poroelastic media. Therefore, a large number of elements are always needed in order to capture the solution. To alleviate this drawback the use of hierarchical basis functions [57, 94] has been attempted. However, in the last decade, most of the authors have converged on the idea that wave based methodologies should be considered for the efficient modeling of waves propagation phenomena in vibroacoustic. Basically, the idea consists in enriching or replacing the piece-wise polynomials used in classical finite element analysis by piece-wise plane waves, as these are exact solution of the homogeneous problem. In this framework, the Wave Based Method [36] (WBM) has been developed and applied, among others, to porous media [35]. Also, the Discontinuous Galerkin Method (DGM) has been applied to poroelastic materials [34]. Differently, the rationale of the enrichment methods is to combine the strengths of finite element and wave based methodologies. In this context, an application of the Partition of Unity FEM (PUFEM) to dissipative acoustic materials can be found in the work of Chazot *et al.* [20].

One could then argue that a possible way to improve the efficiency of finite element based modeling strategies in vibroacoustic applications is by means of hybrid methodologies. Thus, the subsystems characterized by geometrical complexity and longer wavelengths are modeled by standard finite element schemes and modal synthesis, whereas the subsystems with much shorter wavelengths, such as the acoustic treatment, are modeled by means of wave based techniques. Although the aforementioned wave based methodologies can achieve a drastic reduction of the degrees of freedom compared to conventional finite element models, their application to complex three-dimensional systems, possibly in a hybrid context, is still subject of ongoing research. Alternatively, a potential reduction of the computational burden could be obtained by approximating the effect of the soft sub-

structure (e.g. acoustic treatment) on the master subsystems without introducing physical degrees of freedom. In order to do that, the subsystem which exhibits shorter wavelengths has to be assumed homogeneous, flat and of infinite extent. These hypotheses allow to use simple and fast wave based analytical techniques. Namely, the knowledge of simple fundamental solutions (i.e. Green functions) is sufficient to approximate the behavior of the considered substructure. For simple problems, the Green function in the wavenumber domain is known analytically. For instance, in the work of Ji *et al.* [60], the effect of a thin panel on a much stiffer beam is taken into account using the exact analytical solution for the line impedance of the infinite plate. Unfortunately, the calculation of the Green functions of complex multilayered systems cannot be carried out analytically. However, the Transfer Matrix Method [3] (TMM) provides a powerful and efficient tool to obtain the desired Green function for a given circular frequency and wavelength. For instance, in the hybrid methodology proposed by Tournour *et al.* [122], the acoustic treatment is taken into account in a locally reacting sense (i.e. wall impedance [3, 86]) by the frequency dependent coefficients of its transfer matrix. An application of this methodology to an optimization problem can also be found in the work of Yamamoto *et al.* [130]. The approach proposed by Courtois and Bertolini [26] uses, instead, the Inverse Fourier Transform (IFT) to explicitly find the Green functions of the acoustic treatment to be employed in the boundary terms of a standard finite element approximation. These approaches may be referred to as hybrid Finite Element-Transfer Matrix Methods (FE-TMMs). On the other hand, Rhazi and Atalla [92, 93] proposed a different hybrid approach to model flat rectangular plates with attached multilayer treatments. The displacement of a simply supported plate was described in terms of superposition of orthogonal trigonometric functions (i.e. Ritz method) while the effect of the multilayer treatment on each mode was approximated using the TMM. This approach, similar to the one proposed by Ji *et al.* [60] from a methodological standpoint, may be referred to as a hybrid modal-TMM. Conversely, the approach proposed by Fernandez *et al.* [45, 45] tackles the hybrid modeling from a stochastic viewpoint, being the sound package modeled as a fuzzy system [107, 108].

This paper investigates how a transfer matrix model can be used to describe homogeneous and flat acoustic treatments in standard finite element analyses of vibroacoustic systems. In this context, the few works briefly described above do not provide a comprehensive reference, as the generic properties of such hybrid FE-TMMs (i.e. domain of validity of the approximation, accuracy and computational efficiency with respect to well-established finite element based substructuring procedures) can hardly be inferred. The purpose of the present paper is then twofold. (i) The theoretical formulation of the hybrid FE-TMM recently proposed by the authors to account for the effect of acoustic treatments attached

onto a radiating structure [1] is extended to the radiation inside finite element acoustic cavities. Here, the main objective is to provide a comprehensive theoretical framework for this class of hybrid approaches. (ii) Numerical examples are then provided in order to understand the behavior of the hybrid model and its domain of validity. The analysis is limited to flat acoustic treatments, as the effect of the curvature is beyond the scope of this paper.

The paper is organized as follows. In Section 3.3 the theoretical background is presented. First, the boundary operator which accounts for the acoustic treatment in the modal equations of a generic vibroacoustic system is introduced. Second, a finite element substructuring procedure is briefly presented as an exact and well-established methodology to retrieve the boundary operator. Then, the analytical framework involved in the hybrid FE-TMM is introduced as an extension of the formulation proposed by Alimonti *et al.* [1]. Moreover, it is shown how simplified models (i.e. modal [92, 93] and locally reacting [122] approaches) can be deduced from the proposed model. In Section 3.4 the boundary operators obtained by means of the analytical and finite element models are compared. Next, a plate-cavity system is considered to assess the accuracy of the assembled hybrid finite element-transfer matrix model.

3.3 Theoretical background

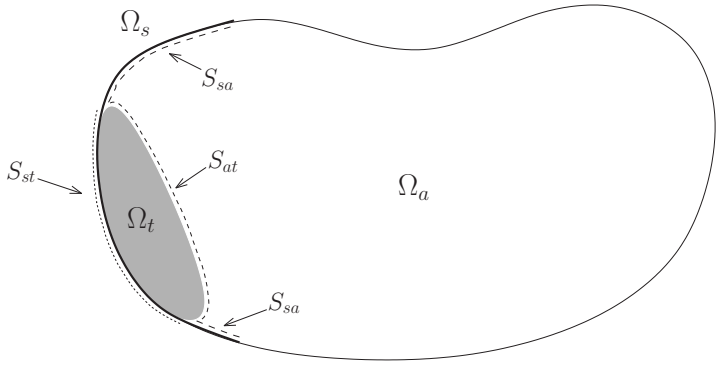

Figure 3.1 Generic vibroacoustic system.

Fig. 3.1 shows a generic vibroacoustic system. The structural and fluid domains are denoted by Ω_s and Ω_a, respectively, while Ω_t refers to the volume occupied by the acoustic treatment. The latter is attached onto the structure over the treated surface S_{st}. The acoustic fluid may be in contact with the structure over the surface S_{sa}. The interface between the fluid and the sound package is denoted by S_{at}. The boundary $\partial\Omega_a - S_{sa} \cup S_{at}$ is assumed to be rigid.

The response of the system in the frequency domain is herein considered (i.e. the time dependency $e^{\imath\omega t}$ is implicitly assumed, where ω denotes the circular frequency and $\imath$ is the complex unit). Given a finite element model of the structural and acoustic domains, the linear system describing the dynamics of the master subsystems in terms of modal amplitudes is

$$\begin{bmatrix} \left((1+\imath\eta_s)\omega_{s,i}^2-\omega^2\right)\delta_{ij} & \tilde{\mathbf{C}} \\ \tilde{\mathbf{C}}^{\mathrm{T}} & \left(\frac{\omega_{a,i}^2}{\omega^2}-\frac{1}{(1+\imath\eta_a)}\right)\delta_{ij} \end{bmatrix} \begin{Bmatrix} \mathbf{q}_s(\omega) \\ \mathbf{q}_a(\omega) \end{Bmatrix} = \begin{Bmatrix} \tilde{\mathbf{F}}_s(\omega) \\ \mathbf{0} \end{Bmatrix} + \begin{Bmatrix} \tilde{\mathbf{R}}_s(\omega) \\ \tilde{\mathbf{R}}_a(\omega) \end{Bmatrix}, \tag{3.1}$$

where the unknowns $\mathbf{q}_s$ and $\mathbf{q}_a$ are the amplitudes of the N_s in-vacuo structural modes and N_a rigid-walled cavity modes, respectively. The symbol $\omega_{s,i}$ (resp. $\omega_{a,i}$) refers to the natural frequency of the i^{th} structural (resp. cavity) mode, while δ_{ij} is the Kronecker delta symbol. The dissipation is introduced in Eq. 3.1 using a structural damping model for both the structure (loss factor η_s) and the fluid (loss factor η_a). The superscript $\tilde{}$ above a matrix or vector indicates that it has been projected onto the modal subspace. Thus, $\tilde{\mathbf{C}}$ is the classical modal coupling matrix which accounts for the fluid-structure interaction over the surface S_{sa}. Vector $\tilde{\mathbf{F}}_s$ accounts for the effect of external loads on the structural domain. Finally, $\tilde{\mathbf{R}}_s$ and $\tilde{\mathbf{R}}_a$ are the interface forces due to the presence of the acoustic treatment. They can be formally expressed in terms of modal amplitudes as follows

$$\begin{Bmatrix} \tilde{\mathbf{R}}_s(\omega) \\ \tilde{\mathbf{R}}_a(\omega) \end{Bmatrix} = \begin{bmatrix} \tilde{\mathbf{Y}}_{ss}(\omega) & \tilde{\mathbf{Y}}_{sa}(\omega) \\ \tilde{\mathbf{Y}}_{sa}^{\mathrm{T}}(\omega) & \tilde{\mathbf{Y}}_{aa}(\omega) \end{bmatrix} \begin{Bmatrix} \mathbf{q}_s(\omega) \\ \mathbf{q}_a(\omega) \end{Bmatrix} = \tilde{\mathbf{Y}}(\omega) \begin{Bmatrix} \mathbf{q}_s(\omega) \\ \mathbf{q}_a(\omega) \end{Bmatrix}. \tag{3.2}$$

The three block matrices $\tilde{\mathbf{Y}}_{ss}$, $\tilde{\mathbf{Y}}_{aa}$ and $\tilde{\mathbf{Y}}_{sa}$ constitute the boundary operator $\tilde{\mathbf{Y}}$. Namely, $\frac{1}{\imath\omega}\tilde{\mathbf{Y}}_{ss}$ is the equivalent boundary impedance over S_{st} seen by the structural modes, $\imath\omega\tilde{\mathbf{Y}}_{aa}$ is the equivalent boundary admittance over S_{at} seen by the acoustic cavity modes over the surface S_{at} and $\tilde{\mathbf{Y}}_{sa}$ is an added coupling operator. Thus, the final system reads

$$\left(\tilde{\mathbf{Z}}(\omega)-\tilde{\mathbf{Y}}(\omega)\right)\mathbf{q}(\omega)=\tilde{\mathbf{F}}(\omega)\,, \tag{3.3}$$

where, for sake of conciseness, the modal amplitudes have been gathered in the vector $\mathbf{q}$. The definition of the generalized modal stiffness matrix $\tilde{\mathbf{Z}}$ and of the external load vector $\tilde{\mathbf{F}}$ follows from Eq. 3.1.

In the following sections, it will be shown how the boundary operator $\tilde{\mathbf{Y}}(\omega)$ can be (i) exactly retrieved from a finite element model of the acoustic treatment or (ii) computed approximately from an analytical model of the same acoustic treatment.

3.3.1 Full finite element substructuring

In this section, the matrix $\tilde{\mathbf{Y}}$ is retrieved by means of a finite element model of the acoustic treatment. The methodology is only briefly recalled as a detailed presentation is beyond the scope of this paper. The reader can refer to the work of Hamdi *et al.* [53] for a comprehensive derivation. In what follows, the (u, p) formulation for poroelastic elements developed by Atalla *et al.* [5] is employed.

Let us consider a finite element model of a generic multilayer acoustic treatment, which is assumed to involve solid, fluid and poroelastic domains. The nodal variables are the displacements $\mathbf{U}$ (i.e. solid and porous solid phase displacements) and pressures $\mathbf{P}$ (i.e. acoustic pressures and interstitial pressures) within the acoustic treatment domain. The nodal unknowns are partitioned as follows:

$$\mathbf{U}(\omega) = \left\{ \begin{array}{c} \mathbf{U}_2(\omega) \\ \mathbf{U}_i(\omega) \end{array} \right\}, \quad \mathbf{P}(\omega) = \left\{ \begin{array}{c} \mathbf{P}_0(\omega) \\ \mathbf{P}_1(\omega) \\ \mathbf{P}_i(\omega) \end{array} \right\}, \tag{3.4}$$

where $\mathbf{U}_2$ is a vector containing the nodal displacements over the acoustic treatment-structure interface S_{st}, while $\mathbf{P}_1$ and $\mathbf{P}_0$ contain the nodal pressures over the impervious and permeable subsets of the acoustic treatment-cavity interface S_{at}. The subscript i indicates the remaining internal degrees of freedom. Similarly, the master degrees of freedom at the interfaces are denoted by $\mathbf{U}_{s,2}$, $\mathbf{P}_{a,0}$ and $\mathbf{P}_{a,1}$. As a result, the continuity conditions are $\mathbf{U}_2 = \mathbf{U}_{s,2}$ and $\mathbf{P}_0 = \mathbf{P}_{a,0}$. Employing a set of Lagrange multipliers (i.e. normal displacements $\mathbf{W}$ over the permeable subset of S_{at}) to ensure the pressure continuity over the permeable interface, the finite element equations of the acoustic treatment seen as a substructure can be written as

$$\begin{bmatrix} \mathbf{Z}_{t,\mathrm{U_2U_2}}(\omega) & \mathbf{Z}_{t,\mathrm{U_2U}_i}(\omega) & \mathbf{Z}_{t,\mathrm{U_2P}}(\omega) & \mathbf{0} \\ \mathbf{Z}^{\mathrm{T}}_{t,\mathrm{U_2U}_i}(\omega) & \mathbf{Z}_{t,\mathrm{U}_i\mathrm{U}_i}(\omega) & \mathbf{Z}_{t,\mathrm{U}_i\mathrm{P}}(\omega) & \mathbf{0} \\ \mathbf{Z}^{\mathrm{T}}_{t,\mathrm{U_2P}}(\omega) & \mathbf{Z}^{\mathrm{T}}_{t,\mathrm{U}_i\mathrm{P}}(\omega) & \mathbf{Z}_{t,\mathrm{PP}}(\omega) & -\mathbf{C}_0 \\ \mathbf{0} & \mathbf{0} & -\mathbf{C}_0^{\mathrm{T}} & \mathbf{0} \end{bmatrix} \begin{Bmatrix} \mathbf{U}_2(\omega) \\ \mathbf{U}_i(\omega) \\ \mathbf{P}(\omega) \\ \mathbf{W}(\omega) \end{Bmatrix} = \\ = \begin{bmatrix} \mathbf{C}_2 & \mathbf{0} & \mathbf{0} \\ \mathbf{0} & \mathbf{0} & -\mathbf{C}_1 \\ \mathbf{0} & \mathbf{0} & \mathbf{0} \\ \mathbf{0} & -\mathbf{C}_0^{\mathrm{T}} & \mathbf{0} \end{bmatrix} \begin{Bmatrix} \mathbf{T}(\omega) \\ \mathbf{P}_{a,0}(\omega) \\ \mathbf{P}_{a,1}(\omega) \end{Bmatrix}, \tag{3.5}$$

where matrix $\mathbf{Z}_t$ is the dynamic stiffness of the whole acoustic treatment, while $\mathbf{C}_0$, $\mathbf{C}_1$ and $\mathbf{C}_2$ are classical finite element coupling matrices involving the integral of shape functions products over the interfaces S_{at} and S_{st}. Vector $\mathbf{T}$ contains the stress components over S_{st}. In order to compute the response of the acoustic treatment as a function of the master degrees of freedom $\mathbf{U}_{s,2}$, $\mathbf{P}_{a,0}$ and $\mathbf{P}_{a,1}$, Eq. 3.5 has to be rearranged to give

$$\begin{bmatrix} \mathbf{Z}_{t,\mathrm{U}_i\mathrm{U}_i}(\omega) & \mathbf{Z}_{t,\mathrm{U}_i\mathrm{P}}(\omega) & \mathbf{0} \\ \mathbf{Z}^{\mathrm{T}}_{t,\mathrm{U}_i\mathrm{P}}(\omega) & \mathbf{Z}_{t,\mathrm{PP}}(\omega) & -\mathbf{C}_0 \\ \mathbf{0} & -\mathbf{C}_0^{\mathrm{T}} & \mathbf{0} \end{bmatrix} \begin{Bmatrix} \mathbf{U}_i(\omega) \\ \mathbf{P}(\omega) \\ \mathbf{W}(\omega) \end{Bmatrix} = - \begin{bmatrix} \mathbf{Z}^{\mathrm{T}}_{t,\mathrm{U_2U}_i}(\omega) & \mathbf{0} & \mathbf{C}_1 \\ \mathbf{Z}^{\mathrm{T}}_{t,\mathrm{U_2P}}(\omega) & \mathbf{0} & \mathbf{0} \\ \mathbf{0} & \mathbf{C}_0^{\mathrm{T}} & \mathbf{0} \end{bmatrix} \begin{Bmatrix} \mathbf{U}_{s,2}(\omega) \\ \mathbf{P}_{a,0}(\omega) \\ \mathbf{P}_{a,1}(\omega) \end{Bmatrix}, \tag{3.6}$$

where the continuity condition $\mathbf{U}_2 = \mathbf{U}_{s,2}$ has been explicitly applied. Formally, the solution of Eq. 3.6 can be obtained as

$$\begin{Bmatrix} \mathbf{U}_i(\omega) \\ \mathbf{P}(\omega) \\ \mathbf{W}(\omega) \end{Bmatrix} = -\overline{\mathbf{Z}}_t^{-1}(\omega)\mathbf{C}(\omega) \begin{Bmatrix} \mathbf{U}_{s,2}(\omega) \\ \mathbf{P}_{a,0}(\omega) \\ \mathbf{P}_{a,1}(\omega) \end{Bmatrix} = -\overline{\mathbf{Z}}_t^{-1}(\omega)\mathbf{C}(\omega)\mathbf{V} \begin{Bmatrix} \mathbf{q}_s(\omega) \\ \mathbf{q}_a(\omega) \end{Bmatrix}, \tag{3.7}$$

where the definition of matrices $\overline{\mathbf{Z}}_t$ and $\mathbf{C}$ follows from Eq. 3.6. The matrix $\mathbf{V}$ represents the modal subspace which maps the modal amplitudes in the nodal variables over the interfaces S_{st} and S_{at}. Once the response has been obtained, the acoustic treatment will, in turn, generate a load on the master degrees of freedom, closing the feedback loop. It can be shown [53] that the interface loads $\tilde{\mathbf{R}}_s$ and $\tilde{\mathbf{R}}_a$ acting on the structural and acoustic modes can be retrieved as

$$\left\{ \begin{array}{c} \tilde{\mathbf{R}}_s(\omega) \\ \tilde{\mathbf{R}}_a(\omega) \end{array} \right\} = \left((\mathbf{C}(\omega)\mathbf{V})^{\mathrm{T}} \overline{\mathbf{Z}}_t^{-1}(\omega) (\mathbf{C}(\omega)\mathbf{V}) - \left[\begin{array}{cc} \mathbf{V}_{\mathrm{U}_2}^{\mathrm{T}} \mathbf{Z}_{t,\mathrm{U}_2\mathrm{U}_2}(\omega)\mathbf{V}_{\mathrm{U}_2} & \mathbf{0} \\ \mathbf{0} & \mathbf{0} \end{array} \right] \right) \left\{ \begin{array}{c} \mathbf{q}_s(\omega) \\ \mathbf{q}_a(\omega) \end{array} \right\} = \\ = \tilde{\mathbf{Y}}_{\mathrm{FE}}(\omega)\mathbf{q}\,, \tag{3.8}$$

where $\mathbf{V}_{\mathrm{U}_2}$ is obtained by a partition of the reduced basis $\mathbf{V}$ according to the definition of $\mathbf{U}_2$. The matrix $\tilde{\mathbf{Y}}_{\mathrm{FE}}$ is thus the boundary operator obtained by a finite element model of the acoustic treatment. Eq. 3.8 shows that a linear system with multiple Right Hand Sides (RHSs) must be solved at each frequency of interest to compute $\overline{\mathbf{Z}}_t^{-1}(\mathbf{CV})$. Since the finite element model of the acoustic treatment typically involves a huge number of degrees of freedom, this methodology might be still computationally expensive.

In this work the linear solver PARDISO [98, 99] was used to perform the matrix operation $\overline{\mathbf{Z}}_t^{-1}(\mathbf{CV})$ at each discrete frequency where the solution of the modal system in Eq. 3.3 was of interest. The selected solver allows for parallel computing.

3.3.2 Green functions based hybrid FE-TMM

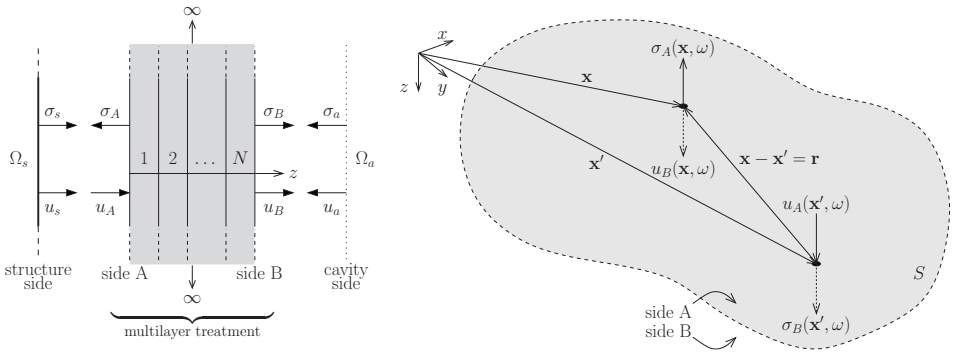

Figure 3.2 Geometry of the acoustic treatment. Through-the-thickness view of the multilayer (left) and top view (right) of the treated surface S.

In this section some approximations are introduced in order to avoid the finite element modeling of the whole acoustic treatment. The latter is, instead, modeled by means of an analytical approach based on the Green functions formalism. In order to employ this simplification, the acoustic treatment is assumed (i) isotropic, (ii) homogeneous in the plane (i.e. thickness, lay-up and material properties do not change over the treated surface), (iii) flat (unwrapped if any curvature is present) and (iv) of infinite extent (lateral boundary conditions are neglected). As a consequence, the interfaces S_{st} and S_{at} formally

coincide and will be referred to as the treated surface S. Therefore, the acoustic treatment can be seen as an equivalent reacting surface in contact with the structure over its side A and with the cavity over its side B (see Fig. 3.2). Only normal displacements and stresses are considered at the two sides of the treatment.

Let $u_A(\mathbf{x},\omega)$ and $\sigma_A(\mathbf{x},\omega)$ be the normal displacement and normal stress over side A of the acoustic treatment. Similarly, $u_B(\mathbf{x},\omega)$ and $\sigma_B(\mathbf{x},\omega)$ are the normal displacement and normal stress over side B in contact with the acoustic cavity. The vector $\mathbf{x}$ indicates the position over the surface S. Under these conditions, the response of the acoustic treatment in terms of reactions σ_A and u_B over the two sides of the surface S can be directly obtained invoking the Green function formalism:

$$\left\{\begin{array}{rcl} \sigma_A(\mathbf{x},\omega) & = & \displaystyle\int_S g_{AA}(r,\omega)u_A(\mathbf{x}',\omega)\,\mathrm{d}\mathbf{x}' + \int_S g_{AB}(r,\omega)\sigma_B(\mathbf{x}',\omega)\,\mathrm{d}\mathbf{x}' \\ u_B(\mathbf{x},\omega) & = & \displaystyle\int_S g_{BA}(r,\omega)u_A(\mathbf{x}',\omega)\,\mathrm{d}\mathbf{x}' + \int_S g_{BB}(r,\omega)\sigma_B(\mathbf{x}',\omega)\,\mathrm{d}\mathbf{x}' \end{array}\right. , \tag{3.9}$$

where r is the module of the distance vector $\mathbf{r} = |\mathbf{x} - \mathbf{x}'|$ pointing from $\mathbf{x}'$ to $\mathbf{x}$. The functions $g_{mn}(r,\omega)$ ($m = A, B$ and $n = A, B$) are the Green functions of the problem. The domain S represents the support of u_A and σ_B, i.e. they are assumed to be zero outside the surface S. It is noted in passing that Eq. 3.9 can be rearranged to account for different boundary conditions outside the area S at the two ends of the treatment. However, in the present paper, the formulation above is adopted for its efficiency, as it allows reactions σ_A and u_B to be directly evaluated (i.e. avoiding any matrix inversion). A set of radially symmetric shape functions obtained by translation is employed to expand the normal displacement u_A and normal stress σ_B in Eq. 3.9 as

$$\begin{array}{rcl} u_A(\mathbf{x},\omega) & = & \psi(|\mathbf{x}-\mathbf{x}_j|)\,a_j(\omega) = \psi_j(r)\,a_j(\omega)\,, \\ \sigma_B(\mathbf{x},\omega) & = & \psi(|\mathbf{x}-\mathbf{x}_j|)\,b_j(\omega) = \psi_j(r)\,b_j(\omega)\,, \end{array} \tag{3.10}$$

where the sum over repeated index is implicitly assumed. The coefficients a_j and b_j are the participation factors of the j^{th} shape function $\psi_j(r)$.

Under the aforementioned hypothesis, it is useful to continue the analysis in the wavenumber domain, where the Green functions can be easily computed. Thus, substituting Eq.

3.10 in Eq. 3.9, integrating over the surface S, projecting onto the shape functions subspace and employing the convolution theorem yields [1]

$$\begin{cases} R_{A_i}(\omega) &= G_{AA}(r_{ij},\omega)\, a_j(\omega) + G_{AB}(r_{ij},\omega)\, b_j(\omega) \\ R_{B_i}(\omega) &= G_{BA}(r_{ij},\omega)\, a_j(\omega) + G_{BB}(r_{ij},\omega)\, b_j(\omega) \end{cases} , \tag{3.11}$$

where $r_{ij} = |\mathbf{r}_{ij}|$ is the Euclidean distance between the nodes $\mathbf{x}_j$ and $\mathbf{x}_i$ over the treated surface. R_{A_i} and R_{B_i} are the normal stress at side A and normal displacement at side B projected onto the i^{th} shape function (i.e. force and displacement flux, respectively). The functions $G_{mn}(r_{ij},\omega)$ ($m = A, B$ and $n = A, B$) are defined as

$$G_{mn}(r_{ij},\omega) = \frac{1}{2\pi}\int_0^\infty \hat{g}_{mn}(k,\omega) J_0(k r_{ij}) k |\hat{\psi}(k)|^2 \,\mathrm{d}k \,, \tag{3.12}$$

where $k = |\mathbf{k}|$ is the modulus of the wavenumber and $J_0(k r_{ij})$ is the Bessel function of zero order of argument $k r_{ij}$. The formalism $\hat{f}(k)$ indicates the radially symmetric Fourier Transform (FT), i.e. Hankel transform, of the function $f(r)$. The fundamental kernels $\hat{g}_{mn}(k,\omega)$ can be sampled over the (k,ω) space using the TMM (see appendix A). The coupling Green functions satisfy the reciprocity condition $\hat{g}_{AB}(k,\omega) = \hat{g}_{BA}(k,\omega)$. Eqs. 3.9 and 3.11 come as a natural extension of what has been recently proposed by the authors in Ref. [1] (see chapter 2).

In this work, linear shape functions with compact support R are employed, i.e.

$$\psi(r) = \begin{cases} 1 - \dfrac{r}{R} & \text{if } r \le R \\ 0 & \text{if } r > R \end{cases} . \tag{3.13}$$

This class of radially symmetric functions has been already used by the authors and has shown good performances compared with a classical linear finite element approximation [1]. Thus, in what follows, the collocation nodes $\mathbf{x}_j$ on the treated surface S are assumed to be associated to a structured finite element mesh which involves elements of the same size. Each nodal displacement and pressure defined on the finite element mesh is then approximated by Eq. 3.13. Consequently, in analogy with the finite element shape functions, the coefficients a_j and b_j are assumed to be the nodal normal displacements U_{A_j}

and stresses Σ_{B_j}, respectively. This choice allows for a simple and direct approximation of the boundary operator. Indeed, under these circumstances, if the collocation nodes also coincide with the finite element nodes of the structural and acoustic domains, the continuity conditions can be easily applied as $\mathbf{R}_s = \mathbf{R}_A$, $\mathbf{R}_a = -\mathbf{R}_B$, $\mathbf{U}_{s,2} = \mathbf{U}_A$ and $\mathbf{P}_{a,0/1} = -\mathbf{\Sigma}_B$ (see Fig. 3.2). Thus Eq. 3.11 can be rearranged in matrix form as

$$\left\{ \begin{array}{c} \mathbf{R}_s(\omega) \\ \mathbf{R}_a(\omega) \end{array} \right\} = \left[\begin{array}{cc} \mathbf{G}_{AA}(\omega) & -\mathbf{G}_{AB}(\omega) \\ -\mathbf{G}_{AB}^{\mathrm{T}}(\omega) & \mathbf{G}_{BB}(\omega) \end{array} \right] \left\{ \begin{array}{c} \mathbf{U}_{s,2}(\omega) \\ \mathbf{P}_{a,0/1}(\omega) \end{array} \right\}, \tag{3.14}$$

where $\mathbf{R}_s$ and $\mathbf{R}_a$ are the nodal loads acting on the master degrees of freedom. The vector $\mathbf{U}_{s,2}$ contains the displacements of the structural domain over S, while $\mathbf{P}_{a,0/1}$ indicates that the nodal pressures of the acoustic domain over S may refer to the permeable or impervious subset given that the acoustic trim is assumed homogeneous (the latter interface condition affects the calculation of the Green functions, but Eq. 3.14 remains formally unchanged). It should be noted that, due to the assumptions inherent within the analytical framework, $\mathbf{R}_s$ and $\mathbf{U}_{s,2}$ refer only to normal components. On the other hand, the exact finite element methodology presented in Section 3.3.1 can account for various coupling conditions (e.g. sound package glued or sliding onto the structure). Projecting Eq. 3.14 onto the modal basis, one obtains

$$\left\{ \begin{array}{c} \tilde{\mathbf{R}}_s(\omega) \\ \tilde{\mathbf{R}}_a(\omega) \end{array} \right\} = \mathbf{V}^{\mathrm{T}} \left[\begin{array}{cc} \mathbf{G}_{AA}(\omega) & -\mathbf{G}_{AB}(\omega) \\ -\mathbf{G}_{AB}^{\mathrm{T}}(\omega) & \mathbf{G}_{BB}(\omega) \end{array} \right] \mathbf{V} \left\{ \begin{array}{c} \mathbf{q}_s(\omega) \\ \mathbf{q}_a(\omega) \end{array} \right\} = \tilde{\mathbf{Y}}_{\mathrm{GF}} \mathbf{q}\,, \tag{3.15}$$

where $\tilde{\mathbf{Y}}_{\mathrm{GF}}$ is the boundary operator obtained using the Green functions computed by means of the TMM. Thus, the efficiency of the present hybrid FE-TMM resides mainly in the numerical quadrature of Eq. 3.12, as matrix inversions are avoided. Moreover, the evaluations of $G_{mn}(r_{ij}, \omega)$ for different values of r_{ij} are completely independent, making the methodology suitable for parallel computing. However, in the present work, a serial implementation was considered.

3.3.3 Interpretation of the analytical model and further approximations

Thanks to the use of radially symmetric shape functions obtained by translation, Eq. 3.12 involves a one-dimensional integration for a given distance r_{ij} between two nodes.

However, in the case of generic functions (i.e. non radially symmetric), the (i, j) component of $G_{mn}(\omega)$ is given by a full integration in the (k_x, k_y) space [1], i.e.

$$G_{mn}(\psi_i, \psi_j, \omega) = \frac{1}{(2\pi)^2} \int_{\mathbf{k}} \hat{\psi}_i^*(\mathbf{k}) \hat{g}_{mn}(|\mathbf{k}|, \omega) \hat{\psi}_j(\mathbf{k}) \, \mathrm{d}\mathbf{k} \,, \tag{3.16}$$

where the superscript * indicates the conjugate of a complex number. Functions $\hat{\psi}_i(\mathbf{k})$ and $\hat{\psi}_j(\mathbf{k})$ can be, for instance, the FTs of the structural and/or cavity modes over the surface S. The integration involved in Eq. 3.16 reveals that the response of the laterally infinite acoustic treatment is given by a continuous set of waves, i.e. all the wavenumber couples (k_x, k_y) are allowed to propagate through the thickness. On the other hand, as a consequence of the presence of lateral boundaries, the response of the bounded system is given by a discrete distribution of travelling waves, i.e. the planar modes of the finite size acoustic treatment. Equivalently (and perhaps more suitably in the context of waves propagation in dissipative media), an interpretation in terms of direct and reflected wave fields [73] might help the reader. Namely, the analytical model (Eq. 3.15 and 3.16) accounts only for direct field effects, as the reflections at the lateral boundaries of the sound package are neglected. Although such approximation may be justified for passive acoustic treatments (i.e. the reflected field is non diffuse), the reflected field might be still important close to the boundaries of the treated surface S. For instance, at some frequencies, the interference between direct and reflected fields may be non negligible, leading to modal resonances. In such case, the analytical model will be able to capture the global behavior of the sound package (i.e. global resonances, which are only functions of the thickness), while the local behavior due to a single modal contribution (i.e. modal resonance) will be, if dominant, missed. As a consequence, it can be argued that the two models are expected to converge to the same solution as the response of the bounded acoustic treatment involves (i) a "sufficient" number of traveling modes and (ii) "enough" dissipation. The impact of these assumptions will be assessed in Section 3.4.

The interpretation of Eq. 3.16 in terms of structural and/or cavity modes allows for further simplifications of the model. For instance, if the modal coupling is neglected (i.e. $G_{mn}(\psi_i, \psi_j, \omega) = 0$ if $i \neq j$), the integrand in Eq. 3.16 is modulated by $|\hat{\psi}_i(\mathbf{k})|^2$, which tends to exhibit a sharp peak around the dominating modal wavenumber component $\mathbf{k}_t$. As a result, if one also assumes that the Green function varies slowly with $\mathbf{k}$ compared to $|\hat{\psi}_i(\mathbf{k})|^2$, then $\hat{g}_{mn}(k, \omega)$ can be sampled at $k_t = |\mathbf{k}_t|$ and carried outside the integral yielding

$$G_{mn}(\psi_i, \omega) = \frac{\hat{g}_{mn}(k_t\left(\psi_i\right), \omega)}{\left(2\pi\right)^2} \int_{\mathbf{k}} |\hat{\psi}_i(\mathbf{k})|^2 \, \mathrm{d}\mathbf{k} \,, \tag{3.17}$$

which is the hybrid modal-TMM proposed by Rhazi and Atalla [92, 93]. However, the approximation can be employed only for the diagonal blocks of $\tilde{\mathbf{Y}}_{\mathrm{GF}}$, since the coupling between different modes is neglected. Moreover, the approach appears convenient only when the modal shapes and their dominating wavenumber components are known analytically, that is, generally speaking, when trigonometric functions can be employed (e.g. Ritz method).

Another approximation of Eq. 3.16 can be obtained if the Green function is assumed to vary slowly over the entire wavenumber spectrum. In such case, the Green function can be approximated by its value at a prescribed wavenumber k_0, yielding

$$G_{mn}(\psi_i, \psi_j, \omega) = \frac{\hat{g}_{mn}(k_0, \omega)}{\left(2\pi\right)^2} \int_{\mathbf{k}} \hat{\psi}_i^*(\mathbf{k}) \hat{\psi}_j(\mathbf{k}) \, \mathrm{d}\mathbf{k} \,, \tag{3.18}$$

which physically represents the behavior of a locally reacting system, whose acoustic impedance [3, 86] is denoted by $\hat{g}_{mn}(k_0, \omega)$ (with an abuse of notation since $\hat{g}_{mn}(k_0, \omega)$ does not have necessarily the dimensions of an impedance). However, the choice of the local kernel $\hat{g}_{mn}(k_0, \omega)$ is, generally speaking, hard to justify since typical acoustic treatments do not exhibit constant Green functions over a wide wavenumber spectrum. However, this approach is typically used for practical applications because of its efficiency. Indeed, the wavenumber integral in Eq. 3.18 involves only the coupling between structural and/or cavity modes and can be computed in the physical domain with negligible computational effort. Therefore, Eq. 3.15 can be simplified to give

$$\left\{ \begin{array}{c} \tilde{\mathbf{R}}_s(\omega) \\ \tilde{\mathbf{R}}_a(\omega) \end{array} \right\} = \left[\begin{array}{cc} \hat{g}_{AA}(k_0, \omega)\, c_{s,i} \delta_{ij} & \hat{g}_{AB}(k_0, \omega)\, \tilde{\mathbf{C}} \\ \hat{g}_{AB}(k_0, \omega)\, \tilde{\mathbf{C}}^{\mathrm{T}} & -\hat{g}_{BB}(k_0, \omega)\, c_{a,ij} \end{array} \right] \left\{ \begin{array}{c} \mathbf{q}_s(\omega) \\ \mathbf{q}_a(\omega) \end{array} \right\} = \tilde{\mathbf{Y}}_{\mathrm{LR}} \mathbf{q} \,, \tag{3.19}$$

where $c_{s,i}$ and $c_{a,ij}$ are coefficients which depend on the adopted normalization for the structural and acoustic modal basis, while $\tilde{\mathbf{C}}$ is the modal coupling matrix describing the

fluid-structure modal interaction over the treated surface S. In what follows, the local kernel is chosen by sampling the Green functions at $k = 0$.

3.4 Results

In this section numerical examples are provided to assess the performance of the hybrid FE-TMM. First, some representative entries of the boundary operators $\tilde{\mathbf{Y}}_{\mathrm{FE}}$ and $\tilde{\mathbf{Y}}_{\mathrm{GF}}$ are compared to quantify the impact of the assumptions inherent within the analytical model of the acoustic treatment. Then, a plate-cavity system is considered to assess the accuracy of the assembled finite element-transfer matrix model in terms of global indicators.

Fig. 3.3 shows the geometry considered for the numerical simulations. A 2 mm thick plate of dimensions $L_{x_p} \times L_{y_p}\,\mathrm{m}^2$ is clamped along its edges and excited by a point force. The acoustic treatment, of uniform thickness h_t, is attached onto the structure and radiates inside an acoustic cavity of dimensions $L_{x_c} \times L_{y_c} \times L_{z_c}\,\mathrm{m}^3$. The plate is made of steel, while the acoustic cavity is filled with air. The mechanical and acoustic properties of the materials are listed in Tab. 3.1. A dissipation is introduced in the acoustic domain by a structural damping model to represent the effect of other dissipative elements within the acoustic cavity. The acoustic treatment can slide along its lateral boundaries, which are assumed to be rigid (i.e. the normal component of the solid phase displacement is fixed) and impervious (i.e. the flux through the boundary is zero). Only normal components are involved in the continuity conditions at the interface between the plate and the acoustic treatment.

3.4.1 Preliminary Assessment of the Green functions based FE-TMM

In this section, the accuracy of the hybrid methodology is assessed at the substructure level (i.e. matrix $\tilde{\mathbf{Y}}_{\mathrm{GF}}$). Namely, the response of the acoustic treatment obtained by the Green functions methodology (Eq. 3.15) is compared with the reference finite element solution (Eq. 3.8). It has been observed in Section 3.3.3 that the main difference between the Green functions and finite element models of the acoustic treatment resides in the number of waves which are allowed to propagate through the thickness, or, equivalently, in the effect of wave reflections at the lateral boundaries. This particular aspect (i.e. finite lateral extent) is discussed here.

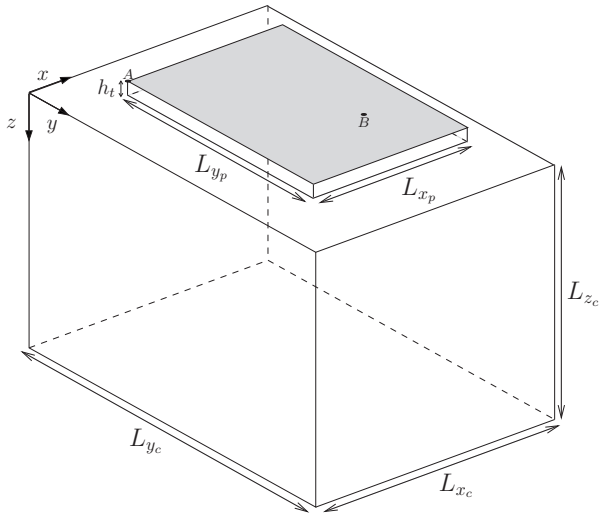

Figure 3.3 Plate-cavity system considered in the numerical simulations. Point A defines the position of the plate over the (x, y) plane. B is the application point of the mechanical force.

The acoustic treatment considered in this analysis has dimensions $L_{x_p} = L_{x_c} = 0.4\,\mathrm{m}$ and $L_{y_p} = L_{y_c} = 0.8\,\mathrm{m}$ (see Fig. 3.3). Two different layups are considered. The first (referred to as *light* treatment) consists of a one layer involving a 2 cm thick melamine foam (poroelastic properties listed in Tab. 3.1). The second lay-up (referred to as *spring-mass* treatment) consists, instead, of two layers, namely a 2 cm thick melamine foam and a $1.2\,\mathrm{kg/m^2}$ heavy layer. The latter was modeled as a 1 mm thick solid layer with negligible stiffness (i.e. limp solid, see Tab. 3.1). The poroelastic layer is attached onto the structure (i.e. side A), while the heavy layer is wetted by the fluid inside the cavity (i.e. side B). Concerning the finite element model, nine Hexa-8 equivalent fluid or poroelastic elements (depending on whether the solid phase is considered limp or not) and one Hexa-8 solid element are used in the thickness direction for the modeling of the poroelastic and solid layers, respectively. The choice of the mesh size over the (x, y) plane was driven by the shortest wavelength exhibited in the considered spectrum by the master subsystems, while the number of elements through the thickness of the acoustic treatment guarantees that the shortest Biot wave is captured correctly over the frequency domain of interest (i.e. eight elements per wavelength were used in the plane and the thickness direction).

The light acoustic treatment is first considered. The frame of the poroelastic material is considered limp, thus the treatment is modeled as an equivalent fluid. Fig. 3.4(a) shows the absolute value of the diagonal entry $\tilde{\mathrm{Y}}_{ii}$ corresponding to the 1^{st} and 100^{th} structural modes (S1 and S100, respectively). The corresponding bending wavenumbers k_s exhibited by the plate modes are $12\,\mathrm{rad/m}$ and $70,9\,\mathrm{rad/m}$, respectively. A perfect agreement between

Table 3.1 Materials used in the numerical simulations.

Material	**Properties**	
	Acoustic	**Mechanical**
Steel		density = $8000\,\mathrm{kg/m^3}$ Young's modulus = $200\,\mathrm{GPa}$ Poisson's ratio = 0.33 damping factor = 0.02
Air	density = $1.21\,\mathrm{kg/m^3}$ speed of sound = $342.2\,\mathrm{m/s}$ damping factor = 0.1	
Melamine	porosity = 0.99 resistivity = $10900\,\mathrm{kg/m^3 s}$ tortuosity = 1.02 viscous length = $100\,\mu\mathrm{m}$ thermal length = $130\,\mu\mathrm{m}$	density = $8.8\,\mathrm{kg/m^3}$ Young's modulus = $80\,\mathrm{kPa}$ Poisson's ratio = 0.4 damping factor = 0.17
Limp solid		density = $1200\,\mathrm{kg/m^3}$ Young's modulus = $10^3\,\mathrm{kPa}$ Poisson's ratio = 0.3 loss factor = 0.5

the finite element and Green functions solutions is observed. Fig. 3.4(b) shows, instead, the imaginary part (i.e. dissipative effects) of the diagonal entry $\tilde{\mathrm{Y}}_{ii}$ corresponding to the 7^{th} and 185^{th} acoustic modes (A7 and A185, respectively). The in-plane acoustic wavenumber k_a exhibited by the cavity modes is $8.8\,\mathrm{rad/m}$ and $37\,\mathrm{rad/m}$, respectively. The figure shows that the Green functions approximation leads to a large overestimation of the damping at low to mid frequencies. This behavior can be explained by the fact that, unlike the case of the clamped plate, the dynamics of the acoustic cavity along the acoustic treatment boundary is important (i.e. maxima of pressure and normal displacement always occur in the considered configuration). As a consequence, finite size effects (i.e. reflected waves) cannot be neglected without loosing accuracy. Moreover, this effect is particularly pronounced for the geometry considered here, since, due to orthogonalities between the limp layer and the cavity modes, the resonance at $500\,\mathrm{Hz}$ is due to one single modal contribution. Thus, the number of propagating modes and the dissipation are not high enough in the low frequency range to meet the requirements for the Green functions model to give reliable results. However, at higher frequency, agreement between the finite element and Green functions solutions is obtained, thanks to the increasing dissipative effects. Moreover, shorter wavelengths (see higher order mode A185 in Fig. 3.4(b)) give a better correlation. The same observations holds for a poroelastic model of the acoustic treatment, since, for the considered problem (i.e. calculation of $\tilde{\mathbf{Y}}_{aa}$ for the light treatment), the structural frame is not particularly excited.

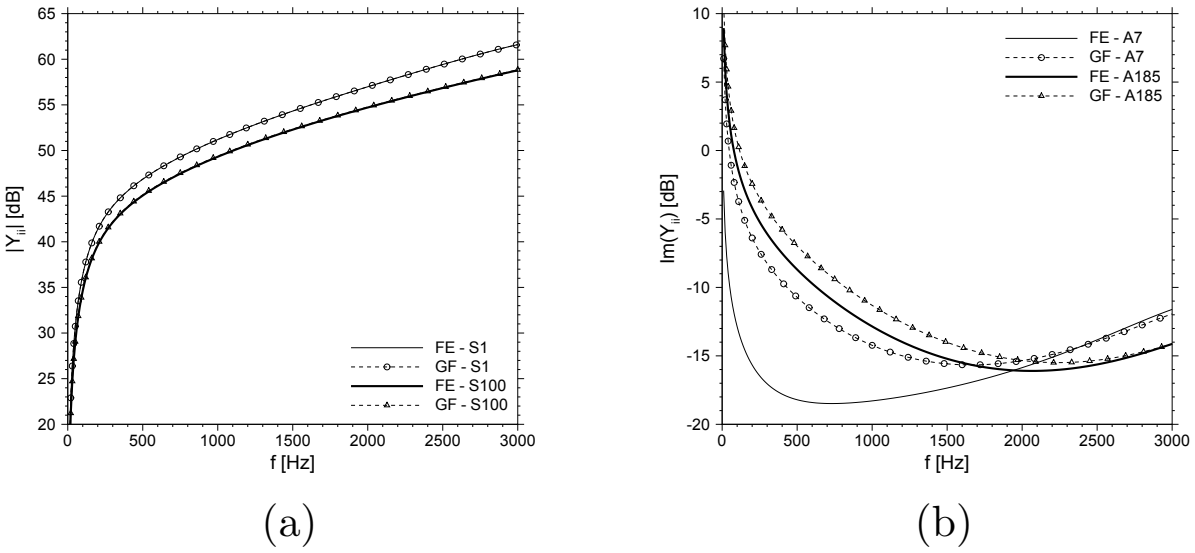

Figure 3.4 Diagonal entry $\tilde{\mathrm{Y}}_{ii}$ of the boundary operator evaluated by the finite element (FE) and the Green functions (GF) methodology. (a): absolute value for structural modes S1 and S100. (b): imaginary part for acoustic modes A7 and A185. Results relative to the light acoustic treatment.

The spring-mass (i.e. foam-heavy layer) acoustic treatment is considered in Fig. 3.5(a). The frame of the poroelastic material is, again, considered limp, so that only the stiffness of the equivalent fluid is involved. Fig. 3.5(a) shows the absolute value of the diagonal entry $\tilde{\mathrm{Y}}_{ii}$ corresponding to the 5^{th} structural mode for a treatment of nominal and doubled planar dimensions (i.e. $0.4 \times 0.8\,\mathrm{m}^2$ and $0.8 \times 1.6\,\mathrm{m}^2$, respectively). The thickness of the treatment remains, instead, unchanged. The bending wavenumber k_s exhibited by the plate mode is about $20\,\mathrm{rad/m}$ ($10\,\mathrm{rad/m}$ for the double size system). The results show that the Green functions approximation suffers from a loss of accuracy around the global peak between 300 and 400 Hz. The response of the sound package is, in fact, non local at the resonance peak so that the effect of the lateral boundaries (i.e. reflected field) is non negligible. Nonetheless, the average response is captured. However, Fig. 3.5(a) shows that when the planar dimensions are doubled, the analytical model gets more accurate. This is not surprising, since the larger is the system the bigger is the portion of acoustic treatment unaffected by the reflected field emanating from the lateral boundaries.

Fig. 3.5(b) refers, instead, to the light acoustic treatment. The coupling between the two phases is now considered within the porous media. Thus, the solid frame of the poroelastic layer is directly excited by the displacement field imposed by the structural domain over side A of the treatment. The same analysis performed above for the spring-

mass acoustic treatment is carried out. However, in this case, the accuracy of the Green functions model at the foam resonances does not improve when the size of the system doubles. This is due to the fact that, for this configuration, the response of the acoustic treatment is controlled by one structure borne wave (i.e. the same mode which would travel through the thickness if the poroelastic layer was modeled considering only its solid phase). Around the peaks, the Green functions model fails as the effect of one dominant modal contribution (or, equivalently, of the reflected field) cannot be predicted by the analytical model. Similarly, it could be shown that the resonances of the indirect coupling term induced by the acoustic treatment (i.e. $\tilde{\mathbf{Y}}_{sa}$ in Eq. 3.2) are underestimated as well. Nevertheless, the global behavior of the system is always captured and the gap between the two curves narrows as the frequency increases (thanks to dissipative effects). The same behavior was observed for the spring-mass acoustic treatment, which is not shown here for the sake of conciseness.

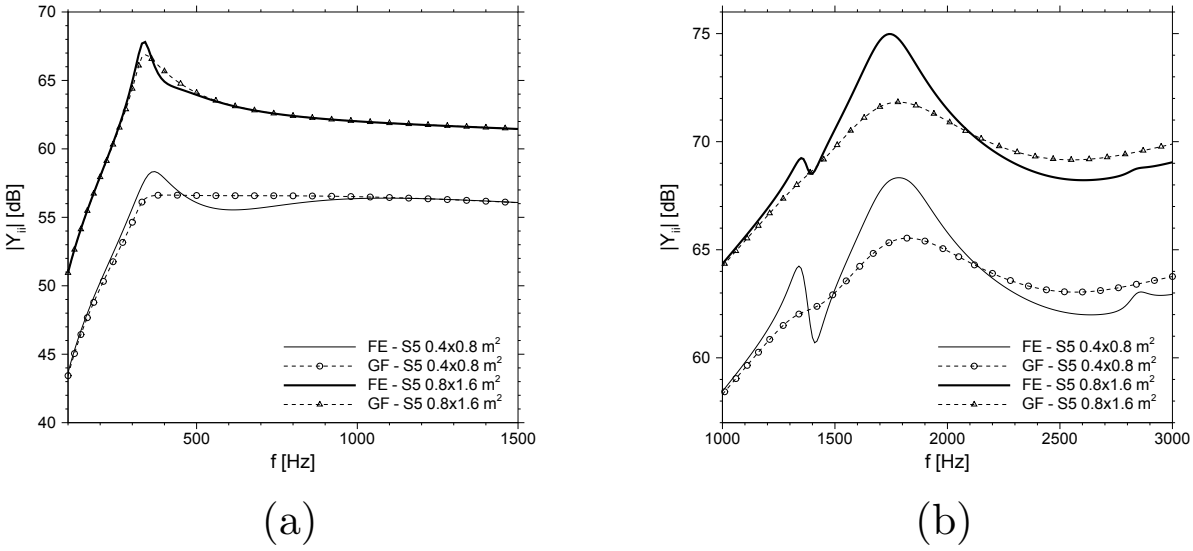

Figure 3.5 Absolute value of the diagonal entry $\tilde{\mathrm{Y}}_{ii}$ of the boundary operator corresponding to the structural mode S5 evaluated by the finite element (FE) and the Green functions methodology (GF). Effect of the acoustic treatment lateral dimensions. (a): spring-mass lay-up, limp model. (b): light lay-up, poroelastic model.

Thus, one can conclude that, generally speaking, the larger are the lateral dimensions of the trimmed area, the better is the accuracy of the analytical model. However, although typical acoustic trim configurations seem to match the requirements for the Green functions model to give reliable results (i.e. short wavelength and dissipation), the accuracy of the model

may, in some cases, worsens. In fact, due to the nature of the coupling between the structure (resp. acoustic cavity) and the sound package, it can occur that only few wave components (one in the cases above) are excited by the master subsystem. Nevertheless, the global behavior of the system is always captured.

3.4.2 Application to a plate-cavity system

The inaccuracies of the analytical model identified in Section 3.4.1 will consequently affect the accuracy of the assembled hybrid model. Namely, when the boundary operator $\tilde{\mathbf{Y}}_{\mathrm{GF}}$ obtained by means of the Green functions model is used in Eq. 3.3 instead of the exact operator $\tilde{\mathbf{Y}}_{\mathrm{FE}}$, discrepancies with the reference solution must be expected. The purpose of this section is to illustrate the effect of the approximation introduced by the hybrid model when the global vibroacoustic parameters of a plate-cavity system are of interest.

The system considered in the numerical simulations involves a structural plate of dimensions $L_{x_p} = 0.595\,\mathrm{m}$, $L_{y_p} = 1.554\,\mathrm{m}$ and an acoustic cavity of dimensions $L_{x_c} = 0.8\,\mathrm{m}$, $L_{y_c} = 1.7\,\mathrm{m}$ and $L_{z_c} = 1\,\mathrm{m}$. Point A (see Fig. 3.2) is located at $(0.074\,\mathrm{m}, 0.056\,\mathrm{m})$. The system is excited by a point force acting on the structure along the z-axis at point B located at $(0.167\,\mathrm{m}, 0.187\,\mathrm{m})$. The two acoustic treatments used in Section 3.4.1 (i.e. light and spring-mass layups) are considered. The vibroacoustic system is solved in the frequency range between 10 Hz and 1 KHz. Eight elements per wavelength were used to mesh the structural and acoustic finite element domains. The finite element mesh along the thickness of the porous layer involves five Hexa-8 poroelastic elements, while for the heavy layer one Hexa-8 solid element is used. The mechanical and acoustic properties of the plate and fluid are reported in Tab. 3.1. Three solution strategies are considered: the full finite element substructuring methodology (referred to as FEM, this is the reference solution for the considered analysis), the Green functions based FE-TMM (referred to as FE-TMM(GF)) and the simplified locally reacting model (referred to as FE-TMM(LR)).

Fig. 3.6 shows the space averaged quadratic velocity of the plate when the light treatment is placed between the structure and the cavity. A few discrepancies between the FE-TMM(GF) solution and the reference finite element prediction are observed between 400 Hz and 600 Hz. In this frequency range, the structural frame of the poroelastic layer strongly interacts with the dynamics of the plate (i.e. a thickness resonance of the sound package falls very close to the resonance of some plate modes, so that the dissipation introduced by the treatment is maximized). However, as already discussed, such effect on the plate dynamics is underestimated by the FE-TMM(GF) for this particular configuration (cf. Fig. 3.5(b)). Nevertheless, overall, both the hybrid models provide a good

prediction of the plate vibrational energy. Conversely, Fig. 3.7 shows that the prediction of the quadratic pressure in the cavity does not exhibit the same accuracy. Indeed, the FE-TMM(GF) is known to introduce overdamping in each cavity mode at low frequency (cf. Fig. 3.4(b)). Consequently, the quadratic pressure gets underestimated as soon as the cavity modes start to participate to the response (first non null acoustic mode occurs at 100 Hz). However, as already observed in Section 3.4.1, a better correlation is observed at higher frequencies, where a convergent behavior can be inferred. On the other hand, the FE-TMM(LR) solution shows that the Green functions of the considered acoustic treatment cannot be considered constant over the frequency band of interest, as a divergent trend from the reference finite element solution is observed. The inaccuracy of the FE-TMM(LR) (for both the structural and acoustic indicators) at higher frequencies was confirmed by further analysis, where a smaller system was considered to allow for the computation of the system response up to 3 KHz. However the results are not shown here for the sake of conciseness.

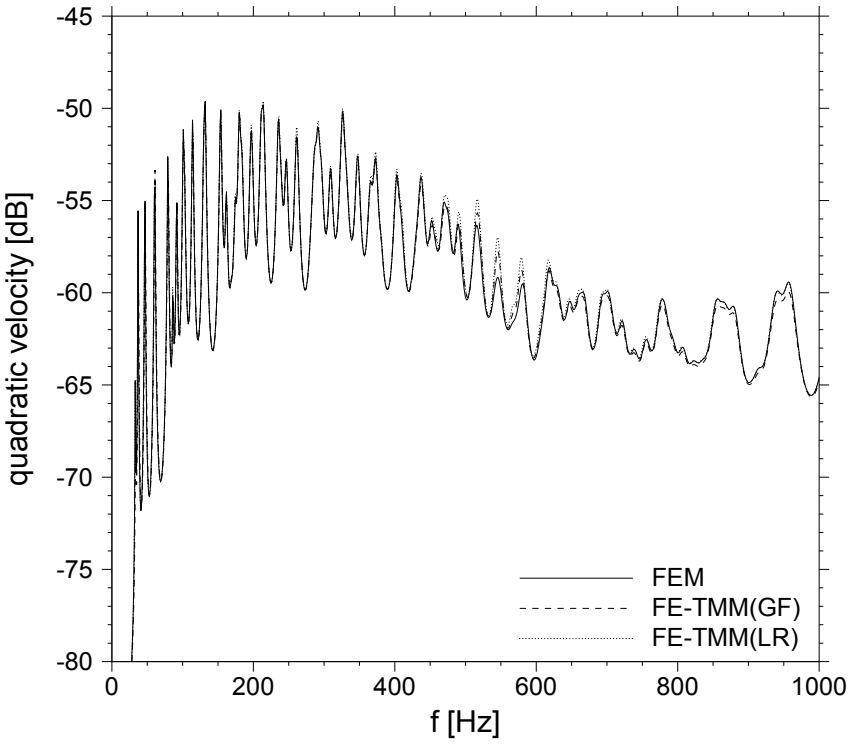

Figure 3.6 Quadratic velocity of the clamped plate. Comparison between the FEM, the FE-TMM(GF) and the FE-TMM(LR). Results relative to the light acoustic treatment.

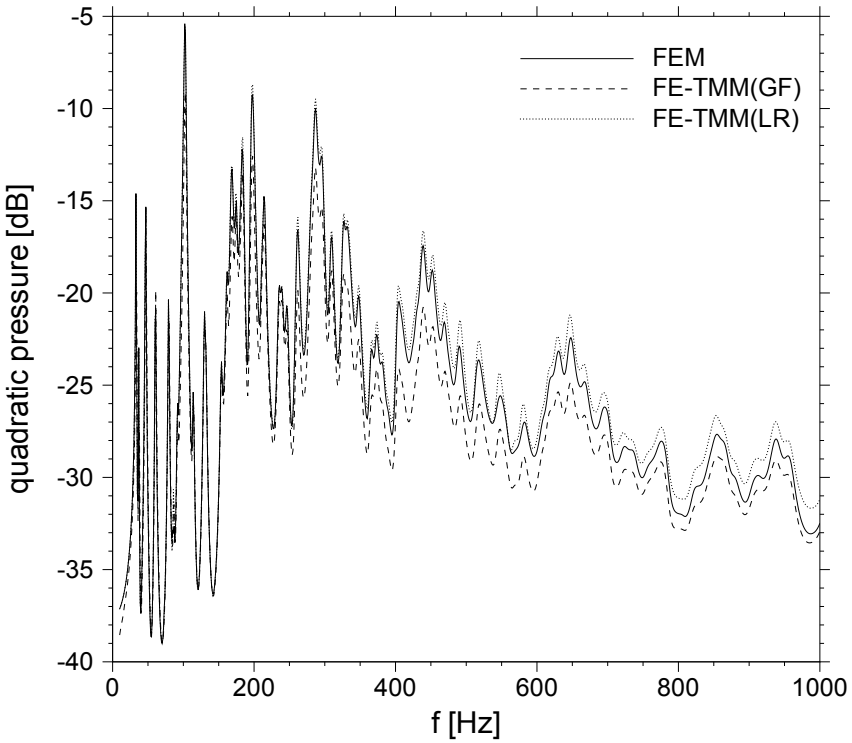

Figure 3.7 Quadratic pressure of the acoustic cavity. Comparison between the FEM, the FE-TMM(GF) and the FE-TMM(LR). Results relative to the light acoustic treatment.

Fig. 3.8 shows the quadratic velocity of the plate when the spring-mass treatment is considered. Now, the effect of the mass at the top of the foam leads to a strong resonance (i.e. double wall resonance) at 350 Hz. The FE-TMM(GF) solution correctly follows the reference, even though the strong interaction at the double wall resonance is, as already observed in Fig. 3.6, only captured on average. On the other hand, the FE-TMM(LR) fails, as neither the damping nor the mass effects introduced by the acoustic treatment are captured correctly. Fig. 3.9 shows the comparison of the three solutions for the quadratic pressure inside the cavity. Once again, it can be observed that the FE-TMM(GF) is not able to capture accurately the structural frame effects at the transmission resonances around 500 Hz and 900 Hz, where the power injected to the cavity is underestimated (and so the quadratic pressure). Nevertheless, the qualitative behavior of the finite element solution is always fulfilled. On the other hand, the FE-TMM(LR) solution confirms that spring-mass treatments cannot be assumed to be locally reacting.

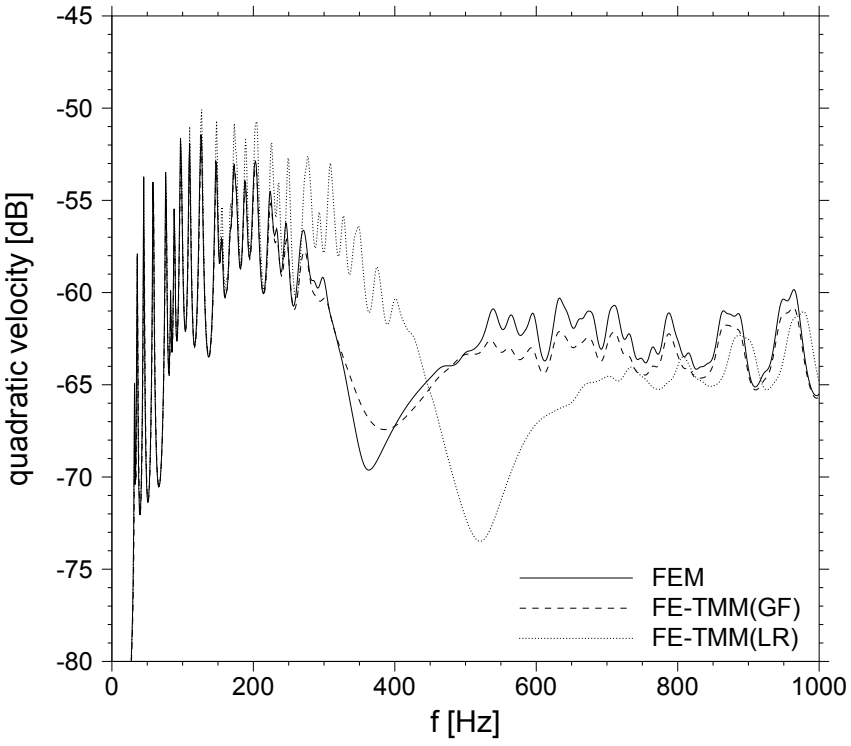

Figure 3.8 Quadratic velocity of the clamped plate. Comparison between the FEM, the FE-TMM(GF) and the FE-TMM(LR). Results relative to the spring-mass acoustic treatment.

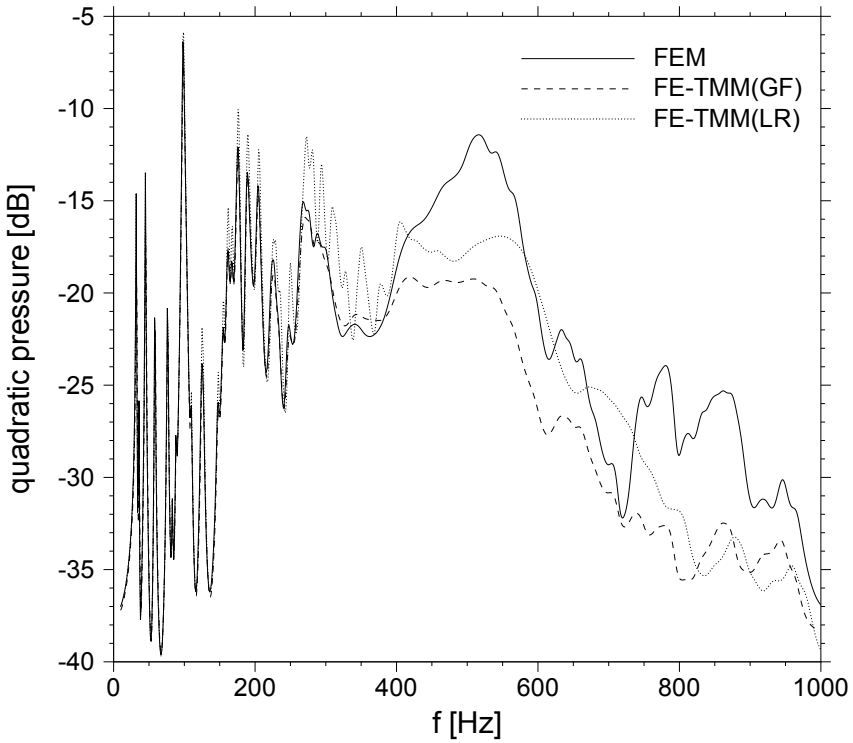

Figure 3.9 Quadratic pressure of the acoustic cavity. Comparison between the FEM, the FE-TMM(GF) and the FE-TMM(LR). Results relative to the spring-mass acoustic treatment.

As already shown in Section 3.4.1, when the frame of the poroelastic layer is not directly excited by the master structure (i.e. a limp model can be assumed), a better correlation should be expected. Indeed, if the poroelastic layer of the spring-mass treatment is modeled as an equivalent fluid, the quadratic velocity of the plate is very well captured by the FE-TMM(GF) (see Fig. 3.10(a)). Also the prediction of the acoustic energy improves (see Fig. 3.10(b)). However, the overall transmission is still underestimated by the FE-TMM(GF), revealing that the effect of the reflected field at the thickness resonance is important to capture the indirect coupling effects between the plate and the cavity. On the other hand, the FE-TMM(LR) remains inaccurate in the observed frequency range.

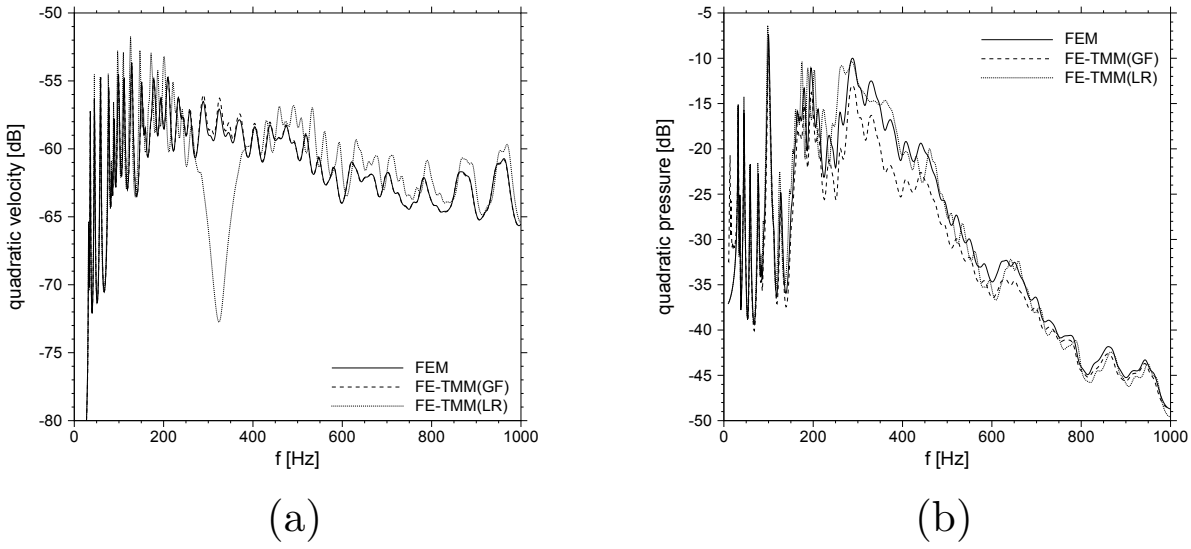

Figure 3.10 Comparison between the FEM, the FE-TMM(GF) and the FE-TMM(LR). Results relative to the spring-mass lay-up (a limp model of the poroelastic layer is assumed). Plate quadratic velocity (a) and cavity quadratic pressure (b).

Finally and for the sake of completeness, information about the computational time is provided here. All the calculations were performed on 48 2.2 GHz AMD processors. The computational time needed by the reference finite element methodology to solve Eq. 3.7 at each frequency step is 177 s and 212 s for the light and spring-mass treatments (i.e. solutions in Figs. 3.8-3.10), respectively. The linear system involves 64898 and 70208 degrees of freedom, respectively. On the other hand, the FE-TMM(GF) involves less computations, as the computational time required to build the nodal boundary operator (Eq. 3.14) is 7 s and 12 s, respectively, at each frequency step. For the light (resp. spring-mass) treatment, this time refers to the integration of the three kernels (Eq. 3.12) over 100

(resp. 200) grid points and the interpolation over the nodal distances r_{ij} (about 3 s for the considered mesh of the treated surface). It has to be recalled that a serial implementation of the FE-TMM(GF) was considered. A parallel implementation would further reduce the computational time and lead to a fairer comparison with the parallel linear solver used by the finite element solution.

3.5 Conclusions

A hybrid FE-TMM was proposed to couple the finite element models of structural and acoustic domains with an analytical model of the acoustic treatment for efficient low to mid frequency analysis. The analytical formulation employs the Green functions of flat, laterally unbounded, homogeneous and isotropic acoustic treatments. Such fundamental solutions are computed efficiently by means of the TMM, which accounts for the exact wave propagation through the thickness of the treatment. The formulation is generic, as simpler models formerly proposed by other authors can be recovered from the proposed framework. Moreover, the proposed methodology is direct, in the sense that it avoids expensive matrix inversions.

A preliminary analysis was performed to assess the accuracy of the analytical model. It was shown that this approach can always capture the global behavior of the system. Such behavior is a function of the thickness configuration (i.e. lay-up) and geometry (i.e. depth of the treatment h_t). Conversely, the effect of reflections at the lateral boundaries is neglected. Despite this limitation, the proposed model provides a good approximation (especially for large trimmed surfaces) as long as the effect of the reflected field is not dominant. However, due to the particular configuration (geometry and/or mounting conditions), the latter condition may not be met and the solution at low frequency might be poorly approximated regardless of the size of the system.

The impact of these errors in the prediction of typical vibroacoustic indicators was assessed for a plate-cavity system. It was found that the absorption in the cavity is typically overestimated by the proposed hybrid model over the entire low frequency range. Nevertheless, convergence to the finite element solution is obtained as the frequency increases. Moreover, when spring-mass layups are considered, the dynamic of the coupled system is well captured far from the global resonances of the treatment, where the power transitted to the cavity is typically underestimated. This effect was observed also for an equivalent fluid model of the poroelastic layer, meaning that the effect of the reflected wave field, even if localized, is important to capture the indirect coupling between structural

and acoustic domains. Nonetheless, the proposed methodology can always predict the qualitative behavior of the system reducing the computational burden with respect to classical finite element approaches and avoiding time consuming preprocessing (i.e. meshing) phases. Moreover, it overcomes limitations and difficulties inherent within the use of simple locally reacting models of the acoustic treatment.

3.6 Further comments

The main contribution of this chapter is a preliminary assessment of finite size effects within the noise control treatment. To further study such effects and propose a correction, an intermidiate step is however required. Namely, a more rigorous formulation is needed to fully understand the behavior of the hybrid FE-TMM. Indeed, as observed throughout this chapter, some arbitrariness seems to arise in the mathematical formulation of the sound package response (Eq. 3.9). This aspect will be extensively discussed in the next chapter.

CHAPTER 4

ENHANCED FORMULATION OF THE FE-TMM

In this chapter an enhanced formulation of the transfer matrix based model of the noise control treatment is presented. Namely, (i) the use of jinc functions in place of the linear shape functions used in chapters 2-3 is proposed to generalize and simplify the construction of the computational model, and (ii) the effect of different baffling conditions at the two ends of the sound package is studied. This analysis, together with those performed in chapters 2 and 3, concludes the assessment of the hybrid FE-TMM by providing a comprehensive overview of its computational *advantages* and accuracy *limitations*. The chapter is presented in the form of a paper (Part I of a two-parts paper). However, the manuscript has not been subitted yet.

Auteurs et affliation:

L. Alimonti: Étudiant au doctorat, Université de Sherbrooke, Faculté de Génie, Department de génie mécanique

N. Atalla: Professeur, Université de Sherbrooke, Faculté de Génie, Department de génie mécanique

Date d'acception: -

État de l'acceptation: -

Revue: -

Référence: -

Titre français: Modélisation efficiente des traitements acoustiques planes et homogénes pour l'analyse vibroacoustique par éléments finis. Partie 1: formulations du champ direct

Contribution au document: Dans ce article, une formulation améliorée du modéle du traitement acoustique est présentée.

Résumé français: Cet article porte sur le développement d'un modèle simplifié pour les traitements de contrôle du bruit afin d'accélérer l'analyse par éléments finis aux applications vibroacoustiques. La méthode repose sur l'hypothèse que le traitement acoustique est plat et homogène. De plus, son étendue latérale finie est négligée. Cette hypothèse est justifiée par une courte longueur d'ondes et une forte dissipation, ce qui suggère que le champ réfléchi émanant des limites latérales de traitement acoustique

n'affecte pas sensiblement la réponse dynamique. Dans ces circonstances, la réponse du traitement de contrôle du bruit peut être formellement obtenue par des intégrales de convolution impliquant les noyaux analytiques simples (i.e. les fonctions de Green). De telles solutions fondamentales peuvent être calculées de manière efficace par la méthode de matrice de transfert. Toutefois, il y a un certain arbitraire dans la formulation du modèle mathématique, d'où des conditions divergentes de cloisonnement aux deux extrémités du traitement à prendre en considération. Ainsi, ce travail examine la possibilité de différentes formulations (c.-à-d. les conditions de bafflage) dans le même cadre hybride élément de matrice de transfert fini, la recherche de la meilleure stratégie en termes de compromis entre l'efficacité et la précision. Des exemples numériques sont proposés pour montrer les points forts ainsi que les limites de la méthodologie proposée.

Note: -

4.1 Abstract

This paper is concerned with the development of a simplified model for noise control treatments to speed up finite element analysis in vibroacoustic applications. The methodology relies on the assumption that the acoustic treatment is flat and homogeneous. Moreover, its finite lateral extent is neglected. This hypothesis is justified by short wavelength and high dissipation, which suggest that the reflected field emanating from the acoustic treatment lateral boundaries does not substantially affect its dynamic response. Under these circumstances, the response of the noise control treatment can be formally obtained by means of convolution integrals involving simple analytical kernels (i.e. Green functions). Such fundamental solutions can be computed efficiently by the transfer matrix method. However, some arbitrariness arises in the formulation of the mathematical model, resulting in different baffling conditions at the two ends of the treatment to be considered. Thus, the paper investigates the possibility of different formulations (i.e. baffling conditions) within the same hybrid finite element-transfer matrix framework, seeking for the best strategy in terms of tradeoff between efficiency and accuracy. Numerical examples are provided to show strengths and limitations of the proposed methodology.

4.2 Introduction

The numerical modeling of multilayered systems used for noise control purposes in aeronautical and automotive applications has met a growing interest in the last two decades. Such components, also called acoustic trims or sound packages, are typically attached onto

the main structure and/or coupled with an acoustic fluid in order to reduce the noise radiated from the vibrating structure or generated within the fluid domain. Highly dissipative materials, such as poroelastic media, are usually employed in one or more layers of the acoustic trim. Nowadays, the prediction of the vibroacoustic response of such build-up systems over a wide range of frequencies remains an open problem.

This work is mainly concerned with the low frequency modeling. In such frequency range (e.g. up to 1 KHz for typical automotive applications), it is common practice to model the whole system by means of the Finite Element Method [10] (FEM). Such approach, although well-established for real life structures (e.g. stiffened plates, junctions etc. . .) and complex shaped acoustic domains, is not always suitable to model noise control treatments. In fact, such subsystems involve typically several layers of soft and dissipative materials like poroelastic media. As a results, two main issues arise from the use of the FEM. First, several degrees of freedom are typically needed to capture the short and damped waves travelling within the poroelastic layers [5, 30, 85], especially as the frequency range of interest increases. Although several attempts have been made (for instance using hierarchical formulations [57, 94] and reduced order models [33, 95, 97]), this aspect is still an open issue. Second, a preprocessing phase is always required to mesh all the layers involved in the treatment. Thus, for each design of the acoustic trim, a new mesh must be created, making the FEM not suitable for the early stage of the design process, when the optimal configuration of the acoustic trim has to be identified.

For the reasons above, simplified models of the acoustic trim are generally preferred. On the one hand, it is common practice to measure the plane wave impedance [3, 86] of the acoustic trim and use it in a standard finite element framework as boundary condition over the acoustically treated area (see for instance Ref. [37]). However, this approach implicitly assumes that the behavior of the acoustic treatment is local, meaning that the impedance at a given point of the multilayer treatment depends only on the local values of displacement and pressure. On the other hand, the fact that the wavelength in poroelastic media becomes rapidly short even at low frequency suggests that high frequency techniques could be successfully used to model such subsystems. In this context, hybrid techniques involving classical finite element based approaches for structural and acoustic domains and high frequency methodologies for the acoustic treatment have been developed. For instance, Fernandez *et al.* proposed a structural fuzzy [107, 108] model for the acoustic trim and applied it to the modeling of practical automotive applications [45, 46]. However, the methodology would still require some input parameters to fully define the "fuzzy acoustic trim" which necessitate experimental measurements and a finite element model of the

acoustic trim itself. Hence, in order to simplify further the modeling problem, there is a growing interest in embedding a simple analytical model of the sound package in the finite element model of the vibroacoustic system. Indeed, the Transfer Matrix Method [3] (TMM) is widely used to study and optimize arbitrarily complex multilayered structures. The analytical formulation of the TMM relies on the assumptions that the system is (i) homogeneous, (ii) flat and (iii) of infinite extent. Although hypotheses (ii) and (iii) cannot be met at low frequency for structural components or acoustic cavities, the short wavelengths and high damping involved in the acoustic trim suggest that the TMM could be successfully employed for such subsystems. This would render the model of the acoustic trim quick and simple, saving computational time and avoiding meshing phases.

In this context, Tournour *et al.* [122] proposed a simple hybrid model where the local impedance of the acoustic trim is evaluated by means of the TMM rather than measuring it experimentally. More sophisticated approaches able to account for the non local behavior of the noise treatment were proposed by Shorter and Mueller [105], Courtois and Bertolini [26] and Alimonti *et al.* [1] (and chapter 3). These methodologies aims at approximating the wall impedance [3, 43, 44, 86] of the homogeneous and flat sound package by its direct field contribution only (i.e. the response of the equivalent laterally infinite acoustic trim). The latter is fully determined by the knowledge of a set of Green functions which can be efficiently computed by means of the TMM. The reflected vibrational field arising from the lateral boundaries of the treatment is, instead, neglected. Nonetheless, the results are promising, as the Green functions based model of the trim can circumvent the limitations of the local impedance model, as shown in Ref. [1] and chapter 3. However, although conceptually similar, the construction of the analytical model (i.e. definition and evaluation of the Green functions) and its integration in a finite element framework substantially differs in the works mentioned above. Thus, the effect of different implementations should be carefully studied, as the accuracy and efficiency of the simplified model of the trim may depend on the adopted formulation.

In Part I of this paper the integral formulation based on the Green functions of the laterally unbounded acoustic treatment is presented. The approach takes advantage from the use of the jinc function [63] to calculate of the acoustic trim direct field response. This choice simplyfies the formulation and allows for different baffling conditions at the two ends of the acoustic trim to be easily accounted for within the same framework. Indeed, the acoustic trim is assumed to be of infinite extent, so that a set of baffling conditions must be specified outside the finite coupling area with the structural and acoustic subsystems. As briefly discussed in chapter 3, such conditions potentially affect the computational efficiency of

the Green functions based model. However, from the accuracy standpoint, it can be argued that the effect of the baffling conditions on the response of the system may not be important. Indeed, the Green functions of typical sound packages are strongly damped so that baffling effects are likely localized along the boundaries of the coupling area. Hence, it is important to study the impact of different formulations (i.e. baffling conditions) on the accuracy of the acoustic trim model in order to identify the best strategy in terms of tradeoff between accuracy and efficiency.

The paper is organized as follows. In section 4.3, the theoretical background is introduced and the motivations of this work are discussed. In section 4.4, the discrete direct field model of the sound package is obtained for two sets of baffling conditions by a standard Galerkin procedure involving a wavenumber representation of the convolution integrals. The models of the acoustic trim are integrated in the finite element equations of the vibroacoustic system and the final hybrid model is assembled. Then, the limitations of the simplified model of the acoustic trim are explicitly recalled and discussed. In section 4.5, the accuracy of the two models is assessed for three typical vibroacoustic applications. Namely, the radiation of a forced structure with an attached sound package in a (i) bounded, (ii) unbounded fluid domain and the (iii) absorption provided by a treated wall in an acoustic cavity are studied. Different combinations of layups, materials and excitations will be considered in order to fully assess the accuracy of the proposed direct field models of the acoustic trim.

4.3 Theoretical background

4.3.1 Wave based representation

The description of any vibrating system (or subsystem from a substructuring standpoint) in the low frequency range typically employs a modal decomposition approach. Each mode (i.e. standing wave) dominates the response at particular frequencies (i.e. the eigenfrequencies). However, generally speaking, a modal behavior is not clearly observed in highly dissipative systems such as sound packages. Besides the softness of the adopted materials, the reason of this resides mainly in the fact that waves impinging onto the boundaries of the system quickly dies out after being reflected, avoiding strong interference phenomena with the incoming waves. Therefore, throughout this paper, a description of the sound package response in terms of direct and reflected wave fields is rather preferred. The direct field is the vibrational field generated by the external disturbance applied to the system in the absence of boundaries (i.e. the response of the equivalent infinitely extended

system). Then, the response of the bounded system is given by the linear superposition of the direct field and the reflected field that emanates from the boundaries to restore prescribed boundary conditions [73, 86]. Such viewpoint is typically employed in high frequency analysis (for instance, see Refs. [64, 67, 106]).

In the context of this work, waves are strongly damped while propagating within the acoustic trim. Hence, one can argue that the effect of the reflected field is likely negligible and the dynamic response may be approximated by the direct field contribution only. Part I of this paper relies on this very assumption to build the simplified model of the acoustic trim and assesses its accuracy. The question is now how to formulate a model of the sound package which can reproduce physically and mathematically the desired dynamic behavior (i.e. no reflected waves). In what follows, the direct field contribution of the sound package response is approximated starting from the knowledge of simple fundamental solutions, i.e. the Green functions, which can be easily computed by means of efficient analytical tools like the TMM.

4.3.2 Green functions of the acoustic trim

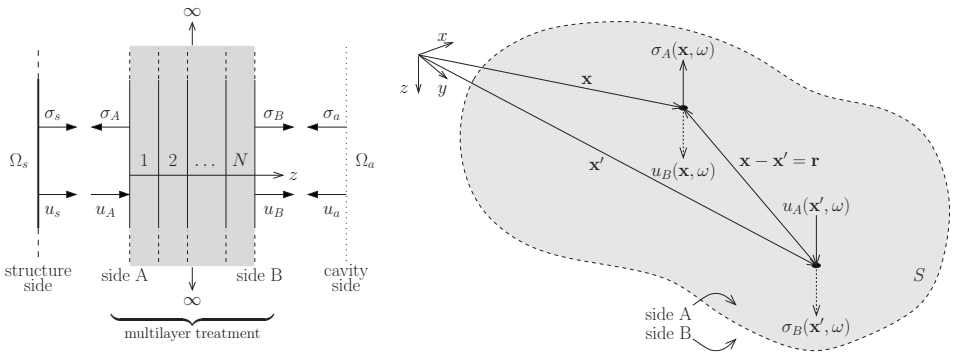

Figure 4.1 Geometry of the acoustic treatment. Through-the-thickness view of the lay-up (left) and top view (right) of the treated surface S.

The present analysis considers the harmonic vibrations of a dynamic system in the frequency domain, i.e. the time dependency $e^{\imath\omega t}$ is implicitly assumed. This section serves as an introduction to the analytical model of the acoustic trim. The latter is assumed to be (i) homogeneous in the plane (i.e. thickness, lay-up and material properties do not change over the trimmed surface), (ii) flat and (iii) of infinite extent (i.e. the lateral boundary conditions are neglected). Although the analytical model can formally handle non isotropic sound packages, the present analysis is limited to isotropic layups. No restrictions are applied in the thickness directions, where several layers of arbitrary material and phase can be employed. A generic multilayered system is sketched in Fig. 4.1. Let $u_A(\mathbf{x},\omega)$ and

$\sigma_A(\mathbf{x},\omega)$ be the normal displacement and normal stress over side A of the acoustic treatment. Similarly, $u_B(\mathbf{x},\omega)$ and $\sigma_B(\mathbf{x},\omega)$ are the normal displacement and stress over side B. The vector $\mathbf{x}$ indicates the position over the surface S, whose boundary ∂S defines the finite planar extension of the actual bounded acoustic trim. Under these conditions, the response of the multilayer treatment can be obtained invoking the Green function formalism. Thus, for instance, the normal stress σ_A at point $\mathbf{x}$ due to an imposed displacement u_A applied over the surface S is given by

$$\sigma_A(\mathbf{x},\omega) = \int_S d(r,\omega) u_A(\mathbf{x}',\omega)\,\mathrm{d}\mathbf{x}'\,, \tag{4.1}$$

where r is the module of the distance vector $\mathbf{r} = |\mathbf{x}-\mathbf{x}'|$ pointing from $\mathbf{x}'$ to $\mathbf{x}$. The function $d(r,\omega)$ is the fundamental solution (i.e. Green function) of the considered problem. For a given set of boundary conditions on the other side of the acoustic trim (e.g. hard wall condition $u_B = 0$ or pressure release condition $\sigma_B = 0$), it accounts for the exact solution (i.e. wave propagation in the thickness coordinate z) when the system is assumed of infinite lateral extent. Eq. 4.1 assumes that the displacement $u_A(\mathbf{x},\omega)$ is zero outside the excited surface S. The system is, thus, said to be baffled over side A. On the other hand, the problem may be reformulated as

$$u_A(\mathbf{x},\omega) = \int_S g(r,\omega) \sigma_A(\mathbf{x}',\omega)\,\mathrm{d}\mathbf{x}'\,, \tag{4.2}$$

which, instead, assumes side A of the acoustic trim to be unbaffled (i.e. pressure release condition outside the surface S). Generally speaking, for a given imposed displacement u_A, Eqs. 4.1 and 4.2 lead to different results, as the specified baffling conditions are different. Moreover, Eq. 4.1 allows for a direct evaluation of the reaction σ_A whereas Eq. 4.2 requires the inversion of the convolution operator (and vice versa if u_A is the output of interest). However, the choice between the two formulations is not arbitrary when a mathematical representation of the direct field part of the system response is sought. For instance, if the acoustic trim is assumed to be an equivalent fluid, the natural formulation accounting for the wave propagation in the laterally unbounded treatment is that employed in Eq. 4.1. On the other hand, if the system in Fig. 4.1 is assumed to be a solid layer, then Eq. 4.2 would ensure the propagation of the disturbance in the homogeneous laterally infinite solid layer.

Unfortunately, the arguments above can hardly be extended to a generic acoustic trim, which may involve several layers of different phases (i.e. solid and/or fluid). However, it

can be argued that, thanks to short wavelengths and dissipation, the effect of different baffling conditions may be important only close to the boundary ∂S. Hence, if the surface S is large "enough", different conditions could be considered equivalent, so that the most efficient approach could be employed circumventing any confusion in the definition of the "exact" direct field formulation. It is worth noting that the argument above is a natural consequence of the main motivation behind the proposed approach: if the effect of the finite lateral extent is assumed to be negligible so must be that of the baffling.

4.4 Hybrid model of the vibroacoustic system

In this section, the response of the laterally unbounded acoustic treatment is obtained by means of two different formulations. The first one can be seen as the "exact" methodology to obtain the direct field response when the whole acoustic trim is assumed to behave like an equivalent fluid. Namely, it considered both ends of the multilayer treatment inserted into an infinite rigid baffle. As a consequence, the normal displacements u_A and u_B are the variables on which the integral operator (i.e. convolution) applies (see Eq. 4.1). For this reason, such formulation is herein referred to as (u, u) formulation of the acoustic trim. The second methodology considered in this paper is, instead, simply justified by its numerical efficiency, as it avoids the inversion of any integral operator. Such formulation will be referred to as (u, σ) formulation of the acoustic trim, as u_A and σ_B are the variables on which the convolution integral applies. Although other two combinations of baffling conditions were considered (i.e. (σ, u) and (σ, σ)), for the sake of conciseness, the present analysis is limited only to (u, u) and (u, σ) formulations, as they can be justified by physical and computational arguments, respectively. In the following sections, the dynamic response of the acoustic trim according to the two considered formulations is obtained and then embedded in the finite element model of the structural-acoustic master system yielding the assembled hybrid model. Finally, for the sake of clarity, the limitations of the proposed approach are briefly summarized and discussed.

4.4.1 (u, u) formulation of the acoustic trim

Referring to Fig. 4.2(a), the acoustic trim is assumed to be attached to a structural domain over side A, while side B radiates into a fluid domain. The structure-trim and fluid-trim coupling areas formally coincide and will be referred to as the treated (or trimmed) surface S. The structural and acoustic domains are modeled by classical finite element based procedures. To account for the acoustic trim in the discrete model of the vibroacoustic

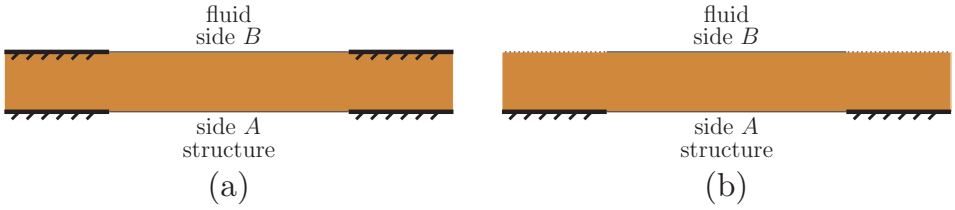

Figure 4.2 Baffling conditions for the (a) (u,u) formulation and (b) (u,σ) formulation.

system, the coupling forces exchanged over the surface S between the master subsystems (i.e. structure and/or fluid domains) and the acoustic trim must be expressed as a function of the master subsystem degrees of freedom (see chapter 3). In this section, such relation is obtained starting from the (u,u) formulation of the laterally infinite sound package, i.e.

$$\begin{cases} \sigma_A(\mathbf{x},\omega) &= \displaystyle\int_S d_{AA}(r,\omega)u_A(\mathbf{x}',\omega)\,\mathrm{d}\mathbf{x}' + \int_S d_{AB}(r,\omega)u_B(\mathbf{x}',\omega)\,\mathrm{d}\mathbf{x}' \\ \sigma_B(\mathbf{x},\omega) &= \displaystyle\int_S d_{BA}(r,\omega)u_A(\mathbf{x}',\omega)\,\mathrm{d}\mathbf{x}' + \int_S d_{BB}(r,\omega)u_B(\mathbf{x}',\omega)\,\mathrm{d}\mathbf{x}' \end{cases}, \tag{4.3}$$

where functions $d_{mn}(r,\omega)$ ($m=A,B$ and $n=A,B$) are the Green functions of the (u,u) formulation. The following approximation for the displacements over sides A and B is employed

$$\begin{aligned} u_A(\mathbf{x},\omega) &= \sum_{j=1}^{n} 2\frac{\mathrm{J}_1(k_s r)}{k_s r}\,a_j(\omega) = \sum_{j=1}^{n} 2\,\mathrm{jinc}(k_s r)\,a_j\,, \\ u_B(\mathbf{x},\omega) &= \sum_{j=1}^{n} 2\frac{\mathrm{J}_1(k_s r)}{k_s r}\,b_j(\omega) = \sum_{j=1}^{n} 2\,\mathrm{jinc}(k_s r)\,b_j\,, \end{aligned} \tag{4.4}$$

where $J_1(k_s r)$ is the Bessel function of first order of argument $k_s r$, r is the modulus of the distance $\mathbf{r}=\mathbf{x}-\mathbf{x}_j$ and k_s is the maximum wavenumber content of the jinc function. Such shape functions were successfully used by Langley [63] for the calculation of the radiation impedance of a vibrating surface. The approximation in Eq. 4.4 can be seen as the discrete form of the interpolation scheme used in the Smoothed Particle Hydrodynamics (SPH) [80]. Given a generic mesh of the trimmed surface S consisting of n points, the j^{th} jinc function is associated to the grid point $\mathbf{x}_j$. Coefficients a_j and b_j are the corresponding participation factors. Substituting Eq. 4.4 in Eq. 4.3, integrating over the surface S,

projecting onto the shape functions subspace and employing the convolution theorem to express the Green functions in the wavenumber domain (see Ref. [1]) one obtains

$$\begin{cases} \mathbf{R}_A(\omega) &= \mathbf{D}_{AA}(\omega)\,\mathbf{a}(\omega) + \mathbf{D}_{AB}(\omega)\,\mathbf{b}(\omega) \\ \mathbf{R}_B(\omega) &= \mathbf{D}_{BA}(\omega)\,\mathbf{a}(\omega) + \mathbf{D}_{BB}(\omega)\,\mathbf{b}(\omega) \end{cases}, \tag{4.5}$$

where vectors $\mathbf{R}_A$ and $\mathbf{R}_B$ gather the projection on each shape function of the normal stress on sides A and B, respectively. The (i, j) components of the generalized stiffness matrices $\mathbf{D}_{mn}$ ($m = A, B$ and $n = A, B$) are defined as

$$D_{mn_{ij}}(\omega) = D_{mn}(r_{ij}, \omega) = \left(\frac{4\pi}{k_s^2}\right)^2 \frac{1}{2\pi} \int_0^{k_s} \hat{d}_{mn}(k, \omega) J_0(k r_{ij}) k \,\mathrm{d}k\,, \tag{4.6}$$

where $k = |\mathbf{k}|$ is the modulus of the wavenumber, $J_0(kr_{ij})$ is the Bessel function of zero order of argument kr_{ij} and $r_{ij} = |\mathbf{r}_{ij}|$ is the Euclidean distance between the nodes $\mathbf{x}_j$ and $\mathbf{x}_i$. Eq. 4.6 implicitly assumes that the acoustic trim is isotropic in the plane. The formalism $\hat{f}(k)$ indicates the radially symmetric Fourier transform, i.e. Hankel transform, of the function $f(r)$. The coupling Green functions satisfy the reciprocity condition $\hat{d}_{AB}(k, \omega) = -\hat{d}_{BA}(k, \omega)$. The procedure to calculate the fundamental kernels $\hat{d}_{mn}(k, \omega)$ by means of the TMM is outlined in appendix A.

In order to integrate the model of the acoustic trim in the finite element equations describing the dynamics of the vibroacoustic system, a suitable mapping must be defined to link the participation factors $\mathbf{a}$ and $\mathbf{b}$ to the structural and acoustic finite element degrees of freedom over the interface S. The procedure to obtain such mapping is detailed in appendix B. Assuming that the nodes associated to each jinc function and those belonging to the finite element structural and fluid domains coincide over the surface S, the following continuity relations hold

$$\begin{aligned} \mathbf{a} &= \mathbf{H}\mathbf{U}_{n_s}\,, \\ \mathbf{R}_B &= -\hat{\mathbf{H}}\mathbf{P}_a\,, \end{aligned} \tag{4.7}$$

where $\mathbf{U}_{n_s}$ and $\mathbf{P}_a$ are the normal displacements and acoustic pressures, respectively, at the finite element nodes over the trimmed surface S. Mapping operators $\mathbf{H}$ and $\hat{\mathbf{H}}$ are

defined in appendix B. Consequently, the interface forces acting on the structural and acoustic finite element degrees of freedom are given by

$$\begin{array}{rcl} \mathbf{R}_s &=& \mathbf{H}^{\mathrm{T}}\mathbf{R}_A\,, \\ \mathbf{R}_a &=& -\ \hat{\mathbf{H}}^{\mathrm{T}}\mathbf{b}\,, \end{array} \tag{4.8}$$

respectively. Eq. 4.8 guarantees conservation of energy at the interface between the finite elements domains and the two ends of the acoustic trim. The minus signs in Eqs. 4.7-4.8 come from the notation used in Fig. 4.1. Using Eq. 4.7-4.8 and Eq. 4.5, solving for $\mathbf{R}_s$ and $\mathbf{R}_a$, one finally obtains

$$\left\{ \begin{array}{c} \mathbf{R}_s \\ \mathbf{R}_a \end{array} \right\} = \left[\begin{array}{cc} \mathbf{H}^{\mathrm{T}}(\mathbf{D}_{AA} + \mathbf{D}_{AB}\mathbf{D}_{BB}^{-1}\mathbf{D}_{AB})\mathbf{H} & -\mathbf{H}^{\mathrm{T}}\mathbf{D}_{AB}\mathbf{D}_{BB}^{-1}\hat{\mathbf{H}}) \\ -\hat{\mathbf{H}}^{\mathrm{T}}\mathbf{D}_{BB}^{-1}\mathbf{D}_{AB}\mathbf{H} & \hat{\mathbf{H}}^{\mathrm{T}}\mathbf{D}_{BB}^{-1}\hat{\mathbf{H}} \end{array} \right] \left\{ \begin{array}{c} \mathbf{U}_{n_s} \\ \mathbf{P}_a \end{array} \right\}, \tag{4.9}$$

where the block matrix can be interpreted as the boundary operator accounting for the structural stiffness, fluid admittance and fluid-structure coupling added to the vibroacoustic system due to the presence of the sound package (see chapter 3 for details). Note that the frequency dependency has been omitted to lighten the notation. Eq. 4.9 reveals that the calculation of the acoustic trim response by means of the (u, u) formulation requires the evaluation of $\mathbf{D}_{BB}^{-1}$ through the solution of a linear system with multiple right hand sides. The dimension of the system to be solved is $n \times n$, where n is the number of trimmed nodes. It can be argued that, for large n, the presence of a matrix inversion might jeopardize the efficiency of the model, as matrix $\mathbf{D}_{BB}$ is fully populated.

4.4.2 (u, σ) formulation of the acoustic trim

The acoustic trim is now assumed to be baffled over side A and unbaffled over side B (see Fig. 4.2(b)). Under these assumptions, the response of the laterally infinite acoustic trim reads

$$\left\{ \begin{array}{rcl} \sigma_A(\mathbf{x},\omega) & = & \displaystyle\int_S g_{AA}(r,\omega) u_A(\mathbf{x}',\omega)\,\mathrm{d}\mathbf{x}' + \int_S g_{AB}(r,\omega)\sigma_B(\mathbf{x}',\omega)\,\mathrm{d}\mathbf{x}' \\ u_B(\mathbf{x},\omega) & = & \displaystyle\int_S g_{BA}(r,\omega) u_A(\mathbf{x}',\omega)\,\mathrm{d}\mathbf{x}' + \int_S g_{BB}(r,\omega)\sigma_B(\mathbf{x}',\omega)\,\mathrm{d}\mathbf{x}' \end{array} \right. , \tag{4.10}$$

where functions $g_{mn}(r,\omega)$ ($m = A, B$ and $n = A, B$) are the Green functions of the (u,σ) formulation. Following the same procedure employed in the previous section, the discrete form of Eq. 4.10 is

$$\left\{ \begin{array}{rcl} \mathbf{R}_A(\omega) & = & \mathbf{G}_{AA}(\omega)\,\mathbf{a}(\omega) + \mathbf{G}_{AB}(\omega)\,\mathbf{b}(\omega) \\ \mathbf{R}_B(\omega) & = & \mathbf{G}_{BA}(\omega)\,\mathbf{a}(\omega) + \mathbf{G}_{BB}(\omega)\,\mathbf{b}(\omega) \end{array} \right. , \tag{4.11}$$

where the (i,j) component of matrices $G_{mn}(\omega)$ is formally equivalent to the definition in Eq. 4.6, taking care of replacing $\hat{d}_{mn}(k,\omega)$ with $\hat{g}_{mn}(k,\omega)$. The reciprocity condition gives $\hat{g}_{AB}(k,\omega) = \hat{g}_{BA}(k,\omega)$. The continuity conditions now read

$$\begin{array}{rcl} \mathbf{a} & = & \mathbf{H}\mathbf{U}_{n_s}\,, \\ \mathbf{b} & = & -\,\mathbf{H}\mathbf{P}_a\,. \end{array} \tag{4.12}$$

Consequently, the interface forces acting on the structural and acoustic finite element degrees of freedom are given by

$$\begin{array}{rcl} \mathbf{R}_s & = & \mathbf{H}^{\mathrm{T}}\mathbf{R}_A\,, \\ \mathbf{R}_a & = & -\,\mathbf{H}^{\mathrm{T}}\mathbf{R}_B\,. \end{array} \tag{4.13}$$

Using Eqs. 4.12-4.13 and Eq. 4.11 one finally obtains

$$\left\{ \begin{array}{c} \mathbf{R}_s \\ \mathbf{R}_a \end{array} \right\} = \left[\begin{array}{cc} \mathbf{H}^{\mathrm{T}}\mathbf{G}_{AA}\mathbf{H} & -\mathbf{H}^{\mathrm{T}}\mathbf{G}_{AB}\mathbf{H} \\ -\mathbf{H}^{\mathrm{T}}\mathbf{G}_{AB}\mathbf{H} & \mathbf{H}^{\mathrm{T}}\mathbf{G}_{BB}\mathbf{H} \end{array} \right] \left\{ \begin{array}{c} \mathbf{U}_{n_s} \\ \mathbf{P}_a \end{array} \right\} . \tag{4.14}$$

Thus, Eq. 4.14 directly gives the boundary operator accounting for the effect of the acoustic trim, avoiding any matrix inversion and allowing for saving computational time compared to the model in Eq. 4.9. It is worth noting that the model of the sound package in Eq. 4.14 is formally equivalent to that proposed in chapter 3, where linear radially symmetric shape functions were employed to approximate the displacements and pressures over the two ends of the trim. In the case of a structured mesh with rectangular elements, it was shown that such choice allows to approximate the mapping operator $\mathbf{H}$ with the identity matrix. On the other hand, the formulation in terms of jinc functions employed in this paper is generic, as no restrictions are applied on the topology of the trimmed area mesh.

4.4.3 Assembled hybrid model

The simplified models of the acoustic trim (Eqs. 4.9 and 4.14) are finally embedded in the finite element equations of the vibroacoustic system, yielding (see chapter 3)

$$\left(\begin{bmatrix} \mathbf{Z}_{ss}(\omega) & \mathbf{Z}_{sa}(\omega) \\ \mathbf{Z}_{sa}^{\mathrm{T}}(\omega) & \mathbf{Z}_{aa}(\omega) \end{bmatrix} - \begin{bmatrix} \mathbf{Y}_{ss}(\omega) & \mathbf{Y}_{sa}(\omega) \\ \mathbf{Y}_{sa}^{\mathrm{T}}(\omega) & \mathbf{Y}_{aa}(\omega) \end{bmatrix} \right) \begin{Bmatrix} \mathbf{q}_s(\omega) \\ \mathbf{q}_a(\omega) \end{Bmatrix} = \begin{Bmatrix} \mathbf{F}_s(\omega) \\ \mathbf{F}_a(\omega) \end{Bmatrix}, \tag{4.15}$$

where $\mathbf{q}_s$ and $\mathbf{q}_a$ are the degrees of freedom of the structural (i.e. displacements and rotations or modal amplitudes) and acoustic (i.e. pressures or modal amplitudes) domains, respectively. The boundary operator $\mathbf{Y}$ accounts for the effect of the sound package on the vibroacoustic system (see chapter 3). With an abuse of notation if Eq. 4.15 is expressed in physical coordinates, the block matrices $\mathbf{Y}_{ss}$, $\mathbf{Y}_{sa}$ and $\mathbf{Y}_{aa}$ refer to those defined in Eqs. 4.9 and 4.14. It should be observed that the second equation can refer to an hard walled as well as an open acoustic cavity. In the latter case, the radiation into an unbounded acoustic domain can be modeled by adding an impedance operator to the block matrix $\mathbf{Z}_{aa}$, for instance employing the Boundary Element Method [6] (BEM) or the Perfectly Matched Layer [11, 12] (PML).

4.4.4 Numerical implementation

The numerical implementation of the acoustic trim model was carried out in MATLAB. The parallel toolbox [123] was exploited in order to speed up the calculations. The implementation mainly involves the following steps.

– Calculation of the Green functions. The functions $\hat{d}_{mn}(k,\omega)$ (or $\hat{g}_{mn}(k,\omega)$) must be evaluated by means of the TMM at each frequency step over a sampled wavenumber space. A grid consisting of n_k points between $k = 0$ and $k = k_s$ must be defined guaranteeing a correct sampling of the oscillatory behavior of the integrand in Eq. 4.6. This step can take advantage from a parallel implementation, as the transfer matrix problems to be solved at each wavenumber grid point k_i are independent.
– Integration of the kernels. The functions $D_{mn}(r_{ij},\omega)$ (or $G_{mn}(r_{ij},\omega)$) are sampled at n_r grid points between $r = 0$ and $r = r_{max}$, where r_{max} is the maximum distance between two points over the trimmed surface S. The integration of Eq. 4.6 at the n_r radius points can be also performed in parallel, as each calculation is entirely independent.
– Matrices assembly. The functions calculated in the previous step must be then interpolated to build the matrices of the adopted formulation. Although this step was not optimized in this work, it was found that an efficient interpolation routine can make the difference when a large number n of trimmed nodes is considered. After this step, if the (u,σ) formulation is employed, the model of the acoustic trim (i.e. Eqs. 4.14) is ready to be embedded into the finite element system.
– Solution of the linear system. If the (u,u) formulation is employed, a linear system must be solved to obtain Eq. 4.9.

Finally, the choice of the maximum wavenumber content k_s of the jinc functions must be defined. In this work, the same approach proposed by Langley [63] was employed, i.e. k_s is uniquely defined by the shortest wavelength captured by the mesh of the trimmed surface S.

4.4.5 Limitations of the model

Given a sound package covering an area S of the interface between a structure and a fluid, the models developed in sections 4.4.1-4.4.2 can be employed if the sound package is (i) flat, (ii) homogeneous and (iii) isotropic in the plane containing S. Conditions (i)-(ii) are the hypotheses on which the analytical formulation is formally based, as they allow to express the Green functions as functions of the distance $\mathbf{r}$ only. In turns, this also allows to calculate the fundamental solutions by means of the TMM, whose analytical framework is based on such assumptions. Nonetheless, it could be argued that the formulation can be extended to moderately curved and non homogeneous sound packages, assuming, respectively, the system to be locally flat and dividing the surface S in homogeneous patches [26]. However, these aspects are beyond the scope of the present work and are not assessed here. Condition (iii) allows to express the entries of matrices $D_{mn_{ij}}(\omega)$

and $G_{mn_{ij}}(\omega)$ as one-dimensional integrals, since the Green functions depend only on the module of the wavenumber k (i.e. the spatial Green functions becomes a function of the module of the distance r). Non isotropic layups, can still be approximated using averaged Green functions to remove the dependency from the heading angle ϕ.

If conditions (i)-(iii) are met, then the accuracy of the Green functions based model depends only on the main assumption that finite size effects within the treatment are negligible, i.e. the direct field part of the acoustic trim response dominates over reflected field contribution. The impact of such assumption is of primary importance and must be fully understood. To this end, only the equivalent fluid behavior of the acoustic treatment (i.e. poroelastic layers are modeled according to the limp approximation [84]) will be considered in this work. Such choice simplifies of the dynamic behavior of the system allowing for an easier interpretation of the results. On the other hand, the effect of a full Biot model has been studied in chapter 3 and is the subject of a specific application in chapter 5.

For the sake of completeness, it should be mentioned that the model of the acoustic trim, as presented in section 4.4, can handle only the continuity of normal displacement and stress at the interface with the structure. However, this is not an intrinsic limitation of the methodology, since the formulation could be, in theory, extended to account for in-plane components. Nonetheless, the assumption of normal continuity is widely used in real life applications, due to practical mounting conditions.

4.5 Results

The accuracy of the hybrid model presented in section 4.4.3 is here assessed. To this end, two different analysis are proposed. First the accuracy of the hybrid model according to the (u, u) and (u, σ) formulations of the acoustic trim is assessed in terms of typical vibroacoustic indicators, i.e. structural space averaged quadratic velocity, acoustic cavity space averaged quadratic pressure and power radiated into an unbounded fluid. Second, the effect of the material properties on the accuracy of the model will be assessed in terms of difference between the vibroacoustic indicators obtained with two different acoustic trim configurations. Throughout this section, the reference solution uses the substructuring approach developed by Hamdi *et al.* [53], which employs a finite element model of the sound package to calculate the boundary operator $\mathbf{Y}$.

The considered benchmark involves a 2 mm thick rectangular steel plate of dimensions $L_x \times L_y \, \mathrm{m}^2$, clamped along its edges. The acoustic trim is attached onto the structure and radiates either into a baffled semi-infinite fluid domain or into a rigid walled cavity

of cubic shape with dimensions $L_x \times L_y \times L_z\,\mathrm{m}^3$. Two different layups are considered for the sound package. Namely, a (i) one-layer lay-up (referred to as *light* trim) consisting of a 4 cm foam and a (ii) two-layers lay-up (referred to as *spring-mass* trim) consisting of a 2 cm foam with a heavy layer attached on top. The materials used for the poroelastic layer are reported in Tab. 4.1, along with the structural properties of the plate and the considered air conditions. The lateral boundaries of the acoustic trim finite element model are assumed to be rigid and impervious (i.e. hard walled).

Table 4.1 Materials used in the numerical simulations.

Material	**Properties**	
	Acoustic	**Mechanical**
Steel		density = $8000\,\mathrm{kg/m^3}$ Young's modulus = 200 GPa Poisson's ratio = 0.33 damping factor = 0.02
Air	density = $1.21\,\mathrm{kg/m^3}$ speed of sound = $342.2\,\mathrm{m/s}$	
Melamine	porosity = 0.99 resistivity = $10900\,\mathrm{kg/m^3s}$ tortuosity = 1.02 viscous length = $100\,\mu$m thermal length = $130\,\mu$m	density = $8.8\,\mathrm{kg/m^3}$ Young's modulus = 80 kPa Poisson's ratio = 0.4 damping factor = 0.17
Felt	porosity = 0.98 resistivity = $26514\,\mathrm{kg/m^3s}$ tortuosity = 1 viscous length = $48\,\mu$m thermal length = $144\,\mu$m	density = $58\,\mathrm{kg/m^3}$ Young's modulus = 6 kPa Poisson's ratio = 0.04 damping factor = 0.15
Heavy layer		density = $1.2\,\mathrm{kg/m^2}$ Young's modulus = 10^3 kPa Poisson's ratio = 0.3 loss factor = 0.5

4.5.1 Assessment of the proposed models

The first case refers to an acoustic cavity of dimensions $0.8 \times 1.7 \times 1\,\mathrm{m}^3$. A proportional structural damping model is used to introduce dissipative effects within the cavity ($\eta_a = 0.01$). Most of the absorption is instead provided by a 4 cm melamine foam attached onto the $0.8 \times 1.7\,\mathrm{m}^2$ rigid wall at $z = 0$. A monopole with constant volume velocity is placed at the corner $(0\,\mathrm{m}, 1.7\,\mathrm{m}, 1\,\mathrm{m})$. The response of the system up to 1 kHz is considered. The finite element model of the cavity involves $24 \times 50 \times 30$ eight-noded fluid elements. The poroelastic layer, assumed to be limp, is modeled with 5 eight-noded equivalent fluid elements along its thickness (same mesh of the acoustic domain in the plane). Fig. 4.3

shows the quadratic pressure inside the acoustic cavity. It can be pointed out that a similar behavior is observed for both the two considered hybrid models. Namely, as a consequence of the infinite lateral extent assumption (i.e. direct field only), none of the two formulations is able to capture the absorption provided by the actual (i.e. laterally bounded) melamine layer in the low frequency range (below 600 Hz). However, as the frequency increases, the effect of the reflected field within the light trim becomes less important and the hybrid models converge to the reference solution. This behavior has already been observed for a plate-cavity system in chapter 3 and it is confirmed by the present analysis, which, in addition, shows that the low frequency absorption remains an issue regardless of the considered baffling conditions. In fact, although it could be pointed out that the (u, u) formulation captures better the qualitative behavior at low frequency (note, for instance, the position of the resonances), the accuracy does not substantially improve compared to the more computationally efficient (u, σ) formulation.

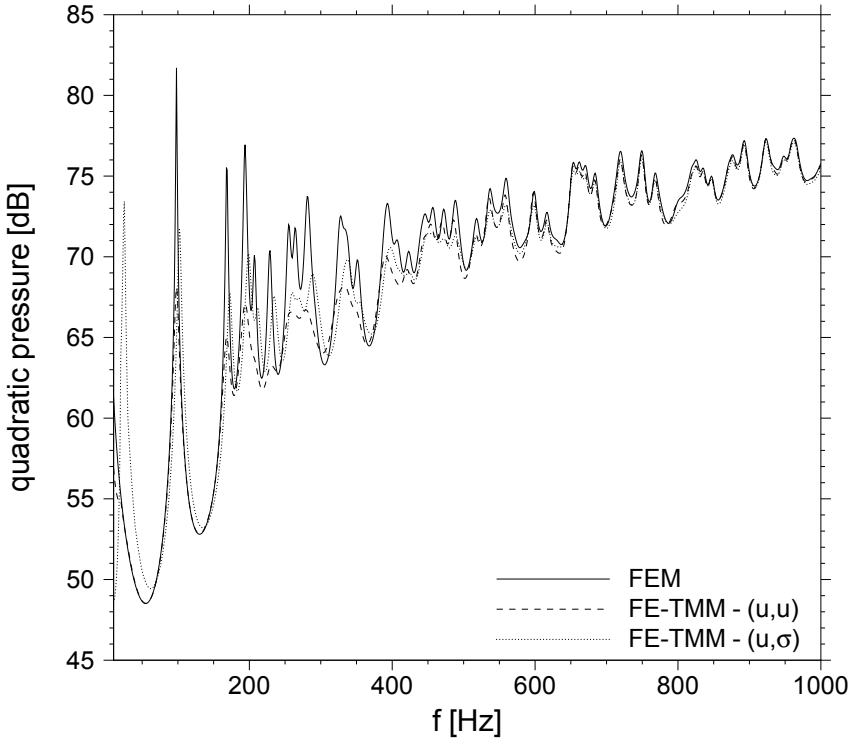

Figure 4.3 Space averaged quadratic pressure of the acoustic cavity excited by a monopole. A 4 cm melamine layer is attached onto the hard wall facing the excitation point. Comparison between the finite element and the hybrid models based on the (u, u) and (u, σ) formulations.

The second case refers to a plate-cavity system of dimensions $0.4 \times 0.85 \times 0.5\,\mathrm{m}^3$. The 4 cm melamine foam is now placed between the plate and the cavity. The response of the system driven by a point force applied on the plate at point $(0.114\,\mathrm{m}, 0.147\,\mathrm{m})$ is considered. The upper limit of the observed frequency range is 3 kHz. The finite element model of the plate and cavity involve 35×75 four-noded plate elements and $35 \times 75 \times 36$ eight-noded fluid elements, respectively. The melamine layer is modeled with 10 eight-noded equivalent fluid elements along its thickness. The simulation refers to the case of a 5% damping provided by the cavity itself (i.e. $\eta_a = 0.05$). The quadratic velocity is very well captured by both the hybrid models (confirming the results in Ref. [1] and chapter 3) and thus not shown here for the sake of conciseness. The quadratic pressure in the cavity is, instead, reported in Fig. 4.4. The previous analysis (Fig. 4.3) would suggest that, after a low frequency region where the absorption seen from the cavity side is overestimated (see, for instance, the acoustic resonance at 200Hz), the hybrid solutions should converge to the reference curve. However, an offset from the reference solution is observed over the whole considered spectrum, showing that the hybrid models cannot quantitavely capture the power flow from the structure to the fluid domain through the acoustic trim. Indeed, the contribution to the indirect fluid-structure coupling (i.e. extra-diagonal block matrix in Eqs. 4.9 and 4.14) of the reflected field emanating from the lateral boundaries of the foam is neglected and a perfect match with the reference solution cannot be expected. Namely, part of the vibrational energy appears to be lost through the lateral extent of the treatment. Nonetheless, the (u, u) and (u, σ) hybrid models follow very well the reference and provide an accuracy within 3 and 2 dB, respectively. Moreover, the hybrid solutions are very close to each other (within 1 dB), confirming that the baffling conditions produce negligible effects.

The transmission issues are confirmed also for the case where side B of the sound package is radiating into a fluid filled half-space (note that the latter is considered baffled regardless of the formulation employed for the sound package). However, when the system is excited by a plane wave, the accuracy of the hybrid models increases. This is shown in Fig. 4.5, where the power radiated into the unbounded fluid is reported for the same plate considered in the previous simulation excited by a $45°/45°$ plane wave. The gap between the hybrid and reference solutions has reduced and a good approximation is obtained. This is not surprising, since the effect of the plane wave is to force the system to vibrate with a given wavenumber (i.e. the projection of the acoustic wavenumber onto the plate surface), minimizing the finite size effects on the system response. As a consequence, an almost perfect match between the two hybrid models is obtained, although few discrepancies are still observed below 200 Hz (where the response is still markedly modal). Similar results

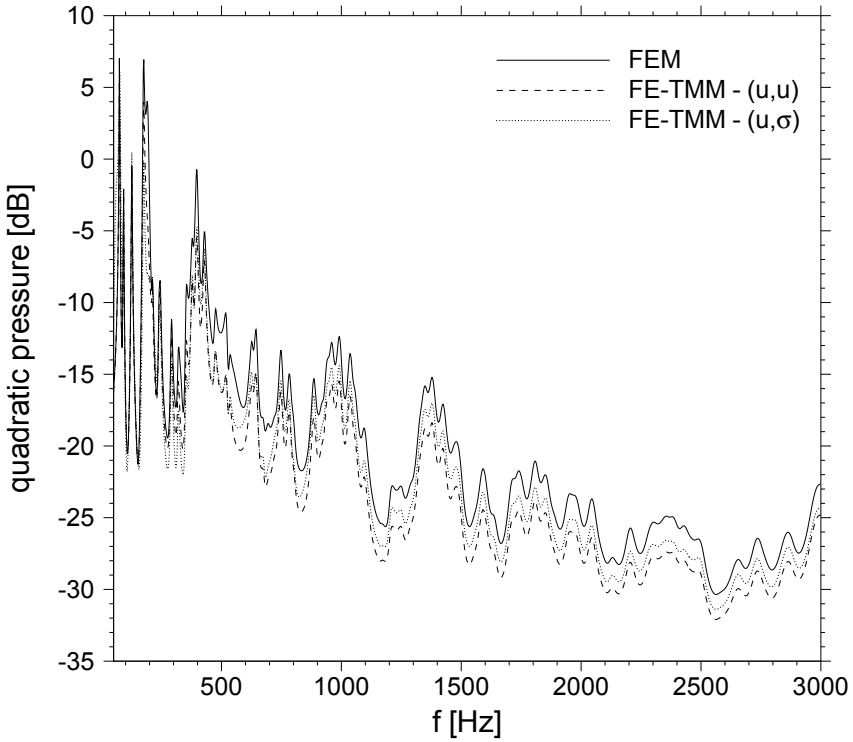

Figure 4.4 Space averaged quadratic pressure of the acoustic cavity. The plate-cavity system is mechanically excited by a point force. Result relative to the light acoustic treatment lay-up (4 cm melamine). Comparison between the finite element and the hybrid models based on the (u, u) and (u, σ) formulations.

could be shown for the quadratic pressure if the plate-foam system is backed by a hard walled acoustic cavity.

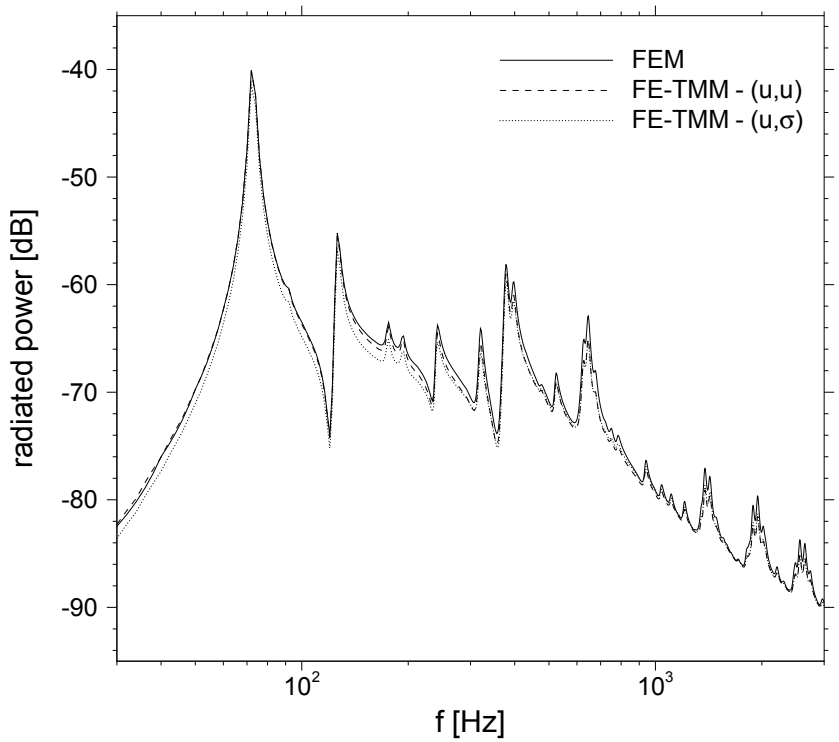

Figure 4.5 Power radiated into the semi-infinite fluid. The plate is acoustically excited by a 45°/45° plane wave. Result relative to the light acoustic treatment lay-up (4 cm melamine). Comparison between the finite element and the hybrid models based on the (u, u) and (u, σ) formulations.

The analysis carried out in Figs. 4.4-4.5 is repeated in Figs. 4.6-4.7 for a larger system acoustically treated by a spring-mass lay-up. The plate dimensions are $0.8 \times 1.7\,\mathrm{m}^2$ while the acoustic cavity is 1 m deep. The finite element model of the plate and cavity involve 43×91 four-noded plate elements and $43 \times 91 \times 30$ eight-noded fluid elements, respectively. The mesh of the acoustic trim employs 5 eight-noded limp elements through the thickness of the melamine layer, while the heavy screen is modeled with one layer of eight-noded solid elements (see Tab. 4.1 for the structural properties). Figs. 4.6 and 4.7 show, respectively, the quadratic pressure inside the cavity when the plate is excited by a point force at $(0.112\,\mathrm{m}, 0.131\,\mathrm{m})$ and the power radiated into the fluid half-space (which replaces the hard walled cavity) when the plate is excited by a 45°/45° plane wave. The results show that, at the double wall resonance of the system around 350 Hz, the reflected field in the

acoustic trim cannot be neglected due to the pronounced non local behavior of the spring-mass lay-up. Indeed, for the point load case (see Fig. 4.6), the hybrid models based on the (u, u) and (u, σ) formulations underestimate the quadratic pressure peak by 4 and 3 dB, respectively. As a consequence, the difference between the two formulations are also confined between 250 and 450 Hz, where a maximum gap of 2 dB is observed in the narrow frequency band between 300 and 400 Hz. However, the qualitative behavior of the reference solution is well reproduced. The structural energy of the plate is instead well captured (see also chapter 3) and thus not shown here for the sake of brevity. On the other hand, Fig. 4.7 confirms that the hybrid models perform better when an acoustic excitation drives the plate.

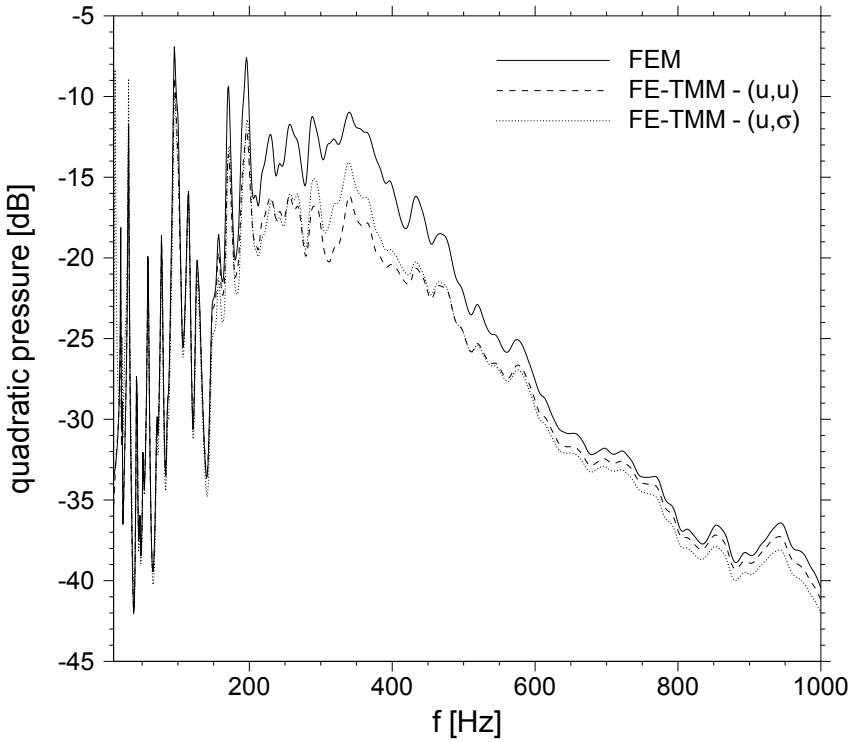

Figure 4.6 Space averaged quadratic pressure of the acoustic cavity. The plate-cavity system is mechanically excited by a point force. Result relative to the spring-mass acoustic treatment lay-up (2 cm melamine with 1.2 $\mathrm{kg/m^2}$ heavy layer on top). Comparison between the finite element and the hybrid models based on the (u, u) and (u, σ) formulations.

Finally, to give an idea about the computational cost of the two hybrid methods, the spring-mass trim case is considered. Concerning the reference solution, the finite element model of the acoustic trim involves 48032 degrees of freedom and requires 90 **s** to build

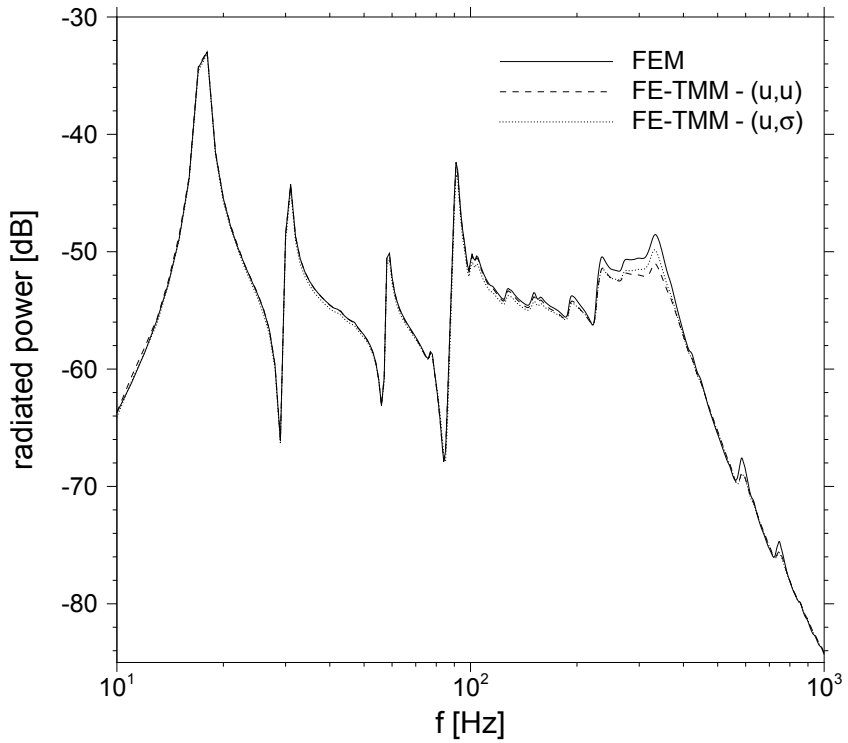

Figure 4.7 Power radiated into the semi-infinite fluid. The plate is acoustically excited by a 45°/45° plane wave. Result relative to the spring-mass acoustic treatment lay-up (2 cm melamine with 1.2 kg/m^2 heavy layer on top). Comparison between the finite element and the hybrid models based on the (u, u) and (u, σ) formulations.

the boundary operator $\mathbf{Y}$ (see Eq. 4.15) at each frequency step. This time refers to the solution of the finite element linear system by means of the MKL based parallel solver PARDISIO [98, 99]. On the other hand, the (u, u) and (u, σ) formulations requires 4.2 and 14.4 s, respectively. This information refers to the sum of the computational time required to perform each step discussed in section 4.4.4 (see Tab. 4.2 for details). The number of trimmed nodes is $n = 4048$, while $n_k = n_r = 606$ uniformly distributed points were employed for the sampling of the analytical functions. All the computations were performed on a desktop computer powered by an intel i7-2600 processor (8 nodes at 3.4 GHz).

Table 4.2 Computational time required to perform each step involved in the (u, u) and (u, σ) formulations. MATLAB *backslash* operator was used to perform the solution step.

	TMM	Integration	Interpolation	Solution	Total	$\frac{\text{Reference}}{\text{Total}}$
(u, u)	0.3 s	2.1 s	1.8 s	10.2 s	14.4 s	6.2
(u, σ)	0.3 s	2.1 s	1.8 s	-	4.2 s	21.4

4.5.2 Effect of different materials

In the previous section it has been shown that, generally speaking, the reflected field within the acoustic trim can play an important role in the response of the vibroacoustic system. Its contribution is neglected by the simplified analytical model of the sound package, so that a modeling error appears. It should be clear at this point that this error is a function of the acoustic trim configuration. Indeed, this has been implicitly proved in the previous section, where a different behavior of the hybrid models were observed for two different acoustic trims. In this section the effect of different materials is assessed. Namely, for a fixed lay-up (light or spring-mass), the results obtained by employing different poroelastic materials are compared. The results are presented in terms of relative difference between the response obtained with two different layups, i.e. , for the generic vibroacoustic indicator X,

$$\Delta[X] = X_{\text{lay-up 1}}\,[\text{dB}] - X_{\text{lay-up 2}}\,[\text{dB}]\,. \tag{4.16}$$

The first case refers to the plate-cavity system of dimensions $0.4 \times 0.85 \times 0.5\,\text{m}^3$. The quadratic pressure due to a point force excitation when the 4 cm melamine foam is attached onto the plate has already been shown in Fig. 4.4. Fig. 4.8(a) shows instead the indicator Δ for the quadratic pressure in the cavity when the performance of the melamine is

compared with a felt layer (properties in Tab. 4.1) of the same thickness. A logarithmic scale on the frequency axis is used to focus on the low frequency range. Moreover, a one-third octave band averaging of the same result is reported in Fig. 4.8(b) to facilitate the interpretation of the result. It can be observed that the hybrid models are able to predict the difference between the two materials with an accuracy of 1 dB (on average) above 200 Hz. This difference is explained by the fact that the absolute accuracy of the hybrid models increases when the felt layer is considered. Indeed, the felt is softer (in terms of equivalent complex speed of sound $c_0(\omega)$) than the melamine, so that the reflected waves emanating from the boundaries exhibit a faster decay rate. Moreover, it can be argued that the (u, u) formulation gives a better quantitative (below 200 Hz) and qualitative (above 200 Hz) correlation with the reference solution. On the other hand, it can also be pointed out that in terms of efficiency/accuracy tradeoff, the (u, σ) formulation gives satisfactory results.

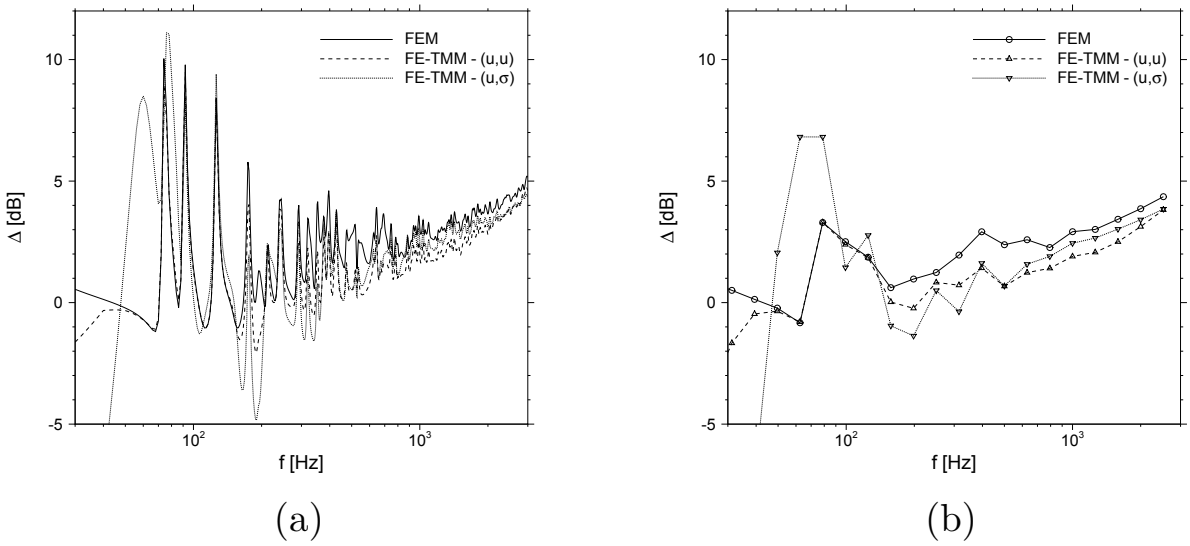

Figure 4.8 Eq. 4.16 applied to the quadratic pressure in the acoustic cavity considering a 4 cm melamine (lay-up 1) and a 4 cm felt (lay-up 2). The plate-cavity system is mechanically excited by a point force. Comparison between the finite element and the hybrid models based on the (u, u) and (u, σ) formulations. Narrow band (a) and third-octave band average (b).

The same analysis is proposed in Fig. 4.9 for the case of a 45°/45° plane wave excitation. The hard walled cavity is replaced by an unbounded fluid domain and the indicator Δ is applied to the radiated power. Besides the fact that the plane wave excitation allows for a better accuracy, the results confirm what already observed in Fig. 4.8. Moreover, it is intersting to note that, for the plane wave excitation, the solution obtained by the hybrid

models is in very good agreement (in terms of band averaging) with the classical TMM above 300 Hz. This mainly corroborate the ability of the TMM to capture non resonant transmission paths.

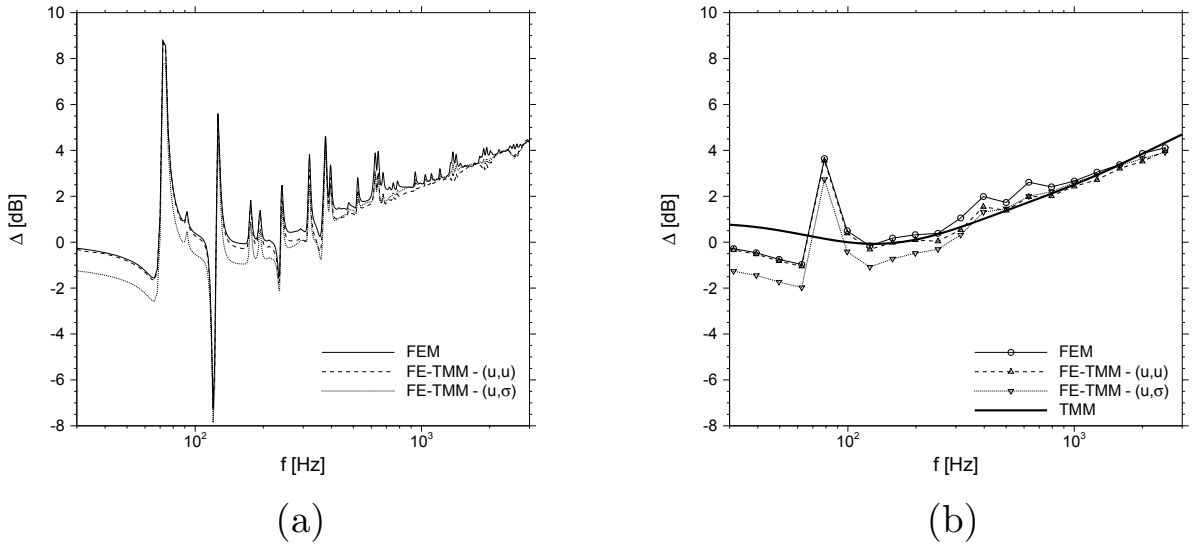

Figure 4.9 Eq. 4.16 applied to the power radiated into the semi-infinite fluid considering a 4 cm melamine (lay-up 1) and a 4 cm felt (lay-up 2). The plate is acoustically excited by a 45°/45° plane wave. Comparison between the finite element and the hybrid models based on the (u, u) and (u, σ) formulations. Narrow band (a) and third-octave band average (b).

Finally, the effect of the material properties on the spring-mass trim is assessed. The same plate-cavity system discussed in Fig. 4.6 in section 4.5.1 is considered for this purpose. Fig. 4.10 shows the difference Δ in the quadratic pressure when the 2 cm melamine layer is replaced with a felt of the same thickness. The acoustic trim finite size effects are now confined around the double wall resonance of the system. As expected, the results confirm that the error depends on the adopted material. Namely, on average a 2 dB gap is observed between 250 and 450 Hz between the prediction obtained with the hybrid models and the reference curve. As already pointed out, this is due the fact that the softer is the poroelastic layer (i.e. felt softer than melamine) the more accurate are the hybrid models. It is noteworthy that, although not shown here, the quadratic velocity is well predicted for both the considered materials.

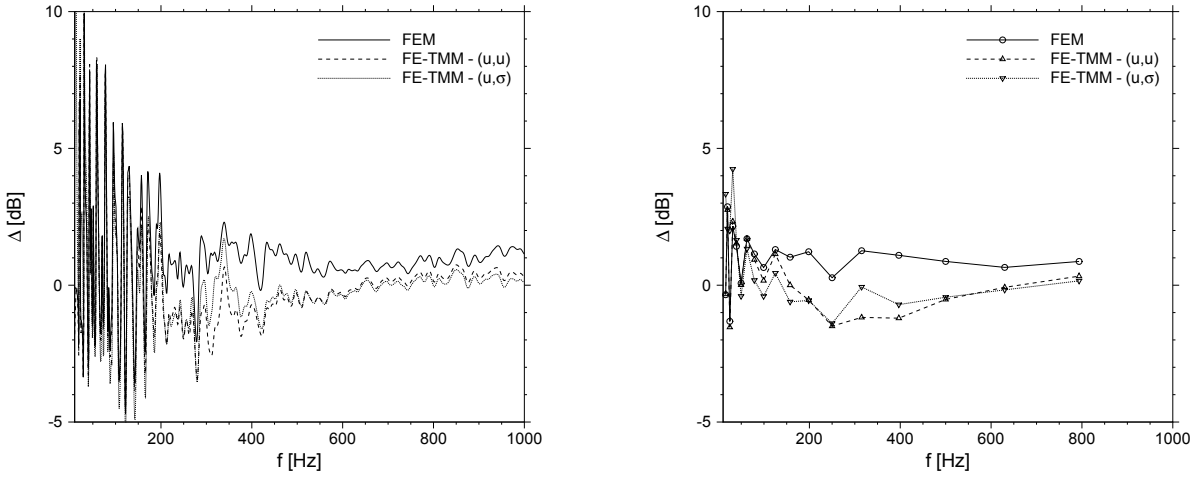

Figure 4.10 Eq. 4.16 applied to the quadratic pressure in the acoustic cavity considering a 2 cm melamine with 1.2 kg/m^2 heavy layer (lay-up 1) and a 2 cm felt with 1.2 kg/m^2 heavy layer (lay-up 2). The plate-cavity system is mechanically excited by a point force. Comparison between the finite element and the hybrid models based on the (u, u) and (u, σ) formulations. Narrow band (a) and third-octave band average (b).

4.6 Conclusions

A simplified modeling strategy to account for acoustic treatments in vibroacoustic finite element analysis was presented. The theoretical framework applies to flat, homogeneous and isotropic acoustic treatments and assumes that finite size effects are negligible. As a result, the response of the acoustic trim is approximated by its direct field contribution only, which can be modeled by employing Green functions formalism. In this work, the effect of different mathematical formulations of the direct field response of the acoustic trim was assessed. These formulations differ by the selection of the boundary conditions imposed outside the trimmed area at the end of the rims (i.e. baffling condition). The considered methodology takes advantage from the use of the jinc function to simplify the calculation of the discrete model matrices and their integration in the finite element equations of the vibroacoustic system.

Two different combination of baffling conditions were considered, leading to the (u, u) and (u, σ) formulations of the acoustic trim problem. The results showed that, for typical acoustic treatments, the effect of the adopted formulation is practically negligible, as the two models were found to give similar results. Namely, the same tendency of the modeling error was observed for both models. Hence, from a practical standpoint, the direct field response of the acoustic trim can be approximated by any of the two considered formulations. This conclusion can be extended to other combinations of baffling conditions (i.e. (σ, σ) and (σ, u) formulations), which were not discussed here for the sake of conciseness. As a result, it can be argued that, given the accuracy that the hybrid models can achieve, the formulation which minimizes the computational cost must be be preferred. In particular, in this paper it has been observed that the (u, σ) formulation allows for the fastest assembly of the hybrid model when the acoustic trim is placed between a finite element structural and acoustic domain.

As a final remark, this work also confirmed the limitation of the direct field model of the acoustic trim (regardless of the adopted formulation) shown in previous publications (Ref. [1] and chapter 3). Namely, although the qualitative behavior of the system is always well captured, the effect of the reflected field must be retrieved if a good accuracy is required. Such conclusion may be not surprising for spring-mass layups at the thickness resonances (where the response is quite non local). This is however less obvious for simple sound packages involving only one soft and dissipative layer (i.e. light layups). A correction to account for finite size effects is proposed in the next chapter.

CHAPTER 5

FINITE SIZE CORRECTION FOR THE FE-TMM

This chapter in concerned with the development of a finite size correction. Namely, the image source method is employed to retrieve the effect of the sound package lateral boundaries. The chapter is presented in the form of a paper (Part II of a two-parts paper), although the manuscript has not been submitted yet. In addition, for the sake of completeness, further results have been added at the end of the chapter to show how the mounting conditions between the noise control treatment and the structure can affect the accuracy of the hybrid FE-TMM.

Auteurs et affliation:

L. Alimonti: Étudiant au doctorat, Université de Sherbrooke, Faculté de Génie, Department de génie mécanique

N. Atalla: Professeur, Université de Sherbrooke, Faculté de Génie, Département de génie mécanique

Date d'acception: -

État de l'acceptation: -

Revue: -

Référence: -

Titre français: Modélisation efficiente des traitements acoustiques planes et homogénes pour l'analyse vibroacoustique par éléments finis. Partie 2: correction de dimension finie par la méthode de la source d'image

Contribution au document: Dans ce article, la méthode de la source d'image est utilisé pour récupérer l'effet des frontiéres latérales du traitement acoustique

Résumé français: Ce travail porte sur la méthodologie fini hybride matrice de transfert d'éléments élaborée dans la première partie de cet article. L'hypothèse principale de cette méthode hybride consiste à négliger l'étendue latérale finie réelle du traitement de contrôle de bruit. Bien qu'une augmentation substantielle de l'efficacité de calcul peut être réalisé, l'effet du champ réfléchi (à savoir les effets de taille finie) peut être parfois important, ce qui empêche le modèle hybride de fournir des résultats quantitatifs significatifs. Pour cette raison, une correction pour tenir compte des réflexions d'ondes aux limites latérales du traitement de contrôle du bruit est recherchée. A cette fin,

il est démontré dans le présent travail que le procédé de la source d'image peut être utilisé avec succès pour extraire les effets de taille finie. En effet, cette méthode est reconnue comme efficace lorsque la réponse du système est une fonction lisse de la fréquence, comme dans le cas des traitements de réduction du bruit fortement dissipatifs. La principale préoccupation de cet article est d'évaluer l'exactitude et la faisabilité de la méthode de la source de l'image dans le cadre de la modélisation de traitements insonorisants. Des exemples numériques démontrent que les performances du modèle hybride standard peuvent être sensiblement améliorées par la correction proposée sans détérioration excessive de l'efficacité de calcul.

Note: -

5.1 Abstract

This work is concerned with the hybrid finite element-transfer matrix methodology developed in part I of this paper. The main assumption behind this hybrid method consists in neglecting the actual finite lateral extent of the noise control treatment. Although a substantial increase of the computational efficiency can be achieved, the effect of the reflected field (i.e. finite size effects) may be sometimes important, preventing the hybrid model from giving quantitative meaningful results. For this reason, a correction to account for wave reflections at the lateral boundaries of the noise control treatment is sought. For this purpose, it is shown in the present paper that the image source method can be successfully employed to retrieve such finite size effects. Indeed, such methodology is known to be effective when the response of the system is a smooth function of the frequency, like in the case of highly dissipative noise control treatments. The main concern of this paper is to assess accuracy and feasibility of the image source method in the context of noise control treatments modeling. Numerical examples show that the performance of the standard hybrid model can be substantially improved by the proposed correction without deteriorating excessively the computational efficiency.

5.2 Introduction

This paper is concerned with the low frequency modeling of vibroacoustic systems with passive noise control treatments. Such acoustic components, often called acoustic trims or sound packages, are typically made of several layers of highly dissipative materials (e.g. porous media, rubbers, thin screens etc. . .) assembled in a multilayer fashion and coupled with structural and acoustic domains. In the low frequency range, the Finite Element

Method [10] (FEM) is typically employed to model such coupled systems. However, two main issues arise from the application of this methodology to the modeling of passive noise control components. First, the acoustic trim involves soft and dissipative materials which, despite the small volume occupied, typically require several degrees of freedom in order to correctly capture the solution. This aspect may become a serious issue when poroelastic materials are involved in the treatment lay-up [30] and simplified equivalent fluid models do not guarantee reliable accuracy [84]. Second, the use of the FEM is intrinsically associated to a preprocessing phase where each layer of the acoustic trim must be carefully meshed. This can be time consuming when several configurations of the same system must be simulated, like, for instance, in an optimization process. Therefore, although the FEM can still be considered an accurate tool in the final validation stage, there is a need for more efficient approaches.

Recently, several authors have proposed simplified modeling strategies for acoustic treatments based on integral formulations [1, 26, 105] (see also chapters 3 and 4) involving analytical kernels (i.e. Green functions) which can be efficiently computed by the Transfer Matrix Method [3] (TMM). These methodologies allow to calculate the surface impedance of the sound package to use in finite element analysis in order to take into account the effect of acoustically treated parts on the vibroacoustic response of a fluid-structure system. The rationale behind these hybrid Finite Element-Transfer Matrix Methods (FE-TMMs) is based on the assumption that size effects due to the finite lateral extent of the trim are negligible. Essentially, the sound package is modeled as an equivalent reacting surface whose dynamic response is given by its direct field contribution only. The reflected field emanating from the lateral boundaries of the surface is, instead, not considered. Formally, the approach assumes the layers involved in the acoustic trim to be flat and homogeneous. Under these conditions, the analytical model of the acoustic trim has shown interesting performance. Namely, the dynamic effects of the actual finite size treatment (i.e. mass, stiffness and damping added to the master structural and acoustic domains) are always qualitatively captured [1] (see chapter 3), thus overcoming the intrinsic limitations of simple local impedance models. However, the accuracy may be sometimes lacking. Indeed, the finite size of the acoustic trim can play an important role at low to mid frequencies depending on the considered materials and lay-up. This argument was confirmed in Part I of this paper (i.e. chapter 4) for typical absorption and transmission problems involving spring-mass as well as light trim configurations. Moreover, finite size effects are maximized when the coupling between the structural and fluid domains with the acoustic trim is characterized by geometrical orthogonalities among the modes, as shown in chapter 3. In such cases, although the analytical model can still capture the exact position of the acoustic

trim resonances, the accuracy at low frequency may be jeopardized. As a result, it can be concluded that the reflected vibrational field emanating from the lateral boundaries, even though confined in a thin region, may be important if a good accuracy is required. Therefore, a correction is needed.

The problem of accounting for the reflected field in mathematical models which neglect the presence of boundaries has been an active subject of research in the past two decades. Most of these works are mainly concerned with the high frequency analysis of vibrating systems in the context of the Statistical Energy Analysis [73] (SEA). Essentially, the system is assumed to be lightly damped, so that the reflected waves emanating from the boundaries actually give rise to a chaotic vibrational field due to multiple consecutive reflections and short wavelengths. A reflected field so characterized, is often called *reverberant* or *diffuse* and can be studied with statistical tools [64, 106]. However, this approach cannot be employed in the present analysis. Indeed, dissipative effects dominates within the acoustic trim, so that the resulting reflected field is rather *non reverberant* and *non diffuse*, as it dies out within few (or none) oscillations before being reflected again by other boundaries. Although other approaches have been proposed to relax the diffuse field hypothesis (a comprehensive overview can be found in Ref. [68]), their application is not straightforward in the context of arbitrary sound packages, because of the complexity of the multilayered treatment in the thickness direction.

On the other hand, the Image Source Method [86] (ISM) is often employed in acoustics to obtain the solution in a bounded domain from the formulation of an equivalent unbounded problem. The classical ISM consists in representing wave reflections at the boundaries by introducing virtual sources in the unbounded domain. Such fictitious sources are mirrors of the original source with respect to the boundaries of the system. The ISM is widely used in room acoustics [4, 16, 78, 101] and has also been applied to structural vibrations [28, 29, 51, 52]. In acoustic applications, the amplitudes of the image sources are given by the product of the amplitude of the original source and the reflection coefficient of the boundary at which the reflection occurs. For constant reflection coefficients (e.g. hard wall conditions in closed acoustic cavities) the method exactly reproduce the prescribed boundary conditions on straight edges. In structural applications, the ISM is not always as powerful, since only few boundary conditions can be reproduced by simple images of the actual source [52]. Unlike the FEM, the efficiency of the ISM increases with short wavelengths and high damping, suggesting that this methodology could be efficiently employed for the acoustic treatments modeling. Indeed, as previously observed, the reflected field within the acoustic

trim is non reverberant so that only few reflections (i.e. few mirror sources) are expected to be important.

The purpose of this work is to provide a first assessment of the ISM in the context of noise control treatments modeling. Namely, the ISM is employed to correct the analytical model for laterally unbounded, flat and homogeneous sound packages proposed in chapter 4. The possibility to represent specific lateral boundary conditions is not contemplated. A straightforward use of the ISM based on physical arguments is rather preferred. On the one hand, this choice is justified by the approximate nature of the analytical model (i.e. some details are already intrinsically lost compared to a finite element approximation). On the other hand, multilayered treatments can be quite complex systems, so that lateral mounting conditions might be either not exactly known, hard to model or, from an industrial standpoint, vary for each realization of the system (e.g. assembled car). Thus, the objective is to assess the feasibility of a simplified image sources based correction to retrieve the accuracy that was intrinsically missing in the unbounded model of the acoustic trim proposed in chapter 4. The study is restriced to hard wall lateral boundary conditions (i.e. lossless) and to rectangular treated areas in order to simplify the image sources generation process.

The paper is organized as follows. In Section 2 the main equations are introduced and the finite size correction is presented by introducing images of the actual sources forcing the acoustic trim over the two ends of the multilayer. Since such correction is exact only if an equivalent fluid behavior is assumed for the whole acoustic trim, physical arguments are provided to justify the methodology for generic configurations. In Section 3, the corrected model of the acoustic trim is validated through a benchmark similar to that proposed in chapter 4. Then, in Section 4, two application are proposed. First, a simplified automotive application is considered. Then, the effectiveness of the proposed correction is assessed in the case of layups whose behavior cannot be assumed equivalent to that of a fluid domain. Namely, an acoustic trim involving a poroelastic layer with non negligible mechanical properties is considered.

5.3 Theoretical background

The acoustic treatment is assumed (i) flat, (ii) homogeneous in the plane (i.e. thickness, lay-up and material properties do not change over the treated surface) and (iii) isotropic. One side of the multilayer (i.e. side A) is considered to be attached onto a structure while the other side (i.e. side B) radiates into a fluid. The coupling surface between the treat-

ment, the structure and the fluid is herein referred to as the trimmed (or, equivalently, treated) area S. Under this circumstances, the analytical model of the the laterally unbounded acoustic trim was presented in chapter 4. The model accounts only for normal displacement and stress at the ends of the treatment. Due to the negligible impact of the boundary conditions to apply outside the surface S (i.e. the absolute complement of S in $\mathbb{R}^2$, i.e. $\mathbb{R}^2 \setminus S$) on the two sides of the trim, two formulations were proposed. Namely, the (u, u) formulation assumes both ends of the treatment inserted in a rigid baffle ($u = 0$ over $\mathbb{R}^2 \setminus S$) while the (u, σ) considers side A baffled ($u = 0$ over $\mathbb{R}^2 \setminus S$) and side B unbaffled ($\sigma = 0$ over $\mathbb{R}^2$ S). The (u, u) formulation is supported by physical arguments (i.e. it exactly gives the direct field response if the acoustic trim is assumed to behave like a fluid) but it requires more computational effort to integrate the response of the trim into the finite element equation of the master structural and acoustic degrees of freedom. On the other hand, the (u, σ) formulation is justified by its efficiency, as it minimizes the number of operations required to build the final hybrid model. A comprehensive derivation of these two formulations can be found in chapter 4. Here, only the final result is used. Considering for instance the (u, u) formulation, the response of the laterally unbounded sound package can be written as

$$\begin{cases} \mathbf{R}_A(\omega) &= \mathbf{D}_{AA}(\omega)\,\mathbf{a}(\omega) + \mathbf{D}_{AB}(\omega)\,\mathbf{b}(\omega) \\ \mathbf{R}_B(\omega) &= \mathbf{D}_{BA}(\omega)\,\mathbf{a}(\omega) + \mathbf{D}_{BB}(\omega)\,\mathbf{b}(\omega) \end{cases}, \tag{5.1}$$

where $\mathbf{a}$ and $\mathbf{b}$ are the coefficients associated to each basis function used to approximate the displacement over sides A (i.e. u_A) and B (i.e. u_B). Namely, a jinc function [63] is associated to each node of the discretized surface S. The entries of the generalized dynamic stiffness matrices are defined as

$$D_{mn_{ij}}(\omega) = D_{mn}(r_{ij}, \omega) = \left(\frac{4\pi}{k_s^2}\right)^2 \frac{1}{2\pi} \int_0^{k_s} \hat{d}_{mn}(k, \omega) J_0(k r_{ij}) k \,\mathrm{d}k\,, \tag{5.2}$$

where $m = A, B$ and $n = A, B$, $k = |\mathbf{k}|$ is the modulus of the wavenumber, $J_0(kr_{ij})$ is the Bessel function of zero order of argument kr_{ij}, $r_{ij} = |\mathbf{r}_{ij}|$ is the Euclidean distance between nodes $\mathbf{x}_j$ and $\mathbf{x}_i$ and k_s is the maximum wavenumber content of the jinc function. The formalism $\hat{f}(k)$ indicates the radially symmetric Fourier transform, i.e. Hankel transform, of the function $f(r)$. Thus, the analytical kernels $\hat{d}_{mn}(k, \omega)$ are the transformed Green

functions. Finally, vectors $\mathbf{R}_A$ and $\mathbf{R}_B$ are the normal stresses acting on the acoustic trim degrees of freedom, i.e.

$$R_{m_i}(\omega) = \int_S 2\,\mathrm{jinc}(k_s r)\sigma_m(\mathbf{x},\omega)\,\mathrm{d}S\,, \tag{5.3}$$

where $r = |\mathbf{x}_i - \mathbf{x}|$ (i.e. the jinc function is centered at $\mathbf{x}_i$).

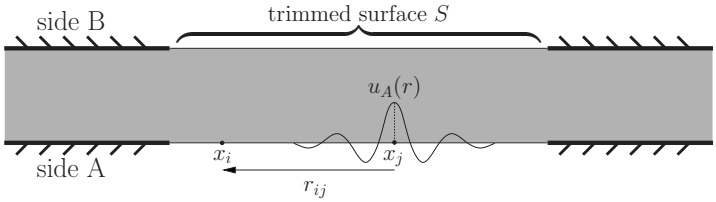

Figure 5.1 Through-the-thickness view of the acoustic trim baffled on both ends (i.e. (u,u) formulation). A jinc-like displacement is applied at point $\mathbf{x}_j$. The module of the distance between the source and the observation point $\mathbf{x}_i$ is r_{ij}.

To facilitate the discussion, let us focus on the following scalar problem taken from Eq. 5.1

$$R_{A_i}(\omega) = D_{AA}(r_{ij},\omega)a_j(\omega) = D^{\infty}(r_{ij},\omega)a_j(\omega)\,, \tag{5.4}$$

where the formalism D^{∞} has been employed in place of D_{AA} to emphasize that the solution assumes an infinite laterally extended system (i.e. direct field response). Eq. 5.4 gives the reaction on node i due to a displacement of the form $2\,\mathrm{jinc}(k_s r)$ centered in $\mathbf{x}_j$ and of amplitude a_j when all other degrees of freedom are fixed to zero. With an abuse of notation due to the finite value of k_s, $D^{\infty}(r_{ij},\omega)$ is the Green function of the multilayer in the physical space, relating the output at a given point (i.e. R_{A_i}) to the source (i.e. a_j). The mathematical problem is sketched in Fig. 5.1. Similar equations can be defined by employing other blocks of Eq. 5.1, or considering the (u,σ) formulation instead. Eq. 5.4 will be used in the next section to develop the finite size correction based on the ISM.

5.3.1 Finite size correction

In the ISM, the reflected field emanating from the boundary of the system is interpreted as the effect of virtual sources, whose position in the space is uniquely determined by the position of the original source. The methodology assumes the domain to have a polygonal

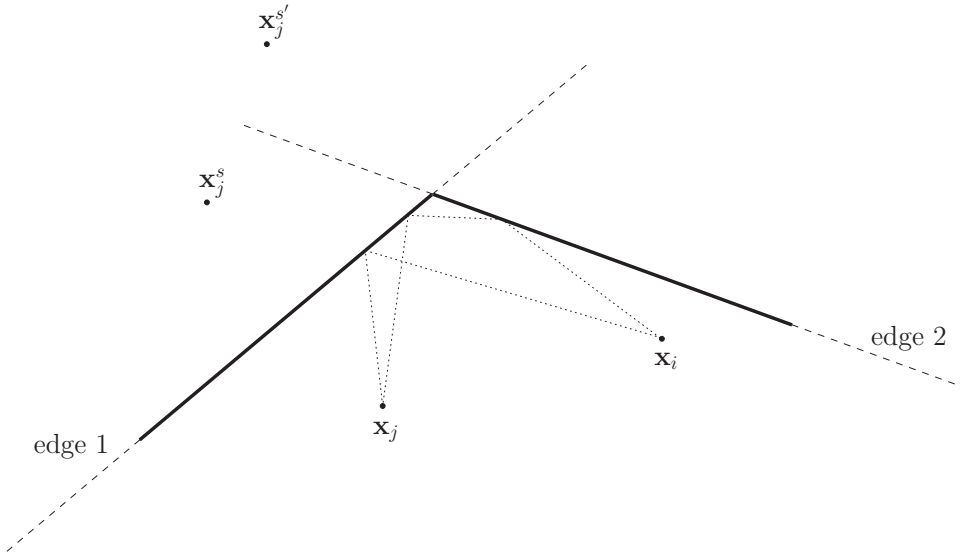

Figure 5.2 Image sources generation process for a convex corner.

shape, i.e. only reflections at straight edges can be modeled. Under these conditions, the two-dimensional process to generate the virtual sources is depicted in Fig. 5.2. Subscripts j and i refers to the source and receiver, respectively. Consider, for instance, the reflection on edge 1 of the wave field generated by a source located at $\mathbf{x}_j$. The reflected field is interpreted as the vibrational field emanating from a source located at $\mathbf{x}_j^s$, whose coordinates are determined by the symmetry of $\mathbf{x}_j$ with respect to edge 1. Then, if waves arising from the image source are reflected again by another boundary along their path, a new reflection must be accounted for. Hence, another image source is generated. For instance, a second order image is located at $\mathbf{x}_j^{s'}$, where the superscript s' indicates that the new source accounts for a second order reflection of the reflected field originally emanated from edge 1. Thus, referring to Eq. 5.4, the total reaction at the observation point $\mathbf{x}_i$ obtained by superposition of direct and reflected field contributions can be written as

$$R_{A_i}(\omega) = D^{\infty}(r_{ij}, \omega) a_j(\omega) + \sum_{p=1}^{N_w} \sum_{q=1}^{\infty} D^S(r_{ij^{(p,q)}}, a_j, \omega)\,, \tag{5.5}$$

where, N_w is the number of straight edges composing the boundary, q is the number of successive reflections (in theory infinite higher order images are required) and $r_{ij^{(p,q)}}$ is the module of the distance between the virtual source associated to the couple (p, q) and the receiver point $\mathbf{x}_i$. The function $D^S(r, a_j, \omega)$ is defined in such a way that some conditions are satisfied for the reflection corresponding to the couple (p, q). For generic boundary conditions, the contribution of the reflected field can be complicated, as simple image

sources might not be sufficient to reproduce the exact effect of the boundary (see, for instance, the application to thin plate vibrations of Gunda *et al.* [52]). However, in this work, the problem is rather simplified. Namely, an equivalent fluid behavior is assumed for the whole acoustic trim. Consequently, the latter can be equivalently seen as a shallow acoustic cavity and classical results for the reflected field can be used [4, 16, 78, 101]. Under this hypothesis, if perfect reflections are considered at lateral boundaries (i.e. lossless walls), Eq. 5.5 becomes

$$R_{A_i}(\omega) = \left(D^{\infty}(r_{ij}, \omega) + \sum_{p=1}^{N_w} \sum_{q=1}^{\infty} D^{\infty}(r_{ij^{(p,q)}}, \omega) \right) a_j(\omega) \,. \tag{5.6}$$

Thus, the reflected field is given by the equivalent direct field emanating from successive image sources with the same intensity of the original source. Formally, Eq. 5.6 is valid only under the aforementioned hypothesis, i.e. only if equivalent fluid layers are involved in the treatment. On the other hand, if different media are considered (e.g. solid and poroelastic layers), Eq. 5.6 should rather be interpreted as an approximation of the exact finite size behavior. Indeed, the reflection of all type of waves (e.g. compressional and shear) propagating within the layers of the treatment occurs at the boundary. Generally speaking, such reflection generates coupling effects among all wave types that one simple image source cannot predict. Nonetheless, the image source guarantees that the energy impinging onto the lateral boundaries is perfectly reflected back, avoiding energy losses. From this standpoint, the proposed methodology is similar to the Ray Tracing Method (RTM, see for instance the application to thin plates of Chae and Ih [18]). Such energetic interpretation suggests that, regardless of the particular boundary conditions, the reflected field should be at least quantitatively captured on average, improving the performance of the laterally unbounded model assessed in chapter 4.

In order to simplify the implementation of the image sources detection algorithm, the present analysis is limited to rectangular treated areas S. In such case, the image sources locations is trivial [4]. Moreover, since the reflected field originated by the image sources is highly damped, multiple reflections do not need to be accounted for. Indeed, it can be argued that, for a sufficiently large trimmed area S, only two kind of reflections needs to be considered, namely (i) first order reflection along the four straight edges and (ii) second order reflection at the corners. With this assumption, the final lattice of virtual sources associated to the generic source located at $\mathbf{x}_j$ assumes the pattern in Fig. 5.3.

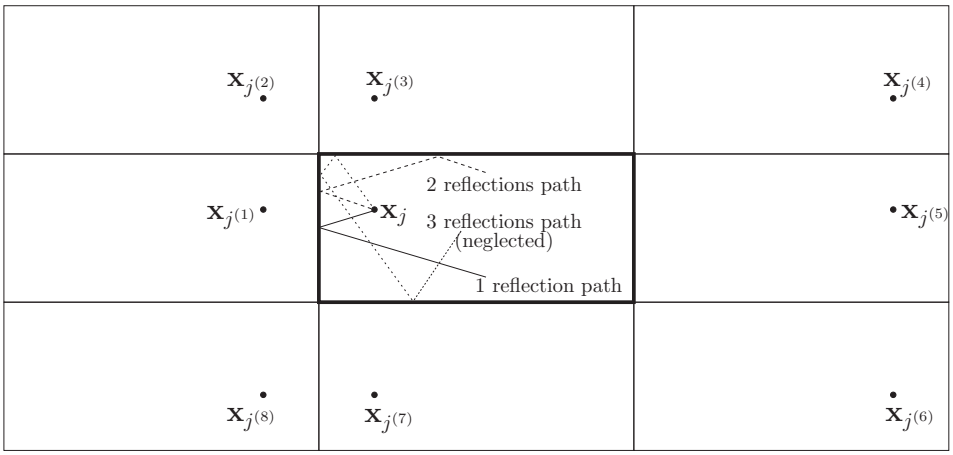

Figure 5.3 Images lattice accounting for up to second order reflections only at corners (i.e. double reflections between two opposite edges are neglected).

Extending the discussion above to the case of multiple sources, the reflected field within the acoustic trim is obtained from eight images of the n trimmed nodes. Hence, the final form of the corrected (u, u) formulation (Eq. 5.1) can be written as

$$\left\{ \begin{array}{rcl} \mathbf{R}_A(\omega) & = & \left(\mathbf{D}_{AA}(\omega) + \sum_{l=1}^{8} \mathbf{D}_{AA}^{(l)}(\omega) \right) \mathbf{a}(\omega) + \left(\mathbf{D}_{AB}(\omega) + \sum_{l=1}^{8} \mathbf{D}_{AB}^{(l)}(\omega) \right) \mathbf{b}(\omega) \\ \mathbf{R}_B(\omega) & = & \left(\mathbf{D}_{BA}(\omega) + \sum_{l=1}^{8} \mathbf{D}_{BA}^{(l)}(\omega) \right) \mathbf{a}(\omega) + \left(\mathbf{D}_{BB}(\omega) + \sum_{l=1}^{8} \mathbf{D}_{BB}^{(l)}(\omega) \right) \mathbf{b}(\omega) \end{array} \right. , \quad (5.7)$$

where, referring to the definition in Eq. 5.2,

$$D_{mn_{ij}}^{(l)}(\omega) = D_{mn}(r_{ij^{(l)}}, \omega) \quad (5.8)$$

with $r_{ij^{(l)}}$ the distance between the receiver node i and the l^{th} image of the node j. For completeness note that the corrected (u, σ) model (see chapter 4) of the trim is formally equivalent to Eq. 5.7, i.e.

$$\left\{ \begin{array}{rcl} \mathbf{R}_A(\omega) & = & \left(\mathbf{G}_{AA}(\omega) + \sum_{l=1}^{8} \mathbf{G}_{AA}^{(l)}(\omega) \right) \mathbf{a}(\omega) + \left(\mathbf{G}_{AB}(\omega) + \sum_{l=1}^{8} \mathbf{G}_{AB}^{(l)}(\omega) \right) \mathbf{b}(\omega) \\ \mathbf{R}_B(\omega) & = & \left(\mathbf{G}_{BA}(\omega) + \sum_{l=1}^{8} \mathbf{G}_{BA}^{(l)}(\omega) \right) \mathbf{a}(\omega) + \left(\mathbf{G}_{BB}(\omega) + \sum_{l=1}^{8} \mathbf{G}_{BB}^{(l)}(\omega) \right) \mathbf{b}(\omega) \end{array} \right. , \quad (5.9)$$

where the coefficients $\mathbf{b}$ are now associated to the normal stress on side B, i.e. σ_B. The reactions on the same side are now defined as (cf. Eq. 5.3)

$$R_{B_i}(\omega) = \int_S 2\,\mathrm{jinc}(k_s r) u_B(\mathbf{x}, \omega)\,\mathrm{d}S\,. \tag{5.10}$$

Matrices $G_{mn}(\omega)$ are formally equivalent to the definition in Eq. 5.2, taking care of replacing $\hat{d}_{mn}(k, \omega)$ with $\hat{g}_{mn}(k, \omega)$.

5.3.2 Assembly of the hybrid model

As shown in details in chapter 4, the acoustic trim models in Eqs. 5.7 and 5.9 can be easily integrated in the finite element equations of the structural-acoustic system. The generic form of the assembled final system reads

$$\left(\begin{bmatrix} \mathbf{Z}_{ss}(\omega) & \mathbf{Z}_{sa}(\omega) \\ \mathbf{Z}_{sa}^{\mathrm{T}}(\omega) & \mathbf{Z}_{aa}(\omega) \end{bmatrix} - \begin{bmatrix} \mathbf{Y}_{ss}(\omega) & \mathbf{Y}_{sa}(\omega) \\ \mathbf{Y}_{sa}^{\mathrm{T}}(\omega) & \mathbf{Y}_{aa}(\omega) \end{bmatrix} \right) \begin{Bmatrix} \mathbf{q}_s(\omega) \\ \mathbf{q}_a(\omega) \end{Bmatrix} = \begin{Bmatrix} \mathbf{F}_s(\omega) \\ \mathbf{F}_a(\omega) \end{Bmatrix}, \tag{5.11}$$

where matrix $\mathbf{Z}$ is a generalized impedance matrix and vectors $\mathbf{q}_s$ and $\mathbf{q}_a$ are the degrees of freedom of the structural (i.e. displacements and rotations or modal amplitudes) and acoustic (i.e. pressures or modal amplitudes) domains, respectively. Vectors $\mathbf{F}_s$ and $\mathbf{F}_a$ are the external disturbances forcing the structural and acoustic domains, respectively. If Eq. 5.11 is expressed in physical coordinates, the boundary operator $\mathbf{Y}$ accounting for the effect of the acoustic trim must be interpreted as acting only on the trimmed area finite element degrees of freedom. Without loss of generality, the second equation in Eq. 5.11 can refer to a hard walled as well as to an open acoustic cavity. Indeed, the radiation into a semi-infinite fluid can be modeled by adding an impedance operator to matrix $\mathbf{Z}_{aa}$ to account for the infinite extent of the acoustic domain, for instance employing the Boundary Element Method [6] (BEM) or the Perfectly Matched Layer [11, 12] (PML).

The hybrid system obtained using the (u, u) model of the acoustic trim involves the following boundary operator (see chapter 4)

$$\mathbf{Y} = \begin{bmatrix} \mathbf{H}^{\mathrm{T}}(\tilde{\mathbf{D}}_{AA} + \tilde{\mathbf{D}}_{AB}\tilde{\mathbf{D}}_{BB}^{-1}\tilde{\mathbf{D}}_{AB})\mathbf{H} & -\mathbf{H}^{\mathrm{T}}\tilde{\mathbf{D}}_{AB}\tilde{\mathbf{D}}_{BB}^{-1}\hat{\mathbf{H}}) \\ -\hat{\mathbf{H}}^{\mathrm{T}}\tilde{\mathbf{D}}_{BB}^{-1}\tilde{\mathbf{D}}_{AB}\mathbf{H} & \hat{\mathbf{H}}^{\mathrm{T}}\tilde{\mathbf{D}}_{BB}^{-1}\hat{\mathbf{H}} \end{bmatrix}, \tag{5.12}$$

where the superscript˜indicates that the direct field matrix has been corrected for finite size effects, i.e. $\tilde{\mathbf{D}}_{mn} = \mathbf{D}_{mn} + \sum_{l=1}^{8} \mathbf{D}_{mn}^{(l)}$. The explicit dependency on the circular frequency ω has been omitted to lighten the notation. Eq. 5.11 together with Eq. 5.12 gives the response of the vibroacoustic system accounting for finite size effects in the acoustic trim. The reciprocity condition $\hat{d}_{AB}(k,\omega) = -\hat{d}_{BA}(k,\omega)$ has been used, leading to the symmetry of the boundary operator. Matrices $\mathbf{H}$ and $\hat{\mathbf{H}}$ are suitable mapping operators between the acoustic trim and finite element nodal degrees of freedom (see chapter 4). As already pointed out in chapter 4, a matrix inversion is involved in the construction of the acoustic trim response, potentially jeopardizing the efficiency of the analytical model when the trimmed surface S involves a large number of nodes n (note that $\tilde{\mathbf{D}}_{BB}$ is fully populated). On the other hand, such drawback is avoided by employing the (u,σ) model of the acoustic trim. In such case, the boundary operator reads (see chapter 4)

$$\mathbf{Y} = \begin{bmatrix} \mathbf{H}^{\mathrm{T}}\tilde{\mathbf{G}}_{AA}\mathbf{H} & -\mathbf{H}^{\mathrm{T}}\tilde{\mathbf{G}}_{AB}\mathbf{H} \\ -\mathbf{H}^{\mathrm{T}}\tilde{\mathbf{G}}_{AB}\mathbf{H} & \mathbf{H}^{\mathrm{T}}\tilde{\mathbf{G}}_{BB}\mathbf{H} \end{bmatrix}, \tag{5.13}$$

where the reciprocity condition $\hat{g}_{AB}(k,\omega) = \hat{g}_{BA}(k,\omega)$ has been used. Differently from Eq. 5.12, Eq. 5.13 does not require any matrix inversion in the construction of the acoustic trim response, allowing to reduce the computational burden for large n.

5.3.3 Overview of the computational cost

Thanks to the simplifications adopted in the previous section, the corrected model of the acoustic trim (Eq. 5.7 and 5.9) essentially requires only the evaluation of the analytical kernels $D_{mn}(r,\omega)$ at the distances between the trimmed nodes and their images. Since functions $D_{mn}(r,\omega)$ are sampled at each frequency over a set of radius points (see chapter 4), only extra interpolations are needed to account for the effect of the reflected field. Such conclusion strictly holds under the previously assumed hypothesis of a rectangular trimmed surface S, as for such geometries the locations of the images can be quickly calculated. However, in the case of generic polygons, the computational time required by a mirror sources detection algorithm (see Cuenca *et al.* [29]) must be also accounted for. Although this aspect is not subject of this work, it can be argued that, since only the first low order images should be generated, efficiency issues are not expected to be encountered. Moreover, for typical sizes of the trimmed area, dissipation effects would also render the images of several trimmed nodes ineffective, as the reflected field emanating from them might not reach other nodes. This physical observation seems to justify the definition

of a tolerance which forces to zero some of the elements of matrices $\mathbf{D}_{mn}^{(l)}$ (resp. $\mathbf{G}_{mn}^{(l)}$). Consequently, the number of interpolations would be minimized and the computational efficiency optimized. This particular aspect will be assessed in Section 3.2.

As a final remark concerning the computational costs, the effect of the finite size correction on the two proposed formulations of the laterally unbounded acoustic trim (i.e. (u, u) and (u, σ)) is worth discussing. In fact, it can be pointed out that the corrected (u, u) and (u, σ) models are expected to reproduce the same finite size behavior although the two formulations use different baffling conditions over the two sides of the treatment. As a result, the corrected hybrid models (Eqs. 5.12 and 5.13) are expected to give the same solution. The effect of the adopted formulation will be discussed in Section 3.1. Once the above argument is confirmed, the most efficient formulation (i.e. (u, σ)) should be always preferred.

5.4 Validation

This section aims at validating the infinite acoustic trim model corrected by means of the ISM presented in Section 5.3. To this end, only the case of acoustic treatments having an equivalent fluid behavior is considered (an example illustrating the accuracy of the model for a poroelastic trim will be given later in section 4). In this case, the exact solution is expected to be retrieved. The effect of the correction on both the (u, u) and (u, σ) formulations is also assessed. Moreover, a convergence study is carried out to justify the assumption of the a priori image sources lattice in Fig. 5.3 and to propose a truncation rule for the images generation process. Throughout this section, the reference solution uses the finite element based substructuring methodology developed by Hamdi *et al.* [53], which employs a finite element model of the acoustic trim to calculate the boundary operator $\mathbf{Y}$ in Eq. 5.11. Typical vibroacoustic indicators such as structural space averaged quadratic velocity, acoustic space averaged quadratic pressure and power radiated into a fluid domain. The mechanical and acoustic properties of the considered materials are reported in Tab. 5.1. Emphasis will be put on mechanical excitations. Indeed, it was observed in chapter 4 that finite size effects in the acoustic trim are maximized when the system is mechanically excited.

5.4.1 Assessment of the finite size correction

To begin with, the absorption provided by a dissipative layer attached onto a wall of a parallelepiped cavity of dimensions $0.8 \times 1.7 \times 1\,\mathrm{m}^3$ excited by an acoustic monopole is

Table 5.1 Materials used in the numerical simulations. Note that m (given in the text) refers to the mass per unit surface of the considered heavy layers.

Material	**Properties**	
	Acoustic	**Mechanical**
Steel		density = $8000\,\mathrm{kg/m^3}$ Young's modulus = $200\,\mathrm{GPa}$ Poisson's ratio = 0.33 damping factor = 0.02
Air	density = $1.21\,\mathrm{kg/m^3}$ speed of sound = $342.2\,\mathrm{m/s}$	
Melamine	porosity = 0.99 resistivity = $10900\,\mathrm{kg/m^3s}$ tortuosity = 1.02 viscous length = $100\,\mu\mathrm{m}$ thermal length = $130\,\mu\mathrm{m}$	density = $8.8\,\mathrm{kg/m^3}$ Young's modulus = $80\,\mathrm{kPa}$ Poisson's ratio = 0.4 damping factor = 0.17
Felt	porosity = 0.98 resistivity = $26514\,\mathrm{kg/m^3s}$ tortuosity = 1 viscous length = $48\,\mu\mathrm{m}$ thermal length = $144\,\mu\mathrm{m}$	density = $58\,\mathrm{kg/m^3}$ Young's modulus = $6\,\mathrm{kPa}$ Poisson's ratio = 0.04 damping factor = 0.15
Polyurethan	porosity = 0.99 resistivity = $6758\,\mathrm{kg/m^3s}$ tortuosity = 1.4 viscous length = $83\,\mu\mathrm{m}$ thermal length = $325\,\mu\mathrm{m}$	density = $29.1\,\mathrm{kg/m^3}$ Young's modulus = $110\,\mathrm{kPa}$ Poisson's ratio = 0.4 damping factor = 0.1
Heavy layer		density = $m \cdot 10^{-3}\,\mathrm{kg/m^3}$ Young's modulus = $10^3\,\mathrm{kPa}$ Poisson's ratio = 0.3 loss factor = 0.5

assessed. A 4 cm melamine foam is attached onto the $0.8 \times 1.7\text{m}^2$ rigid wall at $z = 0$. Moreover, a proportional structural damping model is used to introduce dissipative effects within the cavity itself ($\eta_a = 0.01$). A monopole with constant volume velocity is applied at the corner located at $(0\,\text{m}, 1.7\,\text{m}, 1\,\text{m})$. The response of the system up to 1 kHz is considered. The finite element model of the cavity involves $24 \times 50 \times 30$ eight-noded fluid elements. The foam, assumed to be limp, is modeled with 5 eight-noded equivalent fluid elements along its thickness (same mesh of the acoustic domain in the plane). Fig. 5.4 shows the quadratic pressure inside the acoustic cavity. A perfect correlation is observed between the reference curve and the corrected hybrid models. Consequently, the corrected (u, u) and (u, σ) formulations are equivalent, as expected. The finite size effects can be appreciated by comparison with the solution obtained neglecting the image sources (i.e. direct field only). It can be argued that the reflected field effect must be accounted for to correctly capture the absorption provided by the acoustic treatment below 600 Hz (an error between 5 and 10 dB is observed if the finite size of the treatment is neglected). It is noted in passing that the considered geometry involves orthogonalities between the acoustic cavity and the dissipative fluid layer, i.e. only the cavity modes with the same shape over the trimmed area are coupled by the presence of the acoustic treatment. Nonetheless, Fig. 5.4 shows that the image sources correction exactly retrieves such effect.

A parallelepiped air filled plate-cavity system of dimensions $0.8 \times 1.7 \times 1\,\text{m}^3$ is considered next. The plate, clamped along its edges, covers the $0.8 \times 1.7\,\text{m}^2$ face of the cavity at $z = 0$. A 2 cm polyurethane foam with a 1.5kg/m^2 heavy layer on top is placed between the plate and the cavity. The response of the system driven by a point force applied on the plate at point $(0.112\,\text{m}, 0.131\,\text{m})$ and acting along the z-axis is considered. The finite element model of the plate and cavity involve 43×91 four-noded plate elements and $43 \times 91 \times 30$ eight-noded fluid elements, respectively. The mesh of the acoustic trim employs 5 eight-noded limp elements through the thickness of the polyurethane layer, while the heavy screen is modeled with one layer of eight-noded solid elements (see Tab. 5.1 for the structural properties). The simulation refers to the case of a 5% damping provided by the acoustic cavity itself (i.e. $\eta_a = 0.05$). The quadratic velocity is not reported since the direct field model of the sound package is already accurate enough to capture the damping added to the structure by this type of lay-up [1] (see also chapter 3). The quadratic pressure in the cavity is, instead, reported in Fig. 5.5. It can be observed that the effect of the reflected field is important between 200 and 600 Hz, where the peak of the response associated to the spring-mass resonance of the acoustic trim occurs. In this frequency range, the response of the trim is non local and size effects appears. Such

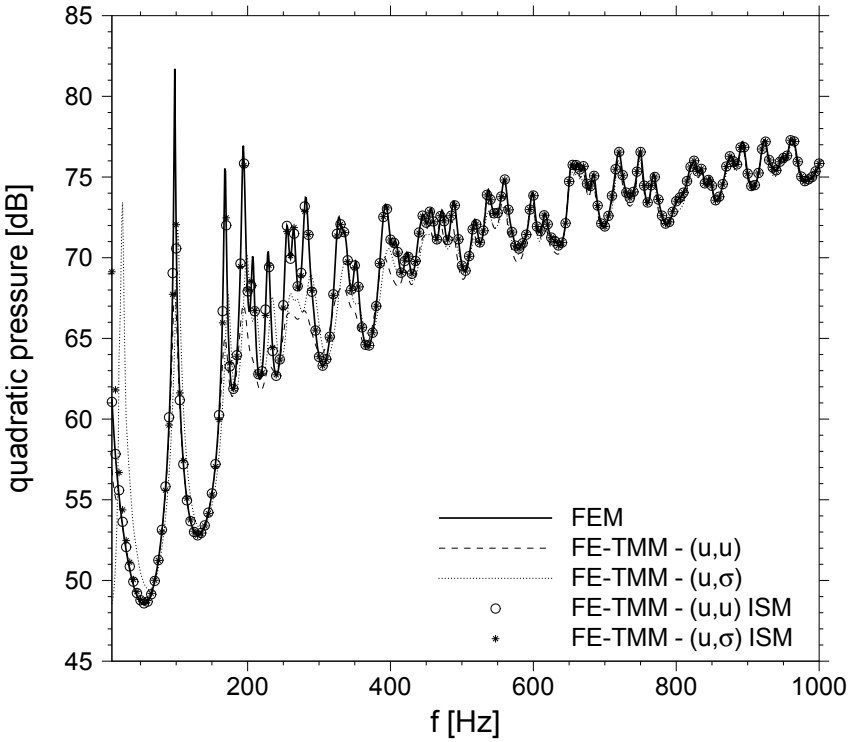

Figure 5.4 Space averaged quadratic pressure of the acoustic cavity excited by a monopole. A 4 cm melamine layer is attached onto the hard wall facing the excitation point. Effect of the finite size correction on the hybrid models based on the (u, u) and (u, σ) formulations.

behavior is exactly retrieved by adding image sources, as a perfect match between the corrected hybrid models and the reference solution is observed.

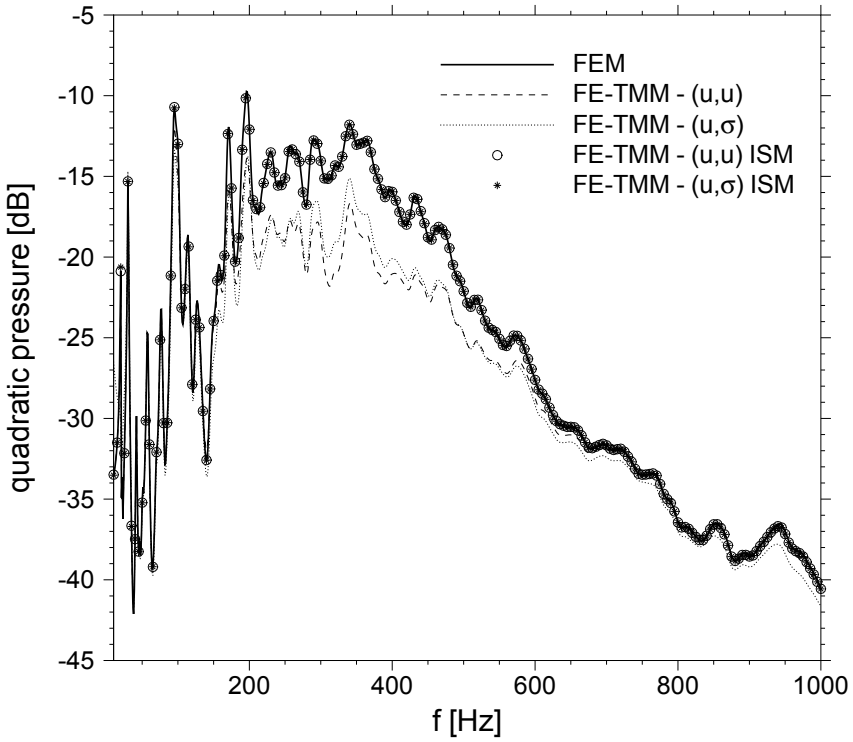

Figure 5.5 Space averaged quadratic pressure of the acoustic cavity. The plate-cavity system is mechanically excited by a point force. A 2 cm polyurethane foam with $1.5\,\mathrm{kg/m^2}$ heavy layer on top is placed between the plate and the cavity. Effect of the finite size correction on the hybrid models based on the (u, u) and (u, σ) formulations.

Finally, to conclude the present validation, the radiation of a clamped plate in an unbounded fluid domain is considered. The surface radiating into the semi-infinite fluid is assumed to be inserted into a infinitely extended rigid baffle. The plate is 0.4 m long and 0.85 m wide. The mechanical force is now located at $(0.114\,\mathrm{m}, 0.147\,\mathrm{m})$. The finite element model of the plate involves 35×70 four-noded plate elements. A light treatment consisting of a 4 cm felt is attached onto the structure and radiates in air. The felt is modeled with 10 eight-noded equivalent fluid (i.e. limp) elements along its thickness (same mesh of the structural domain in the plane). The radiated power is reported in Fig. 5.6. It is observed that the reflected field affects the power radiated into the semi-infinite fluid above 400Hz. Once again, the reference solution in perfectly recovered by the proposed hybrid models when the ISM is employed.

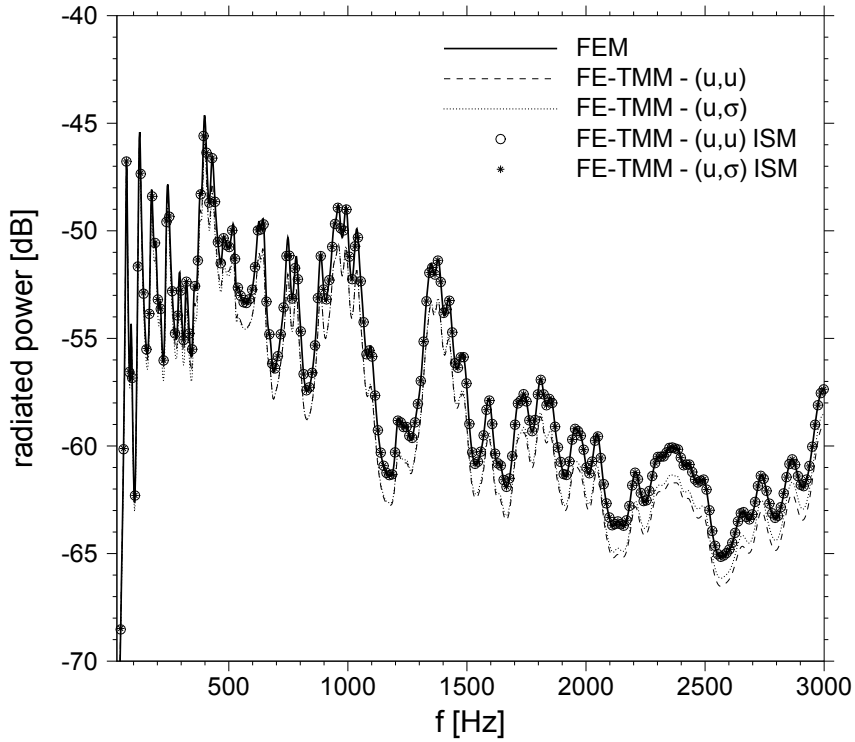

Figure 5.6 Power radiated into the semi-infinite fluid. The plate is mechanically excited by a point force. A 4 cm felt is attached onto the structure and radiates in the fluid. Effect of the finite size correction on the hybrid models based on the (u, u) and (u, σ) formulations.

To conclude, it can be argued that the analysis above confirms the hypotheses and observations discussed in Section 5.3. Namely, (i) the finite size correction by image sources allows to retrieve the exact behavior of acoustic treatments with an equivalent fluid behavior; (ii) the reflected field is non diffuse, as the minimum number of reflections (i.e. one along straight edges and two at corners, see image lattice in Fig. 3) is enough to capture its effects on the system response; (iii) the corrected (u, u) and (u, σ) formulations are equivalent, authorizing the user to choose the most efficient approach (i.e. (u, σ)).

5.4.2 Truncation rule for the image sources generation process

In this section a further analysis is presented to fully assess the hypothesis justifying the use of the ISM. Namely, the strong dissipative effects involved in the acoustic trim allows to overcome the typical issue related to the ISM, that is the number of images to be generated. To prove this argument, the region containing only those images which actually give a contribution to the reflected field must be defined. The analysis proposed in this section follows the work of Cuenca *et al.* [29], where a similar study were conducted for the application of the ISM to damped thin plates.

Although the number of images has already been limited to those accounting for the reflection paths in Fig. 5.3, a further criteria can be introduced to fully take advantage from the non diffuse nature of the reflected field. Namely, the reflected field is expected to be accurately determined by considering only those image sources which actually affect to the solution at the trimmed area nodes. In order to do this, a truncation criteria must be introduced to stop the image generation process. Typically, such criteria is based on the definition of a meaningful characteristic length. Thus, if the distance between the image source $\mathbf{x}_{j^{(l)}}$ (see Fig. 5.3) and the receiver point $\mathbf{x}_i$ is larger than such characteristic length, then the effect of the considered image is neglected. Formally, the condition for the effectiveness of the image source located at $\mathbf{x}_{j^{(l)}}$ reads

$$r_{ij^{(l)}} \leq \epsilon r_c \,, \tag{5.14}$$

where ϵ is a tolerance and r_c is the mean free path [62], i.e.

$$r_c = \frac{\pi S}{p} \,, \tag{5.15}$$

where S is the trimmed surface and p its perimeter. The mean free path is often used in room acoustics and is defined as the average distance a ray of sound travels before it encounters an obstacle and reflects. Equivalently, it may be seen as the average distance between two successive image sources. Since the image sources lattice considered in this work (Fig. 5.3) already assumes only one reflection at straight edges and double reflections at corners, a tolerance around 1 is expected to give reliable results. In what follows, two plate-cavity systems with light and spring-mass treatments are considered to prove the argument above. Only the results relative to the more efficient (u, σ) formulation are reported.

The first case refers to a $0.4 \times 0.85 \times 0.5\,\mathrm{m}^3$ air filled cavity. A clamped plate covers the $0.4 \times 0.85\,\mathrm{m}^2$ face of the cavity at $z = 0$ and is excited by a point force. A 4 cm felt is placed between the plate and the cavity. Fig. 5.7 shows the error between the quadratic pressure inside the cavity obtained with the hybrid model employing all the eight images of the lattice in Fig. 5.3 and that obtained with different values of the tolerance ϵ. The results show a slow convergence below 800 Hz. In this frequency range, the absorption provided by the felt layer must be correctly captured to obtain a good accuracy (cf. Fig. 5.4). Indeed, the first peaks of the error are localized around 200, 340 and 400 Hz, which are the first three non zero natural frequencies of the cavity. Thus, to correctly capture the damping added to each cavity mode an accurate description of the reflected field is required (although still confined in the lattice of Fig. 5.3). It could be argued that a value of the tolerance ϵ around 1.5 already gives an accurate solution apart at the first two resonances at 200 and 340 Hz. On the other hand, in the remaining portion of the considered frequency range, $\epsilon = 0.5$ already gives almost the same solution of the full images lattice. In this frequency range, the absorption is correctly captured even without finite size correction (cf. Fig. 5.4) whereas the transmission is typically underestimated if the reflected field is neglected (see Fig. 5.6). Thus, the power injected into the cavity can be perfectly retrieved considering only the image sources within about 0.2 m (i.e. maximum distance ϵr_c with $\epsilon = 0.5$) from the boundaries. All the images lying outside this cloud can be thus neglected.

The second case refers to a $0.8 \times 1.7 \times 1\,\mathrm{m}^3$ cavity. A clamped plate covers the $0.8 \times 1.7\,\mathrm{m}^2$ face of the cavity at $z = 0$ and is excited by a point force. A 2 cm melamine foam with a $1.2\mathrm{kg/m}^2$ heavy layer on top is placed between the plate and the cavity. The same convergence analysis for the acoustic quadratic pressure previously discussed is reported in Fig. 5.8. For the considered lay-up, the absorption provided by the sound package is now not important, as the peaks of the error at the cavity resonances (below 200 Hz) are not

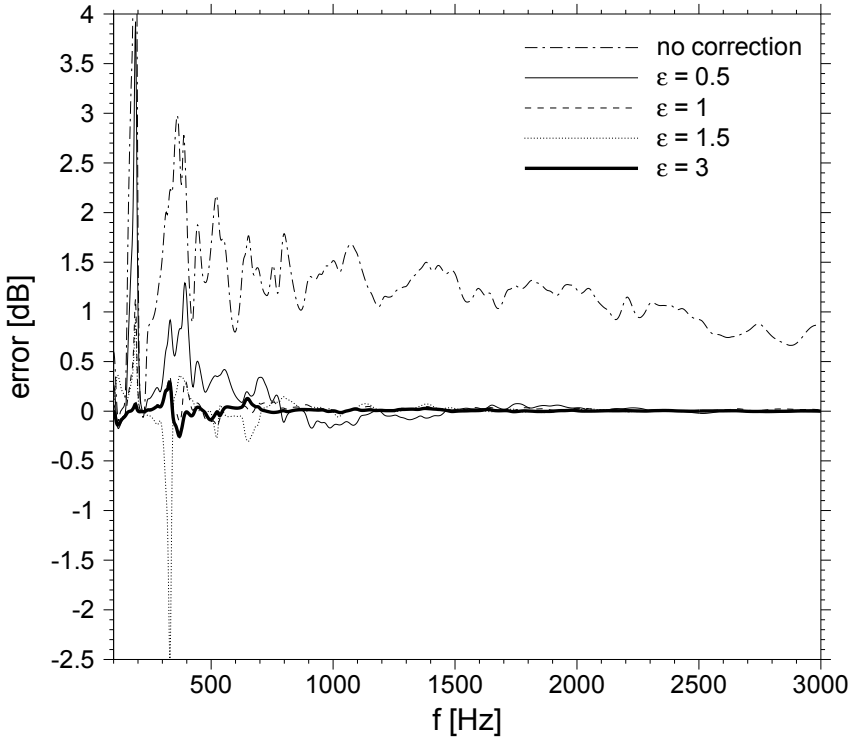

Figure 5.7 Effect of the tolerance ϵ in the approximation of the reflected field within the 4 cm felt treatment. The error refers to the difference between the quadratic pressure obtained with the full images lattice (Fig. 5.3) and that obtained with different values of ϵ. The error relative to the solution without finite size correction is also reported. Results relative to the (u, σ) formulation.

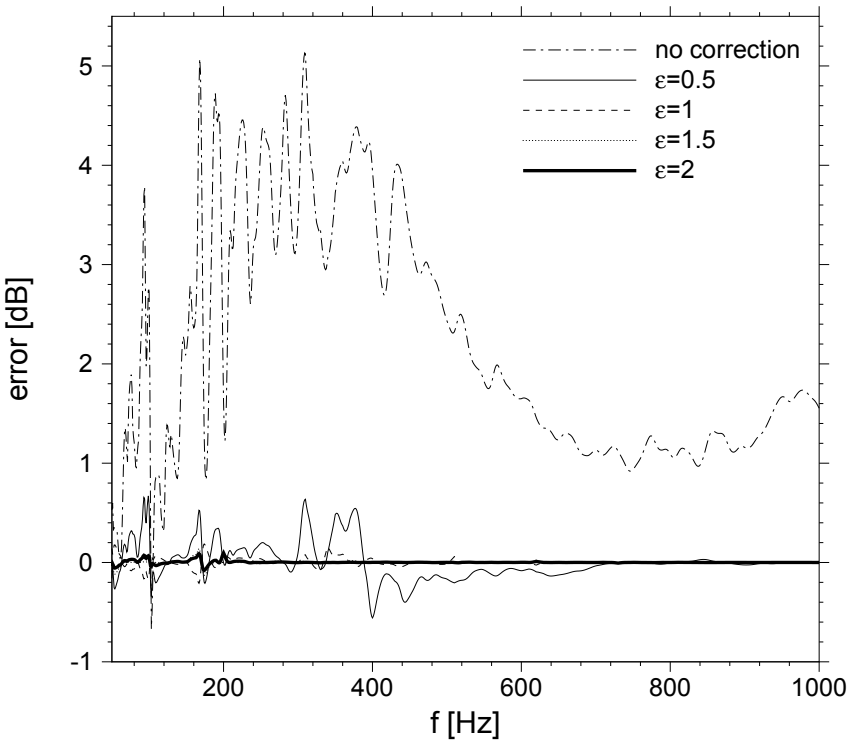

Figure 5.8 Effect of the tolerance ϵ in the approximation of the reflected field within the 2 cm melamine foam with 1.2 $\mathrm{kg/m^2}$ heavy layer on top treatment. The error refers to the difference between the quadratic pressure obtained with the full images lattice (Fig. 5.3) and that obtained with different values of ϵ. The error relative to the solution without finite size correction is also reported. Results relative to the (u, σ) formulation.

particularly pronounced. On the other hand, the maximum value of the error is observed at the resonance around 350 Hz controlled by the spring-mass behavior of the lay-up. Here, a satisfactory accuracy (i.e. ± 0.5 dB) can be achieved by setting $\epsilon = 0.5$, corresponding to an images cloud confined within 0.425 m from the boundaries of the trimmed area.

As a result, the convergence analysis showed that, although some issues may be encountered with the absorption provided by the acoustic trim at low frequencies, the proposed truncation criteria is generally in agreement with the assumed behavior of the reflected field. Namely, for the considered sound packages, a ray emanating from a source over the trimmed area does not hit, on average, more than one wall along its path, that is $\epsilon \leq 1$ typically gives satisfactory results. In other words, the reflected field is confined within less than a mean free path from the lateral boundaries.

To conclude, it should be mentioned that the same study was carried out for the (u, u) formulation and showed a slower convergence with respect to the parameter ϵ. This result is not surprising since a matrix inversion is involved in the construction of the acoustic trim response (see Eq. 5.12), requiring a more accurate description of the reflected field. The results are not reported here for the sake of conciseness.

5.5 Applications

In this section, two applications are considered to compare accuracy and efficiency of the hybrid methodology with classical approaches. The first case consist of a simplified automotive application with a soft three-layers treatment attached onto the main structure. The second case aims at assessing the accuracy of the image sources correction when poroelastic materials with non negligible structural properties are involved in the treatment. A simple plate cavity system is considered for this end.

Three modeling strategies are compared in this section: (i) the full finite element substructuring approach as presented in Refs. [53] and chapter 3 (reference solution); (ii) the hybrid FE-TMM corrected for finite size effects by means of the ISM (Eqs. 5.12 and 5.13) using the full images lattice in Fig. 5.3); (iii) the simplified local impedance approach [122] employing the normal plane wave impedance of the sound package (calculated by means of the TMM). As a result of the analysis carried out in Section 5.4.1, only the (u, σ) formulation of the Green functions based model of the acoustic trim will be considered, as it overperforms the (u, u) formulation in terms of efficiency (see chapter 4).

5.5.1 Application 1: simplified car test case

The first application proposed here consists of a rigid acoustic cavity coupled with a 2 mm thick steel plate (see Fig. 5.9). The same geometry was considered in Ref. [95]. Here, the application is proposed in a different configuration. Namely, a 3-layers acoustic treatment involving a $1\,\mathrm{kg/m^2}$ heavy screen sandwiched between a 2 cm and 1 cm felt layers is attached onto the structure. The presence of other dissipative materials inside the acoustic domain (i.e. carpets, seats, etc...) is modeled introducing a 10% damping in the cavity. The mesh of the plate involves 43×91 four-noded plate elements while fifty eight-noded fluid elements are used through the depth of the cavity. The felt is a very soft material (see Tab. 5.1), and its structural stiffness is typically negligible. Therefore, the bottom and top layers of the trim are modeled using two eight-noded equivalent fluid limp elements. The heavy layer is instead modeled as a limp solid (see Tab. 5.1). The finite element model of the sound packge involves 40618 equations. The number of trimmed nodes is 4048. The system is excited by a point force acting normally to the plate and located at $(0.186\,\mathrm{m}, 1.364\,\mathrm{m}, 0\,\mathrm{m})$. The response of the system up to 500 Hz is considered.

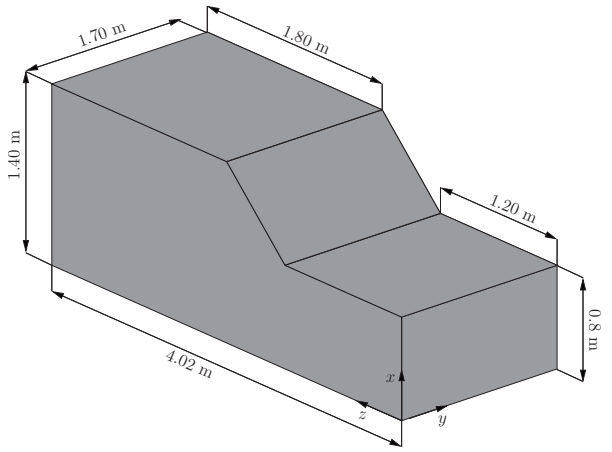

Figure 5.9 Application 1. Geometry of the vibroacoustic system. The plate covers the face located at $z = 0$.

Figs. 5.10 and 5.11 show the plate quadratic velocity and the absolute value of the pressure at driver's ear point at $(0.423\,\mathrm{m}, 1.214\,\mathrm{m}, 3.529\,\mathrm{m})$, respectively. All the considered methodologies are in good agreement below 200 Hz, although it may be pointed out that the absorption provided by the top felt layer is not perfectly captured by the local impedance model. Indeed, small differences (less than 1 dB) are observed in Figs. 5.11 at resonances and anti-resonances between 100 and 200 Hz. On the other hand, above 200 Hz the effect of the thickness resonance of the 3-layers treatment cannot be captured by a locally reacting model, as both the considered indicators are far from the reference

solution. Conversely, the hybrid model based on the acoustic trim Green functions and corrected by the ISM perfectly matches the finite element solution, therefore confirming the accuracy of the methodology for practical layups and local indicators (previously only global indicators were considered). It is noted in passing that the slightly divergent trend at high frequency between the Green functions based hybrid model and the reference solution is due to the finite element model of the solid limp layer involved in the acoustic trim. Indeed, it could be shown that increasing the number of elements along the x and y axes reduces the gap.

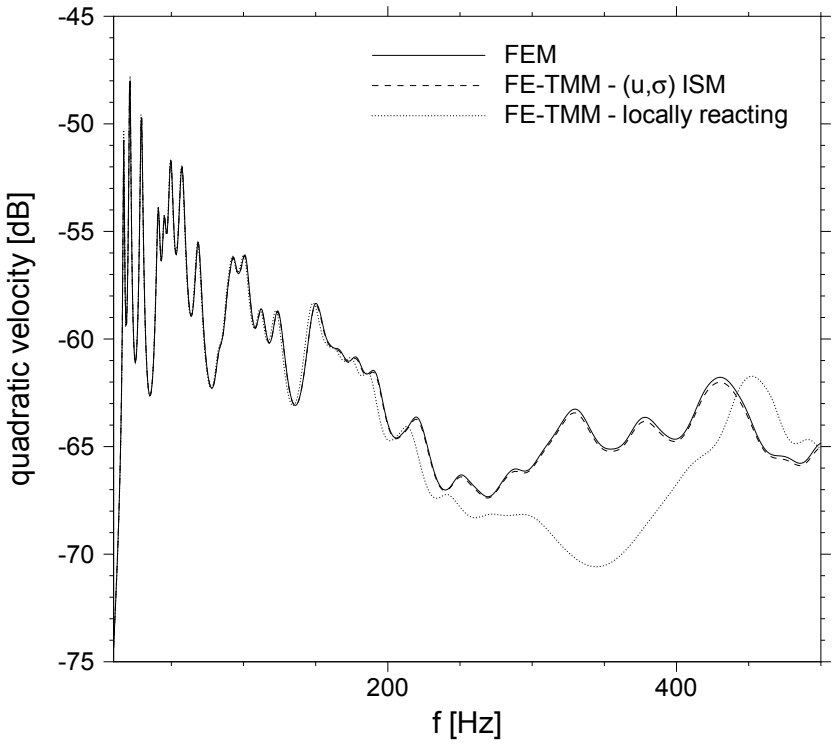

Figure 5.10 Space averaged quadratic velocity of the plate for the case considered in Application 1. Comparison between the finite element (FEM), the hybrid model based on the (u, σ) formulation corrected by means of the ISM (FE-TMM-(u, σ) ISM) and the hybrid model using the plane wave impedance of the trim (FE-TMM-locally reacting).

5.5.2 Application 2: finite size effects in poroelastic materials

The second application consists in the plate-cavity system depicted in Fig. 5.12. The cavity dimensions are $L_{x_c} = 0.8\,\mathrm{m}$, $L_{y_c} = 1.7\,\mathrm{m}$ and $L_{z_c} = 1\,\mathrm{m}$ while the plate is $0.595\,\mathrm{m}$

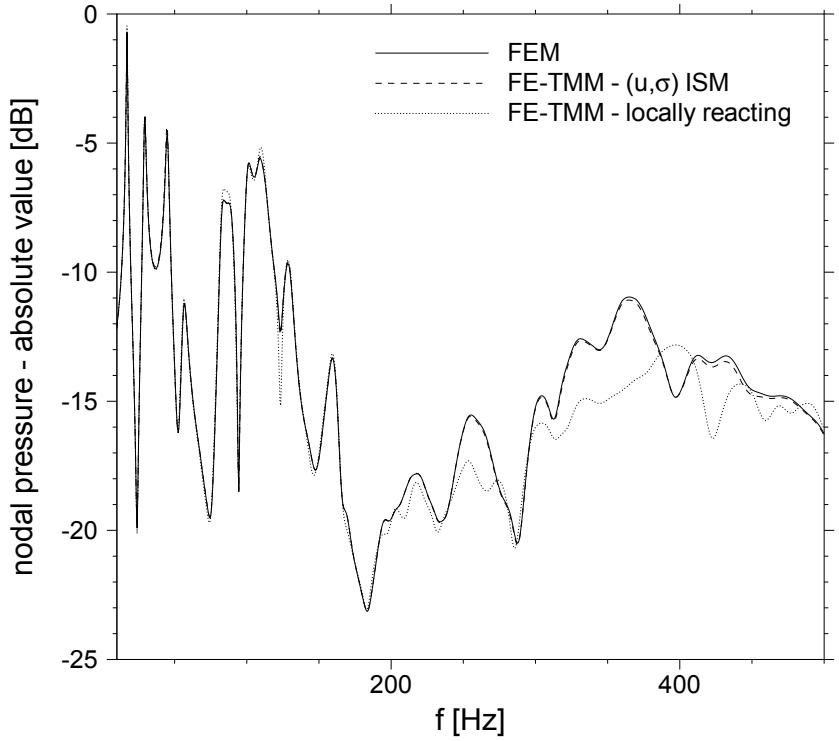

Figure 5.11 Acoustic pressure at driver's hear point for the case considered in Application 1. Comparison between the finite element (FEM), the hybrid model based on the (u, σ) formulation corrected by means of the ISM (FE-TMM-(u, σ) ISM) and the hybrid model using the plane wave impedance of the trim (FE-TMM-locally reacting).

large and 1.554 m wide. Point A (see Fig. 5.12) is located at $(0.074\,\mathrm{m}, 0.056\,\mathrm{m})$. The system is excited by a point force acting on the structure along the z-axis at point B located at $(0.167\,\mathrm{m}, 0.187\,\mathrm{m})$. The mesh of the plate involves 32×83 four-noded plate elements while $43 \times 91 \times 30$ eight-noded fluid elements are used for the finite element model of the acoustic domain. The sound package placed between the plate and the fluid consists of a 1.9 cm melamine foam with a $1.2\,\mathrm{kg/m^2}$ heavy layer on top. The melamine layer is modeled by poroelastic elements (five eight-noded elements through the thickness were used) according to the formulation of Atalla *et al.* [5]. The heavy layer is considered glued onto the top of the foam and is modeled as a limp solid. Such interface condition is very important because it excites solid borne compressional and shear waves in the porous material, making a limp model of the foam not reliable. At the other end of the treatment, the melamine layer is considered to be laid onto the structure, i.e. a 1 mm equivalent fluid layer (same properties of the melamine foam) is placed between the poroelastic layer and the plate. This modeling strategy is typically employed in practical applications to account for the fact that the foam solid frame is not directly connected to the structure. The finite element model of the sound package involves 75978 equations. The number of trimmed nodes is 2774.

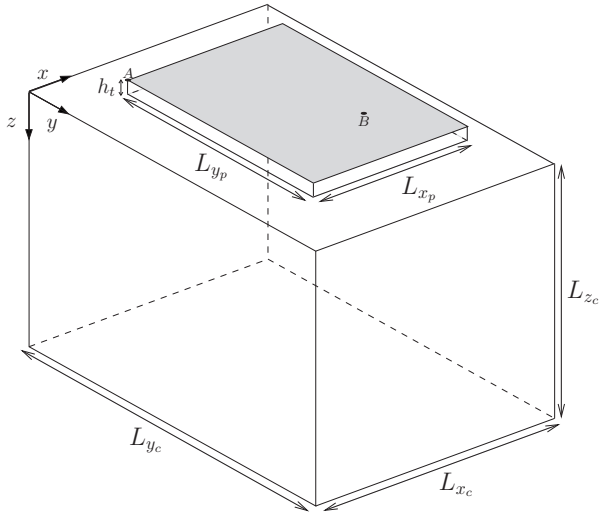

Figure 5.12 Application 2. Geometry of the plate-cavity system.

Figs. 5.13 and 5.14 show the structural and acoustic quadratic velocity and pressure, respectively. Concerning the simplified locally reacting model of the considered sound package, it can be pointed out that it fails over the whole frequency band. Indeed, although it could be argued that the acoustic energy in the cavity somehow follows the reference solution on average, the local behavior of the system is clearly missed. Namely, position and amplitude of the resonance peaks in the structural (Fig. 5.13) and acoustic (Fig. 5.14)

response are not correctly predicted. It could be shown that, although other values of the local impedance could be employed besides the classical plane wave value (i.e. solution of the TMM obtained by setting a null trace wavenumber), an acceptable solution for both the structural and acoustic indicators cannot be retrieved, revealing the limitations of this efficient but extremely simplified model of the trim. On the other hand a very good correlation is observed between the hybrid model based on the trim Green functions corrected by the ISM and the reference solution. More precisely, the structural energy is perfectly retrieved over the entire spectrum (few discrepancies actually appears in the higher portion of the spectrum due to the finite element model of the limp solid layer, see also Fig. 5.10 and associated discussion) while the predicted acoustic energy drifts away from the reference curve only between 750 and 900 Hz. In this frequency range, a local resonance associated to the shear waves propagating in the melamine foam is observed. However, the image sources correction as proposed in this work is not able to exactly captured such size effect. This is not surprising since the reflection of the poroelastic waves at the lateral boundaries cannot be exactly reproduced by means of the classical ISM (see Section 5.3.1). Nonetheless, the proposed finite size correction is still able to retrieve the average level, providing a good approximation of the exact solution.

Therefore, the present analysis suggests that the reflection of the energy carried by the direct field at the lateral boundaries by means of image sources is sufficient to obtain a satisfactory accuracy for generic sound packages.

5.5.3 Computational efficiency

To conclude this section, the efficiency of the proposed methodology is discussed in terms of computational time required to perform the simulations in Sections 5.5.1 and 5.5.2. In what follows, the computational time refers to that required for the calculation of the boundary operator $\mathbf{Y}$ in Eqs. 5.11. The reference methodology requires the solution of a finite element system to perform this step. For the two applications in Sections 5.5.1 and 5.5.2, 124 and 290 s were necessary to solve the linear system by means of the MKL based parallel solver PARDISO [98, 99]. On the other hand, the computational time required by the Green functions model with finite size correction to calculate the same operator $\mathbf{Y}$ by means of Eq. 5.13 is reported in Tab. 5.2 as sum of three steps. Namely, the calculation of the fundamental solutions by the TMM, the integration of the functions defined in Eq. 5.2 over a given set of grid points between the maximum and minimum distance between two trimmed nodes and the interpolation of the integrated function to build the matrices of the acoustic trim model. For application 1 (resp. 2), it can be seen that the proposed

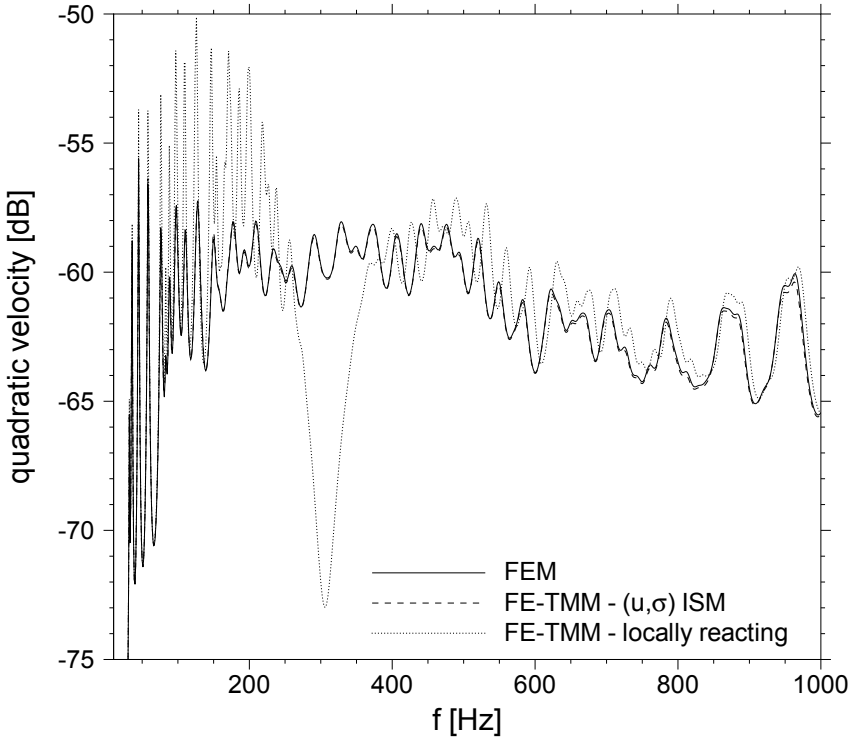

Figure 5.13 Space averaged quadratic velocity of the plate for the case considered in Application 2. Comparison between the finite element (FEM), the hybrid model based on the (u, σ) formulation corrected by means of the ISM (FE-TMM-(u, σ) ISM) and the hybrid model using the plane wave impedance of the trim (FE-TMM-locally reacting).

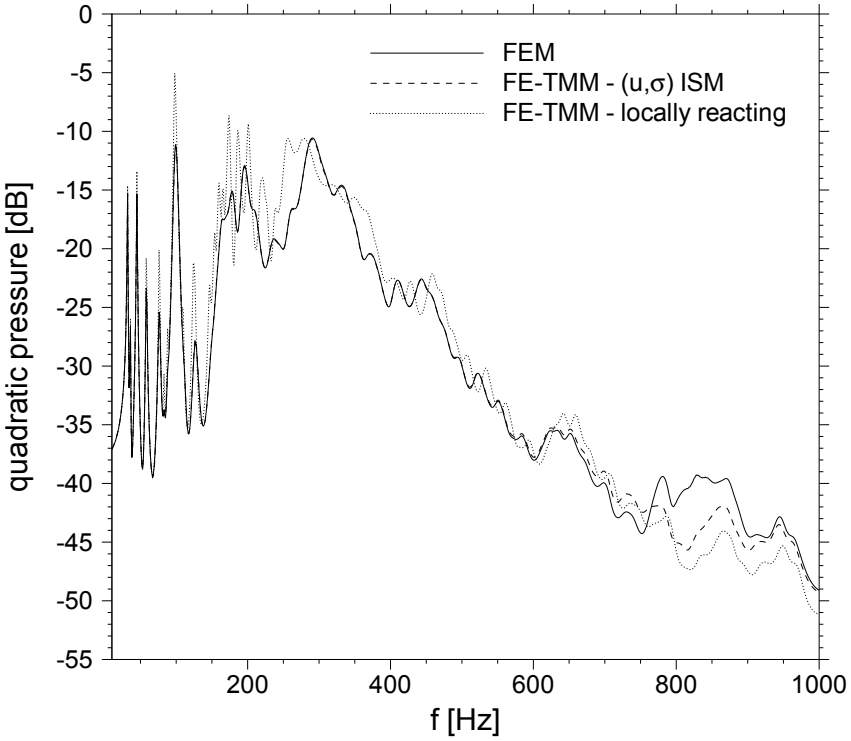

Figure 5.14 Space averaged quadratic pressure of the cavity for the case considered in Application 2. Comparison between the finite element (FEM), the hybrid model based on the (u, σ) formulation corrected by means of the ISM (FE-TMM-(u, σ) ISM) and the hybrid model using the plane wave impedance of the trim (FE-TMM-locally reacting).

methodology is about 7 (resp. 29) times faster than a standard finite element approach. It should be clear that a very appealing saving in the computational time is achieved especially in the second application, since the sound package involves poroelastic instead of equivalent fluid elements. Moreover, a close look at Tab. 5.2 reveals that the interpolation step is clearly the most critical step of the methodology, making the computational time strongly dependent on the number of trimmed nodes. However, it should be noted that a simple implementation in a MATLAB environment of the Green functions approach was considered and the interpolation step was not optimized. Conversely, the reference solution employs the optimized MKL library, so that the present analysis should be seen as a qualitative assessment of the computational performance rather than a rigorous benchmarking. Despite that, given that the reference solution is almost perfectly matched by the proposed methodology (Figs. 5.10-5.11 and 5.13-5.14), a very promising reduction of the computational burden is achieved. All the computations were performed on a Linux machine powered by an intel i7-2600 processor (8 nodes at 3.4 GHz).

Table 5.2 Computational time required to perform each step involved in the Green function model of the acoustic trim with finite size correction.

	TMM	Integration	Interpolation	Total	$\frac{\text{Reference}}{\text{Total}}$
Application 1	1 s	4 s	12 s	17 s	7.3
Application 2	0.5 s	3.5 s	6 s	10 s	29

5.6 Conclusions

In this paper, a numerical tool aimed at simplifying and speeding-up the integration of acoustic treatments in vibroacoustic finite element analysis was proposed. The methodology employs the ISM to account for the finite lateral extension of the acoustic trim (i.e. reflected field effects) within the analytical framework for laterally unbounded, flat and homogeneous treatments presented in Part I (i.e. chapter 4). The use the ISM was justified by the non diffuse nature of the reflected field arising in the sound package. Image sources were employed to reproduce the effect of lossless lateral boundaries. Although this choice allows to exactly retrieve the finite size effects of treatments with an equivalent fluid behavior, it cannot satisfy arbitrary lateral mounting conditions for treatments involving solid-phase layers with non negligible mechanical properties. On the one hand, the methodology only guarantees that the energy impinging onto the boundary is reflected back (the effect of an absorption coefficient to model lossy boundaries was not considered), similarly to ray tracing. On the other hand, it greatly simplyfies the modeling of the acoustic trim; the meshing of complex layups is avoided (simplifying the virtual

prototyping phase) and the knowledge of the actual lateral mounting conditions (which may be different for each realization of the build-up system) is not required.

The results showed that the ISM can substantially improve the accuracy of the direct field model of the acoustic trim presented in Part I (i.e. chapter 4). Namely, the dynamic response of acoustic treatments involving equivalent fluid layers is exactly retrieved. However, as expected, a perfect correlation with a finite element analysis cannot be achieved for the generic case of poroelastic layers, due to the simplifications adopted in the modeling of the lateral boundary conditions. Nonetheless, a satisfactory accuracy is always obtained, at least on average. Furthermore, it was proved that the non diffuse nature of the reflected field arising in the acoustic treatments allows to consider only image sources confined within less than one mean free path from the boundary of the trimmed area (i.e. only one reflections occurs on average), confirming the suitability of the ISM in the modeling of highly dissipative systems. Thus, the proposed finite size correction allows to preserve sufficient accuracy with respect to standard finite element procedures while substantially reducing the computational burden. Results are indeed very promising, as a reduction of the computational time by, at least, a factor 10 is obtained compared to well-established finite element procedures. Moreover, the proposed model can be used for arbitrary sound packages, thus overperforming simple local impedance approaches. However, the image sources correction is intrinsically limited to polygonal treated areas.

5.7 Further results

It has been shown that the finite size correction based on the ISM developed in this chapter is not able to reproduce exactly the reflected field in poroelastic media with non negligible mechanical properties. As shown in Fig. 5.14, this typically leads to a loss of accuracy in localized narrow frequency bands, i.e. around the thickness resonances controlled by compressional and shear solid phase borne waves in the porous layer/s. Conversely, far from these bands and at the resonances controlled by compressional fluid borne waves, a perfect correlation with the FEM is observed.

For the reason above, the effect of the continuity condition between the structure and the first poroelastic layer involved in the sound package must be further assessed. Indeed, the fact that the foam solid frame may be or may be not directly connected to the master structure can strongly affect the participation of the solid phase borne waves to the sound package response in the low frequency range. Clearly, when the mounting conditions become complex (i.e. point or line connections), a detailed model of the interface can

be achieved only by means of a finite element based strategy. However, such boundary conditions may vary for each realization of the system (i.e. industrial process) so that their modeling is rather simplified during the design phase.

In this section, the effect of different interface conditions is studied for a representative spring-mass lay-up. The same plate-cavity system presented in Section 3.4 (Fig. 3.3) is considered to this end. The sound package consists of a 2 cm melamine foam with a $1.2\,\mathrm{kg/m^2}$ heavy layer on top (see Tab. 5.1 table in Part II). The analysis is restricted to the following configurations.

Configuration A (solid phase sliding): the melamine layer is considered glued to the heavy screen while it can slide (i.e. only normal displacement continuity) onto the plate. Thus, the structural normal displacement directly excites the solid frame of the foam. This interface configuration can be model by means of the hybrid method, although a loss of accuracy must be expected at the thickness resonances of the sound package.

Configuration B (equivalent fluid): the melamine layer is considered as an equivalent fluid according to the limp model. Thus, only compressional fluid waves can propagate within it. As proved throughout this chapter, the behavior of this configuration can be exactly retrieved by the hybrid model.

Configuration C (fluid-structure interface): the melamine layer is considered glued to the heavy screen while a 1 mm limp layer is placed at the interface with the plate. Such configuration is typically employed to model the fact that the foam solid frame is not directly connected to the plate, i.e. the sound package is simply laid on the structure. As shown in Fig. 5.14, a loss of accuracy is only expected at the sound package shear waves controlled resonance between 750 and 900 Hz.

Configuration D (solid phase partially glued): the melamine layer is considered glued to the heavy screen and glued onto the structure at the corners of the treated area. Namely, the continuity of the three displacements is enforced between the plate and the foam solid frame over four $0.003\,\mathrm{m^2}$ square patches placed at the corners of the plate. Over the rest of the treated area the skeleton of the foam is considered not directly connected to the plate by introducing a 1 mm limp layer. This configuration is non homogeneous and cannot be modeled by the hybrid method.

Figs. 5.15 and 5.16 show the quadratic velocity and pressure, respectively, of the plate cavity-system when the configuration A is considered and a point force drives the structure at $(0.167\,\mathrm{m}, 0.187\,\mathrm{m})$. The three curves refer to the finite element substructuring methodology (reference) and the hybrid FE-TMM ((u, σ) formulation) with and without image source correction. The results confirm that the exact finite size effects can be only

retrieved on average, as the set of image sources is inappropriate to exactly reproduce the reflection of poroelastic waves at the lateral boundaries of the treatment. Nevertheless, the hybrid solution clearly benefits from the, albeit approximated, finite size correction (see Fig. 5.16), as the gap with the reference curve is reduced. However, it should be noticed that the interface condition considered in this example (i.e. configuration A) is hardly representative of typical applications. Indeed, due to practical reasons (i.e. the vehicle must be accessible for inspections and reparations), the sound package is typically just laid over the structure or, at most, connected over few small areas or points. Therefore, Figs. 5.15 and 5.16 should be rather seen as the result of a numerical test case aiming at fully assessing the limitations of the hybrid methodology. In this context, it may be asserted that the case of a poroelastic layer whose structural frame is directly excited (by continuity condition) over both ends of the layer constitutes a *worst case scenario* for the accuracy of the FE-TMM.

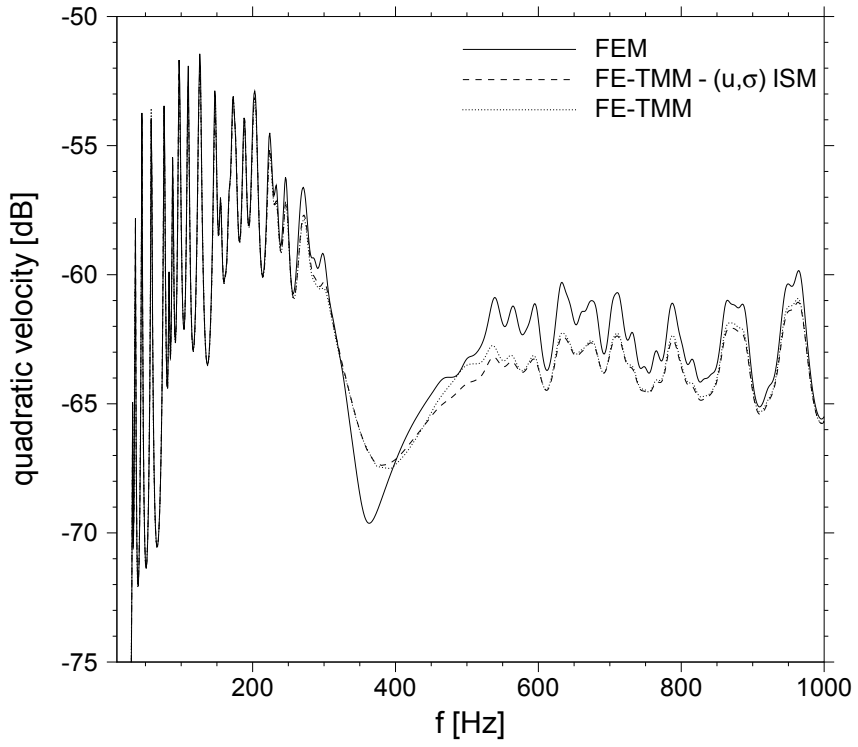

Figure 5.15 Space averaged quadratic velocity of the plate (configuration A). Comparison between the finite element (FEM), the hybrid model based on the (u, σ) formulation with (FE-TMM-(u, σ) ISM) and without finite size correction (FE-TMM-(u, σ)).

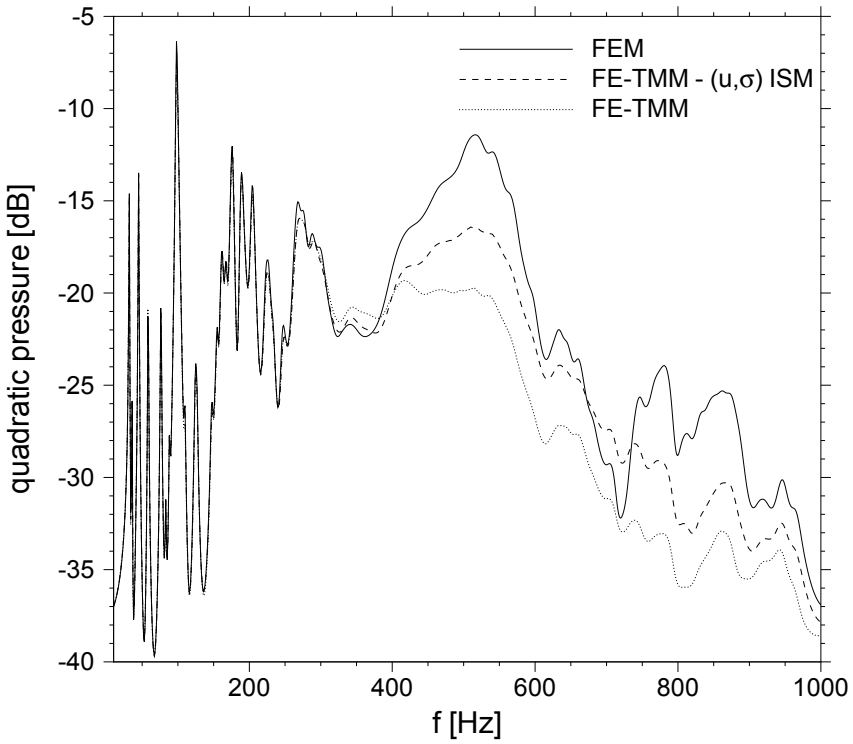

Figure 5.16 Space averaged quadratic pressure of the cavity (configuration A). Comparison between the finite element (FEM) and the hybrid model based on the (u, σ) formulation with (FE-TMM-(u, σ) ISM) and without finite size correction (FE-TMM-(u, σ)).

As a result, more practical configurations should be considered. Namely, the sound package may be considered glued onto the structure over discrete small areas (configuration D). However, to simplify the modeling problem, such interface condition is usually approximated by neglecting the connection between the structure and the foam solid phase. In such case, a small fluid gap is introduced (configuration C). A further simplification may be obtained if the whole poroelastic layer is assumed to behave like an equivalent fluid, thus neglecting the effect of the structural frame also at the interface with the heavy layer (configuration B). In Figs. 5.17 and 5.18 the quadratic velocity and pressure, respectively, of the plate-cavity system with these three configurations are reported. Namely, a finite element analysis was performed to compare configuration D with the simplified configurations B and C. For the latters, also the FE-TMM ((u, σ) formulation) solution obtained with the finite size correction is considered. The quadratic velocity is shown in Fig. 5.17. It can be seen that the effect of the interface conditions with the structure and the heavy layer are very important below 400 Hz. Indeed, the limp model (i.e. configuration B) dissipates less vibrational energy than configurations C and D, which instead almost coincide. In addition, for configurations B and C, the hybrid model matches very well the finite element solutions.

Next, the quadratic pressure is shown in Fig. 5.18. The difference between the three configurations is now appreciable above the transmission resonance at 300 Hz. The sound package glued at the for corners of the trimmed area (i.e. configuration D) gives three clear transmission resonances at 300 Hz, 450 Hz and 850 Hz. The limp approximation (i.e. configuration B) follows quite well the behavior of configuration D between the second and third peak. On the other hand, configuration C follows configuration D on average between 300 and 700 Hz while the two curves get closer to each other at the sound package shear waves resonance around 850 Hz. Consequently, it could be argued that, for the considered system, the simplified interface conditions of configuration C can be considered representative of the actual behavior of the system when the sound package is actually installed onto the structure (configuration D). Furthermore, the finite element solution of configuration C is well approximated by the hybrid model, aside from the loss of accuracy exhibited over the narrow frequency band centered at 850 Hz. Therefore, this analysis, albeit not comprehensive, suggests that the hybrid FE-TMM can be considered an efficient and reliable tool for the prediction of the vibroacoustic performances of practical configurations.

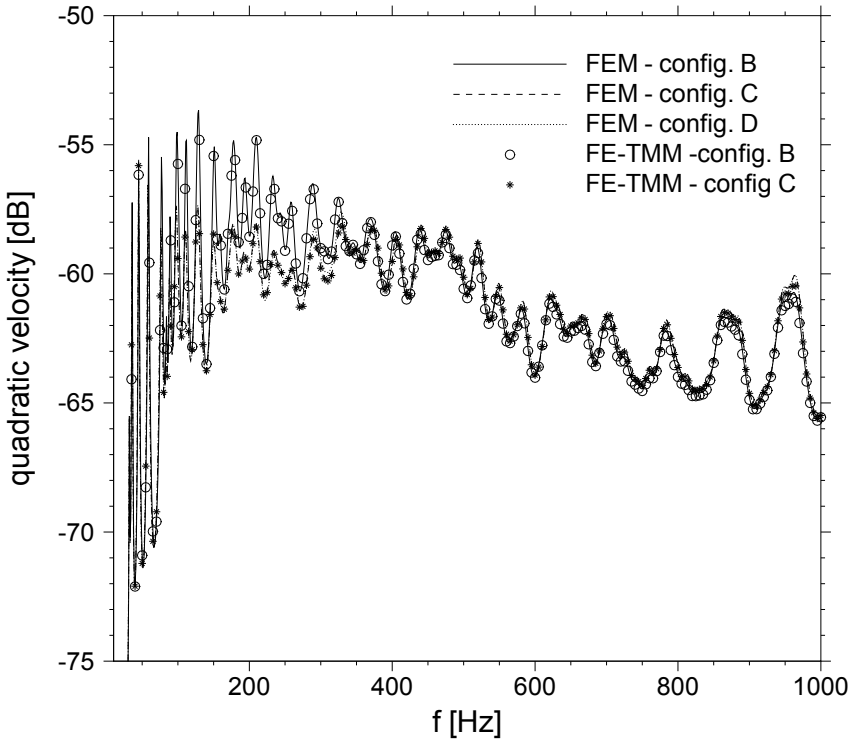

Figure 5.17 Space averaged quadratic velocity of the plate. Comparison between configurations B,C and D. Solutions computed by the FEM and the hybrid model based on the (u, σ) formulation with finite size correction (FE-TMM-(u, σ) ISM).

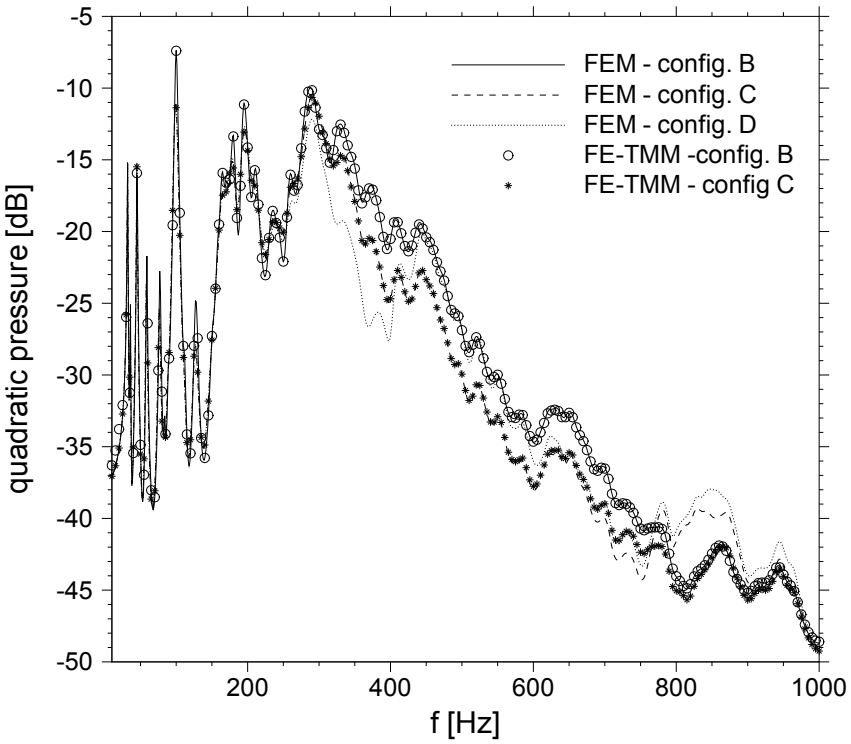

Figure 5.18 Space averaged quadratic pressure of the cavity. Comparison between configurations B,C and D. Solutions computed by the FEM and the hybrid model based on the (u, σ) formulation with finite size correction (FE-TMM-(u, σ) ISM).

CHAPTER 6

EFFICIENT MODELING OF TRANSMISSION PROBLEMS BY THE FE-TMM

This chapter concludes the assessment of the hybrid FE-TMM with a discussion on the numerical modeling of the acoustic radiation of structures with attached noise control treatments. The radiation into an unbounded fluid has already been considered in chapters 4-5. However, no details were therein given on the specific strategy adopted to model the receiver acoustic domain. In this chapter, instead, different hybrid strategies to model efficiently transmission problems are proposed, discussed and compared with the methodology developed in chapter 2. The chapter is organized as follows. In section 6.1, the main equations are introduced. Next, in section 6.2 three different hybrid models are presented. Here, advantages and drawbacks of each strategy are also discussed. Finally, in section 6.3 the considered hybrid models are used to predict the acoustic radiation of a flat structure with an attached typical automotive treatment.

6.1 Introduction

The governing equations of a treated structure radiating in an unbounded fluid domain are given by the following linear system

$$\left(\mathbf{Z}_{ss}(\omega) - \mathbf{Y}_{ss}(\omega)\right)\mathbf{q}_s(\omega) = \mathbf{F}_s(\omega)\,, \tag{6.1}$$

where $\mathbf{Z}_{ss}$ is the structural impedance while $\mathbf{Y}_{ss}$ is the added boundary operator accounting for the effect of the sound package and the external fluid. Vector $\mathbf{q}_s$ gathers the modal amplitudes of the in-vacuo structural modes. Hence, all the operators in Eq. 6.1 are intended to be projected onto the modal basis. The main drawback of Eq. 6.1 consists in the fact that the calculation of $\mathbf{Y}_{ss}$ involves the sound package as well as the unbounded fluid model. In other words, from a substructuring standpoint, the solution of the acoustic treatment and acoustic fluid subdomains are not independent. Conversely, an alternative strategy consists in modeling the radiation from the back of the noise control treatment into the unbounded fluid by an acoustic finite element domain. This would allow to use the framework of chapters 3-4 as it is, thus leading to the following set of equations

$$\left(\begin{bmatrix} \mathbf{Z}_{ss}(\omega) & \mathbf{Z}_{sa}(\omega) \\ \mathbf{Z}_{sa}^{\mathrm{T}}(\omega) & \mathbf{Z}_{aa}(\omega) + \mathbf{Z}_{\infty}(\omega) \end{bmatrix} - \begin{bmatrix} \mathbf{Y}_{ss}(\omega) & \mathbf{Y}_{sa}(\omega) \\ \mathbf{Y}_{sa}^{\mathrm{T}}(\omega) & \mathbf{Y}_{aa}(\omega) \end{bmatrix} \right) \begin{Bmatrix} \mathbf{q}_s(\omega) \\ \mathbf{q}_a(\omega) \end{Bmatrix} = \begin{Bmatrix} \mathbf{F}_s(\omega) \\ \mathbf{F}_a(\omega) \end{Bmatrix}, \tag{6.2}$$

where vectors $\mathbf{q}_s$ and $\mathbf{q}_a$ gathers the modal amplitudes of the uncoupled structural and acoustic modes, so that all the operators in Eq. 6.2 are intended to be projected onto the modal bases. Matrix $\mathbf{Z}_{\infty}$ is the impedance operator accounting for the opening in the acoustic domain, which can be calculated by means of the BEM [6, 17] or PML [11, 12]. Consequently, the calculation of the sound package response (i.e. the boundary operator $\mathbf{Y}$) is decoupled from the unbounded fluid problem (i.e. calculation of $\mathbf{Z}_{\infty}$). This feature can really make the difference when several designs of the acoustic treatment have to be considered.

The hybrid finite element-transfer matrix models based on Eqs. 6.1 and 6.2 will be carefully discussed in the next section.

6.2 Hybrid models

In what follows, three possible modeling strategies are discussed. Namely, the unbounded fluid is accounted for by (i) the simplified model presented in chapter 2 (referred to as model or strategy A), (ii) the exact radiation stiffness attached to the back of the sound package (referred to as model or strategy B) and (iii) the transition through an open finite element cavity (referred to as model or strategy C).

6.2.1 Model A

This is the model already presented in chapter 2. It considers the unbounded fluid to be integrated into the transfer matrix model of the sound package. Thus, the dynamic response is governed by the linear system in Eq. 6.1, where $\mathbf{Y}_{ss}$ accounts for the acoustically treated fluid half space. Employing the jinc function to expand the sound package displacement at the interface with the structure (i.e. side A), it follows from chapter 2 that the entries of $\mathbf{Y}_{ss}$ are given by

$$Y_{ss_{mn}} = V_{s_{mi}} H_{ii} D_{AA_{ij}} H_{jj} V_{s_{jn}} = V_{s_{mi}} H_{ii} \left[\frac{1}{2\pi} \left(\frac{4\pi}{k_s^2} \right)^2 \int_0^\infty \hat{d}_{AA}(k,\omega) J_0(kr) k \, \mathrm{d}k \right] H_{jj} V_{s_{jn}} \,, \tag{6.3}$$

where $\hat{d}_{AA}$ is the Green function accounting for the treated fluid half space (see appendix A), $\mathbf{H}$ is the mapping operator defined in appendix B and $\mathbf{V}_s$ is the structural reduced basis (i.e. modal shapes). The radiated power is computed as follows (see chapter 2)

$$\Pi_{\mathrm{rad}} = \frac{\omega^2}{2} \mathbf{q}_s^*(\omega) \, \mathbf{Z}^{\mathrm{rad}}(\omega) \mathbf{q}_s(\omega) \tag{6.4}$$

where $\mathbf{Z}^{\mathrm{rad}}(\omega)$ is the effective radiation impedance seen by the structure and is given by

$$Z_{mn}^{\mathrm{rad}} = V_{s_{mi}} H_{ii} \left[\frac{1}{2\pi} \left(\frac{4\pi}{k_s^2} \right)^2 \int_0^\infty \mathrm{Re}\left[\hat{Z}_\infty(k,\omega) \right] |\hat{d}_{A\to B}(k,\omega)|^2 J_0(kr) k \, \mathrm{d}k \right] H_{jj} V_{s_{jn}} \,. \tag{6.5}$$

where $\hat{d}_{A\to B}$ is the coupling Green function accounting for the fluid half space (see appendix A). Some comments on advantages and drawbacks of hybrid strategy A are listed below.

- The presence of the unbounded fluid is efficiently accounted for, avoiding expensive boundary element models. Indeed, the computational effort required for the modeling of the external fluid is minimized by embedding its effect into the analytical kernels $\hat{d}_{AA}(k,\omega)$ and $\hat{d}_{A\to B}(k,\omega)$. On the other hand, this model is known to overestimate the fluid loading, as already observed in chapter 2. This is due to the fact that a finite size wetted area on the back of the sound package cannot be taken into account within this framework.
- Due to the fact that the Green functions include the effects of the external fluid, the correction developed in chapter 5 cannot be employed. Indeed, the virtual sources would reproduce the effect of an infinite acoustic waveguide instead of an open space.
- Although the effect of the curvature has not been assessed throughout this thesis, it is worth noting that this model does not allow to account for the curvature of the radiating surface, which can be important at low frequencies.

In conclusions, it can be argued that model A is expected to perform very efficiently, even though the accuracy may be lacking.

6.2.2 Model B

The dynamic stiffness of the unbounded fluid can be also accounted for in the sound package equations according to the (u,u) or (u,σ) formulations introduced in chapter 4. Indeed, several methodologies (for instance the BEM) can be employed to obtain the dynamic stiffness of the semi-infinite fluid, i.e. , without loss of generality,

$$\mathbf{p}_r(\omega) = \mathbf{D}_\infty(\omega)\,\mathbf{u}_n(\omega)\,, \tag{6.6}$$

where $\mathbf{p}_r$ (resp. $\mathbf{u}_n$) gathers the radiated pressures (resp. normal displacements) at the nodes over side B of the treatment. Following appendix B, Eq. 6.6 can be mapped onto the sound package degrees of freedom (i.e. the jinc functions amplitudes), giving the projected dynamic stiffness $\tilde{\mathbf{D}}_\infty$. Therefore, considering for instance the (u,u) formulation, the equations of the acoustic trim wetted by the fluid read

$$\left\{\begin{array}{rcl} \mathbf{R}_A(\omega) & = & \mathbf{D}_{AA}(\omega)\,\mathbf{a}(\omega) + \mathbf{D}_{AB}(\omega)\,\mathbf{b}(\omega) \\ -\tilde{\mathbf{D}}_\infty(\omega)\,\mathbf{a}(\omega) & = & -\mathbf{D}_{AB}(\omega)\,\mathbf{a}(\omega) + \mathbf{D}_{BB}(\omega)\,\mathbf{b}(\omega) \end{array}\right. , \tag{6.7}$$

where matrices $\mathbf{D}_{AA}$, $\mathbf{D}_{AB}$ and $\mathbf{D}_{BB}$ can either refer to those accounting for the response of the laterally unbounded system (i.e. direct field) or to those corrected by means of the ISM. Solving for $\mathbf{R}_A$, the added boundary operator to be used in Eq. 6.1 can be obtained as

$$\mathbf{Y}_{ss} = (\mathbf{H}\mathbf{V}_s)^{\mathrm{T}}(\mathbf{D}_{AA} + \mathbf{D}_{AB}(\mathbf{D}_{BB} + \tilde{\mathbf{D}}_\infty)^{-1}\mathbf{D}_{AB})(\mathbf{V}_s\mathbf{H})\,. \tag{6.8}$$

The radiated power can be calculated as

$$\Pi_{\mathrm{rad}} = \frac{\omega}{2}\mathbf{q}_s^*(\omega)\left[(\mathbf{D}_{BB} + \tilde{\mathbf{D}}_\infty)^{-1}\mathbf{D}_{AB}\mathbf{H}\mathbf{V}_s\right]^{\mathrm{T}}\mathrm{Im}\left[\tilde{\mathbf{D}}_\infty(\omega)\right]\left[(\mathbf{D}_{BB} + \tilde{\mathbf{D}}_\infty)^{-1}\mathbf{D}_{AB}\mathbf{H}\mathbf{V}_s\right]\mathbf{q}_s(\omega)\,. \tag{6.9}$$

Similar equations can be obtained employing the (u,σ) formulation of the sound package. However, it can be pointed out that the use of the latter is no more justified by its computational efficiency, since a matrix inversion is anyway required to obtain the operator $\mathbf{Y}_{ss}$ because of the condensation of the wetted side acoustic trim degrees of freedom.

Some comments on advantages and drawbacks of strategy B are listed below.

– Differently from strategy A, the exact finite size dynamic stiffness matrix of the external fluid is accounted for. A curved radiating surface can be, in principle, considered.
– The finite size effects within the sound package can be approximated following the methodology developed in chapter 5, thus improving substantially the accuracy.
– A (fully-populated) matrix inversion is involved in the computation of the added operator $\mathbf{Y}_{ss}$ (see Eq. 6.8), therefore reducing the computational efficiency for large trimmed areas.

If the analysis is limited to flat systems, model B is thus expected to give accurate results, although efficiency issues may arise when a large number of trimmed nodes are considered. Furthermore, it is noteworthy that simplified models based on the Rayleigh integral can be used in order to speed up the calculation of the open space dynamic stiffness in Eq. 6.6. For instance, the approach proposed by Langley [63] well suits the present framework, as it employs the same methodology (i.e. jinc functions) used for the sound package. This approach (which is employed in the present analysis) is very efficient as it allows for the direct construction of the semi-infinite fluid dynamic stiffness $\mathbf{D}_\infty$, i.e. avoiding the solution of a linear system (which is instead required if the BEM or the PML are employed).

6.2.3 Model C

This model does not require any modification of the acoustic treatment equations (see chapter 4), since the latter is assumed to be inserted between a finite element structural and acoustic domain. Hence, the governing equations in terms of modal amplitudes are those reported in Eq. 6.2. The calculation on the acoustic treatment boundary operator $\mathbf{Y}$ is instead detailed in chapter 4. Some comments on advantages and drawbacks of strategy C follow.

– The exact finite size dynamic stiffness matrix of the external fluid is accounted for. A curved radiating surface can be, in principle, considered.
– The finite size effects within the sound package can be approximated following the methodology developed in chapter 5, thus substantially improving the accuracy..
– It can take advantage from the computational efficiency of the (u, σ) formulation, which has been proved in chapters 4 and 5.
– The construction of the noise control treatment boundary operator $\mathbf{Y}$ is completely independent from calculation of the impedance $\mathbf{Z}_\infty$ of the cavity opening.

– The main drawback resides in the fact that the modal basis of the hard walled cavity may be not effective to describe the dynamic effects of the opening. Consequently a large number of modes may be needed to correctly capture the solution.

It can then be argued that model C should be preferred to model B when several trim layups have to be simulated. Indeed, the operator $\mathbf{Y}$ can be efficiently calculated by means of the (u, σ) formulation (with or without finite size correction) for each configurations, while the effect of the unbounded domain on the acoustic cavity (i.e. $\mathbf{Z}_\infty$) can be computed (independently) only once, improving considerably the efficiency with respect to strategy B. In this work, the BEM is considered to calculate $\mathbf{Z}_\infty$.

6.3 Application to a test case

In this section the models described above are used to predict the power radiated by a structure with an attached four-layers treatment. The 2 mm thick rectangular plate is made of steel (Young's modulus 200 GPa, Poisson's ratio 0.33 and density 8000 $\mathrm{kg/m^3}$), is clamped along its edges and has dimensions $0.8 \times 1.7\,\mathrm{m^2}$. A 1% damping is provided by the structure itself. The acoustic treatment consists of a spring-mass configurations with two further poroelastic layers on top of the heavy screen. The acoustic and mechanical proporties of the layers are reported in Tab. 6.1. The acoustic trim radiates into a semi-infinite fluid domain with density $\rho_0 = 1.21\,\mathrm{kg/m^3}$ and speed of sound $c_0 = 342.2\,\mathrm{m/s}$. Models B and C assume an infinitely baffled radiating surface, while such condition cannot be accounted for in model A, as already discussed in chapter 2. A point force and a $45°/45°$ plane wave are considered as external disturbance. The radiated power and the TL, respectively, are the vibroacoustic indicators of interest.

Concerning the finite element model of the plate, the selected mesh guarantees 8 elements per wavelength at the maximum observed frequency, i.e. 1 KHz. For all the three methodologies, the reduced model involves 170 structural modes, i.e. all the modes resonating in the frequency band $0 - 1300\,\mathrm{Hz}$. Concerning strategy C, the radiation into the unbounded fluid is modeled introducing a fictitious 1 mm deep cavity. The latter is thus coupled with the acoustic trim on one side and with the semi-infinite fluid on the other side. The lateral boundaries of the cavity are assumed to be hard walled. Therefore, the open cavity behaves like a very short waveguide, which is expected to have a negligible tunneling effect [50, 102] on the radiation. The convergence of the solution with the number of kept hard walled acoustic modes was studied and it was fund that the resonating modes in the band $0 - 2000\,\mathrm{Hz}$ suffice to provide an accurate solution.

Fig. 6.1 shows the predicted transmission loss when the 45°/45° plane wave impinges onto the plate. As already observed in chapters 4 and 5, the size effects within the acoustic treatment are negligible when an acoustic excitation is considered. Consequently, it can be argued that the correction based on the ISM is not necessary to get an accurate estimation of the TL. Concerning model A, some inaccuracies are experienced between 100 and 500 Hz, where a maximum error of 2 dB is observed. Hence, model A may be a very efficient strategy to perform quick calculations while improving the accuracy of the classical TMM. The latter, instead, cannot capture the structural modal behavior below 600 Hz since the entire multilayer system is assumed of infinite lateral extent. Such low frequency improvement is obtained at the negligible cost of the solution of an eigenvalue problem and may be very important in case of complex built-up structures (perhaps non flat).

Fig. 6.2 shows instead the predicted radiated power when the plate is excited by a point force. As expected (see chapters 4 and 5), finite size effect are now important. Indeed, a maximum gap of 4 dB is observed between the hybrid models accounting for the reflected field within the acoustic treatment (i.e. finite size correction) and those which do not. Moreover, also model A becomes less accurate compared to the case of acoustic excitation (Fig. 6.1), as already observed in chapter 2. In particular, a maximum error of 5 dB is shown at the system thickness resonance, while an offset between 1 and 2 dB is observed above 500 Hz.

Finally, concerning the accuracy of model C, it can be argued that tunneling effect and modal truncation introduce negligible errors, as an almost perfect correlation with the reference model (i.e. strategy B) is obtained in both Figs. 6.1 and 6.2.

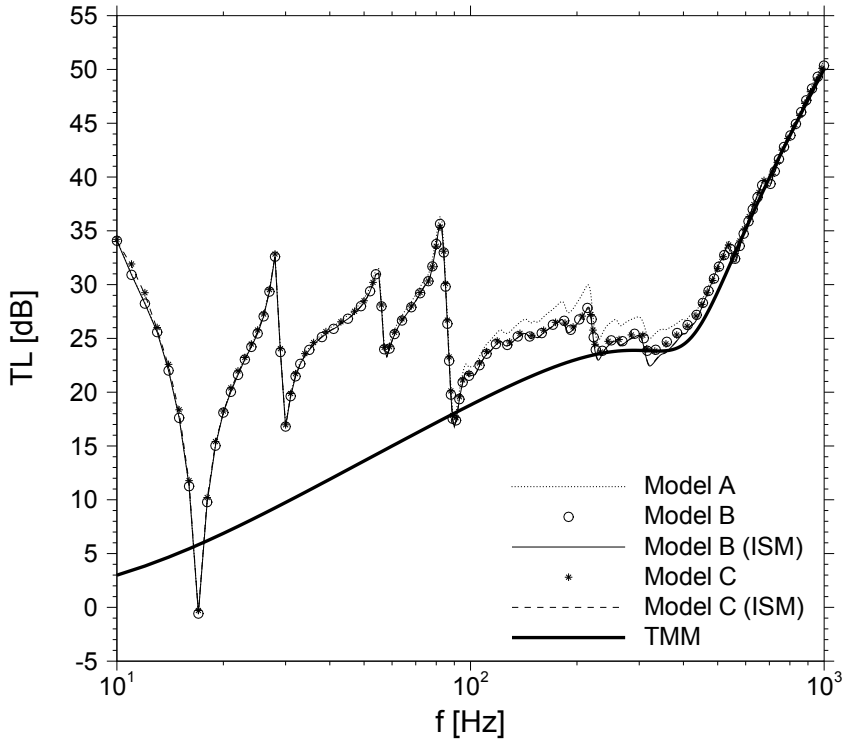

Figure 6.1 Transmission loss provided by the plate with the attached four-layer treatment under a 45°/45° plane wave excitation. Comparison between models A, B (with and without finite size correction by ISM) and C (with and without finite size correction by ISM) and the classical TMM.

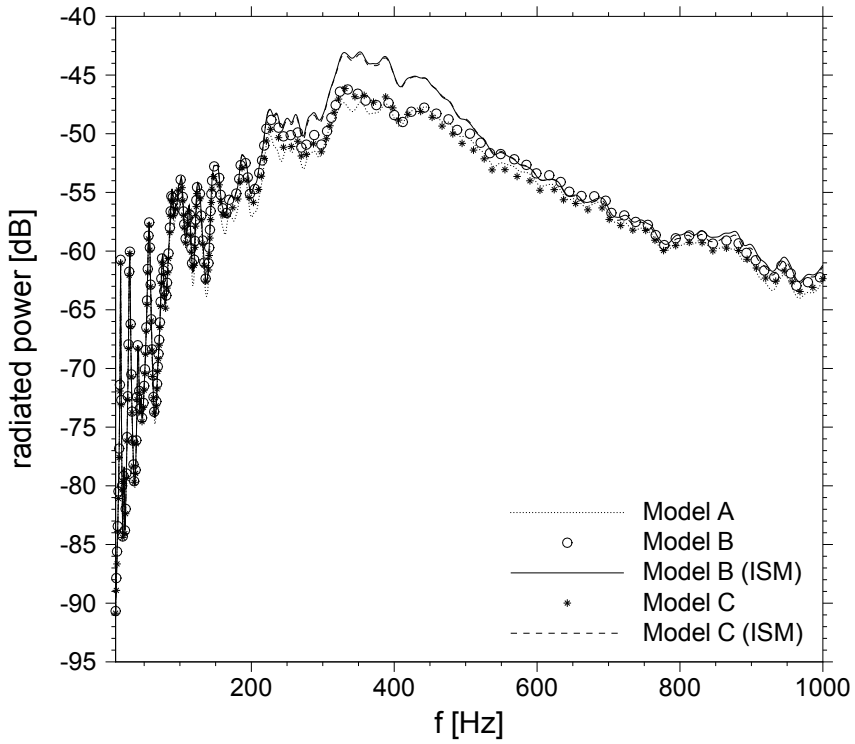

Figure 6.2 Power radiated into the semi-infinite fluid by the plate plus attached four-layer treatment under a point force excitation. Comparison between models A, B (with and without finite size correction by ISM) and C (with and without finite size correction by ISM).

6.3.1 Computational efficiency

In Tab. 6.1 the computational time required for the calculation of the added boundary operator is reported for each methodology considered in the simulations above. To be more precise, the computational time associated to model A and B refers to that required for the calculation of $\mathbf{Y}_{ss}$ in Eq. 6.1. The time required to compute the operator $\mathbf{Y}$ in Eq. 6.2 is instead considered for model C. It is here stressed that the computational time referred to models A and B includes the effect of the semi-infinite fluid, whereas model C requires to consider a further independent step to calculate the impedance of the open end of the cavity attached to the acoustic trim. The time required to perform this step (by means of the BEM) is however not reported here.

Tab. 6.1 reveals that model A is the most efficient strategy, albeit not the most accurate as observed in Figs. 6.1-6.2. Indeed, although model C requires almost the same time for the computation of the sound package operator, it needs a further step to compute the finite element based model of the open cavity, as discussed above. Model B exploits instead the formulation proposed in Ref. [63] based on the Raileigh integral, which allows for a direct calculation of the dynamic stiffness matrix $\mathbf{D}_{\infty}$ (Eq. 6.6). However this methodology is obviously limited to flat radiating surfaces. It is noted in passing that the computational time associated to strategies B and C with finite size correction refers to the model considering the full image sources pattern in Fig. 5.3. However, thanks to the study carried out in section 5.4.2, the number of effective virtual source can be optimized, thus reducing the effort associated to the numerical integration and interpolation steps. Once again, it can be seen from Tab. 6.1 how the latter step is critical for an efficient implementation of the finite size correction based on the ISM.

Table 6.1 Considered acoustic treatment lay-up. Layer 1 is in contact with the structure while layer 4 radiates in air.

Layer	**Thickness**	**Type**	**Properties**	
			Acoustic	**Mechanical**
1	16.5 mm	Porous (Limp)	porosity = 0.95 resistivity = 15797 kg/m^{3}s tortuosity = 1.85 viscous length = 66 μm thermal length = 198 μm	density = 55 kg/m^3 Young's modulus = $5.19 \cdot 10^4$ Pa Poisson's ratio = 0.3 damping factor = 0.23
2	0.57 mm	Plate		density = 1750 kg/m^3 Young's modulus = $1.5 \cdot 10^8$ Pa Poisson's ratio = 0.29 loss factor = 0.1
3	8 mm	Porous (Limp)	porosity = 0.98 resistivity = 26514 kg/m^{3}s tortuosity = 1 viscous length = 48 μm thermal length = 144 μm	density = 58 kg/m^3 Young's modulus = $6 \cdot 10^3$ Pa Poisson's ratio = 0.04 damping factor = 0.15
4	0.4 mm	Porous (Limp)	porosity = 0.95 resistivity = 2500000 kg/m^{3}s tortuosity = 1.2 viscous length = 30 μm thermal length = 60 μm	density = 210 kg/m^3 Young's modulus = $1.5 \cdot 10^3$ Pa Poisson's ratio = 0.3 damping factor = 0.05

Table 6.2 Computational time required to perform each step involved in the (u, u) and (u, σ) formulations. MATLAB *backslash* operator was used to perform the solution step.

	TMM	Integration	Interpolation	Solution	Total
Model A	0.7 s	2 s	1.5 s	-	4.2 s
Model B	0.7 s	2 s	2.4 s	7.3 s	12.4 s
Model B (ISM)	1.3 s	4.5 s	13 s	7.3 s	26.1 s
Model C	0.7 s	1.6 s	1.8 s	-	4.1 s
Model C (ISM)	1.3 s	4 s	12.5 s	-	17.8 s

6.3.2 Conclusions

In this chapter three different finite element-transfer matrix models based on the hybrid framework developed in this thesis have been proposed to predict the noise radiation of an acoustically treated structure into a semi-infinite fluid domain. Each model is specifically designed to respond to a particular need, i.e. from the quick and rough estimation to the accurate prediction of the transmission properties of a built-up structure. As a consequence, a different degree of approximation is involved in the considered models, which inevitably affects their accuracy (Figs. 6.1-6.2) and computational efficiency (Tab. 6.2). Namely, model A is essentially an extension of the TMM to account for the modal behavior of the structure. It allows for quick calculations, although it is based on stringent assumptions. Model B and C are straightforward applications of the hybrid framework developed throughout chapters 3-5. Model C has the advantage of decoupling the acoustic treatment and unbounded fluid substructuring solutions by modeling the radiation from an open acoustic cavity. However, this approach may introduce further difficulties in the use of modal synthesis to reduce the size of the open cavity discrete model.

The three strategies have been used to predict the transmission properties of a steel plate acoustically treated by a typical four-layers automotive lay-up. The hybrid framework allows for an easy and quick virtual prototyping phase, as the finite element model of the sound package is replaced by a much simpler transfer matrix model. For the considered lay-up, the results showed that, when acoustic-borne paths are considered (e.g. plane wave excitation), even simple and quick models (e.g. model A) can give reliable results. Conversely, more accurate models are necessary to capture the resonant transmission due to structure-borne noise (e.g. point force excitation). This conclusion is not surprising and confirms what has been already observed in the previous chapters.

CHAPTER 7

CONCLUSIONS AND PERSPECTIVES

The main concern of this research was to develop a reliable hybrid framework to speed up and simplify the integration of passive acoustic treatment components in vibroacoustic finite element analysis. To this purpose, the finite element models of the main structure and acoustic cavity have been coupled with a simple analytical model of the sound package. Namely, under the hypotheses of homogeneous, flat and laterally infinite acoustic treatments, an approximation of the impedance seen by the finite element domains over the acoustically treated surfaces was obtained starting from a simple transfer matrix model of the treatment itself. The above assumptions are justified by

– the simplifications typically employed in acoustic treatments design and modeling, and
– the short wavelength and dissipation that characterize sound-proofing materials (e.g. poroelastic materials).

The approach, is based on a boundary formulation of the sound package dynamic response. Namely, the reactions of the treatment over its two faces (i.e. the interface surfaces with the structural and acoustic domains) are formally expressed in terms of convolution integrals between external disturbances and Green functions. If the problem is formulated in the wavenumber domain, then the analytical kernels can be quickly sampled by solving successive small transfer matrix problems. In this framework, the discrete dynamic equations of the acoustic treatment can be obtained from a Galerkin projection employing radially symmetric shape functions. In the case of isotropic layups, the latter choice allows to reduce further the computational burden, since two-dimensional integrals can be rearranged as one-dimensional operators. Then, the boundary impedance operator containing the effect of the acoustic trim on the structural and/or acoustic domains can be calculated and thus integrated into the finite element model of the vibroacoustic system.

A comprehensive benchmark of typical test problems (transmission and absorption) involving several acoustic treatment configurations was considered to validate and assess the hybrid FE-TMM. The analysis was limited to flat systems and homogeneous treatments. A systematic comparison with standard approaches showed that, although a substantial improvement is achieved with respect to oversimplified locally reacting models, the accuracy of a detailed finite element model of the acoustic treatment cannot be always retrieved

due to the stringent assumption of infinite lateral extent. Such approximation neglects the presence of a reflected field, whose effect, albeit confined at the boundaries of the treated area, may be important - depending on the considered excitations and materials - to obtain quantitative meaningful predictions. Therefore, a finite size correction based on the ISM has been proposed. The study carried out within this thesis showed that the ISM can be successfully used for the acoustic treatment modeling, thanks to the strong dissipation provided by such subsystems. Although the proposed correction is exact only for sound packages whose dynamic behavior can be approximated by equivalent fluid models (i.e. negligible mechanical properties), the results showed that an accuracy close to that of a reference finite element model can be achieved also for practical configurations. On the other hand, it may be argued that a full finite element analysis might still be needed if the effect of complex details (i.e. practical mounting conditions, curvature) must be assessed.

As a result, depending on the user needs, the hybrid tool developed throughout this thesis (with or without finite size correction) can be successfully used to predict efficiently the response of vibroacoustic systems involving arbitrarily complex flat and homogeneous noise control treatments. Furthermore, a substantial simplification of the modeling is achieved, as time consuming virtual prototyping phases required by standard finite element analysis are replaced by a costless transfer matrix model. This is an important feature when the optimization of the acoustic treatment is sought. Indeed, while the finite element model (possibly of reduced order) of the vibroacoustic system remains unchanged, only simple transfer matrix models must be considered to calculate the boundary operator associated to each layups generated by the optimization process.

7.1 Main achievements

The main achievements of this work can be summarized as follows.

- First of all, the theoretical framework behind the acoustic treatment modeling based on the Green functions has been formally and comprehensively presented, identifying similarities and differences with other approaches proposed in the literature (chapters 2-3). Within the proposed methodology, different formulations have been assessed. Namely, the effect of different shape functions and baffling conditions have been investigated in order to establish the best strategy for the considered applications (chapter 4). This addresses the first objective defined in section 1.4.
- The proposed hybrid FE-TMM has been comprehensively assessed. Although only simplified geometries were considered throughout this thesis, the effects of different

configurations of the acoustic treatment (e.g. materials and interface conditions) and external disturbances on the accuracy of the hybrid model were carefully assessed. This allowed to understand the impact of the main assumption inherent within the hybrid framework (i.e. laterally unbounded acoustic treatments). For instance, it was observed that, broadly speaking, the accuracy provided by the hybrid FE-TMM increases when the sound package materials get softer and acoustic excitations drive the main structure (chapter 4). Moreover, it was pointed out that the dissipation added to the main structure is typically well captured (chapters 2-4), whereas the absorption seen by the acoustic domain is usually poorly captured at low frequencies (chapters 3-4). More complicated was the assessment of the energy transmission through the sound package, which can be only qualitatively captured at low as well as higher frequency (chapters 3-4). This addresses the second objective defined in section 1.4.

- Reference tools (i.e. substructuring FEM [53] and locally reacting impedance model [122]) have been considered to provide systematic comparisons. This allowed, on the one hand, to prove the superiority of the proposed hybrid FE-TMM with respect to locally reacting models. On the other hand, FEM comparable accuracy was achieved while substantially reducing computational costs and resources. This addresses the third objective defined in section 1.4.
- As a result of the three above points, the research went one step forward, improving the accuracy of the noise control treatment model by proposing a finite size correction able to retrieve, at least on average, the effect of the reflected field emanating from the lateral boundaries of the treated surface. In this context, the application of the ISM to the acoustic treatments modeling (chapter 5) constitutes another originality of this work.

To the author's knowledge, no scientific paper dealing with such comprehensive presentation and assessment of hybrid finite element-transfer matrix methodologies applied to passively treated vibroacoustic system was available in the open literature. The present work (in the form of four scientific papers) tries to partially fill this gap by providing (i) a fully validated formulation and (ii) a careful insight into its potentiality (advantages and drawbacks). This should allow for a conscious use of the tool. However, much work is yet to be done, as briefly summarized in the following section.

7.2 Future works

7.2.1 Potential applications

The developed transfer matrix based model for noise control treatments can be also integrated into alternative frameworks beside the finite element application considered in this thesis.

For instance, the FEM-SEA hybrid tool developed by Shorter and Langley [104] to perform efficient mid frequency analysis would greatly take advantage from the proposed formulation to account for noise control treatments. Indeed, a full hybrid framework would be available to perform accurate and quick full-spectrum prediction. For instance, a complex real life system with noise control treatments could be modeled with different strategies depending on frequency range of interest and required accuracy. Namely,

- at low frequency a full finite element model of the main structure and acoustic cavity can be employed together with a transfer matrix model of the acoustic treatment.
- As the frequency increases some details of the structure (i.e. short wavelength subcomponents) and the cabin can be more efficiently modeled as statistical subsystems, while the sound package can still take advantage from the formulation presented in this work.
- At higher frequency a full SEA model can be employed. In this context, the SEA parameters of the acoustically treated subsystems can be estimated by the classical TMM (see Ref. [23, 90]) or by accurate finite element models (for instance using the periodic structure theory [24]) which can, in turn, exploit the simplified Green functions based model to account for multilayer treatments.

A further application of the acoustic treatment model consists in the calculation of self and transfer impedances among patches defined over the two faces of the trim. The Green functions model would provide a user-friendly and quick tool to perform such calculations, avoiding time consuming and cumbersome experimental tests. The impedances can be then used in a PTF methodology, such as the one proposed in Ref. [127].

Finally, it could be argued that the developed hybrid model could be effectively and efficiently employed for uncertainty quantification purposes. Indeed, the parameters of the noise control treatment (e.g. acoustic properties, mechanical properties and thickness) are typically uncertain, so that their propagation in the computational model must be assessed. In this context, given a statistical model for the uncertain data, the hybrid FE-TMM can be used to perform quick Monte Carlo simulations. Indeed, similarly to an optimization procedure, simple transfer matrix models have to be considered to evaluate

the effect of each sample on the vibroacoustic system. The response of each realization is then calculated by solving the reduced order model, so that the confidence intervals for the vibroacoustic indicators of interest can be estimated. It is noted in passing that this approach would only allow to account for *parametric* uncertainties, as the effect of *nonparametric* uncertainties (i.e. modeling errors) have to be accounted for by employing a statistical description of the boundary impedance matrix (see for instance Refs. [69, 111] for an overview of parametric and nonparametric probabilistic approaches of uncertainties). In the latter case, the use of the random matrix theory developed by Soize [109, 110] may be employed to build the computational stochastic model, as performed in Ref. [45].

7.2.2 Further assessments and improvements

Concerning the low frequency range, the following aspects must be still assessed to fulfill the validation of the transfer matrix based acoustic treatment model.

- The effect of the curvature must be quantitatively assessed.
- The modeling of non isotropic configurations must be considered. The model developed in this thesis is not strictly limited to isotropic sound packages, however, non isotropic layups would require an increase of the computational effort, which should be quantified. Alternatively, the use of averaged Green functions (equivalent isotropic kernels) should be considered.
- Non homogeneous configurations must be assessed. In the context of this thesis, different acoustic treatment would be treated as different treated surfaces, thus neglecting coupling phenomena at their interfaces. The effect of this approximation in the dynamic response of the vibroacoustic system must be quantified.
- Finally, the possibility to account for normal components continuity at the structural-acoustic trim interface should be studied. Although it may be argued that this is an unnecessary improvement for noise control treatments (which are typically lied over the structure), it is surely necessary to account for other passive components, such as constrained damping layers.

In addition, depending on the required accuracy, the following improvements of the finite size correction could be considered.

- General implementation of the image sources detection algorithm and application of the to more complex-shaped treated areas to assess the feasibility of the methodology when practical configurations are considered.

- Feasibility study of an alternative correction to account more accurately for the reflected field in materials which do not behave like equivalent fluids (e.g. solids or poroelastic materials with non negligible mechanical properties). However, this aspect appears challenging. Indeed, the wave reflection in solid and porous media may involve complex phenomena (e.g. coupling effects between different wave types) which could be hard to account for without jeopardizing the simplicity of the developed methodology. Moreover, as already pointed out in chapter 5, the usefulness of such correction might be questionable, due to the uncertain knowledge of the acoustic treatment boundary conditions.

It should be noted that to fulfill the above requirements, an alternative methodology may be needed to account for the reflections at the acoustic treatment boundaries.

CONCLUSION FRANÇAIS

L'objectif principal de cette recherche est de développer une méthodologie hybride pour accélérer et simplifier l'intégration des traitements acoustiques dans les modèles par éléments finis du comportement vibroacoustique des structures. À cette fin, les modèles éléments finis de la structure principale et de la cavité acoustique ont été couplés à un modèle analytique du traitement acoustique. Ce dernier est basé sur la méthode des matrices de transfert qui suppose le traitement acoustique plan, homogène et de dimension latérale infinie. L'approche est basée sur une formulation intégrale de la réponse dynamique du traitement acoustique. Formellement, le traitement acoustique est remplacé par des impédances d'interfaces ajoutées aux domaines éléments finis, c.-à-d. à la structure et la cavité. Ces impédances sont exprimées en termes d'intégrales de convolution entre les sollicitations externes et des fonctions de Green judicieusement approximées par la méthode des matrices de transfert.

Un test de performance impliquant plusieurs configurations (absorption, transmission), sollicitations (mécanique, acoustique) et traitements acoustiques (monocouche, bicouche, et multicouche) a été réalisé pour valider et évaluer la précision de la méthodologie hybride éléments finis - matrice de transfert. La comparaison systématique avec la méthode des éléments finis (c.-à-d. modélisation détaillée du traitement acoustique par éléments finis; notre référence) et la méthode d'impédance à réaction localisée (une approximation simple et rapide bien répandue en pratique) a montré que notre approche apporte une amélioration substantielle par rapport à cette dernière. Toutefois, pour quelques excitations et configurations de matériaux, la précision du modèle hybride ne reproduit pas toujours celle des éléments finis en raison de l'hypothèse de l'extension latérale infinie. En effet, cette approximation néglige la contribution du champ réfléchi par les parois latérales du traitement acoustique. Bien que cette contribution soit limitée aux frontières de la surface traitée, elle est nécessaire pour obtenir des prédictions quantitatives utiles. Par conséquent, une correction basée sur la méthode des sources images a été proposée et validée avec succès.

En conclusion, en fonction des besoins de l'utilisateur, la méthodologie hybride développée dans cette thèse peut être utilisée avec succès pour prédire efficacement la réponse vibroacoustique des structures avec traitements acoustiques. En plus du gain en temps de calcul, une simplification substantielle de la modélisation du problème est aussi obtenue.

En effet, le maillage des traitements phoniques, une opération complexe et fastidieuse, est remplacé par un modèle de matrice de transfert simple et rapide. Ceci représente un apport important puisque l'optimisation d'un traitement acoustique, pour un système structure-cavité donné, nécessite le développement et résolution de plusieurs dizaines de modèles.

ANNEX A
CALCULATION OF THE GREEN FUNCTIONS

In this appendix, the methodology employed to calculate the Green functions involved in the (u,u) and (u,σ) formulations is presented. The transfer matrix model of a generic multilayer system leads to the following linear system [3]

$$\mathbf{D}(k,\omega)\mathbf{V}(k,\omega) = \mathbf{0}\,, \tag{A.1}$$

where matrix $\mathbf{D}$ express the continuity conditions at the interfaces between different layers. Without loss of generality, Eq. A.1 refers to the case of an isotropic system, i.e. the final system is only a function of the module of the wavenumber k. Vector $\mathbf{V}$ contains the variables of each layer involved in the acoustic trim. The variables at the two ends of the treatment are defined as

$$\mathbf{V}_A(k,\omega) = \left\{ \begin{array}{c} \sigma_A(k,\omega) \\ v_B(k,\omega) \end{array} \right\} \tag{A.2}$$

$$\mathbf{V}_B(k,\omega) = \left\{ \begin{array}{c} \sigma_B(k,\omega) \\ v_B(k,\omega) \end{array} \right\}, \tag{A.3}$$

where σ_A (resp. v_A) and σ_A (resp. v_B) are the normal stress (resp. velocity) over the two ends of the trim. Since the proposed model accounts only for the normal components at the interface between the sound package and the master acoustic and structural domains, another set of boundary conditions has to be added to Eq. A.1 if the first (i.e. side A) and/or n^{th} (i.e. side B) layers involve also in-plane variables. Imposing the necessary boundary conditions at sides A and B, one gets

$$\left[\begin{array}{ccc} \mathbf{D}_{A_1}(k,\omega) & \mathbf{D}_{A_2}(k,\omega) & \mathbf{0} \\ \mathbf{0} & \mathbf{D}(k,\omega) & \mathbf{0} \\ \mathbf{0} & \mathbf{D}_{B_1}(k,\omega) & \mathbf{D}_{B_2}(k,\omega) \end{array} \right] \left\{ \begin{array}{c} \mathbf{V}_A(k,\omega) \\ \mathbf{V}(k,\omega) \\ \mathbf{V}_B(k,\omega) \end{array} \right\} = \tilde{\mathbf{D}}(k,\omega)\tilde{\mathbf{V}}(k,\omega) = \mathbf{0}\,, \tag{A.4}$$

where matrices $\mathbf{D}_{A_1}$ and $\mathbf{D}_{A_1}$ relates the variables of the first (resp. n^{th}) layer and $\mathbf{V}_A$ (resp. $\mathbf{V}_B$). Eq. A.4 can be rearranged to give

$$\left[\begin{array}{cc} \mathbf{D}_{A_1}(k,\omega) & \mathbf{D}_{A_2}(k,\omega) \\ \mathbf{0} & \mathbf{D}(k,\omega) \\ \mathbf{0} & \mathbf{D}_{B_1}(k,\omega) \end{array} \right] \left\{ \begin{array}{c} \mathbf{V}_A(k,\omega) \\ \mathbf{V}(k,\omega) \end{array} \right\} = \left[\begin{array}{c} \mathbf{0} \\ \mathbf{0} \\ -\mathbf{D}_{B_2}(k,\omega) \end{array} \right] \mathbf{V}_B(k,\omega)\,. \tag{A.5}$$

Solving Eq. A.5 it is possible to define a reduced transfer matrix relating the normal variables on side A and B, i.e.

$$\mathbf{V}_A(k,\omega) = \begin{bmatrix} T_{11}(k,\omega) & T_{12}(k,\omega) \\ T_{21}(k,\omega) & T_{22}(k,\omega) \end{bmatrix} \mathbf{V}_B(k,\omega)\,. \tag{A.6}$$

Thus, the fundamental solutions for the (u,u) formulation read

$$\begin{cases} \hat{d}_{AA}(k,\omega) &= \imath\omega \dfrac{T_{11}(k,\omega)}{T_{21}(k,\omega)} \\ \hat{d}_{AB}(k,\omega) &= -\imath\omega \dfrac{1}{T_{21}(k,\omega)} = -\hat{d}_{BA}(k,\omega) \\ \hat{d}_{BB}(k,\omega) &= -\imath\omega \dfrac{T_{22}(k,\omega)}{T_{21}(k,\omega)} \end{cases}, \tag{A.7}$$

while for the (u,σ) formulation

$$\begin{cases} \hat{g}_{AA}(k,\omega) &= \imath\omega \dfrac{T_{12}(k,\omega)}{T_{22}(k,\omega)} \\ \hat{g}_{AB}(k,\omega) &= \dfrac{1}{T_{22}(k,\omega)} = \hat{g}_{BA}(k,\omega) \\ \hat{g}_{BB}(k,\omega) &= -\dfrac{1}{\imath\omega}\dfrac{T_{21}(k,\omega)}{T_{22}(k,\omega)} \end{cases}, \tag{A.8}$$

where $\imath = \sqrt{-1}$ is the complex unit. Furthermore, the radiation into an unbounded fluid at side B of the acoustic treatment can directly accounted for within the transfer matrix model by adding to the system in Eq. A.6 the impedance condition $\frac{\sigma_B}{v_B} = -\imath\omega \frac{\rho_0 c_0 k_0}{\sqrt{k_0^2 - k^2}} = \hat{Z}_\infty(k,\omega)$. Thus, solving the system one eventually gets

$$\begin{cases} \hat{d}(k,\omega) &= \imath\omega \left(\dfrac{T_{12}(k,\omega)}{T_{22}(k,\omega)} - \dfrac{\frac{1}{T_{22}^2(k,\omega)}\hat{Z}_\infty(k,\omega)}{1 - \hat{Z}_\infty \frac{T_{21}(k,\omega)}{T_{22}(k,\omega)}} \right) \\ \hat{d}_{A\to B}(k,\omega) &= \dfrac{\frac{1}{T_{22}(k,\omega)}\hat{Z}_\infty(k,\omega)}{1 - \hat{Z}_\infty \frac{T_{21}(k,\omega)}{T_{22}(k,\omega)}} \end{cases}. \tag{A.9}$$

ANNEX B

MAPPING BETWEEN JINC FUNCTIONS AMPLITUDES AND NODAL VALUES

In this appendix the mapping from the amplitude of the jinc functions to the value of the physical variable associated to the same node is obtained. Let $u(\mathbf{x}, \omega)$ be the generic physical variable. The approximation of $u(\mathbf{x}, \omega)$ by a finite number of jinc functions is

$$u(\mathbf{x}, \omega) = \sum_{i=1}^{n} 2\,\mathrm{jinc}(k_s r)\, a_i(\omega)\,. \tag{B.1}$$

Following Monaghan [80] and Lanagley [63], the continuous form of Eq. B.1 reads

$$u(\mathbf{x}, \omega) = \int_S 2\,\mathrm{jinc}(k_s r)\, \frac{a(\mathbf{x}', \omega)}{A(\mathbf{x}')}\,, \tag{B.2}$$

where $r = |\mathbf{x} - \mathbf{x}'|$, $A(\mathbf{x}')$ is the area distribution function and S is the support of the function u. Applying the Fourier transform on both sides of Eq. B.2 yields

$$u(\mathbf{k}, \omega) = \left(\frac{4\pi}{k_s^2}\right) \mathrm{FT}\left[\frac{a(\mathbf{x}', \omega)}{A(\mathbf{x}')}\right]\,, \tag{B.3}$$

where the first term in the brackets is the Fourier transform of the jinc function, while the formalism $\mathrm{FT}\,[f(\mathbf{x})]$ indicates the Fourier transform of the argument $f(\mathbf{x})$. Antitransforming Eq. B.3 and using the obtained formula on a specific node $\mathbf{x}_i$ one finally obtains

$$a(\mathbf{x}_i, \omega) = a_i(\omega) = \frac{A(\mathbf{x}_i) k_s^2}{4\pi} u(\mathbf{x}_i, \omega) = H_{ii} u_i(\omega)\,, \tag{B.4}$$

with H_{ii} elements of the diagonal operator $\mathbf{H}$ which maps the physical variables $\mathbf{u}$ onto the amplitudes $\mathbf{a}$. Similarly, the continuous form of the projection onto the jinc function space of the generic variable $u(\mathbf{x}, \omega)$ is

$$R(\mathbf{x}) = \int_S 2\,\mathrm{jinc}(k_s r)\, u(\mathbf{x}', \omega)\,. \tag{B.5}$$

Following the same procedure above, the following mapping between the projected variable and the associated physical variable is obtained

$$R(\mathbf{x}_i, \omega) = R_i(\omega) = \frac{4\pi}{k_s^2} u(\mathbf{x}_i, \omega) = \hat{H}_{ii} u_i(\omega)\,, \tag{B.6}$$

with $\hat{H}_{ii}$ elements of the diagonal operator $\hat{\mathbf{H}}$.

LIST OF REFERENCES

[1] Alimonti, L., Atalla, N., Berry, A. and Sgard, F. (2014). Assessment of a hybrid finite element-transfer matrix model for flat structures with homogeneous acoustic treatments. *The Journal of the Acoustical Society of America*, volume 135, number 5, pp. 2694–2705.

[2] Alimonti, L., Atalla, N., Berry, A. and Sgard, F. (2014). Erratum: Assessment of a hybrid finite element-transfer matrix model for flat structures with homogeneous acoustic treatments [j. acoust. soc. am. 135, 2694-2705 (2014)]. *The Journal of the Acoustical Society of America*, volume 136, number 3, pp. 1441–1442.

[3] Allard, J. F. and Atalla, N. (2009). *Propagation of Sound in Porous Media: Modelling Sound Absorbing Materials*, 2nd edition. John Wiley and Sons.

[4] Allen, J. B. and Berkley, D. A. (1979). Image method for efficiently simulating small-room acoustics. *The Journal of the Acoustical Society of America*, volume 65, number 4, pp. 943–950.

[5] Atalla, N., Panneton, R. and Debergue, P. (1998). A mixed displacement-pressure formulation for poroelastic materials. *The Journal of the Acoustical Society of America*, volume 104, number 3, pp. 1444–1452.

[6] Atalla, N., Sgard, F. and Amedin, C. K. (2006). On the modeling of sound radiation from poroelastic materials. *The Journal of the Acoustical Society of America*, volume 120, number 4, pp. 1990–1995.

[7] Aucejo, M., Maxit, L., Totaro, N. and Guyader, J.-L. (2010). Convergence acceleration using the residual shape technique when solving structure-acoustic coupling with the patch transfer functions method. *Computers & Structures*, volume 88, number 11-12, pp. 728–736.

[8] Avery, P., Farhat, C. and Reese, G. (2007). Fast frequency sweep computations using a multi-point padé-based reconstruction method and an efficient iterative solver. *International Journal for Numerical Methods in Engineering*, volume 69, number 13, pp. 2848–2875.

[9] Barbagallo, M. (2013). *Statistical energy analysis and variational principles for the prediction of sound transmission in multilayered structures*. Ph.D. thesis, KTH Royal Institute of Technology, Stockholm, Sweden.

[10] Bathe, K. J. (1996). *Finite Element Procedures*, 6th edition. Prentice Hall.

[11] Berenger, J.-P. (1994). A perfectly matched layer for the absorption of electromagnetic waves. *Journal of Computational Physics*, volume 114, number 2, pp. 185 – 200.

[12] Bermúdez, A., Hervella-Nieto, L., Prieto, A. and Rodríguez, R. (2010). Perfectly matched layers for time-harmonic second order elliptic problems. *Archives of Computational Methods in Engineering*, volume 17, number 1, pp. 77–107.

[13] Biot, M. A. (1956). Theory of propagation of elastic waves in a fluid-saturated porous solid. I. low-frequency range. *The Journal of the Acoustical Society of America*, volume 28, number 2, pp. 168–178.

[14] Biot, M. A. (1956). Theory of propagation of elastic waves in a fluid-saturated porous solid. II. higher frequency range. *The Journal of the Acoustical Society of America*, volume 28, number 2, pp. 179–191.

[15] Biot, M. A. (1961). Generalized theory of acoustic propagation in porous dissipative media. *Journal of the Acoustical Society of America*, volume 34, number 94, p. 1254.

[16] Borish, J. (1984). Extension of the image model to arbitrary polyhedra. *The Journal of the Acoustical Society of America*, volume 75, number 6, pp. 1827–1836.

[17] Brebbia, C. A. and Dominguez, J. (1996). *Boundary Elements: An Introductory Course*. WIT Press.

[18] Chae, K.-S. and Ih, J.-G. (2001). Prediction of vibrational energy distribution in the thin plate high-frequency bands by using the ray tracing method. *Journal of Sound and Vibration*, volume 240, number 2, pp. 263 – 292.

[19] Chazot, J.-D., Nennig, B. and Chettah, A. (2011). Harmonic response computation of viscoelastic multilayered structures using a zpst shell element. *Computers & Structures*, volume 89, number 23-24, pp. 2522 – 2530.

[20] Chazot, J.-D., Nennig, B. and Perrey-Debain, E. (2013). Performances of the partition of unity finite element method for the analysis of two-dimensional interior sound fields with absorbing materials. *Journal of Sound and Vibration*, volume 332, number 8, pp. 1918 – 1929.

[21] Cherif, R. and Atalla, N. (2014). Radiation efficiency measurement techniques of planar structures. In *Proceedings of noise-con 2014*.

[22] Chronopoulos, D., Ichchou, M., Troclet, B. and Bareille, O. (2013). Predicting the broadband vibroacoustic response of systems subject to aeroacoustic loads by a krylov subspace reduction. *Applied Acoustics*, volume 74, number 12, pp. 1394 – 1405.

[23] Cimerman, B., Bremner, P., Qian, Y. and Van Buskirk, J. (1995). Incorporating layered acoustic trim materials in body structural-acoustic models. *SAE Technical Paper 951307*.

[24] Cotoni, V., Langley, R. and Shorter, P. (2008). A statistical energy analysis subsystem formulation using finite element and periodic structure theory. *Journal of Sound and Vibration*, volume 318, number 4-5, pp. 1077–1108.

[25] Cotoni, V., Shorter, P. and Langley, R. (2007). Numerical and experimental validation of a hybrid finite element-statistical energy analysis method. *The Journal of the Acoustical Society of America*, volume 122, number 1, pp. 259–270.

[26] Courtois, T. and Bertolini, C. (2010). A procedure for efficient trimmed body fe simulations, based on transfer admittance model of the sound package. *SAE Int. J. Passeng. Cars - Mech. Syst.*, volume 3, pp. 1–13.

[27] Craig, R. (1987). A review of time-domain and frequency domain component mode synthesis methods. *Int. J. Anal. Exp. Modal Anal.*, volume 2, number 2, pp. 59–72.

[28] Cuenca, J., Gautier, F. and Simon, L. (2009). The image source method for calculating the vibrations of simply supported convex polygonal plates. *Journal of Sound and Vibration*, volume 322, number 4-5, pp. 1048 – 1069.

[29] Cuenca, J., Gautier, F. and Simon, L. (2012). Harmonic green's functions for flexural waves in semi-infinite plates with arbitrary boundary conditions and high-frequency approximation for convex polygonal plates. *Journal of Sound and Vibration*, volume 331, number 6, pp. 1426 – 1440.

[30] Dauchez, N., Sahraoui, S. and Atalla, N. (2001). Convergence of poroelastic finite elements based on biot displacement formulation. *The Journal of the Acoustical Society of America*, volume 109, number 1, pp. 33–40.

[31] Davidsson, P. (2004). *Structure-Acoustic analysis: finite element modelling and reduction methods*. Ph.D. thesis, Lund University, Lund, Sweden.

[32] Dazel, O., Brouard, B., Dauchez, N., Geslain, A. and Lamarque, C.-H. (2010). A free interface cms technique to the resolution of coupled problem involving porous materials, application to a monodimensional problem. *Acta Acustica united with Acustica*, volume 96, number 2, pp. 247–257.

[33] Dazel, O., Brouard, B., Groby, J.-P. and Göransson, P. (2013). A normal modes technique to reduce the order of poroelastic models: application to 2d and coupled 3d models. *International Journal for Numerical Methods in Engineering*, volume 96, number 2, pp. 110–128.

[34] Dazel, O. and Gabard, G. (2013). Discontinuous galerkin methods for poroelastic materials. *Proceedings of Meetings on Acoustics*, volume 19, number 1, pp. 1–8.

[35] Deckers, E., Hörlin, N.-E., Vandepitte, D. and Desmet, W. (2012). A wave based method for the efficient solution of the 2d poroelastic biot equations. *Computer Methods in Applied Mechanics and Engineering*, volume 201-204, pp. 245 – 262.

[36] Desmet, W. (1998). *A wave based prediction technique for coupled vibro-acoustic analysis*. Ph.D. thesis, Katholieke Universiteit Leuven, Heverlee (Leuven), Belgium.

[37] Deü, J.-F., Larbi, W. and Ohayon, R. (2008). Vibration and transient response of structural-acoustic interior coupled systems with dissipative interface. *Computer Methods in Applied Mechanics and Engineering*, volume 197, number 51-52, pp. 4894 – 4905.

[38] Donders, S., Pluymers, B., Ragnarsson, P., Hadjit, R. and Desmet, W. (2010). The wave-based substructuring approach for the efficient description of interface dynamics in substructuring. *Journal of Sound and Vibration*, volume 329, number 8, pp. 1062–1080.

[39] Duhamel, D., Mace, B. and Brennan, M. (2006). Finite element analysis of the vibrations of waveguides and periodic structures. *Journal of Sound and Vibration*, volume 294, number 1-2, pp. 205–220.

[40] Fahy, F. (1997). Statistical energy analysis: a critical overview. In *Statistical Energy Analysis: An Overview, with Applications in Structural Dynamics*. Cambridge University Press, pp. 431–447.

[41] Farhat, C., Harari, I. and Franca, L. P. (2001). The discontinuous enrichment method. *Computer Methods in Applied Mechanics and Engineering*, volume 190, number 48, pp. 6455 – 6479.

[42] Farhat, C., Harari, I. and Hetmaniuk, U. (2003). A discontinuous galerkin method with lagrange multipliers for the solution of helmholtz problems in the mid-frequency regime. *Computer Methods in Applied Mechanics and Engineering*, volume 192, number 11-12, pp. 1389 – 1419.

[43] Faverjon, B. and Soize, C. (2004). Equivalent acoustic impedance model. part 1: experiments and semi-physical model. *Journal of Sound and Vibration*, volume 276, number 3-5, pp. 571 – 592.

[44] Faverjon, B. and Soize, C. (2004). Equivalent acoustic impedance model. part 2: analytical approximation. *Journal of Sound and Vibration*, volume 276, number 3-5, pp. 593 – 613.

[45] Fernandez, C., Soize, C. and Gagliardini, L. (2009). Fuzzy structure theory modeling of sound-insulation layers in complex vibroacoustic uncertain systems: Theory and experimental validation. *The Journal of the Acoustical Society of America*, volume 125, number 1, pp. 138–153.

[46] Fernandez, C., Soize, C. and Gagliardini, L. (2010). Sound-insulation layer modeling in car computational vibroacoustics in the medium-frequency range. *Acta Acustica united with Acustica*, volume 96, pp. 437–444.

[47] Finnveden, S. (2004). Evaluation of modal density and group velocity by a finite element method. *Journal of Sound and Vibration*, volume 273, number 1-2, pp. 51–75.

[48] Franzoni, L. P., Bliss, D. B. and Rouse, J. W. (2001). An acoustic boundary element method based on energy and intensity variables for prediction of high-frequency broadband sound fields. *The Journal of the Acoustical Society of America*, volume 110, number 6, pp. 3071–3080.

[49] Genechten, B. V., Vandepitte, D. and Desmet, W. (2011). A direct hybrid finite element - wave based modelling technique for efficient coupled vibro-acoustic analysis.

Computer Methods in Applied Mechanics and Engineering, volume 200, number 5-8, pp. 742 – 764.

[50] Gholami, M. (2013). *Un modèle vibroacoustique pour prèvoir l'effet de niche sur la perte par transmission sonore*. M.Sc. thesis, Université de Sherbrooke, Sherbrooke (Quebec), Canada.

[51] Gunda, R., Vijayakar, S. and Singh, R. (1995). Method of images for the harmonic response of beams and rectangular plates. *Journal of Sound and Vibration*, volume 185, number 5, pp. 791 – 808.

[52] Gunda, R., Vijayakar, S. M., Singh, R. and Farstad, J. E. (1998). Harmonic green's functions of a semi-infinite plate with clamped or free edges. *The Journal of the Acoustical Society of America*, volume 103, number 2, pp. 888–899.

[53] Hamdi, M., Atalla, N., Mebarek, L. and Omrani, A. (2000). Novel mixed finite element formulation for the analysis of sound absorption by porous materials. In *Proceedings of 29th International Congress abd Exhibition on Noise Control Engineering*. InterNoise, Nice, France.

[54] Hassan, S. E. (2007). Impedance of pistons on a two-layer medium in a planar infinite rigid baffle. *The Journal of the Acoustical Society of America*, volume 122, number 1, pp. 237–246.

[55] Hetmaniuk, U., Tezaur, R. and Farhat, C. (2012). Review and assessment of interpolatory model order reduction methods for frequency response structural dynamics and acoustics problems. *International Journal for Numerical Methods in Engineering*, volume 90, number 13, pp. 1636–1662.

[56] Hetmaniuk, U., Tezaur, R. and Farhat, C. (2013). An adaptive scheme for a class of interpolatory model reduction methods for frequency response problems. *International Journal for Numerical Methods in Engineering*, volume 93, number 10, pp. 1109–1124.

[57] Hörlin, N.-E., Nordstörm, M. and Göransson, P. (2001). A 3-d hierarchical fe formulation of biot's equations for elasto-acoustic modelling of porous media. *Journal of Sound and Vibration*, volume 245, number 4, pp. 633 – 652.

[58] Jaouen, L., Brouard, B., Atalla, N. and Langlois, C. (2005). A simplified numerical model for a plate backed by a thin foam layer in the low frequency range. *Journal of Sound and Vibration*, volume 280, number 3-5, pp. 681 – 698.

[59] Ji, L., Mace, B. and Pinnington, R. (2001). *Power transmission between long-wavelength sources and short-wavelength receivers* (Technical report). ISVR University of Southampton, 1-75 pp.

[60] Ji, L., Mace, B. and Pinnington, R. (2004). A hybrid mode/fourier-transform approach for estimating the vibrations of beam-stiffened plate systems. *Journal of Sound and Vibration*, volume 274, number 3-5, pp. 547 – 565.

[61] Jonckheere, S., Deckers, E., Genechten, B. V., Vandepitte, D. and Desmet, W. (2013). A direct hybrid finite element - wave based method for the steady-state analysis of acoustic cavities with poro-elastic damping layers using the coupled helmholtz-biot equations. *Computer Methods in Applied Mechanics and Engineering*, volume 263, number 0, pp. 144 – 157.

[62] Kosten, C. W. (1960). The mean free path in room acoustics. *Acta Acustica united with Acustica*, volume 10, number 4, pp. 245–250.

[63] Langley, R. S. (2007). Numerical evaluation of the acoustic radiation from planar structures with general baffle conditions using wavelets. *The Journal of the Acoustical Society of America*, volume 121, number 2, pp. 766–777.

[64] Langley, R. S. (2007). On the diffuse field reciprocity relationship and vibrational energy variance in a random subsystem at high frequencies. *The Journal of the Acoustical Society of America*, volume 121, number 2, pp. 913–921.

[65] Langley, R. S. and Bremner, P. (1999). A hybrid method for the vibration analysis of complex structural-acoustic systems. *The Journal of the Acoustical Society of America*, volume 105, number 3, pp. 1657–1671.

[66] Langley, R. S. and Cordioli, J. A. (2009). Hybrid deterministic-statistical analysis of vibro-acoustic systems with domain couplings on statistical components. *Journal of Sound and Vibration*, volume 321, number 3-5, pp. 893 – 912.

[67] Le Bot, A. (2002). Energy transfer for high frequencies in built-up structures. *Journal of Sound and Vibration*, volume 250, number 2, pp. 247 – 275.

[68] Le Bot, A. and Sadoulet-Reboul, E. (2014). High frequency vibroacoustics: A radiative transfer equation and radiosity based approach. *Wave Motion*, volume 51, number 4, pp. 598 – 605.

[69] Legault, J., Langley, R. and Woodhouse, J. (2012). Physical consequences of a nonparametric uncertainty model in structural dynamics. *Journal of Sound and Vibration*, volume 331, number 25, pp. 5469 – 5487.

[70] Lenzi, M. S., Lefteriu, S., Beriot, H. and Desmet, W. (2013). A fast frequency sweep approach using padé approximations for solving helmholtz finite element models. *Journal of Sound and Vibration*, volume 332, number 8, pp. 1897 – 1917.

[71] Liu, H. (2014). *Wave modeling techniques for medium and high frequency vibroacoustic analysis including porous elastic materials*. Ph.D. thesis, KTH Royal Institute of Technology, Stockholm, Sweden.

[72] Liu, H., Finnveden, S., Barbagallo, M. and Lopez Arteaga, I. (2014). Wave propagation in sandwich panels with a poroelastic core. *The Journal of the Acoustical Society of America*, volume 135, number 5, pp. 2683–2693.

[73] Lyon, R. H. and Dejong, R. G. (1995). *Theory and application of Statistical Energy Analysis*. Butterworth-Heineman.

[74] Mace, B. (2003). Statistical energy analysis, energy distribution models and system modes. *Journal of Sound and Vibration*, volume 264, number 2, pp. 391 – 409.

[75] Mace, B. (2005). Statistical energy analysis: coupling loss factors, indirect coupling and system modes. *Journal of Sound and Vibration*, volume 279, number 1-2, pp. 141 – 170.

[76] Manconi, E. (2008). *Modelling wave propagation in two-dimensional structures using a wave/finite element technique*. Ph.D. thesis, University of Parma, Parma, Italy.

[77] Maxit, L., Aucejo, M. and Guyader, J.-L. (2012). Improving the patch transfer function approach for fluid-structure modelling in heavy fluid. *J. Vib. Acoust.*, volume 134, pp. 1–14.

[78] Mechel, F. (2002). Improved mirror source method in roomacoustics. *Journal of Sound and Vibration*, volume 256, number 5, pp. 873 – 940.

[79] Melenk, J. and Babuska, I. (1996). The partition of unity finite element method: Basic theory and applications. *Computer Methods in Applied Mechanics and Engineering*, volume 139, number 1-4, pp. 289 – 314.

[80] Monaghan, J. (2005). Smoothed particle hydrodynamics. *Reports on Progress in Physics*, volume 68, number 8, p. 1703.

[81] Nguyen, V. P., Rabczuk, T., Bordas, S. and Duflot, M. (2008). Meshless methods: A review and computer implementation aspects. *Mathematics and Computers in Simulation*, volume 79, number 3, pp. 763 – 813.

[82] Orrenius, U., Liu, H., Wareing, A., Finnveden, S. and Cotoni, V. (2014). Wave modelling in predictive vibro-acoustics: Applications to rail vehicles and aircraft. *Wave Motion*, volume 51, number 4, pp. 635 – 649.

[83] Ouisse, M., Maxit, L., Cacciolati, C. and Guyader, J.-L. (2004). Patch transfer functions as a tool to couple linear acoustic problems. *Journal of Vibration and Acoustics*, volume 127, pp. 1–9.

[84] Panneton, R. (2007). Comments on the limp frame equivalent fluid model for porous media. *The Journal of the Acoustical Society of America*, volume 122, number 6, pp. EL217–EL222.

[85] Panneton, R. and Atalla, N. (1997). An efficient finite element scheme for solving the three-dimensional poroelasticity problem in acoustics. *The Journal of the Acoustical Society of America*, volume 101, number 6, pp. 3287–3298.

[86] Pierce, A. D. (1994). *Acoustics*, 3rd edition. Acoustical Society of America.

[87] Pluymers, B., Desmet, W., Vandepitte, D. and Sas, P. (2004). Application of an efficient wave-based prediction technique for the analysis of vibro-acoustic radiation problems. *Journal of Computational and Applied Mathematics*, volume 168, number 1-2, pp. 353–364.

[88] Puri and R.S., Morrey, D. (2011). An arnoldi based projection formulation for fully coupled low frequency structural-acoustic analysis. *Acta Acustica united with Acustica*, volume 97, number 3, pp. 509–518.

[89] Renno, J. M. and Mace, B. R. (2010). On the forced response of waveguides using the wave and finite element method. *Journal of Sound and Vibration*, volume 329, number 26, pp. 5474 – 5488.

[90] Rhazi, D. (2011). *Numerical modeling and experimental validation of the acoustic transmission of aircraft's double-wall structures including sound package*. Ph.D. thesis, Université de Sherbrooke, Sherbrooke (Quebec), Canada.

[91] Rhazi, D. and Atalla, N. (2010). A simple method to account for size effects in the transfer matrix method. *The Journal of the Acoustical Society of America*, volume 127, number 2, pp. EL30–EL36.

[92] Rhazi, D. and Atalla, N. (2010). Transfer matrix modeling of the vibroacoustic response of multi-materials structures under mechanical excitation. *Journal of Sound and Vibration*, volume 329, number 13, pp. 2532 – 2546.

[93] Rhazi, D. and Atalla, N. (2014). Acoustic and vibration response of a structure with added noise control treatment under various excitations. *The Journal of the Acoustical Society of America*, volume 135, number 2, pp. 693–704.

[94] Rigobert, S., Atalla, N. and Sgard, F. C. (2003). Investigation of the convergence of the mixed displacement-pressure formulation for three-dimensional poroelastic materials using hierarchical elements. *The Journal of the Acoustical Society of America*, volume 114, number 5, pp. 2607–2617.

[95] Rumpler, R. (2012). *Efficient Finite Element Approach for Structural-Acoustic Applications including 3D Modelling of Sound Absorbing Porous Materials*. Ph.D. thesis, CNAM-KTH, Stockholm , Sweden.

[96] Rumpler, R., Deü, J.-F. and Göransson, P. (2012). A modal-based reduction method for sound absorbing porous materials in poro-acoustic finite element models. *The Journal of the Acoustical Society of America*, volume 132, number 5, pp. 3162–3179.

[97] Rumpler, R., Göransson, P. and Deü, J.-F. (2013). A residue-based mode selection and sorting procedure for efficient poroelastic modeling in acoustic finite element applications. *The Journal of the Acoustical Society of America*, volume 134, number 6, pp. 4730–4741.

[98] Schenk, O. and Gärtner, K. (2002). Two-level dynamic scheduling in pardiso: Improved scalability on shared memory multiprocessing systems. *Parallel Computing*, volume 28, number 2, pp. 187 – 197.

[99] Schenk, O., Gärtner, K. and Fichtner, W. (2000). Efficient sparse lu factorization with left-right looking strategy on shared memory multiprocessors. *BIT Numerical Mathematics*, volume 40, number 1, pp. 158–176.

[100] Sestieri, A. and Carcaterra, A. (2013). Vibroacoustic: The challenges of a mission impossible? *Mechanical Systems and Signal Processing*, volume 34, number 1-2, pp. 1 – 18.

[101] Sgard, F., Nelisse, H., Atalla, N., Amedin, C. K. and Oddo, R. (2010). Prediction of the acoustical performance of enclosures using a hybrid statistical energy analysis: Image source model. *The Journal of the Acoustical Society of America*, volume 127, number 2, pp. 784–795.

[102] Sgard, F. C., Atalla, N., Gholami, M. and Nelisse, H. (2013). Tunneling effect on the sound transmission loss of a flat structure coupled with a porous material. *Proceedings of Meetings on Acoustics*, volume 19, number 1.

[103] Shorter, P. (2004). Wave propagation and damping in linear viscoelastic laminates. *Journal of the Acoustical Society of America*, volume 115, number 5, pp. 1917–1925.

[104] Shorter, P. and Langley, R. (2005). Vibro-acoustic analysis of complex systems. *Journal of Sound and Vibration*, volume 288, number 3, pp. 669 – 699.

[105] Shorter, P. and Mueller, S. (2008). Modeling the mid-frequency response of poroelastic materials in vibro-acoustics applications. In *Proceedings of SAPEM 2008*.

[106] Shorter, P. J. and Langley, R. S. (2005). On the reciprocity relationship between direct field radiation and diffuse reverberant loading. *The Journal of the Acoustical Society of America*, volume 117, number 1, pp. 85–95.

[107] Soize, C. (1992). Modeling and numerical method in the medium frequency range for vibroacoustic predictions using theory of structural fuzzy. *The Journal of the Acoustical Society of America*, volume 92, number 4, pp. 2365–2365.

[108] Soize, C. (1993). A model and numerical method in the medium frequency range for vibroacoustic predictions using the theory of structural fuzzy. *The Journal of the Acoustical Society of America*, volume 94, number 2, pp. 849–865.

[109] Soize, C. (2000). A nonparametric model of random uncertainties for reduced matrix models in structural dynamics. *Probabilistic Engineering Mechanics*, volume 15, number 3, pp. 277 – 294.

[110] Soize, C. (2003). Random matrix theory and non-parametric model of random uncertainties in vibration analysis. *Journal of Sound and Vibration*, volume 263, number 4, pp. 893 – 916.

[111] Soize, C. (2013). Stochastic modeling of uncertainties in computational structural dynamics-recent theoretical advances. *Journal of Sound and Vibration*, volume 332, number 10, pp. 2379 – 2395.

[112] Soize, C. and Batou, A. (2011). Stochastic reduced-order model in low-frequency dynamics in presence of numerous local elastic modes. *J. Appl. Mech.*, volume 78, number 6, pp. 1–9.

[113] Strouboulis, T., Babuska, I. and Copps, K. (2000). The design and analysis of the generalized finite element method. *Computer Methods in Applied Mechanics and Engineering*, volume 181, number 1-3, pp. 43–69.

[114] Strouboulis, T., Babuska, I. and Hidajat, R. (2006). The generalized finite element method for helmholtz equation: Theory, computation, and open problems. *Computer Methods in Applied Mechanics and Engineering*, volume 195, number 37-40, pp. 4711–4731.

[115] Strouboulis, T., Copps, K. and Babuska, I. (2000). The generalized finite element method: An example of its implementation and illustration of its performance. *International Journal for Numerical Methods in Engineering*, volume 47, number 8, pp. 1401–1417.

[116] Strouboulis, T., Hidajat, R. and Babuska, I. (2008). The generalized finite element method for helmholtz equation. part ii: Effect of choice of handbook functions, error due to absorbing boundary conditions and its assessment. *Computer Methods in Applied Mechanics and Engineering*, volume 197, number 5, pp. 364–380.

[117] Szabo, B. and Babuska, I. (1991). *Finite Element Analysis*. Wiley.

[118] Szabo, B., Duster, A. and Rank, E. (2004). *Encycopedia of Computational Mechanics*, chapter 5. Wiley.

[119] Tanner, G. (2009). Dynamical energy analysis-determining wave energy distributions in vibro-acoustical structures in the high-frequency regime. *Journal of Sound and Vibration*, volume 320, number 4-5, pp. 1023 – 1038.

[120] Totaro, N. and Guyader, J. (2012). Extension of the statistical modal energy distribution analysis for estimating energy density in coupled subsystems. *Journal of Sound and Vibration*, volume 331, number 13, pp. 3114 – 3129.

[121] Tournour, M., Atalla, N., Chiello, O. and Sgard, F. (2001). Validation, performance, convergence and application of free interface component mode synthesis. *Computers & Structures*, volume 79, number 20-21, pp. 1861–1876.

[122] Tournour, M., Kosaka, F. and Shiozaki, H. (2007). Fast acoustic trim modeling using transfer matrix admittance and finite element method. *SAE Technical Paper 2007-01-2166*.

[123] Unknown (2014). *Matlab Parallel Computing Toolbox*. `http://www.mathworks.com/products/parallel-computing/` (page consulted on October 2014).

[124] Van Genechten, B., Vandepitte, D. and Desmet, W. (2011). A direct hybrid finite element - wave based modelling technique for efficient coupled vibro-acoustic analysis. *Computer Methods in Applied Mechanics and Engineering*, volume 200, number 5-8, pp. 742–764.

[125] Van Genechten, B., Vergote, K., Vandepitte, D. and Desmet, W. (2010). A multi-level wave based numerical modelling framework for the steady-state dynamic anal-

ysis of bounded helmholtz problems with multiple inclusions. *Computer Methods in Applied Mechanics and Engineering*, volume 199, number 29-32, pp. 1881–1905.

[126] Vanmaele, C., Vandepitte, D. and Desmet, W. (2007). An efficient wave based prediction technique for plate bending vibrations. *Computer Methods in Applied Mechanics and Engineering*, volume 196, number 33-34, pp. 3178–3189.

[127] Veronesi, G., Christofer, A., Nijman, E., Reilek, J. and Bocquillet, A. (2014). Patch transfer function approach for analysis of coupled vibro-acoustic problems involving porous materials. *SAE Technical Paper 2014-01-2092*.

[128] Viktorovitch, M., Thouverez, F. and Jezequel, L. (2001). An integral formulation with random parameters adapted to the study of the vibrational behaviour of structures in the middle- and high-frequency field. *Journal of Sound and Vibration*, volume 247, number 3, pp. 431 – 452.

[129] Vos, P., Sherwin, S. and Kirby, R. (2010). From h to p efficiently: Implementing finite and spectral/hp element methods to achieve optimal performance for low- and high-order discretisations. *Journal of Computational Physics*, volume 229, number 13, pp. 5161–5181.

[130] Yamamoto, T., Maruyama, S., Nishiwaki, S. and Yoshimura, M. (2008). Thickness optimization of a multilayered structure on the coupling surface between a structure and an acoustic cavity. *Journal of Sound and Vibration*, volume 318, number 1-2, pp. 109–130.